Effective and fundamental quantum fields at criticality

Dissertation

zur Erlangung des akademischen Grades
doctor rerum naturalium (Dr. rer. nat)

vorgelegt dem Rat der Physikalisch-Astronomischen Fakultät
der Friedrich-Schiller-Universität Jena

von Dipl.-Phys. Michael Scherer
geboren am 2. November 1981 in Furtwangen

Gutachter:

1. Prof. Dr. Holger Gies, Jena
2. Prof. Dr. Jan Pawlowski, Heidelberg
3. Prof. Dr. Litim, Sussex

Tag der Disputation: 28. Oktober 2010

Effektive und fundamentale Quantenfelder an der Kritikalität

Zusammenfassung

Die funktionale Renormierungsgruppe in der Formulierung von Wetterich wird als geeignete nicht-störungstheoretische Methode für die qualitative und quantitative Untersuchung universeller Phänomene in Quantenfeldtheorien verwendet. Es werden Flussgleichungen für eine Klasse chiraler Yukawa-Modelle mit und ohne Eichbosonen abgeleitet und deren Fixpunktstruktur untersucht. Die vierdimensionalen chiralen Yukawa-Modelle dienen als Spielzeug-Modelle für den Higgs-Sektor des Standardmodells. Eine Balance bosonischer und fermionischer Fluktuationen ermöglicht asymptotisch sichere Fixpunkte in der untersuchten Näherung, was eine Interpretation dieser Theorie als fundamentale Theorie erlaubt und das Trivialitäts-Problem löst. Außerdem erhalten wir Vorhersagen für die Higgs- und die Topquark-Masse unseres Spielzeugmodells. In drei Dimensionen berechnen wir die kritischen Exponenten, die neue Universalitätsklassen definieren. Damit liefern wir quantitative Vorhersagen für Systeme stark korrelierter chiraler Fermionen, die mit anderen nicht-störungstheoretischen Methoden überprüft werden können. In einem Yukawa-System nicht-relativistischer zweikomponentiger Fermionen wird der Renormierungsgruppen-Fluss ebenfalls durch einen Fixpunkt dominiert, was zu Universalität im BCS-BEC Crossover führt. Wir entwickeln die Methode der funktionalen Renormierung hinzu einem quantitativen Niveau und berechnen unter anderem die kritische Temperatur über den gesamten Crossover. Abschließend liefern wir einen weiteren Hinweis für die Möglichkeit einer asymptotisch sicheren Quantengravitation, indem wir die Existenz eines Fixpunktes im Ultravioletten unter Mitnahme einer Krümmungs-Geist-Kopplung bestätigen.

Effective and fundamental quantum fields at criticality

Abstract

We employ Wetterich's approach to functional renormalization as a suitable method to investigate universal phenomena in non-perturbative quantum field theories both qualitatively and quantitatively. Therefore we derive and investigate flow equations for a class of chiral Yukawa models with and without gauge bosons and reveal fixed-point mechanisms. In four dimensions chiral Yukawa systems serve as toy models for the standard model Higgs sector and show signatures of asymptotically safe fixed points by a balancing of bosonic and fermionic contributions. In the approximations investigated this renders the theory fundamental and solves the triviality problem. Further, we obtain predictions for the Higgs mass and even for the top mass of our toy model. In three dimensions we compute the critical exponents which define new universality classes and provide benchmark values for systems of strongly correlated chiral fermions. In a Yukawa system of non-relativistic two-component fermions a fixed point dominates the renormalization flow giving rise to universality in the BCS-BEC crossover. We push the functional renormalization method to a quantitative level and we compute the critical temperature and the single-particle gap with a considerable precision for the whole crossover. Finally, we provide further evidence for the asymptotic safety scenario in quantum gravity by confirming the existence of an ultraviolet fixed point under inclusion of a curvature-ghost coupling.

Contents

Chapter 1

Invitation

Modern research technology allows to observe physical phenomena on an incredibly large range of different length scales starting from structures smaller than the size of a nucleon in particle collider experiments up to distant galaxies using telescopes. The physical laws and objects we employ for theoretical descriptions are very different from each other on the different length scales. On the level of particle collider experiments, for example, we can describe the dynamics of elementary particles like quarks and gluons by the perturbative regime of quantum chromodynamics whereas at larger length scales physics is better captured in terms of baryons and mesons. Going to even larger length scales we find that atoms are the dominating objects and a system of many atoms is often best described as a fluid following the laws of hydrodynamics. The idea that physical objects, or *degrees of freedom*, and theories describing their properties are different on different scales suggests that we should understand physical theories today as *effective theories* meaning that they are "effectively" valid at some scale. The connection between effective theories on different length scales, might at first sight seem like a technical issue and it is indeed a mathematical formalism, the renormalization group, that establishes this transition by showing how physics changes as the length scale is changed [1, 2]. However, this formalism also provides deep conceptual insight into structure of matter on different scales and has influenced our understanding of physics very profoundly.

The renormalization group is based on the fundament of quantum field theory and statistical physics and a starting point for its formal development was the block spin idea by Leo Kadanoff [3]. It aimed at an understanding of the physics of phase transitions in statistical systems [4–6], i.e. connecting small scale physics with physics on large length scales. However, it is equally important to understand quantum field theory [7] for elementary particle physics. In particular, it provides an explanation for the scale dependence of coupling constants.

The concept of the renormalization group has been further developed since its early days and in this thesis we will employ a modern formulation in terms of the flowing action

[8–10]. The dynamics of the flowing action for the transition between microscopic and macroscopic scales is described by an exact flow equation [11]. This approach constitutes a universal theoretical tool for a description of problems ranging from particle physics like quantum chromodynamics or electroweak physics to critical phenomena and complex many-body systems, see [12–17] for reviews. The exact flow equation allows for systematic approximations containing non-pertubative information and so it is particularly suitable to describe problems involving strong fluctuations of quantum fields and interaction effects as well as the formation and the dynamics of bound states. On the other hand it still allows for an analytical treatment and so to understand the mechanisms and processes going on in strongly interacting problems. It is this conceptual power which we shall employ here to investigate non-perturbative phenomena.

Having an exact flow equation which generally describes the scale dependence of physics it is obvious to ask whether there are conditions under which a certain physical theory does not change as we observe it on different length scales. Under these conditions the system would always look the same no matter with which resolution we observe it, i.e. the system is *scale invariant*. The requirement therefore is the existence of a fixed point in the renormalization group flow. As a physical system is near a renormalization group fixed-point its scale dependence is weak and its behaviour is governed by the fixed-point, giving rise to critical behaviour and universal properties.

The physics of critical phenomena is based on this mechanism and its implications can be explicitly observed, e.g. in the liquid-vapor transition, the Helium superfluid transition, the ferromagnetic phase transition and even in polymer physics. In these systems the renormalization group fixed point dominates the large distance behaviour as it is approached when we study larger and larger length scales, i.e. the infrared limit. For those phenomena we employ effective descriptions for the relevant degrees of freedom and we say that the effective quantum field is at or near criticality resulting in universal scaling laws which are characterized by pure numbers, the critical exponents. However, this mechanism can also work the other way round: A fixed point might be approached as we look at smaller and smaller length scales, i.e. in the ultraviolet limit. This implies the absence of unphysical divergencies as they are often observed in perturbative approaches. A system running into an ultraviolet fixed point can be understood as being fundamental in the sense, that there is no other underlying structure anymore. In this case we have a fundamental quantum field at criticality whose behavior is governed by the ultraviolet fixed point and its properties.

It is not easy to find fixed points in a general theory as e.g. perturbation theory already assumes that the theory sits close to a non-interacting fixed point. Thus it requires non-perturbative tools to do so. The exact flow equation for the flowing action is such a

tool and has successfully been applied to the description of critical phenomena, complex many-body systems as well as in particle physics and gravity.

The idea that an ultraviolet fixed point might exist in a quantum field theory was first realized by Gell-Mann and Low in the context of quantum electrodynamics [2] and later on put in a general framework by Steven Weinberg [18, 19], naming it the *asymptotic safety scenario*. It was also Steven Weinberg who had a special problem in mind, that is today believed to be the most appealing arena for such a scenario: Quantum gravity. Indeed, gravity is non-renormalizable in a perturbative setting, however, it might be renormalizable if an interacting ultraviolet fixed point with suitable properties exists. However, it took another twenty years until this idea was considered more explicitely thanks to the development of functional renormalization, allowing for systematic approaches for the first time [20], see [21–23] for reviews. During the last ten years a lot of evidence has been gathered that such a scenario could be realized [20, 24–49], even discussing possible astrophysical implications [50–52] as well as LHC physics [53, 54]. Especially the pure gravity sector has been investigated, but also interactions with matter have been considered [43–46].

Despite the great advances that have been made in the theoretical description of non-perturbative quantum field theories using the exact renormalization group in the formulation by Wetterich [11] there are still a lot of open issues left which challenge the method on a qualitative as well as on a quantitative level.

An important point concerns the matter sector in asymptotically safe gravity. In order to really constitute a fundamental description of nature not only gravity should be asymptotically safe but the complete standard model plus gravity. A comprehensive discussion of such a complete scenario footing on numerous impressive computations performed by various authors [25–49] during the last ten years can be found in [55]. However, in all the investigations so far the matter sector has been considered as not essential for asymptotically safe mechanisms. On the other hand we know that the standard model is also plagued by problems of (perturbative) non-renormalizability, most prominently represented by the triviality problems in the Higgs sector and quantum electrodynamics. To fill this gap and in order to shed light on the role of the matter sector in asymptotically safe scenarios we investigate the possibility for the standard model to encounter an interacting fixed point for itself, i.e. without the effect of gravity. This is intended to constitute a possible starting point for a complete asymptotically safe scenario including matter, gauge fields and gravity. Looking only to a part of the matter sector we considerably reduce complications found in gravity and other gauge theories caused by gauge fixing.

We briefly introduce the concepts and methods employed here in Chap. 2 and explicitely discuss a paradigm example, namely the $O(N)$-model, to show the conceptual

power and the quantitative accuracy that can be achieved with our method. In Chap. 3, we investigate a simple toy model, namely a Z_2-symmetric Yukawa model exploring the possibility of asymptotic safety. We identify a mechanism that enables this scenario to work and construct a more elaborate chiral Yukawa model with a left/right asymmetry in Chap. 4. This scenario has a high predictive power and allows for the prediction of certain particle masses as, e.g., the Higgs mass. However, we encounter some shortcomings connected to the appearance of Goldstone bosons that are not present in the standard model, which motivates us to take into account gauge fields, see Sec. 4.5.

Another important open issue is represented by critical phenomena of statistical physics systems in lower dimensions including fermions. In the past, $d = 3$ dimensional fermionic systems with chiral symmetries such as QED_3 or the Thirring model have been under investigation in a variety of scenarios [127–136] with applications to condensed-matter physics, high-T_c cuprate superconductors [137, 138] and, recently, graphene [139, 140]. In some of these models, the number of fermion flavors serves as a control parameter for a quantum phase transition. Thus the critical number of fermions is an important quantity and nonperturbative information about these models for varying flavor number N_f is required. Since chiral fermions for arbitrary N_f still represent a challenge, e.g., for lattice simulations, other powerful nonperturbative techniques are urgently needed. Chiral fermion models offer the possiblity for quantitative comparisons between field-theoretical methods, e.g. by computation of critical exponents at an interacting fixed point. In Chap. 5 we investigate a three-dimensional chiral fermion model with a left/right asymmetry. We classify all four-fermion interaction terms and identify fixed-point mechanisms. The critical exponents define new universality classes and provide quantitative benchmark values for systems of strongly correlated chiral fermions.

The pursuit of quantitative precision using functional renormalization group methods for quantum fields at criticality is further pushed forward in Chap. 6. We investigate aspects of the BCS-BEC crossover in ultracold fermionic atom gases. Indeed, also here it is an underlying fixed-point structure giving rise to universal properties of the system. This model is very well suited as a testing ground for non-perturbative methods and we will show that our approach to functional renormalization can provide quantitative results for strongly interacting quantum physics. Thereby, we apply recent conceptual advances, namely bosonization, to include particle-hole fluctuations. Moreover, fluctuations of the fermionic self-energy are considered to finally compute the critical temperature and the single-particle gap with a considerable precision for the whole crossover.

As a last issue we turn to the subject of asymptotically safe gravity. Here, also the ghost sector in quantum gravity is expected to have some possibly important influence on the ultraviolet fixed point. However, this sector has been poorly understood up to now as it was only considered in a classical treatment. A first attempt to fill this gap

is presented in Chap. 7, where we provide further evidence for the asymptotic safety scenario in quantum gravity by confirming the existence of an ultraviolet fixed-point under inclusion of a curvature-ghost coupling. Conclusions are drawn in Chap. 8. We would like to point out that throughout this work, rather technical and computational issues are deferred to the appendix, in particular derivations of flow equations.

The compilation of this thesis is solely to the author, however, a large part of the work presented here has been published in a number of articles and in collaboration with various authors, which I cordially appreciate. Asymptotic safety for Yukawa systems has been investigated in collaboration with Holger Gies and Stefan Rechenberger [56–58]. For the three dimensional Yukawa systems Lukas Janssen joined the collaboration [59]. The work on QEG was done with Holger Gies and Astrid Eichhorn [42]. The investigations on the BCS-BEC crossover where done with Stefan Floerchinger, Sebastian Diehl and Christof Wetterich [60, 61].

Chapter 2

Concepts and methods for quantum fields at criticality

Quantum and statistical field theory constitute the fundament of our theoretical understanding of modern physics. In this chapter we introduce the basic methods and concepts that are employed in this thesis to investigate problems in those two closely related areas. Indeed, quantum field theory describing phenomena in particle physics and statistical physics can be described in the same conceptual setting of (euclidean) functional integrals, which store the physical information in terms of correlation functions, see Sec. 2.1. The functional integral representation of quantum field theory can be put in terms of an exact renormalization group equation (ERGE), the Wetterich equation, see Sec. 2.2. Being a universal theoretical method the Wetterich equation establishes a connection between short- and long-distance physics in terms of the effective average or *flowing* action by acting like a microscope with variable resolution. It allows for systematic non-perturbative approximations of the effective action and the computation of universal as well as non-universal quantities in field theory. Fixed-points of the renormalization group flow induce universal critical dynamics in their vicinity, see Sec. 2.3, i.e. they provide universality as observed in the critical behaviour of phase transitions, see Sec. 2.4. However, they can also reveal underlying mechanisms that render a quantum field theory non-perturbatively renormalizable and therefore a possible candidate for a fundamental and predictive theory, see Sec. 2.5.

2.1 Functional integrals and effective action

In modern quantum field theory the basic objects are functional integrals allowing to calculate the physical observables in terms of expectation values and correlation functions on an incredibly huge configuration space. For quantum statistical physics one starts from the partition function $Z = \mathrm{Tr}\, \exp(-\frac{1}{T}H)$ which can be written in the form of a $(D+1)$-

dimensional functional integral, where $D \in \{0, 1, 2, 3\}$ is the number of space dimensions. Particle physics can be studied from a Wick-rotated four-dimensional functional integral, conventionally known as the Feynman path integral. There is no difference between the formulation of particle physics, i.e. quantum field theory, and the theory of many-body statistical systems, besides the different symmetries.

Generating functional

Here and throughout this thesis we work in euclidean spacetime. A standard way to define a continuum quantum field theory in the functional integral representation is given by the generating functional,

$$Z[J] = \int \mathcal{D}\varphi \, e^{-S[\varphi]+J^T\cdot\varphi} \,, \tag{2.1}$$

where $S[\varphi]$ is the microscopic action subject to quantization and $J = J(x)$ are arbitrary *sources* or *external fields*. The form of $S[\varphi]$ is governed by the field content and the underlying symmetries of the theory we aim to describe and φ should be understood as a composed superfield vector, for instance, in a Nambu-Gorkov formalism containing all the field degrees of freedom. As an example we write down the field content of an N-component scalar model

$$\varphi(x) = (\phi_1, \phi_2, ..., \phi_N)(x) \,. \tag{2.2}$$

These models, equipped with an $O(N)$-symmetry, are paradigmatic for quantum field theories and have numerous applications in physics. The description of fermions requires the introduction of anticommuting Grassmann fields. A common example therefore is a bosonized Gross-Neveu model corresponding to a Yukawa model with the field content

$$\varphi(x) = (\phi, \psi^T, \bar{\psi})(x) \,, \tag{2.3}$$

where ϕ is a real scalar field and ψ represents a Dirac spinor. In Chap. 3 we shall investigate a four-dimensional relativistic theory with such a field content, mimicking the Higgs sector of the standard model. Moreover in Chaps. 4 and 5 we study similar but more complicated theories including different numbers of left- and right-handed fermions, complex bosons and even gauge fields.

In condensed matter physics non-relativistic models such as ultracold fermionic atoms with two energetically accessible hyperfine states in thermal equilibrium are subject to investigations, see Chap. 6. Depending on the interaction strength they can form molecules or collective bosonic states. This can be described with the aid of the following field vector:

$$\varphi(x) = (\phi, \phi^*, \psi_1, \psi_2, \psi_1^*, \psi_2^*)(x) \,. \tag{2.4}$$

For a quantum field theory of gravity, see Chap. 7, we consider the metric field $g_{\mu\nu}(x)$ as the field content of (2.1). Then the superfield vector φ reads

$$\varphi(x) = (g_{\mu\nu}, c^{\mu}, \bar{c}_{\mu})(x)\,, \tag{2.5}$$

where c^{μ} and $\bar{c}_{\mu}$ represent Faddeev-Popov ghost fields required for the gauge fixing procedure.

The source terms J in the partition function (2.1) are introduced corresponding to the field content in the microscopic action, where bosonic entries are real or complex and the fermionic entries are Grassmann-valued. For brevity we define the following short-hand notation for the scalar product:

$$J^T \cdot \varphi = \int_x J_i(x)\varphi_i(x)\,. \tag{2.6}$$

Expectation values and correlation functions

Correlation functions are obtained by functional differentiation with respect to the source terms $J_i(x)$ evaluated at $J = 0$. The two point Green's function is generated by the operation

$$G_{ij}(x,y) = \langle\varphi_i(x)\varphi_j(y)\rangle = \frac{1}{Z[0]}\frac{\delta}{\delta J_i(x)}\frac{\delta}{\delta J_j(y)}Z[J]\Big|_{J=0}\,, \tag{2.7}$$

whereas the connected part of the Green's functions is obtained from the *Schwinger functional*

$$W[J] = \log Z[J]\,. \tag{2.8}$$

Explicitely, the *connected two-point function* which is the (full) propagator is

$$W^{(2)}_{ij}(x,y) \;=\; \frac{\delta}{\delta J_i(x)}\frac{\delta}{\delta J_j(y)}W[J]\Big|_{J=0} = \langle\varphi_i(x)\varphi_j(y)\rangle - \langle\varphi_j(y)\rangle\,\langle\varphi_i(x)\rangle\;. \tag{2.9}$$

The one-point functions are the field expectation values in vacuum (for $J = 0$) and read

$$\Phi_i(x) := \langle\varphi_i(x)\rangle = \frac{\delta W[J]}{\delta J_i(x)}\Big|_{J=0}. \tag{2.10}$$

Effective action

An efficient way to store the physical information is given by the *effective action* Γ, being the generating functional of one-particle irreducible (1PI) correlation functions. It is defined by a Legendre transform:

$$\Gamma[\Phi] = \sup_J\left(J\cdot\Phi - W[J]\right). \tag{2.11}$$

The effective action $\Gamma[\Phi]$ governs the dynamics of the expectation value $\Phi = \langle\varphi\rangle$, and the minimum of Γ for vanishing source J defines the vacuum state of the fully quantized system.

Now, we define J_{sup} to be the source field where $J\cdot\Phi - W[J]$ approaches its supremum (Γ is convex). With $J = J_{\text{sup}}$ we get

$$0 = \frac{\delta}{\delta J_i(x)}(J\cdot\Phi - W[J]) \quad \Longrightarrow \quad \Phi = \frac{\delta W[J]}{\delta J} = \langle\varphi\rangle_J\,. \tag{2.12}$$

Thus, Φ is the expectation value of φ in presence of the source J.

The quantum equation of motion is obtained by taking the derivative with respect to Φ evaluated at $J = J_{\text{sup}}$:

$$\Gamma[\Phi]\frac{\overleftarrow{\delta}}{\delta\Phi_i(x)} = \frac{\delta J_j(y)}{\delta\Phi_i(x)}\cdot\Phi_j(y) + J_i(x) - \frac{\delta J_j(y)}{\delta\Phi_i(x)}\cdot\frac{\delta W[J]}{\delta J_j(y)} = J_i(x)\,. \tag{2.13}$$

We further add the following important identity (where continuous indices are omitted for simplicity)

$$\Gamma^{(2)}_{ij}\cdot W^{(2)}_{jl} = \frac{\delta J_j}{\delta\Phi_i}\cdot\frac{\Phi_l}{\delta J_j} = \mathbb{1},\ \text{where}\ \Gamma^{(2)}_{ij} = \frac{\overrightarrow{\delta}}{\delta\Phi_i(x)}\Gamma\frac{\overleftarrow{\delta}}{\delta\Phi_j(y)} \tag{2.14}$$

This equation states that the second functional derivative of the effective action is the inverse propagator. Distinguishing between left and right derivatives also takes care of the possible Grassmann nature of field variables.

2.2 Functional renormalization

Renormalization group (RG) methods allow to investigate the scale dependence of quantum field theories and to construct non-perturbative approximate solutions to the full effective action Γ. For our renormalization group approach [11] we introduce the concept of the *flowing action* Γ_k, where k is a momentum scale and Γ_k interpolates between the microscopic action $S = \Gamma_\Lambda$ and the full effective action $\Gamma = \Gamma_0$ that includes all quantum and statistical fluctuations. The Wetterich equation establishes the interpolation procedure by means of an exact flow equation for Γ_k and we obtain an initial value problem.

2.2.1 Flowing action and Wetterich equation

We define the IR regulated generating functional by

$$Z_k[J] \equiv \mathrm{e}^{W_k[J]} = \int_\Lambda \mathcal{D}\varphi\,\mathrm{e}^{-S[\varphi]-\Delta S_k[\varphi]+J^T\cdot\varphi}, \tag{2.15}$$

where $W_k[J]$ is the scale-dependent Schwinger functional and

$$\Delta S_k[\varphi] = \frac{1}{2}\int \frac{\mathrm{d}^d q}{(2\pi)^d}\,\varphi(-q)R_k(q)\varphi(q) \tag{2.16}$$

is a regulator term which is quadratic in φ. The regulator function $R_k(q)$ should satisfy

$$\lim_{q^2/k^2\to 0} R_k(q) > 0,\quad \lim_{k^2/q^2\to 0} R_k(q) = 0,\quad \lim_{k^2\to\Lambda\to\infty} R_k(q) \to \infty, \tag{2.17}$$

which implements an IR regularization, guarantees that we start with the classical action S at the UV cutoff Λ and yields the full effective action Γ at $k = 0$. In principle the choice of the regulator is only restricted by the requirements formulated in (2.17). The concrete choice should be guided by symmetry considerations, see below.

We define the corresponding effective or *flowing* action Γ_k again by a modified Legendre transform,

$$\Gamma_k[\Phi] = \sup_J \left(J\cdot\Phi - W_k[J]\right) - \Delta S_k[\Phi]. \tag{2.18}$$

At $J = J_{\mathrm{sup}}$, the conjugate field variable Φ satisfies as before:

$$\Phi(x) = \frac{\delta W_k[J]}{\delta J(x)} = \langle\varphi(x)\rangle, \tag{2.19}$$

implying that $\Gamma_k[\Phi]$ governs the dynamics of the expectation value Φ, where the quantum averaging procedure has been performed from microscopic fluctuations at a UV cutoff Λ down to a momentum scale k. Note that similar to Eq. (2.14) we find $(\Gamma_k^{(2)}+R_k)\cdot W_k^{(2)} = \mathbb{1}$.

The scale dependence of Γ_k for fixed Φ and at $J = J_{\mathrm{sup}}$ is governed by the Wetterich equation [11]

$$\partial_t\Gamma_k[\Phi] = \frac{1}{2}\,\mathrm{STr}\left[\partial_t R_k\left(\Gamma_k^{(2)}[\Phi] + R_k\right)^{-1}\right], \tag{2.20}$$

where $\partial_t = k\frac{\mathrm{d}}{\mathrm{d}k}$ and STr is the trace operation in super-field space and involves an integration over momenta (or coordinates) as well as a summation over internal indices. In momentum space the second functional derivative is more explicitly represented by

$$\left(\Gamma_k^{(2)}[\Phi]\right)_{ij}(p_1,p_2) = \frac{\overrightarrow{\delta}}{\delta\Phi_i(-p_1)}\Gamma_k[\Phi]\frac{\overleftarrow{\delta}}{\delta\Phi_j(p_2)} \tag{2.21}$$

Eq. (2.20) can straightforwardly be derived from the definitions Eqs. (2.15) and (2.18), see App. A. The regulator function $R_k(q)$ provides an infrared cutoff for the theory by adding a mass term to the propagator and thereby cutting off all small-momentum divergencies. Another important property is that it also acts as an ultraviolet regulator by means of the derivative insertion $\partial_t R_k$ that cuts off large momentum modes. This leads

to the fact that at each renormalization step only a narrow shell of momentum modes is integrated out by the flow equation. The flow equation forms the starting point of our further investigations.

From the perspective of perturbation theory, the solution of the Wetterich equation (2.20) corresponds to a resummation of infinitely many Feynman diagrams. Finding exact solutions to equation (2.20) for non-trivial theories is not possible in general and it is necessary to use *truncations* in the space of action functionals to find approximate solutions. However, approximations do not have to rely on the existence of a small expansion parameter like the interaction strength and they are therefore of a non-perturbative nature. For reviews of the functional renormalization group method see [12–16].

2.2.2 Truncations

The Wetterich equation represents a functional differential equation for $\Gamma_k[\Phi]$. Approximate solutions can be constructed by choosing truncations in the space of possible action functionals by making an ansatz of the form

$$\Gamma_k[\Phi] = \int_x \sum_i g_{i,k} \mathcal{O}_i[\Phi] \,, \tag{2.22}$$

with $\mathcal{O}_i[\Phi]$ being field operators and $g_{i,k}$ are generalized coupling constants. Generally, the set of field operators cannot be chosen to constitute a complete set and we are left to choose a finite or infinite subspace for an ansatz that can be inserted into the Wetterich equation. Systematical truncations are usually given in terms of expansions, e.g. the *derivative expansion* for N-component scalar fields Φ_a:

$$\Gamma_k[\Phi] = \int_x \left\{ U_k(\rho) + \frac{1}{2} Z_k(\rho) \partial_\mu \Phi^a \partial^\mu \Phi_a + \frac{1}{4} Y_k(\rho) \partial_\mu \rho \partial^\mu \rho + \mathcal{O}(\partial^4) \right\} \tag{2.23}$$

where we include a scalar potential $U_k(\rho)$ with $\rho = \frac{1}{2}\Phi_a \Phi^a$ that can be expanded as a polynomial in ρ. We deal with this type of expansion in Chaps. 3, 4, 5 and 6.

Choosing a suitable truncation generally requires also some experience and insight into the physical problem. The derivative expansion has been well investigated in a variety of systems and proved to contain the relevant degrees of freedom, yielding quantitatively satisfactory results. RG flows in derivative expansions for Yukawa systems have, for instance, been successfully studied for QCD applications [62–65], critical phenomena [66, 67], and ultra-cold fermionic atom gases [60, 68, 69].

Symmetries

Another essential guiding principle for the choice of the truncation are symmetries. If the regulator term ΔS_k is chosen to respect the symmetries of the microscopic action and

no anomalies are generated by the functional measure also the flowing action Γ_k respects those symmetries. The constraints from the symmetries are modified if this is not the case, which is reflected in modified Ward identities [16].

As a common strategy to find a truncation one can take the microscopic action S or an effective action functional Γ derived from another approximation scheme like, e.g. perturbation theory. Subsequently, we can add further field operators $\mathcal{O}_i[\Phi]$ compatible with the symmetries of the microscopic action and promote the appearing couplings to be dependent on the scale k.

We encounter various different symmetries in this thesis ranging from Lorentz-invariance in Chaps. 3 and 4 to Galilean-inavariance (Chap. 6 for $T = 0$), diffeomorphism invariance (Chap. 7), but also discrete symmetries like parity, charge-conservation and time reversal, see Chap 5. Further discrete and continuous symmetries are discussed for the different models in the corresponding chapters .

Regulators and optimization

The regulator couples through the flow equation to all vertex functions of the theory, so the flow trajectory of the effective average action Γ_k depends on the regulator. In this way the regulator also modifies the effective interactions at intermediate scales $k \neq 0$, which means that the effective action still remembers some details of how the process of integrating out momentum-shells has been performed. For the *full flow* however, this regulator dependence is of no relevance, since the convergence towards the full quantum effective action for any regulator ensures that the regulator induced interactions vanish in the physical limit.

Approximations imply that certain vertices and/or the momentum dependence thereof are neglected in the theory. Then the cancellation of regulator induced interactions during the flow in the limit for $k \to 0$ can not completely be performed. The consequence is, that approximations to the full effective action depend on the regulator scheme and the question raises how it is possible to identify a regulator scheme, that "optimizes" the physical content of an approximation [16, 70, 71]. A way to do this is, e.g., derived in [71]. The basic idea consits of maximising the gap

$$\min_{q^2 \geq 0}(\Gamma_k^{(2)} + R_k) = Ck^2 > 0\,. \tag{2.24}$$

that appears in the denominator on the r.h.s. of the Wetterich equation, so that the contribution to the flow is as small as possible. The same result can be obtained by an alternative criterion formulated in [16]. Optimized regulators stabilise the flow and lead to faster convergence of expansions, as advocated in [71]. The physical information is mainly stored in the few leading terms, that are relevant for the theory, while the other contributions from higher vertex functions remain small.

Example: $O(N)$-model in 3d (Truncation, regulator, flow equations)

As an explicit example we discuss an N-component scalar field theory in three dimensions with $O(N)$-symmetry and a truncation based on Eq. (2.23). The optimization procedure leads to a regulator reading

$$R_k = Z_k(k^2 - q^2)\Theta(k^2 - q^2)\,. \tag{2.25}$$

We truncate as in (2.23) and set $Z_k(\rho) = Z_k,\ Y_k(\rho) = 0, \ldots$. Further we introduce dimensionless quantities $\tilde{\rho} = Z_k\rho/k,\ u_k(\tilde{\rho}) = U_k(\rho)/k^3$. Plugging this ansatz into the Wetterich equation yields flow equations for the dimensionless effective potential u_k and the wave function renormalization Z_k, expressed in terms of the anomalous dimension $\eta_\phi = -\partial_t Z_k/Z_k$:

$$\partial_t u_k = -3u_k + (1+\eta_\phi)\tilde{\rho}u_k' + \frac{\left(1-\frac{\eta_\phi}{5}\right)}{6\pi^2}\left\{\frac{N-1}{(1+u_k')} + \frac{1}{(1+u_k'+2\tilde{\rho}u_k'')}\right\}, \tag{2.26}$$

$$\eta_\phi = \frac{2\rho u_k''^2}{3\pi^2\left(1+u_k'\right)^2\left(1+u_k'+2\tilde{\rho}u_k''\right)^2}\,, \tag{2.27}$$

where primes should be understood as derivatives with respect to $\tilde{\rho}$.

2.3 Fixed points in quantum field theory

Nowadays we understand most theories of physics as being "effective" theories. They describe phenomena at some typical momentum scale k with a reasonable accuracy. On the other hand, they neglect phenomena that are not relevant at this momentum scale. Often, the relevant degrees of freedom change with the scale, as e.g. in Quantum Chromodynamics (QCD) where in the high energy regime we find quarks and gluons, whereas in the low energy limit physics is best described by mesons and baryons. Functional renormalization describes this transition between different regimes going from one (effective) theory to another.

A particular role in the context of scale dependent theories is played by *fixed points* in the renormalization group flow. In the vicinity of a fixed-point the renormalization group running is very slow and the physics of a system can be largely dominated by the properties of the fixed point, e.g. giving rise to universality of critical phenomena, see Sec. 2.4. Moreover, there is a widespread belief that quantum field theory in most cases only accounts for effective theories and that it is not suited to constitute a fundamental theory but should be replaced by another concept at some microscopic scale. This is due to the apparent non-renormalisability of important action functionals, e.g. the Einstein-Hilbert action describing gravity [72–75]. A similar problem arises in the standard model

of particle physics which is plagued by the problem of triviality in the sector describing quantum electrodynamics (QED) [2, 76–78] as well as in the Higgs sector [7, 79–84] and cannot be extended beyond a certain ultraviolet scale. In this context RG fixed points offer a more general conceptual understanding of quantum field theroy with the possibility to promote a theory to be fundamental (and not only effective). This was elucidated by Steven Weinberg when he introduced the idea of asymptotic safety [18, 22, 85] based on the existence of an ultraviolet fixed point, see also Sec. 2.5 for more details. Here, we introduce the technical basics for the discussion of RG fixed points.

2.3.1 The effective field theory picture

The notion of an effective field theory includes the idea that an action functional $\Gamma_k[\Phi]$ can describe physical phenomena at some momentum scale k and that a tree level evaluation suffices to describe physics at that scale. It is implicitely supposed that all the fluctuations of quantum fields with momenta larger than k of an underlying microscopic action have been integrated out to yield $\Gamma_k[\Phi]$. The dominating microscopic degrees of freedom describing physics at scales $\Lambda \gg k$ might be quite different from the degrees of freedom gathered in the super-field vector Φ for the scale k, e.g., compare quarks and gluons to mesons and baryons. Note that in the context of this section $\Gamma_k[\Phi]$ should be understood in the spirit of the concept of effective field theories not necessarily relying on the developements from the previous chapter on Wetterich's renormalization group approach. However, we can expand a general action functional for an effective field theory as before in terms of (dimensionless) running couplings $g_{i,k}$ and field operators $\mathcal{O}_i$

$$\Gamma_k[\Phi] = \sum_i g_{i,k}\mathcal{O}_i[\Phi], \text{ e.g. } \mathcal{O}_i[\Phi] = \left\{\Phi^2, \Phi^4, (\partial\Phi)^2, \dots\right\} . \tag{2.28}$$

2.3.2 Renormalization group flow, β functions

The dependence of an effective theory on the scale k can be obtained from a renormalization group approach. The renormalization group flow in the theory space of action functionals is by definition given in terms of the β functions:

$$\partial_t \Gamma_k[\Phi] = \sum_i \beta_{i,k}\mathcal{O}_i[\Phi] . \tag{2.29}$$

Here, the scale dependence of the effective field theory $\Gamma_k[\Phi]$ is formulated in terms of the scale dependence of running couplins

$$\partial_t g_{i,k} = \beta_{i,k}(g_{1,k}, g_{2,k}, ...) . \tag{2.30}$$

The field operators span the theory space, as is shown in Fig. 2.1. In the left panel of

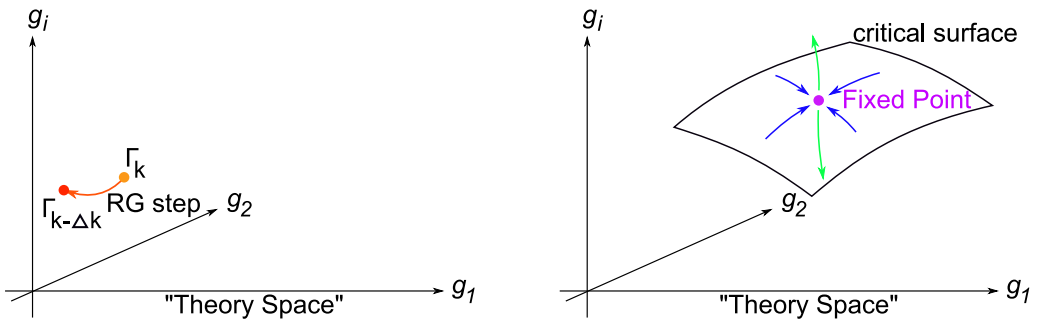

Figure 2.1: Sketch of a 3-dimensional subspace of theory space.

Fig. 2.1 a sketch of the renormalization group flow in a subspace of three operators with associated couplings g_1, g_2 and g_i is shown. The position of the effective average action $\Gamma_k[\Phi]$ in theory space is given by a set of coordinates of running couplings $\{g_{i,k}\}$. As we lower the scale from k to $k - \Delta k$ by an RG step, the transformation of the running couplings and so the change of position in theory space is described by the β functions and we end up at a different effective field theory $\Gamma_{k-\Delta k}[\Phi]$ at the new scale.

Renormalization group fixed point

A fixed-point is a point $g^* = \{g_i^*\}$ in theory space where the running of all dimensionless coupling constants vanishes and so the β functions vanish

$$\beta_{i,k}(g_1^*, g_2^*, ...) = 0 \quad \forall\, i\,. \tag{2.31}$$

A fixed point is called *non-Gaußian*, if at least one fixed-point coupling is nonzero $g_j^* \neq 0$.

Example: $O(N)$ model in 3d (β functions, fixed points)

For the scalar $O(N)$-model we display the β functions computed by means of the Wetterich equation for an effective potential u_k expanded in terms of a running non-vanishing minimum κ_k and a four-boson interaction $\lambda_{2,k}$:

$$u_k = \frac{\lambda_{2,k}}{2}(\tilde{\rho} - \kappa_k)^2\,. \tag{2.32}$$

This ansatz yields flow equations for κ_k and $\lambda_{2,k}$

$$\beta_\kappa = \partial_t \kappa_k = -(1+\eta_\phi)\kappa_k + \frac{\left(1-\frac{\eta_\phi}{5}\right)}{6\pi^2}\left((N-1) + \frac{3}{(1+2\kappa_k\lambda_{2,k})^2}\right) \tag{2.33}$$

$$\beta_\lambda = \partial_t \lambda_{2,k} = (-1+2\eta_\phi)\lambda_{2,k} + \frac{\left(1-\frac{\eta_\phi}{5}\right)\lambda_{2,k}^2}{\pi^2}\left((N-1) + \frac{9}{(1+2\kappa_k\lambda_{2,k})^3}\right), \tag{2.34}$$

as well as one algebraic equation for η_ϕ

$$\eta_\phi = \frac{2\kappa_k \lambda_{2,k}^2}{3\pi^2(1+2\kappa_k\lambda_{2,k})^2}\,. \tag{2.35}$$

Setting equations (2.33) and (2.34) equal to zero and using equation (2.35) yields fixed-points solutions $\{\kappa^*, \lambda_2^*\}$, e.g. for $N = 3$ we obtain $\{\kappa^*, \lambda_2^*\}$=$\{0.0490,6.711\}$.

2.3.3 Critical behaviour near a fixed point

The stability or instability of small deviations from a fixed point determine the topology of the flow in the space of coupling constants. In the vicinity of a fixed point $g^* = \{g_i^*\}$ we can study the behaviour of the renormalization group trajectories using the linearized flow equations

$$\partial_t g_i = B_i{}^j (g_j - g_j^*) + \mathcal{O}\big((g-g^*)^2\big)\,, \text{where} \quad B_i{}^j = \frac{\partial \beta_i}{\partial g_j}\Big|_{g^*}\,, \tag{2.36}$$

is the stability matrix. We diagonalize the stability matrix $B_i{}^j$,

$$B_i{}^j\, V_j^I = -\Theta^I V_i^I, \tag{2.37}$$

in terms of right-eigenvectors V_i^I enumerated by the index I which labels the order of the RG eigenvalues Θ^I according to their real part, starting with the largest one, Θ_1. The RG eigenvalues allow for a classification of physical parameters by analyzing the solution of the coupling flow in the fixed-point regime which is given by

$$g_i = g_i^* + \sum_I C^I\, V_i^I \left(\frac{k_0}{k}\right)^{\Theta^I}\,. \tag{2.38}$$

Here the integration constants C^I =const. define the initial conditions at a reference scale k_0. Eigendirections with $\mathrm{Re}\{\Theta^I\} > 0$ are called *relevant* directions and drive the system away from the fixed point as we evolve the flow towards the infrared. Those infrared unstable directions determine the macroscopic physics. Eigendirections with $\mathrm{Re}\{\Theta^I\} < 0$ die out and flow into the fixed point towards the infrared. They are thus called the *irrelevant* (infrared stable) directions. For the marginal directions $\mathrm{Re}\{\Theta^I\} = 0$, it depends on the higher-order terms in the expansion about the fixed point. The number of relevant and marginally-relevant directions determines the number of physical parameters to be fixed. For the flow away from the fixed point, the linearized fixed-point flow Eq. (2.38) generally is insufficient and the full nonlinear β functions have to be taken into account.

2.4 Critical behaviour of phase transitions

In statistical physics, one finds that completely different thermodynamic systems show the same quantitative behavior near a critical point, e.g. a phase transition. As an example consider a gas-fluid system or a ferromagnet at the critical point. Looking through a microscope we will see droplets (or domains) of various sizes. We will find droplets in bubbles and bubbles in droplets as a manifestation of strong fluctuations. A change of magnification and contrast of the microscope, which basically consitutes a change of the observation scale, yields the same overall picture for the system and we say the system is *scale invariant* at criticality. In the vicinity of these critical points long-range fluctuations of the field are important and the behavior of the theory is independent of its microscopic details. There it can be described by a set of scaling relations and pure numbers, the *critical exponents*. This phenomenon is called *universality*. Typical scaling relations can be studied with the two-point correlation function $G(x,0)$ (see Eq. (2.7)) between fluctuations at the origin and at spacetime point x, e.g. for an $O(1)$ model. Near a critical point we expect $G(x,0)$ to decay exponentially

$$G(x,0) \sim e^{-|x|/\xi}, \tag{2.39}$$

where ξ is the correlation length. The critical point is reached by tuning the temperature T to the critical temperature T_c, which results in an increase to infinity for the correlation length according to the scaling law

$$\xi \sim \left(\frac{T-T_c}{T_c}\right)^{-\nu}, \tag{2.40}$$

where we defined the critical exponent ν. At the critical temperature the correlation function decays as a power law

$$G(x,0) \sim |x|^{2-d-\eta}, \tag{2.41}$$

with the critical exponent η and d denotes the number of euclidean spacetime dimensions. Such scaling laws cannot be deduced from any fixed order perturbation theory calculation, since there are inherently nonperturbative phenomena underlying these laws. The idea to postulate such relations goes back to Ben Widom [86] and can be proved through a general RG analysis [4, 5].

For ultracold fermion gases near a so-called Feshbach resonance we can even observe an *enhanced* universality, where the complete phase diagram is determined in terms of only two parameters. We will come to this issue in Chap. 6.

RG perspective

At a critical point of a second order phase transition one expects a scaling behaviour of the dimensionless rescaled effective potential $u_k(\tilde{\rho})$. An RG trajectory starting at some arbitrary $u_\Lambda(\tilde{\rho})$ at a microscopic scale Λ can have an evolution that flows towards the k-independent scaling solution and stays close to it over a very large range of scales k. At the end of the RG running ($k \to 0$), for a system close to the phase transition, deviations from the scaling solution occur and the system ends up either in the symmetric phase characterized by a vanishing order parameter or in the phase of spontaneously broken symmetry. Such a "near-critical" trajectory becomes insensitive to the details of the microscopic theory which determines the initial conditions for the RG evolution. The trajectory can be tuned to be close to criticality by the relevant parameters in $u_k(\tilde{\rho})$ and then the infrared shape of $u_k(\tilde{\rho})$ becomes independent of the choice of irrelevant parameters in $u_\Lambda(\tilde{\rho})$, implying the universal behaviour. Examples for relevant parameters are temperature and external magnetic field in an uniaxial ferromagnet or pressure and temperature for a normal fluid.

Naturally, scale-invariance of a system is found at a renormalization group fixed point. The critical exponents characterizing the critical point are connected to the RG eigenvalues Θ^I of the fixed-point. They define the *universality class* of a system. The largest (positive) RG eigenvalue Θ_1 is associated with the strongest RG relevant direction. The parameter corresponding to a relevant direction can be used to tune the system to or away from criticality and so it is related to the distance of the temperature from the critical temperature, cf. Eq. (2.40). Thereby a relation between Θ_1 and the critical exponent ν can be established, reading $\nu = 1/\Theta_1$. Similarly, we can identify the critical exponent η with the fixed-point value of the anomalous dimension $\eta = \eta^*_\phi$. Further, the first subleading exponent is traditionally called $\omega = -\Theta_2$.

Example: $O(N)$-model in 3d (RG eigenvalues, critical exponents)

From the fixed-points present in the $O(N)$-models we can extract the RG eigenvalues Θ_I and compute the critical exponents. In Tab. 2.1 we list the critical exponents ν and η for $N \in \{0, 1, 2, 3, 4, 10\}$ obtained using the next-to-leading order derivative expansion with a polynomial expansion for the effective potential up to 12th order in field monomials. A simple mathematica-notebook [87] computing the leading critical exponents for arbitrary N in this approximation using the Wetterich equation can be found here:

`http://www.tpi.uni-jena.de/qfphysics/homepage/scherer/3dONmodel.nb` .

We compare our results to high accuracy computations by J. Zinn-Justin *et al.* using resummed perturbation expansions [88], see Tab. 2.1. Given the simplicity of our approximation our results show a very reasonable agreement. A more detailed analysis of the

	Application in $d = 3$	ν	ν_{ZJ}[88]	η	η_{ZJ}[88]
N=0	Polymer chains	0.59	0.5882(11)	0.040	0.0284(25)
N=1	Liquid-vapor transition	0.64	0.6304(13)	0.044	0.0335(25)
N=2	Helium superfluid transition	0.68	0.6703(15)	0.044	0.0354(25)
N=3	Ferromagnetic phase transtion	0.73	0.7073(35)	0.041	0.0355(25)
N=4		0.77	0.741(6)	0.037	0.035(4)
N=10		0.89	0.859	0.021	0.024

Table 2.1: Critical exponents for $O(N)$-models in three dimensions.

convergence and stability of functional RG methods for three-dimensional $O(N)$-models can be found in [89].

2.5 Asymptotic safety

In an asymptotically safe quantum field theory the microscopic action entering the functional integral approaches an (interacting) fixed point for the limit of an infinite ultraviolet cutoff. This renders the theory well-defined in the limit of arbitrarily high energies and therefore can promote an effective quantum field theory to a candidate for a fundamental theory [18, 22, 85].

Suppose there is a (possibly non-Gaußian) ultraviolet fixed point Γ^* in the theory space of action functionals, coordinatized by the subset of essential couplings (see r.h.s. of figure 2.1). The essential couplings are those couplings that cannot be absorbed by field reparametrizations. If we can find an RG trajectory which connects Γ^* with a meaningful physical theory represented by an effective average action Γ_{IR} at some infrared scale, then we have found a quantum field theory, which can be extended to arbitrarily high scales, since for the cutoff scale $\Lambda \to \infty$ we just run into the fixed point and the theory is *asymptotically safe*, i.e. free from pathological divergencies, see left panel of Fig. 2.2, left panel.

2.5.1 Critical behaviour of asymptotic safety

In section 2.3.3 we already discussed the critical behaviour in the vicinity of a fixed point, however, with a perspective where we evolve the RG scale k towards the infrared. For the concept of asymptotic safety, where the fixed-point is supposed to govern the theory in the ultraviolet we invert the discussion. For convenience we display again equation (2.38) for the linearized flow in the fixed-point regime

$$g_i = g_i^* + \sum_I C^I V_i^I \left(\frac{k_0}{k}\right)^{\Theta^I} .$$

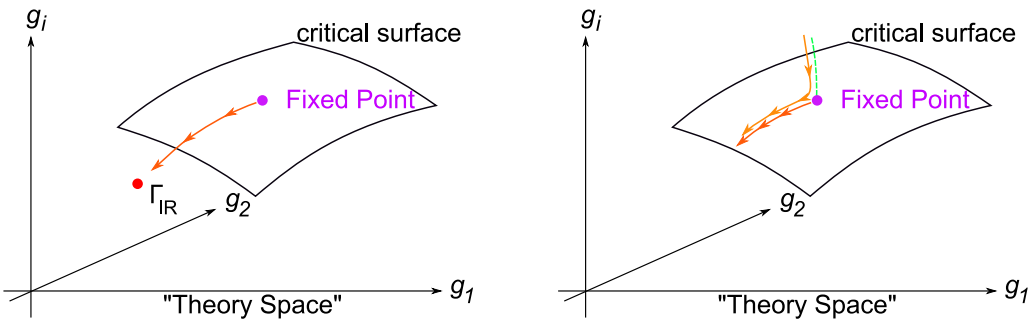

Figure 2.2: Asymptotic safety in theory space.

For the flow towards the ultraviolet, the relevant directions ($\mathrm{Re}\{\Theta_I\} > 0$) are attracted towards the fixed point. We define the *critical hypersurface* S as the set of all points in theory space that run towards the fixed point as $k \to \infty$, i.e. the points lying on RG relevant trajectories. The tangential space of S is spanned by the relevant RG eigenvectors V_i^I, see (2.37) and the number of linearly independent relevant directions at the fixed point corresponds to the dimension of S. As before these directions determine the infrared physics and the number of physical parameters to be fixed. Therefore the theory is predictive if $\dim(S)$ is finite. The directions with $\mathrm{Re}\{\Theta_I\} < 0$ run away from the fixed point as we increase k, see left panel of Fig. 2.2. Contrary, as we decrease k, the irrelevant directions rapidly approach the critical surface, as displayed in Fig. 2.2, right panel. Therefore, the observables in the IR are all dominated by the properties of the fixed point, independently of whether the flow has started exactly on or near the critical surface. This establishes the predictive power of the asymptotic safety scenario.

An RG eigenvalue Θ_I much larger than zero, say of $\mathcal{O}(1)$, implies that the RG trajectory rapidly leaves the fixed-point regime towards the IR. Therefore, separating a typical UV scale where the system is close to the fixed point from the IR scales where, e.g., physical masses are generated requires a significant fine-tuning of the initial conditions. In the context of the standard model, the size of the largest Θ^I is a quantitative measure of the hierarchy problem.

2.5.2 A simple example

Suppose an action functional of a theory can be sensibly parametrized by only two field operators with the corresponding couplings $\{g_{1,k}, g_{2,k}\}$. Further, suppose that this action functional has a (non-Gaußian) RG fixed-point $\{g_1^*, g_2^*\}$ with one relevant direction ($\Theta_1 > 0$) and one irrelevant direction ($\Theta_2 < 0$). According to (2.38) the equations for the linearized flow read

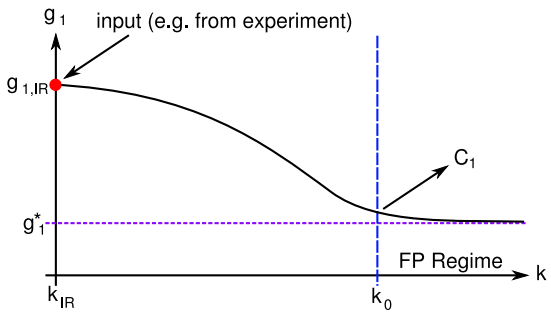

Figure 2.3: Predictivity in the asymptotic safety scenario.

$$g_{1,k} = g_1^* + C_1 V_1^1 \Big(\frac{k_0}{k}\Big)^{\Theta_1} + C_2 V_1^2 \Big(\frac{k_0}{k}\Big)^{\Theta_2} \tag{2.42}$$

$$g_{2,k} = g_2^* + C_1 V_2^1 \Big(\frac{k_0}{k}\Big)^{\Theta_1} + C_2 V_2^2 \Big(\frac{k_0}{k}\Big)^{\Theta_2} . \tag{2.43}$$

When we are close to the fixed point and increase the scale k, i.e. we run towards the ultraviolet, the relevant term containing the critical exponent Θ_1 vanishes. However, the irrelevant term grows large as $\Theta_2 < 0$. In order to make sure, we run into the fixed point for $k \to \infty$ we set $C_2 = 0$ and the linearized flow equations become even simpler

$$g_{1,k} = g_1^* + C_1 V_1^1 \Big(\frac{k_0}{k}\Big)^{\Theta_1} , \; g_{2,k} = g_2^* + C_1 V_2^1 \Big(\frac{k_0}{k}\Big)^{\Theta_1} . \tag{2.44}$$

We observe that there is only the parameter C_1 left to fix. This is where we have to get some input, e.g. from an experiment that gives us an infrared value, e.g. for the coupling $g_{1,\mathrm{IR}}$. We now have to pick the RG trajectory of the full flow that connects the UV fixed point regime with $g_{1,\mathrm{IR}}$. As the RG trajectories do not intersect, this choice is unique. From this procedure we can find C_1 at some chosen reference scale (see Fig. 2.3). The flow is now completely fixed (from the input $g_{1,\mathrm{IR}}$) and we can evolve it from the UV to the IR which provides us with a prediction for $g_{2,\mathrm{IR}}$. This visualizes the predictive power of the asymptotic saftey scenario.

2.5.3 Candidates for asymptotically safe systems

A paradigm example for an asymptotically safe theory are four-fermion models such as the Gross-Neveu model in $2 < d < 4$ dimensions [90–92]. Even though these models are perturbatively not renormalizable and thus seemingly trivial, they are nonperturbatively renormalizable at a non-Gaußian fixed point and hence can be extended to arbitrarily high scales.

Further, the scenario has been applied to a number of models ranging from various other four-fermion models [93, 94] and nonlinear sigma models in $d > 2$ [95] to extra-dimensional gauge theories [96]. However, it is especially in the context of gravity that

the idea of asymtpotic safety has gained considerable attention during the last 10 years. In fact, there is a lot of evidence that such an interacting fixed point exists for diffeomorphism invariant actions, allowing for a formulation of a non-perturbative renormalizable quantum field theory of gravity [20, 24–49]. A contribution to this evidence is given in Chap. 7

In the subsequent chapter we will pave the way for an asymptotically safe setting for the standard model by investigating various Yukawa systems as toy models. Our approach does not introduce new degrees of freedom or further symmmetries and thus no new parameters. Indeed, asymptotic safety can lead to a reduction of parameters and have high predictive power. Comprehensive reviews on asymptotic safety can be found in [21–23].

2.5.4 Asymptotic safety mechanisms in Yukawa Systems

The standard model of particle physics is a very successful theory that is in agreement with numerous high-precision experiments. One crucial building block is the Higgs sector which renders the perturbative expansion of correlation functions well defined and parameterizes the masses of matter fields and weak gauge bosons. So far, the Higgs sector has only been indirectly tested by the precision data of particle collider experiments. In the next years it will be directly explored at the LHC. Beyond this success, two problems of the standard model persist: the triviality problem and the hierarchy problem. At first sight the Landau poles of perturbation theory in the QED and the Higgs sector suggest that one should introduce new degrees of freedom or a new concept. However, in the perturbative setting of the standard model, the only fixed point is the Gaußian fixed point, which is not connected to a physically sensible (non-trivial) effective action in the IR. It is in this context that an asymptotically safe scenario is very appealing. A non-perturbative computation of the Higgs sector including fermions and also gauge fields can reveal whether the problem of triviality still persists or whether the theory can be asymptotically safe in Weinberg's sence, i.e. by acquiring a fixed point in the ultraviolet. As a step towards such a scenario we investigate the fixed-point structure of various Yukawa systems representing toy models for the standard model.

Triviality in the standard model

The triviality problem is a severe problem inhibiting an extension of the standard model to arbitrarily high momentum scales. The scale of maximum ultra-violet (UV) extension $\Lambda_{\mathrm{UV,max}}$ induced by triviality is related to the Landau pole of perturbation theory. Triviality problems occur in both the Higgs sector [7, 79, 81–84] as well as the U(1) gauge sector [2, 76–78]. However, since $\Lambda_{\mathrm{UV,\,max}}$ of the Higgs sector is much smaller than that of the U(1) sector [78], evading triviality in the Higgs sector is of primary importance. In fact for heavy Higgs boson masses, the scale of maximum UV extension $\Lambda_{\mathrm{UV,max}}$ could be

much smaller than the Planck or GUT scale [97–102]. For supersymmetrically extended models, $\Lambda_{\mathrm{UV,max}}$ can be even smaller than in the standard model [103].

Traces of the triviality problem can already be found in perturbation theory. The relation between bare and renormalized four-Higgs-boson coupling $\lambda\phi^4$ in one-loop RG-improved perturbation theory is given by

$$\frac{1}{\lambda_{\mathrm{R}}} - \frac{1}{\lambda_\Lambda} = \beta_0 \,\mathrm{Log}\left(\frac{\Lambda}{m_{\mathrm{R}}}\right), \;\; \beta_0 = \text{const.} > 0, \tag{2.45}$$

where λ_Λ is the bare and λ_{R} the renormalized coupling; Λ is the UV cutoff scale and m_{R} denotes a renormalized mass scale. The first β function coefficient β_0 is generically positive for ϕ^4 theories. Keeping λ_{R} and m_{R} fixed, say as measured in an experiment at an infrared (IR) scale, an increase of the UV cutoff Λ has to be compensated by an increase of the bare coupling λ_Λ. But λ_Λ eventually hits infinity at a finite UV scale $\Lambda_{\mathrm{L}} = m_{\mathrm{R}} \exp[1/(\beta_0\lambda_{\mathrm{R}})]$. This Landau pole provides for a first estimate of the scale of maximum UV extension $\Lambda_{\mathrm{L}} \simeq \Lambda_{\mathrm{UV,max}}$.

Of course, perturbation theory is useless for a reliable estimate of $\Lambda_{\mathrm{UV,max}}$, since it is an expansion about zero coupling. Near the Landau pole, nonperturbative physics can set in and severely modify the picture. In fact, the QED Landau pole has been shown to be outside the physical parameter space, since it is screened by the nonperturbative phenomenon of chiral symmetry breaking [77, 78]. (Still, there remains a finite scale of maximum UV extension $\Lambda_{\mathrm{UV,max}} < \infty$.) A study of the triviality problem therefore mandatorily requires a nonperturbative tool.

The hierarchy problem

The hierarchy problem is not a fundamental problem in the sense of rendering the standard model ill-defined instead it is a fine-tuning problem of initial conditions and arises also from the properties of the Higgs sector. For generic values of the initial squared bare Higgs mass scale $m_\Lambda^2 \sim \Lambda^2$ at UV cutoff Λ, the system is either in the symmetric phase exhibiting no electroweak symmetry breaking or it is in the broken phase with gauge-boson, Higgs-boson and fermion masses of order Λ. Both phases are separated by a quantum phase transition at a critical value $m^2_{\Lambda,\mathrm{cr}}$. A large hierarchy, i.e., a large separation of particle masses from the cutoff scale, requires an extremely fine-tuned value of m_Λ^2 close to the critical value. For instance, separating the scale of electroweak symmetry breaking Λ_{EW} from the UV scale, e.g., given by a GUT scale Λ_{GUT}, requires to fine-tune m_Λ^2 to $m_{\Lambda,\mathrm{cr}}$ within a precision of $\Lambda^2_{\mathrm{EW}}/\Lambda^2_{\mathrm{GUT}} \sim 10^{-28}$.

This problem of "unnatural" initial conditions stems from the fact that the mass parameter in the Higgs sector renormalizes quadratically $\sim \Lambda^2$. In a renormalization group (RG) language, the critical value $m^2_{\Lambda,\mathrm{cr}}$ denotes a strongly IR repulsive fixed point

with critical exponent $\Theta = 2$. Again, these statements hold in the vicinity of the Gaußian fixed point, where all couplings are small and perturbation theory can be applied. We stress that there is nothing conceptually wrong with fine-tuned initial conditions but it is generally considered as unsatisfactory. A solution of the hierarchy problem should either explain the fine-tuned initial conditions within an underlying theory or correspond to a UV extension of the standard model which has no critical exponents significantly larger than zero, implying a slow, say logarithmic, running of the parameters.

Asymptotic Safety of Yukawa Systems

Yukawa models can be used as simple toy models mimicking some important features of the Higgs sector of the standard model. A non-perturbative computation of the RG flow and an analysis of its fixed points gives insight to the question if the theory might be asymptotically safe. Such a fixed-point can be induced by a balancing of the fermionic and the bosonic fluctuations of in Yukawa models.

Conformal vacuum expectation value

The RG flow of a four-dimensional Yukawa model can be in the symmetric (SYM) regime or in the regime of spontaneous symmetry breaking (SSB) where the bosonic field expectation value v is nonzero, $v > 0$. Whereas we do not find interacting fixed points in the SYM regime, the structure of the flow becomes richer in the SSB regime, since new interactions can be mediated by the condensate. Our central idea is that the contributions with opposite sign from bosonic and fermionic fluctuations to the vacuum expectation value (vev) can be balanced such that the vev exhibits a conformal behavior, $v \equiv \langle\varphi\rangle \sim k$. The dimensionless squared vev $\kappa = \frac{1}{2}v^2/k^2$ has a flow equation of the form

$$\partial_t \kappa \equiv \partial_t \frac{v^2}{2k^2} = -2\kappa + \text{interaction terms}. \tag{2.46}$$

If the interaction terms are absent, the Gaußian fixed point $\kappa = 0$ is the only conformal point, corresponding to a free massless theory. If the interaction terms are nonzero, e.g., if the couplings approach interacting fixed points by themselves, the sign of these terms decides about a possible conformal behavior. A positive contribution from the interaction terms gives rise to a fixed point at $\kappa > 0$ which can control the conformal running over many scales. If they are negative, no conformal vev is possible. Since fermions and bosons contribute with opposite signs to the interaction terms, the existence of a fixed point $\kappa_* > 0$ crucially depends on the relative strength between bosonic and fermionic fluctuations. Roughly speaking, the bosons have to win out over the fermions.

In Fig. 2.4, we sketch various options for the flow of the dimensionless squared vev κ. The solid line depicts the free massless theory with a trivial Gaußian fixed point at

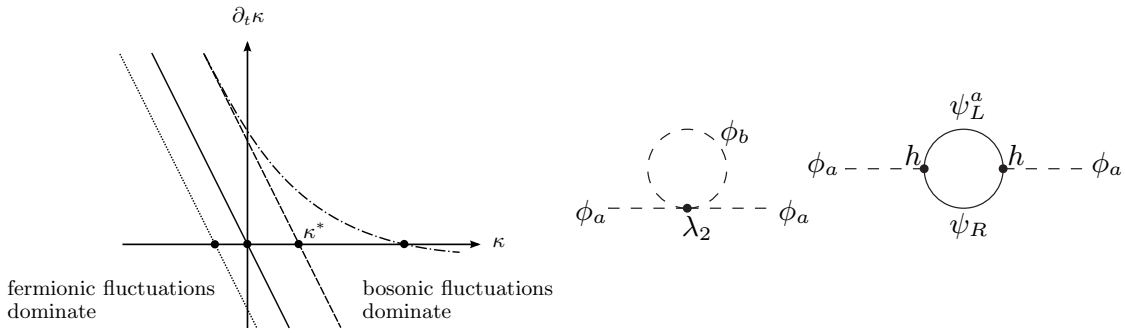

Figure 2.4: Left panel: β-function of the dimensionless squared Higgs vacuum expectation value κ. Right panel: Loop contributions to the renormalization flow of the vev.

$\kappa = 0$. If the fermions dominate, the interaction terms are negative and the fixed point is shifted to negative values (being irrelevant for physics), cf. dotted line. If the bosonic fluctuations dominate, the κ flow develops a non-Gaußian fixed point at positive values $\kappa^* > 0$ that can support a conformal behavior over many orders of magnitude, cf. dashed line. This fixed point is UV attractive, implying that the vev is a relevant operator near the fixed point. If the interaction terms are approximately κ independent, the slope of $\partial_t\kappa$ near the fixed point is still close to -2, corresponding to a critical exponent $\Theta \simeq 2$ and a persistent hierarchy problem. An improvement of "naturalness" could arise from a suitable κ dependence of the interaction terms that results in a flattening of the κ flow near the fixed point, cf. dot-dashed line. Whether or not this happens is not an input but a result of and can be computed within the theory.

The simplest system we investigate is a Z_2-invariant Yukawa system with an number N_f of Dirac fermions and a single component real scalar field, see Chap. 3. Here, we find fermionic dominance for one or more fermion flavors, excluding an asymptotic safety scenario of this kind. In fact, a careful analysis of the model in the SYM regime as well as the SSB regime reveals that no non-Gaußian fixed point exists in the accessible parameter range neither for strong coupling nor induced by balanced threshold behavior. Nevertheless, this fermion dominance is not an unavoidable property of the system, but a result of the algebraic details of the model. This is illustrated by treating the flavor number N_f as a continuous variable. We observe boson dominance for $N_\mathrm{f} \lesssim 0.3$, implying the existence of a suitable non-Gaußian fixed point and a non-trivial interacting fundamental theory valid on all scales. We also find a dependence of the largest critical exponent on the flavor number, supporting also reductions from the value $\Theta = 2$. However, a significant hierarchy always remains in the simple models considered here.

Two features render our mechanism particularly attractive: first, the UV fixed-point properties are such that the system has one parameter less than expected; in other words, once the top mass and the vev are fixed, the Higgs mass is a true prediction of the theory. Second, the set of all possible flows that start from the UV fixed point lead to a constrained set of physical low-energy values; most importantly, the top mass does

generically not become much lighter than the vev, offering a natural explanation for the large mass of the top.

In a second step, we construct a model with standard-model-like symmetries along these lines of research, see Chap. 4. We introduce N_L left-handed fermion species ψ_L^a ($a \in \{1, ..., N_\mathrm{L}\}$) and one right-handed fermion ψ_R, as well as N_L complex bosons ϕ^a. All fields live in the fundamental representation of the left-handed chiral symmetry group $\mathrm{U}(N_\mathrm{L})_\mathrm{L}$. The Yukawa coupling is then realized by a term $\bar{h}(\bar{\psi}_\mathrm{R}\phi^{a\dagger}\psi_\mathrm{L}^a - \bar{\psi}_\mathrm{L}^a\phi^a\psi_\mathrm{R})$.

In comparison to left-right symmetric models, this model has an interesting new feature concerning the relative weight of the boson interaction terms contributing to the renormalization of the dimensionless vev κ (see right panel of figure 2.4): diagrammatically speaking, the inner structure of fermion components in the fermion loop for a specific choice of external boson legs is fully determined. On the other hand, the boson loop obtains contributions from all N_L components and so is linear in N_L. In this way, N_L serves as a control parameter for boson dominance and for the potential existence of a non-Gaußian fixed point. Already at this qualitative level of the discussion, it is worthwhile to stress that the standard model has such a left-right asymmetric structure which can support the conformal-vev fixed point.

In a last step we also include gauge fields in our left-right asymmetric models, to overcome some problems discovered with the model without the gauge bosons, see Sec. 4.5.2.

Chapter 3

Fixed-point structure of Z_2-invariant Yukawa systems

In this chapter, we study a possible asymptotic safety scenario for a four-dimensional Z_2-invariant Yukawa theory. The model involves one real scalar field ϕ and N_f Dirac fermions ψ. It mimics the Higgs sector of the standard model in the sense that spontaneous symmetry breaking (SSB) in the scalar sector generates fermion masses. As a further important feature no Goldstone bosons are generated due to the discreteness of the symmetry. We investigate the fixed-point structure of the RG flow of this model to see if it allows for asymptotic safety which would allow to understand the scalar field ϕ and the fermion field ψ as fundamental quantum fields.

In the spirit of perturbative power-counting near the Gaußian fixed point, the microscopic action subject to perturbative quantization would read

$$S = \int d^4x \left(\frac{1}{2}(\partial_\mu \phi)^2 + \frac{\bar{m}^2}{2}\phi^2 + \frac{\bar{\lambda}}{8}\phi^4 + \bar{\psi}\mathrm{i}\partial\!\!\!/\psi + \mathrm{i}\bar{h}\phi\bar{\psi}\psi \right), \tag{3.1}$$

where the bare parameter space would be spanned by the boson mass $\bar{m}$, the boson interaction $\bar{\lambda}$ and the Yukawa coupling $\bar{h}$. Here, however, we allow for more general actions also near interacting fixed points and only impose the discrete chiral symmetry,

$$\psi \to \mathrm{e}^{\mathrm{i}\frac{\pi}{2}\gamma_5}\psi, \quad \bar{\psi} \to \bar{\psi}\mathrm{e}^{\mathrm{i}\frac{\pi}{2}\gamma_5}, \quad \phi \to -\phi\,. \tag{3.2}$$

We restrict the truncation for the flowing action to bilinears in the fermions and expand the bosonic part in powers of field derivatives, yielding at next-to-leading order

$$\Gamma_k = \int d^4x \left(\frac{Z_{\phi,k}}{2}(\partial_\mu \phi)^2 + U_k(\rho) + Z_{\psi,k}\bar{\psi}\mathrm{i}\partial\!\!\!/\psi + \mathrm{i}\bar{h}_k\phi\bar{\psi}\psi \right), \tag{3.3}$$

where $\rho = \frac{1}{2}\phi^2$. We also confine ourselves to a Yukawa term linear in ϕ. In many cases, it suffices qualitatively to expand the effective potential in powers of ρ, see below. Keeping the wave function renormalizations $Z_{\phi,k}, Z_{\psi,k}$ fixed defines the leading-order derivative expansion. At next-to-leading order, the flows of the wave function renormalizations are described in terms of anomalous dimensions $\eta_\phi = -\partial_t \ln Z_{\phi,k},\ \eta_\psi = -\partial_t \ln Z_{\psi,k}$. In order to fix the standard RG invariance of field rescalings, we define the renormalized fields as $\tilde{\phi} = Z_{\phi,k}^{1/2}\phi,\ \tilde{\psi} = Z_{\psi,k}^{1/2}\psi$ and introduce the dimensionless renormalized quantities

$$\tilde{\rho} = Z_{\phi,k} k^{-2}\rho, \quad h_k^2 = Z_{\phi,k}^{-1} Z_{\psi,k}^{-2} \bar{h}_k^2, \quad u_k(\tilde{\rho}) = k^{-4} U_k(\rho)|_{\rho = k^2\tilde{\rho}/Z_{\phi,k}}\,, \tag{3.4}$$

including the dimensionless renormalized Yukawa coupling and the dimensionless potential. The flow equation for the effective potential for an arbitrary number of dimensions d has been derived in [66, 104]. For our purposes, we specialize to $d = 4$ and use an optimized regulator function R_k (see App. B), yielding

$$\partial_t u_k(\tilde{\rho}) = -4u_k + (2+\eta_\phi)\tilde{\rho}u_k' + \frac{1}{32\pi^2}\Big[\underbrace{\frac{(1-\frac{\eta_\phi}{6})}{1+u_k'+2\tilde{\rho}u_k''}}_{\text{regularized scalar loop}} - \underbrace{N_{\rm f}\frac{4(1-\frac{\eta_\psi}{5})}{1+2\tilde{\rho}h_k^2}}_{\text{regularized fermion loop}} \Big], \tag{3.5}$$

The effective potential encodes information about the symmetry status of the system. The vacuum expectation value of the quantum field corresponds to the minimum $\phi_{\rm min}$ of the effective potential which satisfies the field equation $\frac{\partial U_k}{\partial \phi}|_{\phi_{\rm min}} = 0$. In the symmetric regime (SYM), we have $\phi_{\rm min} = 0$ such that the dimensionless effective potential can be expanded around zero field,

$$u_k \;=\; \sum_{n=1}^{N_p} u_{n,k}\tilde{\rho}^n = m_k^2\tilde{\rho} + \frac{\lambda_{2,k}}{2!}\tilde{\rho}^2 + \frac{\lambda_{3,k}}{3!}\tilde{\rho}^3 + \dots\,, \tag{3.6}$$

where $m_k^2, \lambda_{2,k}, \lambda_{3,k}, \dots$ are dimensionless mass and coupling parameters, respectively.

In the SSB regime, where the minimum of the effective potential u_k acquires a nonzero value $\phi_{\rm min} \neq 0$, we expand the effective potential about $\kappa_k := \tilde{\rho}_{\rm min} = Z_{\phi,k}\phi_{\rm min}^2/(2k^2) > 0$,

$$u_k = \sum_{n=2}^{N_p} u_{n,k}(\tilde{\rho}-\kappa_k)^n = \frac{\lambda_{2,k}}{2!}(\tilde{\rho}-\kappa_k)^2 + \frac{\lambda_{3,k}}{3!}(\tilde{\rho}-\kappa_k)^3 + \dots. \tag{3.7}$$

Given the flow of u_k (3.5), the flows of m_k^2 or $\lambda_{n,k}$ in both phases can be read off from an expansion of the flow equation and a comparison of coefficients. For the flow of κ_k, we use the fact that the first derivative of u_k vanishes at the minimum, $u_k'(\kappa_k) = 0$,

$$0 = \partial_t u_k'(\kappa_k) = \partial_t u_k'(\tilde{\rho})|_{\tilde{\rho}=\kappa_k} + (\partial_t\kappa_k)u_k''(\kappa_k) \quad \Rightarrow \quad \partial_t\kappa_k = -\frac{1}{u_k''(\kappa_k)}\partial_t u_k'(\tilde{\rho})|_{\tilde{\rho}=\kappa_k}\,. \tag{3.8}$$

The flow equations for the running parameters are given explicitly in the following sections for SYM and SSB separately. For convenience, we suppress the index k from now on.

Parameter constraints

As our truncation is based on a derivative expansion, satisfactory convergence is expected if the higher derivative operators take little influence on the flow of the leading-order terms. In the present case, the leading-order effective potential and Yukawa coupling receive higher-order contributions only through the anomalous dimensions. Therefore, convergence of the derivative expansion requires

$$\eta_{\psi,\phi} \lesssim O(1). \tag{3.9}$$

Here and in later chapters, this condition will serve as an important quality criterion for our truncation.

The SYM regime is characterized by a minimum of u_k at vanishing field. A simple consequence is that the mass term needs to be positive, $m^2 > 0$. Also, the potential should be bounded from below, which in the polynomial expansion translates into a positive highest nonvanishing coefficient $\lambda_{N_p} > 0$. In the SSB regime, the minimum must be positive, $\kappa > 0$, the potential should be bounded, and in addition the potential at the minimum must have positive curvature $\lambda_2 > 0$. Finally, Osterwalder-Schrader positivity requires $h^2 > 0$ and we obtain the set of constraints

$$h^2,\, m^2,\, \kappa,\, \lambda_2,\, \lambda_{N_p} > 0. \tag{3.10}$$

The symmetric regime

In addition to the flow of the effective potential (3.5) we have flow equations for h^2 and the anomalous dimensions in the SYM regime which read [66, 104]:

$$\partial_t h^2 = (\eta_\phi + 2\eta_\psi)h^2 + \frac{h^4}{8\pi^2}\Big[\frac{(1-\frac{\eta_\psi}{5})}{(1+m^2)} + \frac{(1-\frac{\eta_\phi}{6})}{(1+m^2)^2}\Big], \tag{3.11}$$

$$\eta_\phi = N_{\rm f}\frac{h^2}{16\pi^2}(4-\eta_\psi), \quad \eta_\psi = \frac{h^2}{16\pi^2}\frac{(1-\frac{\eta_\phi}{5})}{(1+m^2)^2}. \tag{3.12}$$

There is no acceptable fixed point in the symmetric regime. This can be traced back to the properties of the Yukawa coupling flow: Eq. (3.12) together with the parameter constraint on the anomalous dimensions Eq. (3.9) imply that the anomalous dimensions should be positive as h^2 is positive and small $\eta_{\phi,\psi}$ cannot cause a negative sign in Eq. (3.12). As a result all the contributions in the equation for the Yukawa coupling, Eq. (3.11), are positive, which is confirmed by a detailed analysis given in [56]. However, for

a fixed point to exist it requires a negative contribution on the right-hand side of Eq. (3.11). So, the simple Yukawa system in SYM shows no sign of asymptotic safety.

3.1 Regime of spontaneous symmetry breaking

In the SSB regime further effective interactions arise owing to possible couplings to the condensate giving rise to negative contributions in the Yukawa flow. On the other hand, the flow in the SSB regime generically has the tendency to induce decoupling of massive modes and thus an unwanted freeze-out of the flow. This problem is automatically avoided if the expectation value of the field exhibits a conformal behavior. Therefore, we analyze the SSB flow in the following with an emphasis on the running of the expectation value. From the effective potential (3.5), together with Eq. (3.8), the flow of the dimensionless expectation value κ occurring in the expansion (3.7) can be derived:

$$\partial_t\kappa = -(2+\eta_\phi)\kappa + \underbrace{\frac{(3\lambda_2+2\kappa\lambda_3)}{32\pi^2}\frac{(1-\frac{\eta_\phi}{6})}{\lambda_2(1+2\kappa\lambda_2)^2}}_{\text{bosonic fluctuations}} - \underbrace{N_{\rm f}\frac{h^2}{4\pi^2}\frac{(1-\frac{\eta_\psi}{5})}{\lambda_2(1+2h^2\kappa)^2}}_{\text{fermionic fluctuations}}, \quad (3.13)$$

The scalar couplings, cf. (3.7), flow according to the equations

$$\begin{aligned}\partial_t\lambda_2 &= \lambda_3\partial_t\kappa + 2\eta_\phi\lambda_2 + (2+\eta_\phi)\kappa\lambda_3 \quad (3.14)\\ &\quad + \frac{(1-\frac{\eta_\phi}{6})}{16\pi^2(1+2\kappa\lambda_2)^2}\Big(\frac{(3\lambda_2+2\kappa\lambda_3)^2}{(1+2\kappa\lambda_2)} - \frac{5\lambda_3}{2}\Big) - N_{\rm f}\frac{(1-\frac{\eta_\psi}{5})h^4}{\pi^2(1+2\kappa h^2)^3},\\ \partial_t\lambda_3 &= (2+3\eta_\phi)\lambda_3 + \frac{15\lambda_3(3\lambda_2+2\kappa\lambda_3)(1-\frac{\eta_\phi}{6})}{16\pi^2(1+2\kappa\lambda_2)^3} \quad (3.15)\\ &\quad - \frac{3(3\lambda_2+2\kappa\lambda_3)^3}{16\pi^2}\frac{(1-\frac{\eta_\phi}{6})}{(1+2\kappa\lambda_2)^4} + N_{\rm f}\frac{6(1-\frac{\eta_\psi}{5})h^6}{\pi^2(1+2\kappa h^2)^4}.\end{aligned}$$

The full flow of the Yukawa coupling as first derived in [104] is:

$$\begin{aligned}\partial_t h^2 &= (\eta_\phi+2\eta_\psi)h^2 + \frac{h^4}{8\pi^2}\frac{1}{(1+2\kappa h^2)(1+2\kappa\lambda_2)}\left(\frac{1-\frac{\eta_\psi}{5}}{1+2\kappa h^2}+\frac{1-\frac{\eta_\phi}{6}}{1+2\kappa\lambda_2}\right) \quad (3.16)\\ &\quad - \frac{h^4(3\kappa\lambda_2+2\kappa^2\lambda_3)}{4\pi^2}\frac{\left(\frac{1-\frac{\eta_\psi}{5}}{1+2\kappa h^2}+\frac{2(1-\frac{\eta_\phi}{6})}{1+2\kappa\lambda_2}\right)}{(1+2\kappa h^2)(1+2\kappa\lambda_2)^2} - \frac{h^6\kappa}{2\pi^2}\frac{\left(\frac{2(1-\frac{\eta_\psi}{5})}{1+2\kappa h^2}+\frac{1-\frac{\eta_\phi}{6}}{1+2\kappa\lambda_2}\right)}{(1+2\kappa h^2)^2(1+2\kappa\lambda_2)}.\end{aligned}$$

Finally, the anomalous dimensions in SSB read

$$\eta_\phi = \frac{N_{\rm f}h^2}{16\pi^2}\Big(\frac{4(1-2\kappa h^2)}{(1+2\kappa h^2)^4}+\frac{2(1-\eta_\psi)}{(1+2\kappa h^2)^3}-\frac{(2-\eta_\psi)}{(1+2\kappa h^2)^2}\Big)+\frac{\kappa(3\lambda_2+2\kappa\lambda_3)^2}{16\pi^2(1+2\kappa\lambda_2)^4}, \quad (3.17)$$

$$\eta_\psi = \frac{h^2}{16\pi^2}\frac{(1-\frac{\eta_\phi}{5})}{(1+2\kappa h^2)(1+2\kappa\lambda_2)^2}. \quad (3.18)$$

Fixed-point search to leading order at $N_\mathrm{f} = 1$

Let us start with the leading-order derivative expansion, $\eta_\phi,\ \eta_\psi = 0$, confining ourselves initially to the ϕ^4 truncation with three parameters κ, h^2, λ_2 and all $\lambda_{\geq 3} = 0$ at $N_\mathrm{f} = 1$.

We first consider the two fixed-point equations $\partial_t h^2 = 0$ and $\partial_t \lambda_2 = 0$, and let the value for κ be undetermined for the moment. The resulting equations can be solved analytically, revealing a set of solutions. Only one of them fulfills the requirement $\lambda_2 > 0$ and $h^2 > 0$. This solution reads

$$h^{*2} \approx \frac{0.0616116}{\kappa}, \quad \lambda_2^* \approx \frac{0.0880079}{\kappa}. \tag{3.19}$$

Plugging these pseudo-fixed-point values into the fixed-point equation for κ, we find

$$\partial_t \kappa = -2\kappa - 0.0071873 \neq 0 \text{ for } \kappa > 0\,, \tag{3.20}$$

so there is no nontrivial fixed point at leading-order derivative expansion in the ϕ^4 truncation for $N_\mathrm{f} = 1$. This conclusion holds also for all higher flavor numbers N_f.

In order to test the reliability of the ϕ^4 truncation, we next include the λ_3 coupling and its flow equation (3.15) still keeping the anomalous dimensions at zero. Unfortunately, we have not been able to find an analytical solution of the resulting fixed point equations. Hence, we start numerically with a given (arbitrary) value of κ, we solve the fixed-point equations for λ_2, λ_3 and h^2. For the numerics, we choose values of κ ranging from 10 down to 0.001.

As is visible in Tab. 3.1, the values of the h^{*2} and λ_2^* are only slightly changed compared to the ϕ^4 truncation for κ between 10 and 0.01. We still observe a scaling $h^{*2}, \lambda_2^* \propto 1/\kappa$ in this regime, so that the effect of λ_3 can be considered as a small perturbation. The value for λ_3^* approximately scales as $1/\kappa^3$. For even smaller values of κ ($\kappa < 0.01$), λ_3^* grows large and exerts a quantitative influence on the flow. Nevertheless, we still find no indications for a non-Gaußian fixed point in the κ flow. Even for the smallest κ values which are accessible by our numerics, we observe a monotonous increase of $\partial_t\kappa/\kappa$, whereas an approach to a fixed point would require a decrease of this combination towards zero.

κ	h^{*2}	λ_2^*	λ_3^*	$\partial_t\kappa$	$\partial_t\kappa_{\phi^4}$
10	0.00616	0.00880	$4.67 \cdot 10^{-8}$	-20.0	-20.0
1	0.0615	0.0880	$4.67 \cdot 10^{-5}$	-2.01	-2.01
0.1	0.609	0.882	$4.61 \cdot 10^{-2}$	-0.210	-0.207
0.01	5.57	8.96	38.5	-0.026	-0.027
0.001	47.1	91.0	10800	-0.0056	-0.0092
0.0001	451	912	$1.26 \cdot 10^6$	-0.0033	-0.0074
0.00001	4490	9120	$1.29 \cdot 10^8$	-0.0031	-0.0072

Table 3.1: Pseudo-fixed-point values for the fixed-point equations for $h^2,\ \lambda_2$ and λ_3.

κ	h^{*2}	λ_2^*	η_ϕ^*	η_ψ^*	$\partial_t\kappa_t$
10	0.0185	0.0210	$1.11\cdot10^{-4}$	$4.24\cdot10^{-5}$	-20.008
1	0.185	0.210	$1.11\cdot10^{-3}$	$4.24\cdot10^{-4}$	-2.008
0.1	1.85	2.10	0.0111	$4.23\cdot10^{-3}$	-0.2083
0.01	18.5	21.1	0.111	0.0413	-0.0282
0.001	181.7	221.0	1.07	0.32	-0.0098
0.0001	1516	1602	1.73	2.98	-0.0027
0.00001	12030	9778	4.42	3.90	-0.0016
0.000001	68411	93113	4.92	4.16	-0.0012

Table 3.2: Pseudo-fixed-point values for the fixed-point equations for h^2, λ_2 including anomalous dimensions.

Fixed-point search including anomalous dimensions at $N_\mathrm{f} = 1$

The inclusion of the anomalous dimensions is, in principle, straightforward. The corresponding equations for η_ψ and η_ϕ (3.17) and (3.18) can be solved analytically; their solution can then be plugged into the flows of κ, h^2, λ_2, ... In practice, the inclusion of the anomalous dimensions increases the nonlinearities of the flow equations substantially. For our simplified strategy of first fixing a value of κ and then solving for possible pseudo-fixed point values of h^2 and λ_2, an exhaustive search of all possible pseudo-fixed point values appears numerically not feasible. Hence, we have used an algorithm that searches for one pseudo-fixed point of h^2 and λ_2 for a given value of κ and given seed values h^2_seed and $\lambda_{2,\mathrm{seed}}$. We have chosen the seed values on a grid of reasonable values compatible with the constraints (3.10). This procedure leads to the results shown in Tab. 3.2. In the regime of small anomalous dimensions ($\eta_{\phi,\psi} < 1$), we again observe a $1/\kappa$-behavior for the pseudo-fixed-point values of λ and h^2,

$$h^{*2} \approx \frac{0.185059}{\kappa},\ \lambda^* \approx \frac{0.21018}{\kappa}\,. \tag{3.21}$$

An inclusion of the anomalous dimensions does not lead to a vanishing of $\partial_t\kappa$ within the range of κ values studied here. Also, the ratio $\partial_t\kappa/\kappa$ does not exhibit a tendency towards zero as it should if a fixed point existed in the vicinity of the present parameter range.

3.2 Asymptotic safety at small flavor number

Since no acceptable asymptotically safe Yukawa system has been found in the studies above, the question arises as to whether there is a fundamental obstacle against a conformal behavior of the Higgs vacuum expectation value, or whether the class of simple systems has been too restrictive so far. This motivates a small-N_f study by remarking that the conformal behavior of the scalar expectation value is inhibited by the dominance of the fermionic fluctuations in the κ flow, as is visible, e.g., in Eqs. (3.13) and (3.20).

Since fermionic loops are proportional to the number of flavors, this fermionic dominance can be expected to vanish for small N_f.

Following our strategy introduced above, we first pick a value for κ and then solve the fixed-point equations of h^2 and λ_2, yielding pseudo fixed-point values h^{*2} and λ_2^*. Plugging these values into the κ flow, results in

$$\partial_t \kappa = -2\kappa + c(N_\mathrm{f})\,, \tag{3.22}$$

where $c(N_\mathrm{f})$ denotes an N_f-dependent constant. As observed above, $c(N_\mathrm{f})$ is negative for $N_\mathrm{f} = 1$ or larger, cf. Eq. (3.20), which corresponds to the observed absence of an acceptable fixed point. Decreasing N_f, $c(N_\mathrm{f})$ becomes positive for $N_\mathrm{f} \lesssim 0.25$ and so gives rise to a true non-Gaußian fixed point $\kappa^* = c(N_\mathrm{f})/2$ within this ϕ^4 truncation. This demonstrates that a conformal behavior of the Higgs expectation value is indeed possible as a matter of principle and can support asymptotic safety of Yukawa systems.

Fixed-point analysis at leading order

In order to illustrate the fixed-point properties, we choose $N_\mathrm{f} = 1/10$ for the sake of definiteness. The non-universal fixed-point values read $\{\kappa^*, \lambda_2^*, h^{*2}\} = \{0.00165, 27.3, 81.1\}$. The RG eigenvalues Θ_I are deduced from the stability matrix $B_i{}^j$ of the linearized flow around this fixed point. For $N_\mathrm{f} = 1/10$, we find

$$\Theta_1 = 2.372, \quad \Theta_2 = 0.592, \quad \Theta_3 = -2.859. \tag{3.23}$$

We observe two relevant directions, corresponding to $\Theta_{1,2} > 0$, i.e., the universality class of the theory defined by this fixed point has two physical parameters.

Fixed-point analysis at next-to-leading order

A full treatment of the anomalous dimensions confirms this qualitative behavior. The critical fermion number increases slightly: below $N_\mathrm{f} \lesssim 0.33$, a non-Gaußian fixed point exists. For $N_\mathrm{f} = 1/10$, we find $\{\kappa^*, \lambda_2^*, h^{*2}\} = \{0.00163, 42.8, 191.2\}$ and for the anomalous dimensions $\eta_\phi^* = 0.086$ and $\eta_\psi^* = 0.565$. The coupling fixed points λ_2^* and h^{*2} exhibit larger variations. Reliable quantitative predictions hence may require the inclusion of further boson-fermion interaction terms in the truncation. On the contrary, the prediction for the κ fixed point is little affected and the anomalous dimensions are small. We conclude that our result of a conformal behavior of the Higgs expectation value is robust in the derivative expansion.

The number of relevant directions at the fixed point is also robust: two RG eigenvalues have a positive real part. In comparison with the leading-order result, the Θ_I values do not

only differ quantitatively, but also qualitatively. The relevant directions are now described by a pair of complex Θ_I, implying that the UV flow spirals out of the fixed-point region towards the IR,

$$\Theta_{1,2} = 1.619 \mp 0.280i, \quad \Theta_3 = -3.680. \tag{3.24}$$

3.3 Predictivity of asymptotically safe systems

The present simple Yukawa system for a small number of fermion flavors $N_\mathrm{f} \lesssim 0.3$ supports a non-Gaußian fixed point, rendering the system asymptotically safe and the number of positive Θ_I corresponds to the number of physical parameters. The value of the real part of the largest Θ_I is a measure for the severeness of the hierarchy problem, see Sec. 2.5.1.

UV fixed-point regime and mass hierarchy

Repeating the above analysis of the eigenvalues of the stability matrix $B_i{}^j$ for various values of N_f yields the values of Θ_max as displayed in Fig. 3.1. In the limit $N_\mathrm{f} \to 0$, the standard-model value $\Theta_\mathrm{max} = 2$ is approached (even though the system is not in the standard-model universality class, but at the non-Gaußian fixed point). For increasing N_f, Θ_max decreases and approaches a minimum. At next-to-leading order, the minimum is indeed close to $N_\mathrm{f} = 1/10$ where $\Theta_\mathrm{max} \simeq 1.6$. Here, the hierarchy problem is not really overcome but at least somewhat softened compared to the standard model. Beyond this minimum, Θ_max increases again and eventually diverges at the critical flavor number.

Higgs mass from asymptotic safety

For all values of N_f below the critical value, we find that two of the RG eigenvalues have positive real parts, implying that the number of physical parameters of these systems is two. As the SSB phase is characterized by three standard-model parameters, top mass m_top, Higgs mass m_Higgs and vacuum expectation value v, only two of them are needed

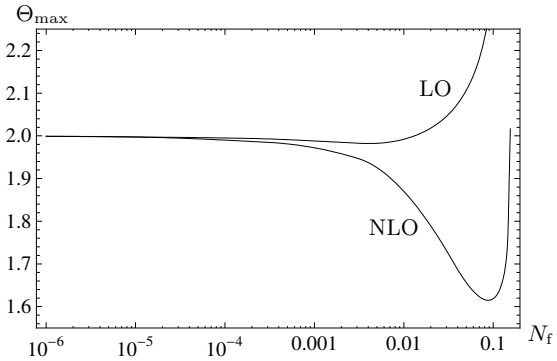

Figure 3.1: Θ_max vs. N_f as a measure for the hierarchy problem.

to fix the Yukawa system at the non-Gaußian fixed point. The third parameter, say the Higgs mass, is a true prediction of the asymptotically safe model. This should be compared to the Gaußian fixed point with perturbative critical exponents of the order $\Theta_\kappa \simeq 2$, $\Theta_{\lambda_2} \simeq 0$, and $\Theta_h \simeq 0$, implying that 3 physical parameters need to be fixed for Gaußian models.

The physical parameters are related to the renormalized couplings κ, h^2, λ_2 by

$$v = \lim_{k\to 0} \sqrt{2\kappa} k, \quad m_{\text{top}} = \sqrt{h^2} v, \quad m_{\text{Higgs}} = \sqrt{\lambda_2} v. \tag{3.25}$$

An asymptotically safe RG trajectory has to emanate from the non-Gaußian fixed point in the deep UV. The possible trajectories are further constrained by the necessity that the system ends up in the SSB phase in order to describe chiral symmetry breaking and dynamical mass generation.

In practice, we start the flow at a UV scale Λ_{UV} in the vicinity of the non-Gaußian fixed point, say at $(\kappa^* + \delta\kappa, \lambda_2^*, h^{2*} + \delta h^2)$. Then, the perturbations $\delta\kappa$ and δh^2 are then tuned such that the top mass and the vacuum expectation value match their desired physical IR values. The resulting Higgs mass is then a parameter-free prediction of the system.

This can be explicitly checked by varying the starting point, i.e., adding irrelevant directions, under the constraint of keeping v and m_{top} fixed. As another check of asymptotic safety, the UV scale Λ_{UV} can be changed. The constraint of keeping v and m_{top} fixed corresponds to staying on the line of constant physics. Asymptotic safety then guarantees that the Higgs mass remains the same and that the starting point approaches the non-Gaußian fixed point for increasing Λ_{UV}.

Of course, the present theory with a small number of fermion flavors cannot be expected to resemble the standard model also quantitatively. For instance, for the $N_{\text{f}} = \frac{1}{10}$ model in the leading-order truncation, we have not found an RG trajectory connecting the non-Gaußian fixed point with an IR limit where the Yukawa coupling approaches its standard-model value $h_{k\to 0} = m_{\text{top}}/v \simeq 0.711$. As a simple example, we have studied a universe with a top mass given by $m_{\text{top}} = hv|_{k\to 0}$ with $h_{k\to 0} = 20.0$. Our prediction for the Higgs mass then is $m_{\text{Higgs}} = \sqrt{6.845} v$. We have explicitly checked that m_{Higgs} indeed does not depend on the starting point in the fixed-point regime nor on the UV cutoff scale Λ_{UV}. In Fig. 3.2, a generic flow of the three running couplings of the ϕ^4 truncation is depicted.

An interesting property of this asymptotically safe system is that the set of possible IR values for the renormalized couplings is generically bounded, i.e., not all conceivable values of the physical parameters lie on RG trajectories that emanate from the non-Gaußian fixed point. In the present case, we observe that it is not possible to tune the flow for $h_{k\to 0}$ below a certain value $h_{\min}$, implying that a lower bound on m_{top}/v exists.

The mechanism behind this property can easily be understood. The RG flow passes essentially three regimes: the fixed-point regime in the UV, the decoupling regime in the IR, and a crossover regime in-between. In the UV fixed-point regime, the system behaves conformally and all couplings stay close to their fixed point values. The decoupling regime in the IR is characterized by the freeze-out of the dimensionful Higgs vacuum expectation value v. This generates Higgs and top masses which decouple from the flow at scales $k \ll v$. No massless modes remain and all running couplings freeze out and approach their IR values. The crossover regime in-between connects the UV fixed-point with the IR decoupling regime. Here, all couplings run fast and the full nonperturbative dynamics becomes important. Generically all β functions are sizeable here, so that the system spends little "RG time" in the crossover regime. This implies that the Yukawa coupling has little RG time to run from its large UV fixed-point value to its physical IR value before it freezes out due to decoupling.

Technically, we observe that there is a very robust IR fixed point in the SSB flow equations that attracts the flow towards the IR in the crossover regime. In the simple ϕ^4 truncation, it is characterized by fixed-point values $\kappa^*_{\rm IR}, h^{*2}_{\rm IR}, \lambda^*_{2,\rm IR}$. This fixed point is not directly physically relevant as $\kappa^*_{\rm IR} < 0$. The SSB constraint $\kappa > 0$ implies, however, that the physical Yukawa coupling is bounded by this IR fixed-point value, $h_{k\to 0} > h^*_{\rm IR}$. We conclude that an asymptotically safe Yukawa system offers a natural explanation for a large top mass.

Whereas Yukawa systems with $N_{\rm f} \lesssim 0.3$ are unlikely to be relevant for the true Higgs sector of the standard model, our results clearly indicate that an asymptotic safety scenario based on a conformal threshold behavior requires a balancing between bosons and fermions. We expect that a variety of realistic models exists where the fermion contributions are balanced by a sufficiently large bosonic sector. Indeed, the work on chiral Yukawa models with a left-right asymmetry presented in the next chapter provides evidence for this boson-fermion balancing for a wide range of integer fermion numbers.

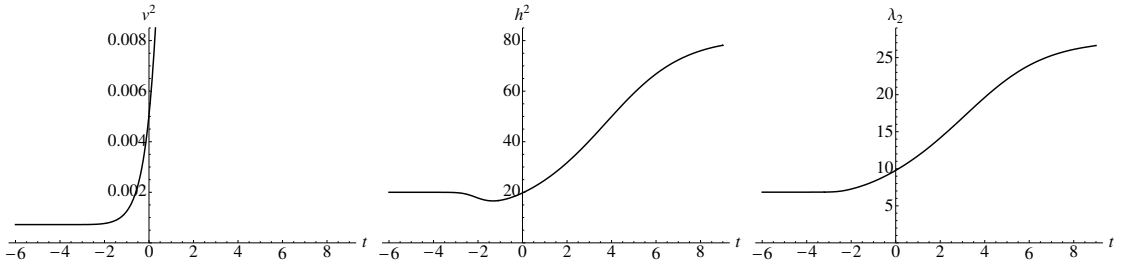

Figure 3.2: Typical flows from the non-Gaußian UV fixed point to the IR.

Further discussion

We would like to emphasize that our scenario goes beyond typical models involving four-fermi interactions to explain the Higgs scalar as a fermionic bound state [105–107]. As pointed out in [108, 109], these models are equivalent to standard Higgs-Yukawa models at a particular point in parameter space (with $Z_\phi \to 0$ and $U \to \bar{m}^2\phi^2/2$ for $k \to \Lambda$) and with the regularization belonging to the definition of the model. In agreement with [108], our results show that the Gross-Neveu variant of these models is not more predictive than the corresponding Yukawa system and still suffers from the triviality problem. By contrast, our asymptotically safe system for small N_f does not correspond to a local four-fermion theory at the fixed point. As the scalar kinetic term does not vanish in the UV and the effective potential is not Gaußian, integrating out the scalar field first yields a non-local and non-polynomial fermionic theory. Asymptotic safety is then encoded in the momentum dependence of the resulting fermionic vertices.

In the light of our results, a search for asymptotically safe Yukawa systems also by other methods would be highly welcome. For the present simple system, small-N_f expansion techniques appear to be most promising. These indeed exist within the worldline approach to quantum field theory, where subclasses of infinitely many Feynman diagrams can be resummed into closed worldline expressions order by order in a small-N_f expansion [110]. These methods have been shown to work in pure scalar models so far [111] and need to be generalized to fermions. Of course, also many non-perturbative lattice studies of Yukawa systems exist, see e.g. [112, 113], recently also employing chirally-invariant lattice fermions [114, 115]. The fact that no non-Gaußian fixed points have been found in standard settings so far is well in accord with our findings. Since lattice realizations often have a large fermion number, the resulting fermion dominance generically inhibits a conformal threshold behavior required for our scenario. Moreover, since our non-Gaußian fixed point has two relevant directions, a tuning of two bare parameters is required in order to take the corresponding continuum limit on a line of constant physics. Even though this is certainly possible on the lattice, this point can easily be missed during a general lattice study. Nevertheless, our results predict the existence of such a non-Gaußian fixed point for small-N_f systems, as they may be realized on the lattice, e.g., with rooted staggered fermions. An investigation of our model including gravitational effects has been performed in [116].

Chapter 4

Renormalization flow of chiral Yukawa systems

In this chapter we investigate a chiral $U(N_{\rm L})_{\rm L}\otimes U(1)_{\rm R}$ Yukawa model including one right-handed fermion and $N_{\rm L}$ left-handed fermions. The fermions are coupled to $N_{\rm L}$ complex bosons via a simple Yukawa interaction. This is motivated from the model in the previous chapter with the purpose to have a handle on the amplitude of the bosonic fluctuations by tuning an external parameter, namely the number of left-handed fermions $N_{\rm L}$. Our chiral Yukawa system mimics the coupling between the standard-model Higgs scalar and the left- and right-handed components of the top quark, also involving Yukawa couplings to the left-handed bottom (for $N_{\rm L}=2$) and further bottom-like quarks (for $N_{\rm L}>2$) in the same family. If the scalar field develops a vev upon symmetry breaking, the top quark acquires a Dirac mass, whereas the bottom-type quarks remain massless, similar to neutrinos in the standard model. For $N_{\rm L}=2$, we ignore the Yukawa coupling $\sim \bar{\psi}_{\rm R}\epsilon_{ab}\phi^{a\dagger}\psi^b_{\rm L}$ in our model, which provides for a mass term for the bottom quark in the standard model, since it does not generalize to other $N_{\rm L}$.

4.1 Truncation and flow equations

We choose the truncated action to be a next-to-leading order derivative expansion

$$\Gamma_k=\int_x\Big\{i(Z_{{\rm L},k}\bar{\psi}^a_{\rm L}\partial\!\!\!/\psi^a_{\rm L}+Z_{{\rm R},k}\bar{\psi}_{\rm R}\partial\!\!\!/\psi_{\rm R})+Z_\phi(\partial_\mu\phi^{a\dagger})(\partial^\mu\phi^a)+U_k(\rho)+\bar{h}_k(\bar{\psi}_{\rm R}\phi^{a\dagger}\psi^a_{\rm L}-\bar{\psi}^a_{\rm L}\phi^a\psi_{\rm R})\Big\}.$$

The fermion fields $\psi^a_{\rm L}$ and $\psi_{\rm R}$ have standard kinetic terms but can acquire different wave function renormalizations $Z_{{\rm L},k}$ and $Z_{{\rm R},k}$. The index a runs from 1 to $N_{\rm L}$. The projections on the left-/right-handed fermion contributions are carried out via the projection operators $P_{\rm L/R}=\frac{1}{2}(1\pm\gamma_5)$. The bosonic sector involves a standard kinetic term with wave function renormalization $Z_{\phi,k}$ and an effective potential $U_k(\rho)$, defining the invariant

$\rho := \phi^{a\dagger}\phi^a$. The bosons can also be expressed in terms of a real field basis $\phi^a = \frac{1}{\sqrt{2}}(\phi_1^a + i\phi_2^a)$ and $\phi^{a\dagger} = \frac{1}{\sqrt{2}}(\phi_1^a - i\phi_2^a)$, where $\phi_1^a, \phi_2^a \in \mathbb{R}$. The truncated effective action including the Yukawa interaction is invariant under $\mathrm{U}(N_\mathrm{L})_\mathrm{L}$ transformations of the left-handed fermion and the boson as well as $\mathrm{U}(1)_\mathrm{R}$ transformations of the right-handed fermion and the boson.

The flow of the wave function renormalizations $Z_{\phi,k}, Z_{\mathrm{L},k}$ and $Z_{\mathrm{R},k}$ is put in terms of scale-dependent anomalous dimensions $\eta_\phi = -\partial_t \ln Z_{\phi,k}$ and $\eta_{\mathrm{L,R}} = -\partial_t \ln Z_{\mathrm{L,R},k}$, where $Z_{\mathrm{L},k}$ and $Z_{\mathrm{R},k}$ acquire different loop contributions and we define the renormalized fields as $\tilde{\phi} = Z_{\phi,k}^{1/2}\phi$, $\tilde{\psi}_{\mathrm{L,R}} = Z_{\mathrm{L,R}}^{1/2}\psi_{\mathrm{L,R}}$. The dimensionless renormalized quantities required for the fixed-point search read

$$\tilde{\rho} \;=\; Z_{\phi,k}k^{2-d}\rho, \quad h_k^2 = Z_{\phi,k}^{-1}Z_{\mathrm{L},k}^{-1}Z_{\mathrm{R},k}^{-1}k^{d-4}\bar{h}_k^2, \quad u_k(\tilde{\rho}) = k^{-d}U_k(\rho)|_{\rho=k^{d-2}\tilde{\rho}/Z_{\phi,k}}. \tag{4.1}$$

Flow equations

Detailed information on the derivation of the flow equations for this truncation in arbitrary spacetime dimensions d is given in App. C. The flow of the effective potential given in terms of threshold functions which are given in App. B reads

$$\begin{aligned}\partial_t u_k \;=\;& -du_k + \tilde{\rho}u_k'(d-2+\eta_\phi) + 2v_d\big\{(2N_\mathrm{L}-1)l_0^d(u_k') + l_0^d(u_k'+2\tilde{\rho}u_k'') \\ & -d_\gamma\big((N_\mathrm{L}-1)l_{0,\mathrm{L}}^{(\mathrm{F})d}(0) + l_{0,\mathrm{L}}^{(\mathrm{F})d}(\tilde{\rho}h_k^2) + l_{0,\mathrm{R}}^{(\mathrm{F})d}(\tilde{\rho}h_k^2)\big)\big\},\end{aligned} \tag{4.2}$$

where the primes denote derivatives w.r.t. $\tilde{\rho}$, and $v_d = 1/(2^{d+1}\pi^{d/2}\Gamma(d/2))$. For the SYM and the SSB regime the effective potential is expanded as defined in Eqs. (3.6) and (3.7).

In the SSB regime, the flow of the Yukawa coupling and the scalar anomalous dimension for the Goldstone mode can, in principle, be different from that of the radial mode. As the Goldstone modes as such are not present in the electroweak sector of the standard model, we compute the Yukawa coupling and the scalar anomalous dimension by projecting the flow onto the radial scalar operators in the SSB regime. Note that this strategy is different from that used for critical phenomena in other Yukawa or bosonic systems, where the Goldstone modes can dominate criticality, see Chap. 5.

We derive the flow of the Yukawa coupling h_k in App. C, and we end up with

$$\begin{aligned}\partial_t h_k^2 \;=\;& (d-4+\eta_\phi+\eta_\mathrm{L}+\eta_\mathrm{R})h_k^2 \\ & +4v_d h_k^4\Big\{(2\tilde{\rho}u_k'')l_{1,2}^{(\mathrm{FB})d}(\tilde{\rho}h_k^2, u_k') - (6\tilde{\rho}u_k'' + 4\tilde{\rho}^2u_k''')l_{1,2}^{(\mathrm{FB})d}(\tilde{\rho}h_k^2, u_k'+2\tilde{\rho}u_k'') \\ & \quad -l_{1,1}^{(\mathrm{FB})d}(\tilde{\rho}h_k^2, u_k') + l_{1,1}^{(\mathrm{FB})d}(\tilde{\rho}h_k^2, u_k'+2\tilde{\rho}u_k'') \\ & \quad +2\tilde{\rho}h_k^2 l_{2,1}^{(\mathrm{FB})d}(\tilde{\rho}h_k^2, u_k') - 2\tilde{\rho}h_k^2 l_{2,1}^{(\mathrm{FB})d}(\tilde{\rho}h_k^2, u_k'+2\tilde{\rho}u_k'')\Big\}.\end{aligned} \tag{4.3}$$

Finally, we list the expressions for the anomalous dimensions

$$\eta_\phi = \frac{8v_d}{d}\tilde{\rho}(3u_k'' + 2\tilde{\rho}u_k''')^2 m_{22}^d(u_k' + 2\tilde{\rho}u_k'') + (2N_{\rm L} - 1)\frac{8v_d}{d}\tilde{\rho}u_k''^2 m_{22}^d(u_k') \tag{4.4}$$
$$+\frac{8v_d d_\gamma}{d}h_k^2 m_4^{({\rm F})d}(\tilde{\rho}h_k^2) - \frac{8v_d d_\gamma}{d}\tilde{\rho}h_k^4 m_2^{({\rm F})d}(\tilde{\rho}h_k^2),$$
$$\eta_{\rm L} = \frac{8v_d}{d}h_k^2[m_{12}^{({\rm FB})d}(\tilde{\rho}h_k^2, u_k' + 2\tilde{\rho}u_k'') + m_{12}^{({\rm FB})d}(\tilde{\rho}h_k^2, u_k')], \tag{4.5}$$
$$\eta_{\rm R} = \frac{8v_d}{d}h_k^2[m_{12}^{({\rm FB})d}(\tilde{\rho}h_k^2, u_k' + 2\tilde{\rho}u_k'') + m_{12}^{({\rm FB})d}(\tilde{\rho}h_k^2, u_k') + (2N_{\rm L} - 2)m_{12}^{({\rm FB})d}(0, u_k')]. \tag{4.6}$$

The arguments of the threshold functions have to be evaluated at the minimum of the effective potential. In this chapter, we will concentrate on the case of $d = 4$ dimensions.

4.2 Fixed point analysis in four dimensions

For notational convenience we suppress the index k at the parameters of the truncation.

The Symmetric Regime (SYM)

A simple analysis like in the previous chapter reveals that within the validity regime of our truncation, we find only the Gaußian fixed point for the Yukawa coupling $h^* = 0$ in SYM. Since the flow of the Yukawa coupling is proportional to itself, an initial zero value for h^2 will leave the system non-interacting at $h^2 = 0$ for all scales. The remaining interacting system is purely bosonic and does not show any nontrivial fixed point in agreement with triviality of ϕ^4 theory. We conclude that the chiral Yukawa model in the SYM regime is not asymptotically safe within the subsector of theory space spanned by our truncation.

4.2.1 Regime of Spontaneous Symmetry Breaking (SSB)

In the SSB regime the flow equations have a richer structure than in the symmetric regime and here the system can support the fixed-point scenario with a conformal vev.

Fixed-point search to leading order

For the fixed-point search, we use a polynomial expansion of the effective potential about its minimum, cf. Eq. (3.7). As a check of the quality of this expansion, the convergence properties of physical quantities have to be determined with respect to increasing orders in this expansion. In general, we expect that this expansion gives a good approximation of the full effective potential only in the vicinity of the potential minimum. Nevertheless, this can still lead to sufficient information for a quantitative estimate of a variety of physical quantities, as they are mostly related to properties of the potential near the minimum.

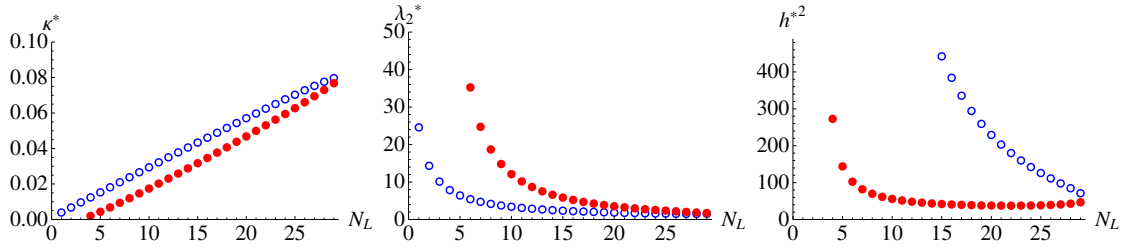

Figure 4.1: Fixed-point values vs. N_{L} for the two physically admissible fixed points.

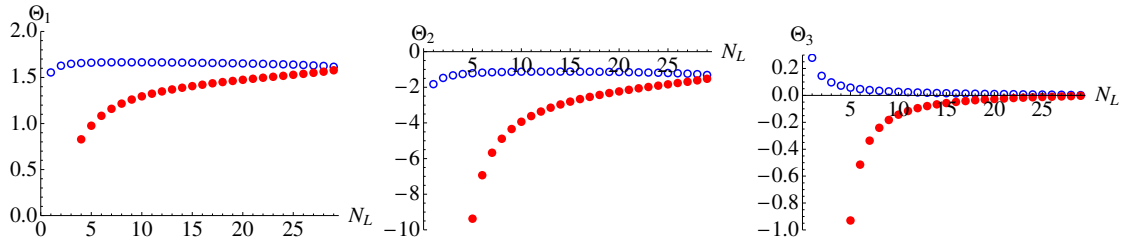

Figure 4.2: Leading order truncation: Critical exponents as a function of N_{L}.

For a first glance, we use the simplest nontrivial approximation of the effective potential, $u = \frac{\lambda_2}{2}(\tilde{\rho} - \kappa)^2$, which facilitates a purely analytical treatment of the fixed-point equations. We also confine ourselves to the leading-order approximation in the derivative expansion, where the anomalous dimensions vanish, $\eta_{\mathrm{L,R},\phi} = 0$. The resulting set of fixed-point equations $\{\partial_t\kappa = 0, \partial_t\lambda_2 = 0, \partial_t h^2 = 0\}$ can be solved analytically. We give the flow equation for κ explicitely to demonstrate the dependence of the bosonic fluctuations on the external parameter N_{L},

$$\partial_t\kappa = -2\kappa + \underbrace{\frac{1}{32\pi^2}\left[(2N_{\mathrm{L}} - 1) + \frac{3}{(1+2\kappa\lambda_2)^2}\right]}_{\text{bosonic fluctuations}} - \underbrace{\frac{1}{4\pi^2}\frac{h^2}{\lambda_2(1+\kappa h^2)^2}}_{\text{fermionic fluctuations}}. \tag{4.7}$$

For a given N_{L}, we obtain a large number of fixed points but only up to two fixed points fulfill the constraints given in Eq. (3.10). For $N_{\mathrm{L}} < 4$, we find only one admissible non-Gaußian fixed point (NGFP). For $4 \leq N_{\mathrm{L}} \leq 29$, two admissible NGFPs occur. For $30 \leq N_{\mathrm{L}} \leq 57$, there is again only one NGFP, whereas larger N_{L} do not give rise to any physically admissible fixed points. The fixed-point values κ^*, h^{*2}, and λ_2^* as a function of N_{L} can be read off from Fig. 4.1. The critical exponents as a function of N_{L} are shown in Fig. 4.2 for this simple truncation. It is remarkable that one NGFP has two relevant directions and the other even only one relevant direction with a positive critical exponent. This implies that the corresponding model is fixed by only two or one physical parameter, respectively. Moreover, the largest critical exponent of both NGFPs is smaller than the perturbative maximal value, $\Theta_{\max} < 2$. As a consequence, these models defined at the NGFPs have an improved hierarchy behavior.

Benchmark fixed point for $N_{\mathrm{L}} = 10$

For further investigations and by way of example, we concentrate on one particular fixed point. We use a fixed point with only one relevant direction, as it is phenomenologically most appealing due to the reduction of physical parameters. We choose $N_{\mathrm{L}} = 10$ in the following, since the corresponding fixed point does not give rise to extreme coupling values, implying numerical stability. In addition, this particular value of N_{L} may also be of relevance for certain unification scenarios.

Furthermore, we extend the lowest-order polynomial expansion studied above to higher operators in $\tilde{\rho}$, cf. Eq. (3.7). From a technical viewpoint, the fixed-point analysis becomes much more involved at higher orders. In particular, we have not found any analytical solutions to the higher-order fixed-point equations. Due to the intrinsic nonlinearity of the fixed-point equations, also a numerical search is nontrivial: a complete identification of all possible fixed points appears out of reach.

Therefore, we start with the assumption that the simple truncation involving only h^2, λ_2 and κ gives already a satisfactory fixed-point estimate. As a next step, we can search for a fixed-point of the subsequent higher-order system in the vicinity of the previous lower-order fixed point. This procedure turns out to be self-consistent and can be iterated to higher orders. The results for the associated fixed-point values are summarized in Tab. 4.1. The resulting fixed-point values show a satisfactory convergence behavior, indicating that the polynomial expansion is quantitatively reliable already at low orders.

Whereas the fixed-point potential is scheme dependent, also the stability of the universal RG eigenvalues can be checked under the inclusion of higher orders in the polynomial expansion. The results are also summarized in Tab. 4.1. The leading exponents vary only on the 10% level upon the inclusion of higher-order terms. Most importantly, the number of relevant directions is not changed at higher orders, and the maximal RG eigenvalue tends to smaller values at higher orders which leads to an improved hierarchy behavior. We conclude that the fixed point exists at leading-order in the derivative expansion. It possesses many desirable properties and can well be approximated by a polynomial expansion.

	h_*^2	κ_*	λ_2^*	Θ_1	Θ_2	Θ_3	Θ_4	Θ_5	Θ_6	Θ_7
$N_{\mathrm{p}} = 2$	55.8	0.0174	12.11	1.294	-0.143	-3.94	-	-	-	-
$N_{\mathrm{p}} = 4$	56.0	0.0158	12.09	1.167	-0.170	-2.50	-5.53	-13.61	-	-
$N_{\mathrm{p}} = 6$	57.4	0.0152	12.13	1.056	-0.175	-2.35	-4.97	-8.49	-14.02	-25.54

Table 4.1: Fixed-points and RG eigenvalues for $N_{\mathrm{L}} = 10$ at different orders in the the effective potential. N_{p} is the largest exponent of ρ in the polynomial expansion (3.7)).

4.3 Top- and Higgs-mass predictions from asymptotic safety

We illustrate the predictive power of this asymptotically safe model, using the flow of our system in the local-potential approximation as a model in its own right. We relate the physical IR parameters (the Higgs vev v, the Higgs mass $m_{\rm Higgs}$ and the top mass $m_{\rm top}$) to the renormalized couplings κ, h^2, λ_2 by Eq. (3.25), as in the previous chapter. The bottom-type quarks remain massless in our model.

The non-Gaußian fixed point has only one relevant direction, so there is only one physical parameter which we relate to the vev $v = 246$ GeV. In fact, fixing v to its physical value merely corresponds to fixing the absolute scale. Dimensionless couplings or mass ratios are even independent of this fixing scale and thus are completely parameter-free predictions of the theory. In practice, we have to start the flow at some finite value of the auxiliary UV cutoff Λ (in arbitrary units), solve the flow, and then associate the resulting value of v with its correct value in physical units. This also fixes the value of Λ in units of, say, GeV. In the model with $N_{\rm L} = 10$, we then end up with a top and a Higgs mass at the IR scale

$$m_{\rm top} = 5.78v, \quad m_{\rm Higgs} = 0.97v, \tag{4.8}$$

where the proportionality factors are approached in the limit $v/\Lambda \ll 1$. In this limit, this result is robust as we vary the UV cutoff, which demonstrates the cutoff independence of our prediction and the top and the Higgs mass are pure predictions of the theory itself.

Whereas the Higgs mass is of the order of the vev as expected, $m_{\rm Higgs} \simeq 239$GeV for $v = 246$GeV, the top mass is significantly larger in our model: $m_{\rm top} \simeq 1422$GeV. This is an indirect consequence of the comparatively large value of the fixed point of the Yukawa coupling. In order to elucidate this relation, let us recall from the previous chapter that the flow can be subdivided into three different regimes: the UV fixed-point regime, a crossover region and a freeze-out region in the IR. The dynamics in the crossover region is an intrinsic parameter-free property of the model that occurs only in a rather narrow window of momentum scales. Hence, the couplings have only a finite "RG time" – similar to the number of e-foldings in inflationary cosmology [117] – to run from their UV initial

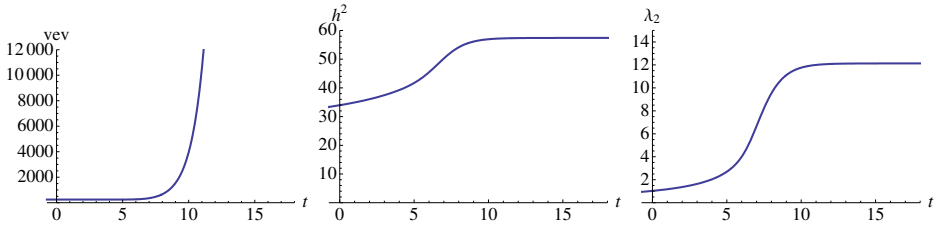

Figure 4.3: Flow of the leading couplings within the lowest-order truncation.

conditions to their IR-frozen values. As the initial fixed-point Yukawa coupling in our model is large, a sizeable IR value remains and gives rise to a large top mass.

Realistic scenarios with a physical value of the top mass require either a smaller fixed-point Yukawa coupling, or a sufficiently large number of crossover e-foldings that facilitates a long running of the Yukawa coupling to its physical value. As the number of e-foldings of the crossover window is mainly dictated by the RG speed at which the physical vev builds up, large numbers of e-foldings can occur if the largest critical exponent dominating the κ flow is small. We conclude that a reduced hierarchy problem and a realistic value of the top mass can go hand in hand with each other.

Finally, we have to address an artifact of our flow in the IR. As can be read off from Fig. 4.3, the perturbatively marginal couplings h^2 and λ_2 still exhibit a slow log-like running in the IR. This running can be traced back to the Goldstone modes which are a particularity of our model, but are not present in the standard model. However, even if we considered the Goldstone modes as physical, the log-like running is still an artifact of our truncation in the IR, arising from the Cartesian decomposition of the scalar field, $\phi = \frac{1}{\sqrt{2}}(\phi_1 + i\phi_2)$. Here the vev is associated with the ϕ_1 direction and ϕ_2 is populated with Goldstone modes. This decomposition leads to log-like divergencies in the diagrams with internal ϕ_2 loops coupling to external ϕ_1 legs. However, as becomes clear from a proper nonlinear decomposition of the scalar field $\phi = \sqrt{\rho}e^{i\theta}$, the true Goldstone modes encoded in the field θ do not couple to the radial mode via the potential, as $U(\phi^\dagger\phi) = U(\rho)$ is independent of θ. We conclude that the log-like running would be absent in a proper nonlinear field basis in the broken regime [118].

In practice, we read off our estimates for the IR values of h^2 and λ_2 at a dynamically defined scale $k_{\rm IR}$. For the identification of this scale, we note that higher-order couplings $\lambda_{n>2}$ are not affected by the Cartesian basis and safely flow to zero due to the leading-order Gaußian flow $\partial_t\lambda_n = 2(n-2)\lambda_n + ...$ as expected, see Fig. 4.4. We define the scale $k_{\rm IR}$ by that scale at which the coupling λ_3 approaches its zero IR fixed point from above within an accuracy of 0.1%. The IR predictions listed in Eq. (4.8) have been read off at this scale. Of course, in the presence of this flow artifact, these predictions actually depend on the choice of $k_{\rm IR}$. Nevertheless, the generic mechanisms in the UV and crossover regimes outlined above are not affected by the IR artifact.

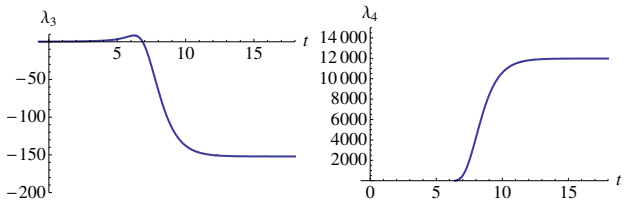

Figure 4.4: Flow of the higher-order couplings λ_3 and λ_4 of the effective potential.

4.4 Derivative expansion at next-to-leading order

We have analyzed the chiral Yukawa model in a derivative expansion of the effective action. As a simple criterion for this expansion to be valid, the anomalous dimensions measuring the influence of higher-derivative terms should be small, cf. Eq. (3.9). As a first check of this criterion, we use our fixed-point results from the lowest-order polynomial expansion in the local-potential approximation and insert them into the right-hand sides of the anomalous dimensions Eqs. (4.19)-(4.21). For this estimate, we ignore the RG improvement in the form of the back-reactions of nonzero η's on the flow of the couplings. The results as a function of N_{L} are shown in Fig. D.12. Whereas the criterion for the magnitude of the anomalous dimension, Eq. (3.9), is satisfied for η_ϕ and η_{L} for $N_{\mathrm{L}} > 5$, the anomalous dimension η_{R} of the right-handed fermion violates the criterion for all N_{L}.

One reason for the magnitude of η_{R} lies in the fact that the massless Goldstone modes and massless bottom-type fermions contribute strongly. This is because they (i) are not damped by massive threshold effects induced by couplings to the condensate, and (ii) contribute with a large multiplicity $\sim N_{\mathrm{L}}$. We conclude that the leading-order derivative expansion does not allow for self-consistent estimates of the fixed-point structure of the chiral Yukawa model as such. Nevertheless, since the Goldstone as well as the massless fermion modes are not present in the standard model but a particularity of our reduced toy model, we expect that the local-potential approximation of the present model provides for a better picture of a possible fixed-point structure of the standard-model Higgs sector than the literal version of our model including its massless modes.

It is still an interesting question within the chiral Yukawa model, whether the nonlinearities induced by the anomalous dimension gives rise to admissible fixed points if the full RG improvement is taken into account. For this, we have first followed the evolution of our leading-order fixed points upon gradually switching on the anomalous dimensions. Our numerical results are compatible with a destabilization of this fixed point. A numerical search of further admissible fixed points upon the full inclusion of the anomalous dimension remained inconclusive and a systematic search in this high-dimensional parameter space is computationally expensive and beyond the scope of this work.

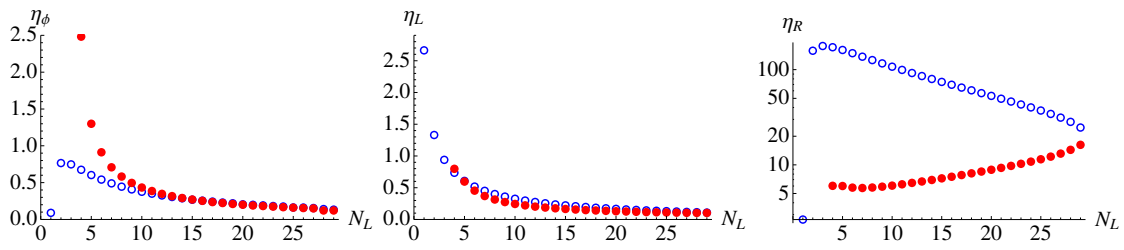

Figure 4.5: Leading-order estimate of the anomalous dimensions.

Summary

As a main result of the present study, a number of conclusions about the requirements for a more realistic model can be drawn.

1. The appearance of the conformal-vev mechanism depends crucially on the algebraic structure of the theory. Boson dominance is required and can be induced by a chiral left-right asymmetry.

2. If the conformal vev breaks a continuous global symmetry, Goldstone bosons are generated. As they are not controlled by threshold effects, they may have the tendency to destabilize the UV fixed point. A model with spontaneous breaking of gauged symmetries will not be affected by this problem.

3. Even though the threshold effects of the conformal vev are nonperturbative, our mechanism does technically not require strong coupling. Comparatively small UV fixed-point couplings would also be allowed if not phenomenologically preferred.

4. The present model predicts a very large top mass. For a realistic top mass, either the Yukawa UV fixed-point value should not be too large or the crossover from the UV regime to the IR freeze-out should extend over many "e-foldings", i.e., a larger range of RG time.

These requirements together with the remarkable predictive power of our scenario are a strong motivation to extend the present set of ideas to gauged chiral Yukawa models, thereby making another step towards a realistic standard-model Higgs sector.

4.5 Inclusion of gauge bosons

The extension of our chiral Yukawa model without gauge bosons to the NLO derivative expansion was plagued by the destabilization of the UV fixed point. This is at least partly caused by large contributions from Goldstone bosons and a large value of the fixed-point Yukawa coupling h_*^2.

In this section, we introduce gauge bosons to investigate more realistically the electroweak sector of the Standard Model, corresponding to $\mathrm{SU}(N) \otimes \mathrm{U}(1)$ with $N = 2$. In this case $2N - 1 = 3$ Goldstone modes appear but are removed from the spectrum of the theory by the $N^2 - 1 = 3$ gauge bosons which acquire a mass. The gauge boson corresponding to an abelian subgroup U(1) remains massless. In the same spirit we investigate our left/right asymmetric chiral Yukawa model including gauge bosons. The gauge bosons can remove Goldstone contributions but also yield further terms in the Yukawa flow resulting in a possible decrease of its fixed-point value. This has the potential to render the derivative expansion well defined also at next-to-leading order.

For arbitrary N_L we promote the global $\mathrm{SU}(N_\mathrm{L})_\mathrm{L}$ symmetry to a local one with $U(x) = e^{-ig\omega^i(x)T^i}$ and $(i = 1, \ldots, N_\mathrm{L}^2 - 1)$. Here, g is the gauge coupling constant, T^i are the generators of the gauge group and $\omega^i(x)$ is a position dependent parameter. The gauge fields are given by $W_\mu^i = \partial_\mu \omega^i$ and the partial derivatives are replaced by the covariant derivatives,

$$\partial_\mu \to D_\mu = \partial_\mu - igW_\mu^i T^i. \tag{4.9}$$

The fields transform under the $\mathrm{SU}(N_\mathrm{L})_\mathrm{L}$ according to

$$\phi^a \to U\phi^a, \quad \psi_\mathrm{L}^a \to U\psi_\mathrm{L}^a, \quad \psi_\mathrm{R} \to \psi_\mathrm{R}, \quad W_\mu^i T^i \to UW_\mu^i T^i U^{-1} - \frac{i}{g}(\partial_\mu U)U^{-1}. \tag{4.10}$$

4.5.1 Truncation

To extend the truncation we have to replace the partial derivatives by covariant derivatives in the kinetic term of the bosons and the kinetic term of the left-handed fermions. The covariant derivatives provide a Yukawa interaction between the left-handed fermions and the gauge bosons, $gZ_{\mathrm{L},k}\bar{\psi}_\mathrm{L}^a \not{W}^i T^i \psi_\mathrm{L}^a$. Further we include a kinetic term for the gauge bosons

$$\frac{Z_F}{4} F_{\mu\nu}^i F^{i\mu\nu}, \text{ with } \quad F_{\mu\nu}^i = \partial_\mu W_\nu^i - \partial_\nu W_\mu^i + g f^{ijk} W_\mu^j W_\nu^k, \text{ and } \quad [T^i, T^j] = i f^{ijk} T^k. \tag{4.11}$$

To implement gauge fixing, we employ the Faddeev-Popov method. We introduce the gauge fixing condition

$$G(W_\mu^i) = \partial_\mu W_\mu^i + 2i\alpha v g T_{Na}^i \Delta\phi^a = 0\,, \tag{4.12}$$

with a gauge-fixing parameter α and excluding the term with $\Delta\phi_1^N$. The bosonic field is separated into the vacuum expectation value (vev) and fluctuations around the vev v,

$$\phi^a = v\delta^{a,N} + \Delta\phi^a, \quad \text{where} \quad \Delta\phi^a = \frac{1}{\sqrt{2}}(\Delta\phi_1^a + i\Delta\phi_2^a). \tag{4.13}$$

The gauge-fixing condition is contained in the gauge -fixing action reading

$$\Gamma_\mathrm{gf} = \frac{Z_\phi}{2\alpha} \int d^dx (\partial_\mu W_\mu^i + 2i\alpha v g T_{Na}^i \Delta\phi^a)(\partial_\mu W_\mu^i - 2i\alpha v g \Delta\phi^{a\dagger} T_{aN}^i). \tag{4.14}$$

Last, we include a Fadeev-Popov ghost term, with ghost fields c^i and $\bar{c}^i$, reading $-\bar{c}^i \mathcal{M}^{ij} c^j$ with

$$\mathcal{M}^{ij} = \frac{\delta G(W^\omega)}{\delta\omega^j} = -\partial_\mu^2 \delta^{ij} - g\partial_\mu W^{k\mu} f^{ikj} + 2\alpha v g^2 T_{Na}^i T_{ab}^j \phi_b. \tag{4.15}$$

Combining all these ingredients yields the truncation

$$\Gamma_k = \int d^dx \big[U_k(\rho) + Z_{\phi,k}(D^\mu\phi)^\dagger(D_\mu\phi) + i(Z_{L,k}\bar\psi^a_L \not{D}\psi^a_L + Z_{R,k}\bar\psi_R\not{\partial}\psi_R) \\ + \bar h_k\bar\psi_R\phi^{a\dagger}\psi^a_L - \bar h_k\bar\psi^a_L\phi^a\psi_R + \frac{Z_F}{4}F^i_{\mu\nu}F^{i\mu\nu} - \bar c^i\mathcal{M}^{ij}c^j\big] + \Gamma_{\rm gf}, \tag{4.16}$$

The vev v is chosen to be in the $N_{\rm L}$ direction.

In this formalism the unitary gauge corresponds to the case $\alpha \to \infty$ and Landau gauge to $\alpha \to 0$. The gauge-fixing terms result in a mass term for the Goldstone bosons that is proportional to $m^2_{\rm Goldstone} \sim \alpha g^2 v^2$. In unitary gauge the Goldstone modes therefore become infinitely heavy and decouple. This is the usual Higgs mechanism, where the gauge bosons remove the Goldstone bosons from the spectrum of the theory. We will work in Landau gauge as this is a fixed point of the RG flow [119, 120] and it simplifies the computations. In this case, the Goldstone modes remain massless. However, for Landau gauge we expect a balancing of effects of the Goldstone and the gauge contributions in the flow equations, mimicking the effect of a removal of the Goldstone bosons in unitary gauge.

4.5.2 Flow equations with gauge fields

We derive the flow equations for the effective potential, the Yukawa coupling and the anomalous dimensions in App. D. Further, we define the mass terms m^2_A of the gauge bosons which result from the diagonalization of the matrix $Z_\phi g^2\phi^{a\dagger}\{T^i,T^j\}_{ab}\phi^b$. Introducing threshold functions as listed in App. B and using the dimensionless quantities $\tilde m^2_A = \frac{m^2_A}{Z_{\rm F}k^2}$ and $\tilde g^2 = \frac{g^2}{Z_{\rm F}k^{4-d}}$, the RG flow equations for the effective potential and the Yukawa coupling read

$$\begin{aligned}\partial_t u_k &= -du_k + \tilde\rho u_k'(d-2+\eta_\phi) + 2v_d\big\{(2N_{\rm L}-1)l^d_0(u_k') + l^d_0(u_k'+2\tilde\rho u_k'') \\ &\quad -d_\gamma\big((N_{\rm L}-1)l^{({\rm F})d}_{0,{\rm L}}(0) + l^{({\rm F})d}_{0,{\rm L}}(\tilde\rho h_k^2) + l^{({\rm F})d}_{0,{\rm R}}(\tilde\rho h_k^2)\big)\big\} \\ &\quad +2v_d\sum_{A=1}^{N_{\rm L}^2-1}\Big[(d-1)l^{({\rm GB})d}_{0{\rm T}}(\tilde m^2_A) + l^{({\rm GB})d}_{0{\rm L}}(0)\Big] - 4v_d\left(N_{\rm L}^2-1\right)l^{({\rm G})d}_0(0).\end{aligned} \tag{4.17}$$

$$\begin{aligned}\partial_t h_k^2 &= (d-4+\eta_\phi+\eta_{\rm L}+\eta_{\rm R})h_k^2 + 4v_d h_k^4\Big\{(2\tilde\rho u_k'')l^{({\rm FB})d}_{1,2}(\tilde\rho h_k^2,u_k') \\ &\quad -(6\tilde\rho u_k''+4\tilde\rho^2u_k''')l^{({\rm FB})d}_{1,2}(\tilde\rho h_k^2,u_k'+2\tilde\rho u_k'') - l^{({\rm FB})d}_{1,1}(\tilde\rho h_k^2,u_k') \\ &\quad +l^{({\rm FB})d}_{1,1}(\tilde\rho h_k^2,u_k'+2\tilde\rho u_k'') + 2\tilde\rho h_k^2 l^{({\rm FB})d}_{2,1}(\tilde\rho h_k^2,u_k') - 2\tilde\rho h_k^2 l^{({\rm FB})d}_{2,1}(\tilde\rho h_k^2,u_k'+2\tilde\rho u_k'')\Big\} \\ &\quad -h_k^2\sum_{a=1}^{N_{\rm L}}\sum_{A=1}^{N_{\rm L}^2-1}\tilde g^2 d_\gamma T^A_{Na}T^A_{aN}(d-1)8v_d m^{({\rm FBE})}_{1,1,1}(u_k',\tilde\rho h_k^2\delta^{aN},\tilde m^2_A).\end{aligned} \tag{4.18}$$

The flow equations for the anomalous dimensions are given by:

$$\begin{aligned}
\eta_\phi &= \frac{8v_d}{d}\tilde{\rho}(3u_k'' + 2\tilde{\rho}u_k''')^2 m_{22}^d(u_k' + 2\tilde{\rho}u_k'') + \frac{(2N_\mathrm{L}-1)8v_d}{d}\tilde{\rho}u_k''^2 m_{22}^d(u_k') \qquad (4.19)\\
&\quad + \frac{8v_d d_\gamma}{d}h_k^2 m_4^{(\mathrm{F})4}(\tilde{\rho}h_k^2) - \frac{8v_d d_\gamma}{d}\tilde{\rho}h_k^4 m_2^{(\mathrm{F})4}(\tilde{\rho}h_k^2) - \frac{8v_d}{d}\tilde{g}^2\sum_{a=1}^{N_\mathrm{L}}\sum_{A=1}^{N_\mathrm{L}^2-1} T_{Na}^A T_{aN}^A\\
&\quad \times\left[dl_{1,1}^{(\mathrm{BGB})d}(u_k', \tilde{m}_A^2) + 3m_{1,2}^{(\mathrm{BGB})d}(u_k', \tilde{m}_A^2) - m_4^{(\mathrm{BGB})d}(u_k', \tilde{m}_A^2)\right]\\
\eta_\mathrm{L} &= \frac{8v_d}{d}h_k^2[m_{12}^{(\mathrm{FB})d}(\tilde{\rho}h_k^2, u_k' + 2\tilde{\rho}u_k'') + m_{12}^{(\mathrm{FB})d}(\tilde{\rho}h_k^2, u_k')], \qquad (4.20)\\
&\quad -8v_d d_\gamma \tilde{g}^2\sum_{a=1}^{N_\mathrm{L}}\sum_{A=1}^{N_\mathrm{L}^2-1} T_{aN}^A T_{Na}^A m_{1,2}^{(\mathrm{FGB})d}(\delta^{aN}\tilde{\rho}h_k^2, \tilde{m}_i^2).\\
\eta_\mathrm{R} &= \frac{8v_d}{d}h_k^2[m_{12}^{(\mathrm{FB})d}(\tilde{\rho}h_k^2, u_k' + 2\tilde{\rho}u_k'') + m_{12}^{(\mathrm{FB})d}(\tilde{\rho}h_k^2, u_k') + 2(N_\mathrm{L}-1)m_{12}^{(\mathrm{FB})d}(0, u_k')].
\end{aligned}$$

4.5.3 Fixed points in the gauged chiral Yukawa model

The set of fixed-point equations is highly non-trivial and it is rather involved to identify fixed points in this system. By numerical iteration, starting from suitable seed values for the couplings, we identified a number of interesting fixed points for $N_\mathrm{L} \in \{3, 4, 5\}$ as a function of the squared gauge coupling g^2 which we use as an external parameter here. Analytical understanding, of course, is eligible and investigations on the underlying fixed-point mechanisms still go on. Therefore, we refer to our work in preparation [121]. As an example we discuss the system for $N_\mathrm{L} = 3$. Further results for $N_\mathrm{L} \in \{4, 5\}$ are given in App. D. At $N_\mathrm{L} = 3$ we observe two fixed points at small values of $g^2 = 0$, see Fig. 4.6. The truncation used here is a NLO derivative expansion with an effective potential up to 6th order in $\tilde{\rho}$. One of the fixed points (red circles in Fig. 4.6) is clearly emerging from the limiting case of the Gaußian fixed point (GFP) at $g^2 = 0$. The corresponding non-Gaußian fixed point values at $g^2 \neq 0$ can be understood as a trivial generalization of the GFP due to the influence of the gauge bosons and are not true NGFPs. The second fixed point (blue circles in Fig. 4.6), however, does not emerge from the GFP in the limit of vanishing gauge coupling, as the fixed-point value κ_* diverges. Note, that the corresponding (blue) fixed-point values for h_*^2 and λ_* do not vanish for $g^2 \neq 0$, cf. Fig. 4.10.

We show the fixed-point values of the anomalous dimensions in Fig. 4.7. They are compatible with the requirement that their magnitude should be $\lesssim 1$ for the generalization of the GFP (red circles) as well as for the conjectured NGFP (blue circles) and confirm the reliability of the derivative expansion. The conjecture that the second fixed point is a real NGFP is further substantiated by the real parts of its RG eigenvalues that run

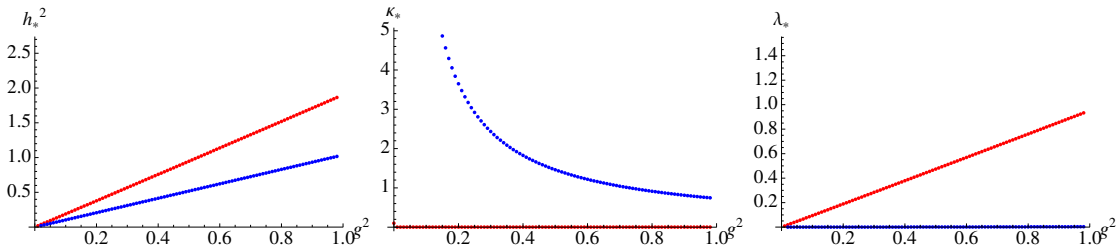

Figure 4.6: Fixed points for $N_{\rm L} = 3$ at NLO with u up to 6th order in ρ.

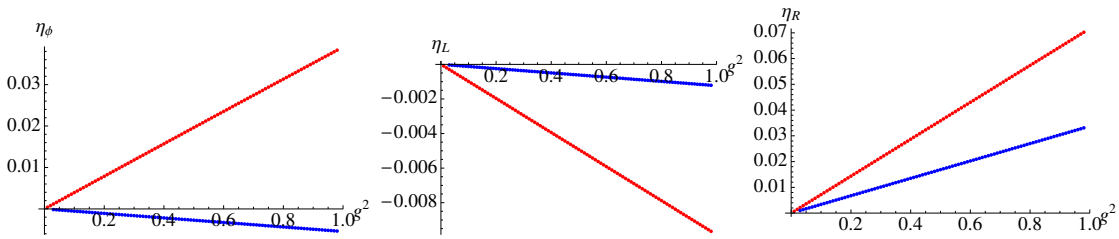

Figure 4.7: Fixed-point anomalous dimensions for $N_{\rm L} = 3$.

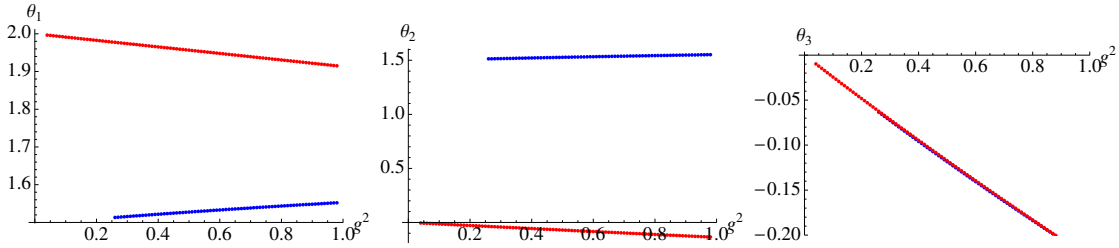

Figure 4.8: Real parts of the RG eigenvalues for $N_{\rm L} = 3$.

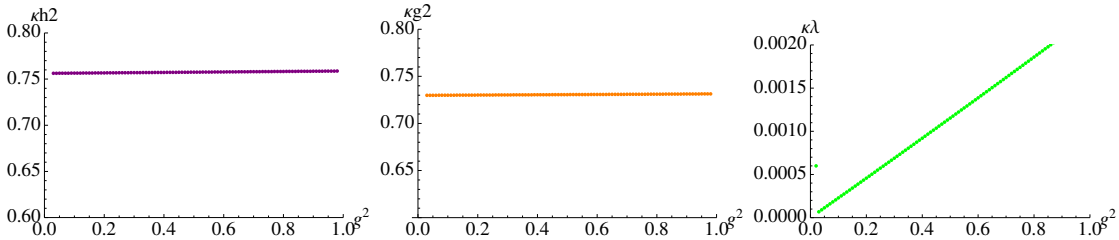

Figure 4.9: Masses for $N_{\rm L} = 3$ at NLO with u up to 6th order in ρ.

towards 1.5 for $\theta_{1,2}$ for $g^2 \to 0$ and not towards its canonical power counting values 2 and 0, see blue circles in Fig. 4.8.

In Fig. 4.9 we show the products of the fixed-point values $\kappa_* h_*^2$, $\kappa_* g^2$ and $\kappa_* \lambda_*$ as a function of the squared gauge coupling g^2. These products represent the dimensionless masses of the top quark, gauge boson and the Higgs boson respectively and we see that they remain constant as $g^2 \to 0$.

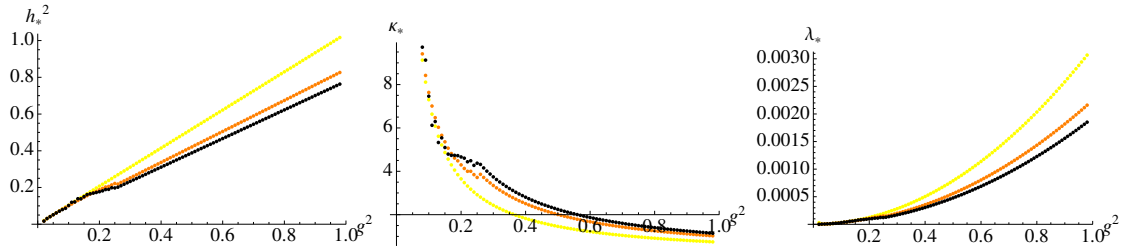

Figure 4.10: Convergence of NPFP values for $N_{\mathrm{L}} = 3$ at NLO with u up to 2nd, 4th and 6th order in ρ.

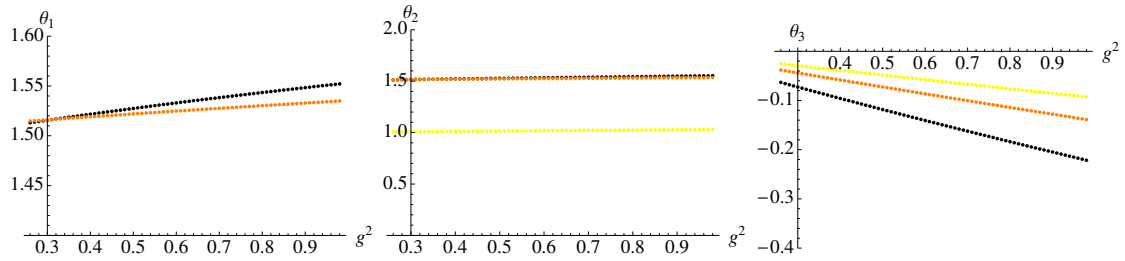

Figure 4.11: Convergence of the NGFP RG eigenvalues for $N_{\mathrm{L}} = 3$ at NLO with u up to 2nd, 4th and 6th order in ρ.

It is important to check the convergence of the fixed-point solution for the NGFP (blue circles in previous Figs.) in order to establish the reliability of our results. In Fig. 4.10 we show the fixed-point values for the lowest order couplings in three different approximation schemes, namely a NLO derivative expansion with an effective potential up to 2nd (yellow circles), 4th (orange circles) and 6th (black circles) order in $\tilde{\rho}$. In Fig. 4.11 we plot the same analysis for the RG eigenvalues of the NGFP.

The same plots for $N_{\mathrm{L}} \in \{4, 5\}$ are given in App. D. They show a similar behavior as discussed here. The observation of NGFPs in this system is very encouraging for a possible asymptotic safety scenario for the standard model. However, the results presented here are still of a preliminary nature and a careful analytical analysis should be done to understand the model and the underlying fixed-point structure. Indeed, the fact that the Higgs and the gauge boson mass remain constant in the limit $g^2 \to 0$ indicates that also an analytical treatment should be possible, potentially revealing a genuine fixed-point mechanism. Work in this direction is under way [121].

Chapter 5

Chiral fermion models in three dimensions

Critical phenomena of statistical physics systems in lower dimensions offer the possiblity for quantitative comparisons between field-theoretical methods, e.g. by computation of critical exponents of second-order phase transitions.

In this chapter we aim at a construction of a statistical-physics model which has structural similarities to the Higgs-Yukawa sector in the standard model: A chiral four-fermion model with a $\mathrm{U}(N_\mathrm{L})_\mathrm{L} \times \mathrm{U}(1)_\mathrm{R}$ symmetry. We are motivated by the fact that a profound understanding of electroweak symmetry breaking or alternative scenarios may require a quantitative control of fluctuating chiral fermions and bosons beyond perturbation theory. In fact, relativistic fermionic models such as the Gross-Neveu model in three dimensions are known to exhibit a second-order phase transition; corresponding studies of the critical behavior have been performed by various methods, e.g. [66, 122–126]. It is also worth a remark that those models are sometimes referred to as a paradigm example for an asymptotically safe theory [91]

In contrast to the two previous chapters we do not aim at a fundamental theory here but at the description of effective quantum fields at and near criticality. In particular, we understand the boson fields as being composed out of the fermion fields whereas in Chaps. 3 and 4 the boson fields were supposed to be fundamental quantum fields.

In the past, $d = 3$ dimensional fermionic systems with left/right symmetric chiral symmetries such as QED_3 or the Thirring model have been under investigation in a variety of scenarios [127–136] with applications to condensed-matter physics, high-T_c cuprate superconductors [137, 138] and, recently, graphene [139, 140]. In some of these models, the number of fermion flavors serves as a control parameter for a quantum phase transition. As the critical number of fermions is an important quantity, nonperturbative information about these models for varying flavor number N_f is required. Since chiral fermions

for arbitrary N_f still represent a challenge, e.g., for lattice simulations, other powerful nonperturbative techniques are urgently needed.

After a classification of possible fermionic models, we concentrate on strong correlations in a scalar parity-conserving channel. We analyze this effective Yukawa model in Sec. 5.2 in a derivative expansion.

The resulting models and quantitative findings constitute and characterize a new set of universality classes, classified by the chiral symmetry content. In particular, we provide for quantitative predictions for the critical exponents for these universality classes which have not been investigated with any other method so far. We believe that these can serve as a first benchmark for other nonperturbative methods which are urgently needed for a study of chiral phase transitions in systems of strongly correlated chiral fermions.

5.1 Classical action and symmetry transformations

Let us first consider a general fermionic model in $d = 2{+}1$ Euclidean dimensions with local quartic self-interaction, being invariant under chiral $\mathrm{U}(N_\mathrm{L})_\mathrm{L} \otimes \mathrm{U}(N_\mathrm{R})_\mathrm{R}$ transformations. The Dirac algebra

$$\{\gamma_\mu, \gamma_\nu\} = 2\delta_{\mu\nu}, \tag{5.1}$$

could minimally be realized by an irreducible representation in terms of 2×2 matrices. As this representation does not permit a chiral symmetry, the massless theory could not be separated from the massive theory by an order-disorder transition. We therefore work exclusively with a 4×4 *reducible* representation of the Dirac algebra,

$$\gamma_\mu = \begin{pmatrix} 0 & -\mathrm{i}\sigma_\mu \\ \mathrm{i}\sigma_\mu & 0 \end{pmatrix}, \quad \mu = 1, 2, 3, \tag{5.2}$$

with $\{\sigma_1, \sigma_2, \sigma_3\}$ being the 2×2 Pauli matrices. Such models have extensively been studied in a variety of applications, see e.g. [141] for a review. There are now *two* other 4×4 matrices which anticommute with all γ_μ as well as with each other,

$$\gamma_4 = \begin{pmatrix} 0 & \mathbb{1} \\ \mathbb{1} & 0 \end{pmatrix} \quad \text{and} \quad \gamma_5 = \gamma_1\gamma_2\gamma_3\gamma_4 = \begin{pmatrix} \mathbb{1} & 0 \\ 0 & -\mathbb{1} \end{pmatrix}. \tag{5.3}$$

Together with

$$\mathbb{1},\ \sigma_{\mu\nu} := \frac{\mathrm{i}}{2}[\gamma_\mu, \gamma_\nu] \quad (\mu < \nu), \tag{5.4}$$

$$\mathrm{i}\gamma_\mu\gamma_4,\ \mathrm{i}\gamma_\mu\gamma_5,\ \mathrm{i}\gamma_4\gamma_5, \tag{5.5}$$

these 16 matrices form a complete basis of the 4×4 Dirac algebra,

$$\{\gamma_A\}_{A=1,\ldots,16} = \{\mathbb{1}, \gamma_\mu, \gamma_4, \sigma_{\mu\nu}, \mathrm{i}\gamma_\mu\gamma_4, \mathrm{i}\gamma_\mu\gamma_5, \mathrm{i}\gamma_4\gamma_5, \gamma_5\}\,. \tag{5.6}$$

We define chiral projectors $P_{\mathrm{L/R}} = \frac{1}{2}(\mathbb{1} \pm \gamma_5)$ that allow us to decompose a Dirac fermion ψ into the left- and right-handed Weyl spinors $\psi_{\mathrm{L/R}} = P_{\mathrm{L/R}}\psi$ and $\bar{\psi}_{\mathrm{L/R}} = \bar{\psi}P_{\mathrm{R/L}}$, where ψ and $\bar{\psi}$ are considered as independent field variables in our Euclidean formulation. Note that there is a certain freedom of choice of the notion of chirality here: we could have chosen just as well $\tilde{P}_{\mathrm{L/R}} = (\mathbb{1} \pm \gamma_4)/2$ or $\hat{P}_{\mathrm{L/R}} = (\mathbb{1} \pm \mathrm{i}\gamma_4\gamma_5)/2$ as chiral projectors. This would have led us to different definitions of the decomposition into Weyl spinors. All these chiralities remain conserved under Lorentz transformations since all three projectors commute with the generators of the Lorentz transformation of the Dirac spinors, $[\gamma_5, \sigma_{\mu\nu}] = [\gamma_4, \sigma_{\mu\nu}] = [\mathrm{i}\gamma_4\gamma_5, \sigma_{\mu\nu}] = 0$.

Continuous symmetries

We consider N_{R} right-handed and N_{L} left-handed fermions, where N_{R} and N_{L} do not have to be identical. We impose a chiral $\mathrm{U}(N_{\mathrm{L}})_{\mathrm{L}} \otimes \mathrm{U}(N_{\mathrm{R}})_{\mathrm{R}}$ symmetry with corresponding field transformations which act independently on left- and right-handed spinors,

$$\mathrm{U}(N_{\mathrm{L}})_{\mathrm{L}}: \quad \psi^a_{\mathrm{L}} \mapsto U^{ab}_{\mathrm{L}}\psi^b_{\mathrm{L}}, \quad \bar{\psi}^a_{\mathrm{L}} \mapsto \bar{\psi}^b_{\mathrm{L}}(U^\dagger_{\mathrm{L}})^{ba}, \tag{5.7}$$

$$\mathrm{U}(N_{\mathrm{R}})_{\mathrm{R}}: \quad \psi^a_{\mathrm{R}} \mapsto U^{ab}_{\mathrm{R}}\psi^b_{\mathrm{R}}, \quad \bar{\psi}^a_{\mathrm{R}} \mapsto \bar{\psi}^b_{\mathrm{R}}(U^\dagger_{\mathrm{R}})^{ba}. \tag{5.8}$$

Here, U_{L} and U_{R} are unitary $N_{\mathrm{L}} \times N_{\mathrm{L}}$ and $N_{\mathrm{R}} \times N_{\mathrm{R}}$ matrices, respectively. For $U^{ab}_{\mathrm{L}} = \mathrm{e}^{\mathrm{i}\alpha}\,\delta^{ab}$ and $U^{ab}_{\mathrm{R}} = \mathrm{e}^{-\mathrm{i}\alpha}\,\delta^{ab}$ we obtain the usual $\mathrm{U}(1)_{\mathrm{A}}$ axial transformations, whereas for $U^{ab}_{\mathrm{L}} = \mathrm{e}^{\mathrm{i}\alpha}\,\delta^{ab}$ and $U^{ab}_{\mathrm{R}} = \mathrm{e}^{\mathrm{i}\alpha}\,\delta^{ab}$ we get $\mathrm{U}(1)_{\mathrm{V}}$ phase rotations. Thus, the symmetry is

$$\mathrm{U}(N_{\mathrm{L}})_{\mathrm{L}} \otimes \mathrm{U}(N_{\mathrm{R}})_{\mathrm{R}} \cong \mathrm{SU}(N_{\mathrm{L}})_{\mathrm{L}} \otimes \mathrm{SU}(N_{\mathrm{R}})_{\mathrm{R}} \otimes \mathrm{U}(1)_{\mathrm{A}} \otimes \mathrm{U}(1)_{\mathrm{V}}, \tag{5.9}$$

with chiral $\mathrm{SU}(N_{\mathrm{L,R}})$ factors.

Discrete symmetries

Due to the reducible representation of the Dirac algebra, there is also some freedom in the definition of the discrete transformations [132, 133]. Charge conjugation may be implemented by either

$$\mathcal{C}:\ \psi^a_{\mathrm{L/R}} \mapsto \left(\bar{\psi}^a_{\mathrm{L/R}}C\right)^T,\ \bar{\psi}^a_{\mathrm{L/R}} \mapsto -\left(C^\dagger\psi^a_{\mathrm{L/R}}\right)^T, \tag{5.10}$$

with $C = \gamma_2\gamma_5$, or

$$\tilde{\mathcal{C}} : \psi^a_{\mathrm{L/R}} \mapsto \left(\bar{\psi}^a_{\mathrm{R/L}}\tilde{C}\right)^T, \bar{\psi}^a_{\mathrm{L/R}} \mapsto -\left(\tilde{C}^\dagger\psi^a_{\mathrm{R/L}}\right)^T, \tag{5.11}$$

with $\tilde{C} = \gamma_2\gamma_4$, or a unitary combination thereof. In the same manner, the parity transformation corresponding to

$$(x_1, x_2, x_3) \mapsto (-x_1, x_2, x_3) =: \tilde{x}, \tag{5.12}$$

with (x_1, x_2) as space coordinates and x_3 as the (Euclidean) time coordinate, may be implemented by either

$$\mathcal{P} : \psi^a_{\mathrm{L/R}}(x) \mapsto P\psi^a_{\mathrm{L/R}}(\tilde{x}), \bar{\psi}^a_{\mathrm{L/R}}(x) \mapsto \bar{\psi}^a_{\mathrm{L/R}}(\tilde{x})P^\dagger, \tag{5.13}$$

with $P = \gamma_1\gamma_4$, or

$$\tilde{\mathcal{P}} : \psi^a_{\mathrm{L/R}}(x) \mapsto \tilde{P}\psi^a_{\mathrm{R/L}}(\tilde{x}), \bar{\psi}^a_{\mathrm{L/R}}(x) \mapsto \bar{\psi}^a_{\mathrm{R/L}}(\tilde{x})\tilde{P}^\dagger, \tag{5.14}$$

with $\tilde{P} = \gamma_1\gamma_5$. Similarly, time reversal corresponding to

$$(x_1, x_2, x_3) \mapsto (x_1, x_2, -x_3) =: \hat{x} \tag{5.15}$$

reads either

$$\mathcal{T} : \psi^a_{\mathrm{L/R}}(x) \mapsto T\psi^a_{\mathrm{L/R}}(\hat{x}), \bar{\psi}^a_{\mathrm{L/R}}(x) \mapsto \bar{\psi}^a_{\mathrm{L/R}}(\hat{x})T^\dagger, \tag{5.16}$$

with $T = \gamma_2\gamma_3$, or

$$\tilde{\mathcal{T}} : \psi^a_{\mathrm{L/R}}(x) \mapsto \tilde{T}\psi^a_{\mathrm{R/L}}(\hat{x}), \bar{\psi}^a_{\mathrm{L/R}}(x) \mapsto \bar{\psi}^a_{\mathrm{R/L}}(\hat{x})\tilde{T}^\dagger, \tag{5.17}$$

with $\tilde{T} = \gamma_1$. Note that every matrix $\in \{C, \tilde{C}, P, \tilde{P}, T, \tilde{T}\}$ is unitary, such that charge conjugation and parity inversion are unitary, and time reversal is anti-unitary.

In order to derive the explicit transformation properties of the bilinears, it is useful to recall that γ_1 and γ_3 are antisymmetric and purely imaginary, whereas γ_2, γ_4, and γ_5 are symmetric and real. The results are listed in Table 5.1, where we have introduced

$$\tilde{\gamma}_\mu := (-\gamma_1, \gamma_2, \gamma_3)_\mu, \tag{5.18}$$

$$(\tilde{\sigma}_{12}, \tilde{\sigma}_{13}, \tilde{\sigma}_{23}) := (-\sigma_{12}, -\sigma_{13}, \sigma_{23}), \tag{5.19}$$

$$\hat{\gamma}_\mu := (\gamma_1, \gamma_2, -\gamma_3)_\mu, \tag{5.20}$$

$$(\hat{\sigma}_{12}, \hat{\sigma}_{13}, \hat{\sigma}_{23}) := (\sigma_{12}, -\sigma_{13}, -\sigma_{23}). \tag{5.21}$$

	$\mathcal{C}$	$\tilde{\mathcal{C}}$	$\mathcal{P}$	$\tilde{\mathcal{P}}$	$\mathcal{T}$	$\tilde{\mathcal{T}}$
$\bar{\psi}^a_{\mathrm{L}}\psi^b_{\mathrm{R}}$	$\bar{\psi}^b_{\mathrm{R}}\psi^a_{\mathrm{L}}$	$\bar{\psi}^b_{\mathrm{L}}\psi^a_{\mathrm{R}}$	$\bar{\psi}^a_{\mathrm{L}}\psi^b_{\mathrm{R}}$	$\bar{\psi}^a_{\mathrm{R}}\psi^b_{\mathrm{L}}$	$\bar{\psi}^a_{\mathrm{L}}\psi^b_{\mathrm{R}}$	$\bar{\psi}^a_{\mathrm{R}}\psi^b_{\mathrm{L}}$
$\bar{\psi}^a_{\mathrm{L}}\gamma_\mu\psi^b_{\mathrm{L}}$	$-\bar{\psi}^b_{\mathrm{L}}\gamma_\mu\psi^a_{\mathrm{L}}$	$-\bar{\psi}^b_{\mathrm{R}}\gamma_\mu\psi^a_{\mathrm{R}}$	$\bar{\psi}^a_{\mathrm{L}}\tilde{\gamma}_\mu\psi^b_{\mathrm{L}}$	$\bar{\psi}^a_{\mathrm{R}}\tilde{\gamma}_\mu\psi^b_{\mathrm{R}}$	$-\bar{\psi}^a_{\mathrm{L}}\hat{\gamma}_\mu\psi^b_{\mathrm{L}}$	$-\bar{\psi}^a_{\mathrm{R}}\hat{\gamma}_\mu\psi^b_{\mathrm{R}}$
$\bar{\psi}^a_{\mathrm{L}}\sigma_{\mu\nu}\psi^b_{\mathrm{R}}$	$-\bar{\psi}^b_{\mathrm{R}}\sigma_{\mu\nu}\psi^a_{\mathrm{L}}$	$-\bar{\psi}^b_{\mathrm{L}}\sigma_{\mu\nu}\psi^a_{\mathrm{R}}$	$\bar{\psi}^a_{\mathrm{L}}\tilde{\sigma}_{\mu\nu}\psi^b_{\mathrm{R}}$	$\bar{\psi}^a_{\mathrm{R}}\tilde{\sigma}_{\mu\nu}\psi^b_{\mathrm{L}}$	$-\bar{\psi}^a_{\mathrm{L}}\hat{\sigma}_{\mu\nu}\psi^b_{\mathrm{R}}$	$-\bar{\psi}^a_{\mathrm{R}}\hat{\sigma}_{\mu\nu}\psi^b_{\mathrm{L}}$
$\bar{\psi}^a_{\mathrm{L}}\gamma_4\psi^b_{\mathrm{L}}$	$\bar{\psi}^b_{\mathrm{L}}\gamma_4\psi^a_{\mathrm{L}}$	$-\bar{\psi}^b_{\mathrm{R}}\gamma_4\psi^a_{\mathrm{R}}$	$-\bar{\psi}^a_{\mathrm{L}}\gamma_4\psi^b_{\mathrm{L}}$	$\bar{\psi}^a_{\mathrm{R}}\gamma_4\psi^b_{\mathrm{R}}$	$\bar{\psi}^a_{\mathrm{L}}\gamma_4\psi^b_{\mathrm{L}}$	$-\bar{\psi}^a_{\mathrm{R}}\gamma_4\psi^b_{\mathrm{R}}$
$\bar{\psi}^a_{\mathrm{L}}\mathrm{i}\gamma_\mu\gamma_4\psi^b_{\mathrm{R}}$	$\bar{\psi}^b_{\mathrm{R}}\mathrm{i}\gamma_\mu\gamma_4\psi^a_{\mathrm{L}}$	$-\bar{\psi}^b_{\mathrm{L}}\mathrm{i}\gamma_\mu\gamma_4\psi^a_{\mathrm{R}}$	$-\bar{\psi}^a_{\mathrm{L}}\mathrm{i}\tilde{\gamma}_\mu\gamma_4\psi^b_{\mathrm{R}}$	$\bar{\psi}^a_{\mathrm{R}}\mathrm{i}\tilde{\gamma}_\mu\gamma_4\psi^b_{\mathrm{L}}$	$\bar{\psi}^a_{\mathrm{L}}\mathrm{i}\hat{\gamma}_\mu\gamma_4\psi^b_{\mathrm{R}}$	$-\bar{\psi}^a_{\mathrm{R}}\mathrm{i}\hat{\gamma}_\mu\gamma_4\psi^b_{\mathrm{L}}$

Table 5.1: Properties of fermion bilinears under discrete transformations. The arguments of the transformed fields are $\tilde{x} = (-x_1, x_2, x_3)$ in the case of parity and $\hat{x} = (x_1, x_2, -x_3)$ in the case of time reversal. The bilinears with $(\mathrm{L} \leftrightarrow \mathrm{R})$ transform analogously.

Field bilinears and 4-fermi terms

The transformation properties with respect to the discrete symmetries facilitate a discussion of possible bilinears and 4-fermi terms in the action of our model. In addition to Lorentz invariance, we impose an invariance of our theory under $\mathrm{U}(N_{\mathrm{L}})_{\mathrm{L}} \otimes \mathrm{U}(N_{\mathrm{R}})_{\mathrm{R}}$ chiral transformations, $\mathcal{C}$ charge conjugation, $\mathcal{P}$ parity inversion, and $\mathcal{T}$ time reversal. The theory then automatically is also invariant under $\tilde{\mathcal{C}}\tilde{\mathcal{P}}$, $\tilde{\mathcal{P}}\tilde{\mathcal{T}}$, and $\tilde{\mathcal{C}}\tilde{\mathcal{T}}$ transformations, since $\tilde{\mathcal{C}}\tilde{\mathcal{P}} = \mathcal{C}\mathcal{P}$, $\tilde{\mathcal{P}}\tilde{\mathcal{T}} = \mathcal{P}\mathcal{T}$, and $\tilde{\mathcal{C}}\tilde{\mathcal{T}} = \mathcal{C}\mathcal{T}$. (The equivalence holds up to $\mathrm{U}(1)_{\mathrm{V}}$ phase rotations of the spinors.) As a consequence, no bilinears to zeroth order in derivatives are permitted. To first order, only the standard chiral kinetic terms

$$\bar{\psi}^a_{\mathrm{L}}\mathrm{i}\partial_\mu\gamma_\mu\psi^a_{\mathrm{L}} \quad \text{and} \quad \bar{\psi}^a_{\mathrm{R}}\mathrm{i}\partial_\mu\gamma_\mu\psi^a_{\mathrm{R}} \tag{5.22}$$

can appear. In particular, all possible mass terms are excluded by symmetry: $\bar{\psi}^a_{\mathrm{L}}\psi^a_{\mathrm{R}}$ and $\bar{\psi}^a_{\mathrm{R}}\psi^a_{\mathrm{L}}$ are not chirally symmetric, and $\bar{\psi}^a_{\mathrm{L}}\gamma_4\psi^a_{\mathrm{L}}$ as well as $\bar{\psi}^a_{\mathrm{R}}\gamma_4\psi^a_{\mathrm{R}}$ are not invariant under $\mathcal{P}$ parity transformations. The same holds for terms involving $\mathrm{i}\gamma_4\gamma_5$. On the level of 4-fermi operators, the interaction terms must have the form

$$\left(\bar{\psi}^a_{\mathrm{L}}\gamma_A\psi^b_{\mathrm{L}}\right)\left(\bar{\psi}^b_{\mathrm{L}}\gamma_A\psi^a_{\mathrm{L}}\right), \quad \left(\bar{\psi}^a_{\mathrm{R}}\gamma_A\psi^b_{\mathrm{R}}\right)\left(\bar{\psi}^b_{\mathrm{R}}\gamma_A\psi^a_{\mathrm{R}}\right) \quad \text{with} \quad \gamma_A \in \{\gamma_\mu, \gamma_4\}, \tag{5.23}$$

$$\left(\bar{\psi}^a_{\mathrm{L}}\gamma_B\psi^b_{\mathrm{R}}\right)\left(\bar{\psi}^b_{\mathrm{R}}\gamma_B\psi^a_{\mathrm{L}}\right) \quad \text{with} \quad \gamma_B \in \{\mathbb{1}, \mathrm{i}\gamma_\mu\gamma_4\}, \tag{5.24}$$

or, with inverse flavor structure,

$$\left(\bar{\psi}^a_{\mathrm{L}}\gamma_A\psi^a_{\mathrm{L}}\right)\left(\bar{\psi}^b_{\mathrm{L}}\gamma_A\psi^b_{\mathrm{L}}\right), \quad \left(\bar{\psi}^a_{\mathrm{R}}\gamma_A\psi^a_{\mathrm{R}}\right)\left(\bar{\psi}^b_{\mathrm{R}}\gamma_A\psi^b_{\mathrm{R}}\right), \quad \left(\bar{\psi}^a_{\mathrm{R}}\gamma_A\psi^a_{\mathrm{R}}\right)\left(\bar{\psi}^b_{\mathrm{L}}\gamma_A\psi^b_{\mathrm{L}}\right). \tag{5.25}$$

Terms with $\gamma_A \in \{\mathrm{i}\gamma_\mu\gamma_5, \mathrm{i}\gamma_4\gamma_5\}$ or $\gamma_B \in \{\gamma_5, \sigma_{\mu\nu}\}$ are equal to these up to a possible sign, since ψ_{L} and ψ_{R} are eigenvectors of γ_5, and $\sigma_{\mu\nu} = -\mathrm{i}\epsilon_{\mu\nu\rho}\gamma_\rho\gamma_4\gamma_5$. Terms with $\gamma_A \in \{\mathbb{1}, \gamma_5, \mathrm{i}\gamma_\mu\gamma_4, \sigma_{\mu\nu}\}$ or $\gamma_B \in \{\gamma_\mu, \mathrm{i}\gamma_\mu\gamma_5, \gamma_4, \mathrm{i}\gamma_4\gamma_5\}$ are identically zero, as $P_{\mathrm{R}}P_{\mathrm{L}} = P_{\mathrm{L}}P_{\mathrm{R}} = 0$.

Fierz transformations

The terms in Eq. (5.25) are not independent of the terms in Eqs. (5.23), (5.24), but are related by Fierz transformations:

$$\left(\bar{\psi}^a_{\mathrm{L}}\gamma_\mu\psi^a_{\mathrm{L}}\right)\left(\bar{\psi}^b_{\mathrm{L}}\gamma_\mu\psi^b_{\mathrm{L}}\right) = \frac{1}{2}\left(\bar{\psi}^a_{\mathrm{L}}\gamma_\mu\psi^b_{\mathrm{L}}\right)\left(\bar{\psi}^b_{\mathrm{L}}\gamma_\mu\psi^a_{\mathrm{L}}\right) + \frac{3}{2}\left(\bar{\psi}^a_{\mathrm{L}}\gamma_4\psi^b_{\mathrm{L}}\right)\left(\bar{\psi}^b_{\mathrm{L}}\gamma_4\psi^a_{\mathrm{L}}\right), \tag{5.26}$$

$$\left(\bar{\psi}^a_{\mathrm{L}}\gamma_4\psi^a_{\mathrm{L}}\right)\left(\bar{\psi}^b_{\mathrm{L}}\gamma_4\psi^b_{\mathrm{L}}\right) = \frac{1}{2}\left(\bar{\psi}^a_{\mathrm{L}}\gamma_\mu\psi^b_{\mathrm{L}}\right)\left(\bar{\psi}^b_{\mathrm{L}}\gamma_\mu\psi^a_{\mathrm{L}}\right) - \frac{1}{2}\left(\bar{\psi}^a_{\mathrm{L}}\gamma_4\psi^b_{\mathrm{L}}\right)\left(\bar{\psi}^b_{\mathrm{L}}\gamma_4\psi^a_{\mathrm{L}}\right), \tag{5.27}$$

$$\left(\bar{\psi}^a_{\mathrm{R}}\gamma_\mu\psi^a_{\mathrm{R}}\right)\left(\bar{\psi}^b_{\mathrm{L}}\gamma_\mu\psi^b_{\mathrm{L}}\right) = -\frac{3}{2}\left(\bar{\psi}^a_{\mathrm{R}}\psi^b_{\mathrm{L}}\right)\left(\bar{\psi}^b_{\mathrm{L}}\psi^a_{\mathrm{R}}\right) - \frac{1}{2}\left(\bar{\psi}^a_{\mathrm{R}}\mathrm{i}\gamma_\mu\gamma_4\psi^b_{\mathrm{L}}\right)\left(\bar{\psi}^b_{\mathrm{L}}\mathrm{i}\gamma_\mu\gamma_4\psi^a_{\mathrm{R}}\right), \tag{5.28}$$

$$\left(\bar{\psi}^a_{\mathrm{R}}\gamma_4\psi^a_{\mathrm{R}}\right)\left(\bar{\psi}^b_{\mathrm{L}}\gamma_4\psi^b_{\mathrm{L}}\right) = -\frac{1}{2}\left(\bar{\psi}^a_{\mathrm{R}}\psi^b_{\mathrm{L}}\right)\left(\bar{\psi}^b_{\mathrm{L}}\psi^a_{\mathrm{R}}\right) + \frac{1}{2}\left(\bar{\psi}^a_{\mathrm{R}}\mathrm{i}\gamma_\mu\gamma_4\psi^b_{\mathrm{L}}\right)\left(\bar{\psi}^b_{\mathrm{L}}\mathrm{i}\gamma_\mu\gamma_4\psi^a_{\mathrm{R}}\right). \tag{5.29}$$

Here, we have suppressed the analogous equations with $(\mathrm{L}\leftrightarrow\mathrm{R})$ for simplicity. We thus end up with six independent 4-fermi terms preserving $\mathrm{U}(N_{\mathrm{L}})_{\mathrm{L}}\otimes\mathrm{U}(N_{\mathrm{R}})_{\mathrm{R}}$ chiral and $\mathcal{C}$, $\mathcal{P}$, and $\mathcal{T}$ symmetry,

$$\left(\bar{\psi}^a_{\mathrm{L}}\psi^b_{\mathrm{R}}\right)\left(\bar{\psi}^b_{\mathrm{R}}\psi^a_{\mathrm{L}}\right), \tag{5.30}$$

$$\left(\bar{\psi}^a_{\mathrm{L}}\gamma_4\psi^b_{\mathrm{L}}\right)\left(\bar{\psi}^b_{\mathrm{L}}\gamma_4\psi^a_{\mathrm{L}}\right), \quad \left(\bar{\psi}^a_{\mathrm{R}}\gamma_4\psi^b_{\mathrm{R}}\right)\left(\bar{\psi}^b_{\mathrm{R}}\gamma_4\psi^a_{\mathrm{R}}\right), \tag{5.31}$$

$$\left(\bar{\psi}^a_{\mathrm{L}}\gamma_\mu\psi^b_{\mathrm{L}}\right)\left(\bar{\psi}^b_{\mathrm{L}}\gamma_\mu\psi^a_{\mathrm{L}}\right), \quad \left(\bar{\psi}^a_{\mathrm{R}}\gamma_\mu\psi^b_{\mathrm{R}}\right)\left(\bar{\psi}^b_{\mathrm{R}}\gamma_\mu\psi^a_{\mathrm{R}}\right), \tag{5.32}$$

$$\left(\bar{\psi}^a_{\mathrm{L}}\mathrm{i}\gamma_\mu\gamma_4\psi^b_{\mathrm{R}}\right)\left(\bar{\psi}^b_{\mathrm{R}}\mathrm{i}\gamma_\mu\gamma_4\psi^a_{\mathrm{L}}\right). \tag{5.33}$$

Note that the corresponding set in $d = 3+1$ dimensions would be smaller as the γ_4 terms would be constrained by a larger Lorentz symmetry.

Up to this point our classification is very general to this point and also includes, e.g., the NJL and the Thirring model.

Partial bosonization

In a (partially) bosonized language after a Hubbard-Stratonovich transformation, we encounter six boson-fermion interactions: The first one corresponding to Eq. (5.30) couples the fermions to a scalar boson (scalar with respect to $\mathcal{P}$ parity), the second and the third (5.31) to a pseudo-scalar boson, the fourth and the fifth (5.32) to a vector boson, and the sixth (5.33) to a pseudo-vector boson. Further bosonic structures in the flavor-singlet channels appear in the corresponding Fierz transforms of Eqs. (5.30)-(5.33).

We expect that a general model based on these interactions exhibits a rich phase structure, being controlled by the relative strength of the various interaction channels. Aiming at an analogue of the electroweak phase transition, we focus in this work on the $\mathcal{P}$ parity-conserving and Lorentz-invariant condensation channel, parameterized in terms of the first interaction term. This channel is also invariant under time reversal $\mathcal{T}$, whereas the boson transforms into its complex conjugate under charge conjugation $\mathcal{C}$. Moreover,

we confine ourselves to the case of $N_{\mathrm{R}} = 1$ right-handed fermion flavor and $N_{\mathrm{L}} \geq 1$ left-handed fermion flavors. The microscopic action of our model in the purely fermionic language then reads

$$S_{\text{4-fermi}} = \int \mathrm{d}^3x \big\{ \bar{\psi}^a_{\mathrm{L}} \mathrm{i}\partial\!\!\!/ \psi^a_{\mathrm{L}} + \bar{\psi}_{\mathrm{R}} \mathrm{i}\partial\!\!\!/ \psi_{\mathrm{R}} + 2\lambda \left(\bar{\psi}^a_{\mathrm{L}} \psi_{\mathrm{R}}\right) \left(\bar{\psi}_{\mathrm{R}} \psi^a_{\mathrm{L}}\right) \big\}. \tag{5.34}$$

Via Hubbard-Stratonovich transformation, we obtain the equivalent Yukawa action

$$S_{\mathrm{Yuk}} = \int \mathrm{d}^3x \big\{ \frac{1}{2\lambda} \phi^{a\dagger} \phi^a + \bar{\psi}^a_{\mathrm{L}} \mathrm{i}\partial\!\!\!/ \psi^a_{\mathrm{L}} + \bar{\psi}_{\mathrm{R}} \mathrm{i}\partial\!\!\!/ \psi_{\mathrm{R}} + \phi^{a\dagger} \bar{\psi}_{\mathrm{R}} \psi^a_{\mathrm{L}} - \phi^a \bar{\psi}^a_{\mathrm{L}} \psi_{\mathrm{R}} \big\}, \tag{5.35}$$

where the complex scalar ϕ^a serves as an auxiliary field. The purely fermionic model can be recovered by use of the algebraic equations of motion for ϕ^a and $\phi^{a\dagger}$: $\phi^a = -2\lambda \bar{\psi}_{\mathrm{R}} \psi^a_{\mathrm{L}}$ and $\phi^{a\dagger} = 2\lambda \bar{\psi}^a_{\mathrm{L}} \psi_{\mathrm{R}}$. Here, we can read off the transformation properties of the scalar field under the chiral symmetry,

$$\phi^a \mapsto U^{ab}_{\mathrm{L}} \phi^b U^\dagger_{\mathrm{R}}, \quad \phi^{a\dagger} \mapsto U_{\mathrm{R}} \phi^{b\dagger} (U^\dagger_{\mathrm{L}})^{ba}. \tag{5.36}$$

The composite scalar field ϕ^a represents an order parameter for an order-disorder transition. As long as ϕ^a has a vanishing expectation value, the system is in the symmetric phase with full chiral $\mathrm{U}(N_{\mathrm{L}})_{\mathrm{L}} \times \mathrm{U}(1)_{\mathrm{R}}$ symmetry; the fermions are massless, whereas the scalars are generically massive as determined by the symmetry-preserving effective potential for the scalars. If ϕ^a acquires a vacuum expectation value the chiral $\mathrm{SU}(N_{\mathrm{L}})$ factor is broken down to a residual $\mathrm{SU}(N_{\mathrm{L}} - 1)$ symmetry. In addition, the axial $\mathrm{U}(1)_{\mathrm{A}}$ is broken, whereas the charge-conserving vector $\mathrm{U}(1)_{\mathrm{V}}$ is preserved. In the broken phase, the spectrum consists of one massive Dirac fermion, one massive bosonic radial mode, $N_{\mathrm{L}} - 1$ massless left-handed Weyl fermions and $2N_{\mathrm{L}} - 1$ massless Goldstone bosons.

Near the phase transition we expect the order-parameter fluctuations to dominate the critical behavior of the system. Universality suggests that the degrees of freedom parameterized by the action (5.35) are sufficient to quantify the critical behavior of this transition, independently of the presence of further microscopic fermionic interactions of Eqs. (5.30)-(5.33). Concentrating on the action (5.35), we observe that the purely scalar sector, i.e., the scalar mass term, has a larger symmetry group of $\mathrm{O}(2N_{\mathrm{L}})$-type. It is therefore instructive to compare the critical behavior of our fermionic model with that of a standard scalar $\mathrm{O}(2N_{\mathrm{L}})$ model which is known to undergo a second order phase transition associated with a Wilson-Fisher fixed point. Differences in the corresponding critical behaviors can then fully be attributed to fermionic fluctuations near the phase transition.

5.2 Effective average action and RG flow

We constrain the flow of the action functional to lie in the subspace of the full theory space spanned by the ansatz known from Chap. 4:

$$\Gamma_k = \int_x \Big\{ Z_{\mathrm{L},k}\bar{\psi}^a_{\mathrm{L}}\mathrm{i}\partial\!\!\!/\psi^a_{\mathrm{L}} + Z_{\mathrm{R},k}\bar{\psi}_{\mathrm{R}}\mathrm{i}\partial\!\!\!/\psi_{\mathrm{R}} + Z_{\phi,k}\left(\partial_\mu\phi^{a\dagger}\right)\left(\partial^\mu\phi^a\right) + U_k(\rho) + \bar{h}_k(\bar{\psi}_{\mathrm{R}}\phi^{a\dagger}\psi^a_{\mathrm{L}} - \bar{\psi}^a_{\mathrm{L}}\phi^a\psi_{\mathrm{R}})\Big\}.$$

This represents the next-to-leading order in a systematic derivative expansion of the effective potential in the scalar sector and a leading-order vertex expansion in the fermionic sector. For definitions about the field content, rescalings and the introduction of dimensionless quantities, see section 4.1. As known from the previous chapter the flow of the effective potential is then given by Eq. (4.2). Whereas the flow of the Yukawa coupling is unambiguous in the symmetric regime, the Goldstone and radial modes can generally develop different couplings in the broken regime. Here, we concentrate on the Goldstone-mode Yukawa coupling to the fermions, as the radial mode becomes massive and decouples in the broken regime. The flow of the Yukawa coupling as derived in App. C reads

$$\partial_t h_k^2 = (\eta_\phi + \eta_{\mathrm{L}} + \eta_{\mathrm{R}} + d - 4)h_k^2 - 8v_d h_k^4 \kappa_k u_k'' l_{111}^{(\mathrm{FB})d}(\kappa_k h_k^2, u_k' + 2\kappa_k u_k'', u_k'). \tag{5.37}$$

The flows of the anomalous dimensions w.r.t the Goldstone-mode are (also App. C)

$$\eta_\phi = \frac{16v_d}{d} u_k''^2 \kappa_k m_{22}^d(u_k' + 2\kappa_k u_k'', u_k') + \frac{8v_d d_\gamma}{d}\left[\kappa_k h_k^4 m_2^{(\mathrm{F})d}(\kappa_k h_k^2) + h_k^2 m_4^{(\mathrm{F})d}(\kappa_k h_k^2)\right], \tag{5.38}$$

$$\eta_{\mathrm{L}} = \frac{8v_d}{d} h_k^2 \left[m_{12}^{(\mathrm{FB})d}(h_k^2\kappa_k, u_k' + 2\kappa_k u_k'') + m_{12}^{(\mathrm{FB})d}(h_k^2\kappa_k, u_k')\right], \tag{5.39}$$

$$\eta_{\mathrm{R}} = \frac{8v_d}{d} h_k^2 \left[m_{12}^{(\mathrm{FB})d}(h_k^2\kappa_k, u_k' + 2\kappa_k u_k'') + m_{12}^{(\mathrm{FB})d}(h_k^2\kappa_k, u_k') + 2(N_{\mathrm{L}} - 1)m_{12}^{(\mathrm{FB})d}(0, u_k')\right].$$

5.3 Fixed points and critical exponents

In order to analyze the fixed point structure of this model, we will again distinguish two different regimes the symmetric regime (SYM) and the regime of spontaneously broken symmetry (SSB). As boson and fermion fluctuations generically contribute with opposite sign, the existence of a fixed point requires a balancing between both contributions together with potential dimensional scaling terms (such as, e.g., the first term on the right-hand side of Eq. (5.37)). In three dimensions we observe that this balancing is indeed possible in both regimes, depending on the number of left-handed fermion flavors, as the scalar loop carries a weight $\sim N_{\mathrm{L}}$ and all scalar degrees of freedom can contribute, whereas the left/right asymmetry structure leads to a weight $\sim \mathcal{O}(1)$ for the fermion loops, Fig. 2.4. In the following we analyze the different regimes in detail.

5.3.1 The symmetric regime

Here and in the following, we drop the subscript k indicating the scale dependence of the running couplings for simplicity. We also set $d = 3$ in the flow equations from now on.

In the symmetric regime we employ the usual expansion of the effective potential u, Eq. (3.6). We write down the explicit expression for the Yukawa coupling which in the SYM regime reduces to $\partial_t h^2 = (\eta_\phi + \eta_\mathrm{L} + \eta_\mathrm{R} - 1)h^2$. This tells us that an interacting fixed point ($h \neq 0$) can only occur if

$$\eta_\phi + \eta_\mathrm{L} + \eta_\mathrm{R} = 1. \tag{5.40}$$

Conversely, if a fixed point exists in the SYM regime, the sum rule (5.40) has to be satisfied by the anomalous dimensions. This statement holds exactly in the present truncation but may receive corrections from higher orders. We comment further on the relevance of this sum rule in the conclusions of this chapter. The expressions for the anomalous dimensions $\{\eta_\phi,\ \eta_\mathrm{L},\ \eta_\mathrm{R}\}$ constitute a linear system of equations which can be solved analytically. Its solution expresses the anomalous dimensions in terms of the couplings h^2 and m^2,

$$\eta_\phi = \frac{2h^2(2h^2(N_\mathrm{L}+1) - 15\pi^2(1+m^2)^2)}{h^4(N_\mathrm{L}+1) - 18\pi^4(1+m^2)^2},\ \eta_\mathrm{L} = \frac{h^2(5h^2 - 12\pi^2)}{h^4(N_\mathrm{L}+1) - 18\pi^4(1+m^2)^2},\ \eta_\mathrm{R} = N_\mathrm{L}\eta_\mathrm{L}.$$

These expressions can be plugged into the sum rule (5.40), resulting in a conditional fixed point for h^2 depending on the size of m^2, which reads

$$\begin{aligned} h^2_\mathrm{cond} \;=\; & \frac{3\pi^2}{8(N_\mathrm{L}+1)}\Big\{7 + 5m(2+m) + 2N_\mathrm{L} \\ & -\sqrt{33 + m(2+m)(54 + 25m(2+m)) + 12N_\mathrm{L} + 4m(2+m)N_\mathrm{L} + 4N_\mathrm{L}^2}\Big\}. \end{aligned} \tag{5.41}$$

For another solution with a positive root, we have not been able to identify a true fixed point of the full system by numerical means. Hence, this solution is ignored in the following. The solution with the negative root, however, does give a fixed point and will be analyzed in the following. This solution is positive for all $m^2 > 0$ and monotonously increasing. Its values range from

$$h^2(m^2 = 0) = \frac{3\pi^2}{8}\frac{\left(7 + 2N_\mathrm{L} - \sqrt{33 + 4N_\mathrm{L}(3+N_\mathrm{L})}\right)}{(N_\mathrm{L}+1)},\ \text{to}\quad h^2(m^2 = \infty) = \frac{3\pi^2}{5}, \tag{5.42}$$

which is very convenient because it ensures that the fixed point value for h^2 is bounded from above and from below in a very narrow window for all m^2. A true fixed point of the system requires fixed points for all scalar couplings $(m^2(=\lambda_1), \lambda_2, \lambda_3, ...)$. The flow equation of a coupling λ_n is always a function of the lower order couplings from the effective potential up to λ_{n+1}, i.e. $\partial_t \lambda_n = f_n(h^2, \lambda_1, ..., \lambda_{n+1})$. Inserting the conditional fixed point

N_L	h_*^2	m_*^2	λ_2^*	η_ϕ^*	η_L^*	η_R^*	ν	ω
1	4.496	0.326	5.099	0.716	0.142	0.142	1.132	0.786
2	3.364	0.104	3.643	0.512	0.162	0.325	1.100	0.809

Table 5.2: Fixed-point values and critical exponents in the SYM regime.

for the Yukawa couplings into these flows leaves us with the problem of searching for a scalar fixed-point potential. We solve the fixed-point equations $\partial_t \lambda_n = 0$ approximately by a polynomial expansion of the potential up to some finite order N_p, see Eq. (3.6). Dropping the higher-order couplings $\lambda_{n>N_p} = 0$, the resulting system of fixed-point equations can be solved explicitly. We find suitable fixed-point solutions in the symmetric regime for $N_\mathrm{L} \in \{1, 2\}$. The non-universal fixed-point values as well as the universal values for the anomalous dimensions at the fixed point and the first two critical exponents can be read off from Tab. 5.2. For these results, we have expanded the effective potential up to λ_6 at next-to-leading order in the derivative expansion and computed the corresponding stability matrix, c.f. Eq. (2.36), including the Yukawa coupling flow.

We emphasize that a corresponding scalar $\mathrm{O}(2N_\mathrm{L})$ model does not exhibit a fixed-point potential in the SYM regime but only in the SSB regime. We conclude that the nature of the phase transition and the corresponding critical behavior is characteristic for our fermionic model. In particular for small N_L, the fermionic fluctuations contribute with a comparatively large weight to the critical behavior, as discussed in Fig. 2.4.

In order to estimate the error on our results arising from the polynomial expansion of the effective potential, we study the convergence of the fixed-point values and of the critical exponents as a function of increasing truncation order for $N_\mathrm{L} = 2$. Tab. 5.3 displays our results for a truncation beyond order $\rho^n \sim \phi^{2n}$ for $n = 2, 4, 6, 7$. All quantities show a satisfactory convergence with a variation on the 1% level among the highest-order truncations. The full truncation error introduced by the derivative expansion is much harder to determine and depends on the specific quantity. By analogy with the bosonic $\mathrm{O}(N)$ models, we expect the leading critical exponent to be our most accurate quantity. On the same truncation level, the critical exponent ν in $\mathrm{O}(N)$ models agrees with the best known value already on the 3% level, see App. 2.4. The subleading exponents as

n	h_*^2	m_*^2	λ_2^*	ν	ω
2	3.462	0.137	3.400	1.001	0.795
4	3.374	0.108	3.621	1.099	0.764
6	3.364	0.104	3.643	1.100	0.809
7	3.367	0.105	3.636	1.098	0.800

Table 5.3: Error estimate for $N_\mathrm{L} = 2$: fixed-point values $h^2, h_*^2, m_*^2, \lambda_2^*$ and the two leading critical exponents ν, ω as a function of the highest-order term n in the ρ expansion of the effective potential.

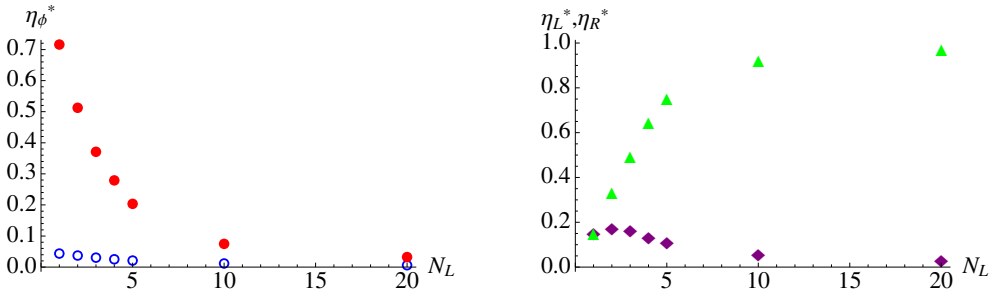

Figure 5.1: Left: η_ϕ^* in the $\mathrm{U}(N_\mathrm{L})_\mathrm{L}\otimes\mathrm{U}(1)_\mathrm{R}$ model (red dots) in comparison with that of the analogous $\mathrm{O}(2N_\mathrm{L})$ model (blue circles). Right: η_L^* (purple diamonds) and η_R^* (green triangles) in the chiral Yukawa model.

well as the anomalous dimensions usually are less well approximated to this order of the derivative expansion and require more refined techniques for a better resolution of the momentum dependence, e.g., as suggested in [142, 143].

5.3.2 The regime of spontaneous symmetry breaking (SSB)

For increasing left-handed fermion number, the scalar fixed-point potential must eventually lie in the regime of spontaneous symmetry breaking as the potential flow Eq. (4.2) of our model approaches that of an $\mathrm{O}(2N_\mathrm{L})$ model in the limit $N_\mathrm{L} \to \infty$. In three dimensions the latter is known to exhibit a Wilson-Fisher fixed-point potential in the SSB regime with a nonzero $\kappa^* > 0$.

We observe the transition of the fixed-point potential from the symmetric to the SSB regime already near $N_\mathrm{L} = 3$. The flow equations in the SSB regime are more involved due to additional loop contributions which arise from the coupling to the vev. This higher degree of nonlinearity inhibits a simple analytical study of the fixed-point structure at NLO in the derivative expansion. Instead, we start at the Wilson-Fisher fixed point for the analogous $\mathrm{O}(2N_\mathrm{L})$ model and obtain a fixed point of the full chiral Yukawa system by numerical iteration. This confirms that the presence of the fermions generically shifts the scalar fixed-point values only slightly. However, our chiral Yukawa system represents a different universality class, and so the critical exponents and the anomalous dimensions are special to this system. Numerical results are displayed in Figs. 5.1 and 5.2. The models were investigated with anomalous dimensions and expanded up to order $\sim \phi^{12}$ in the effective potential.

The fixed-point values of the anomalous dimensions as plotted in Fig. 5.1 are universal (even though slight regulator dependencies can be induced by the truncation). The left panel shows η_ϕ^* for our $\mathrm{U}(N_\mathrm{L})_\mathrm{L}\otimes\mathrm{U}(1)_\mathrm{R}$ model (red dots) in comparison with the analogous $\mathrm{O}(2N_\mathrm{L})$ model (blue circles). Whereas η_ϕ^* in both models approaches a common value for large N_L, we observe larger differences for smaller N_L which can directly be attributed to the fermionic loop contributions. The fermion anomalous dimensions η_L^* and η_R^* are shown

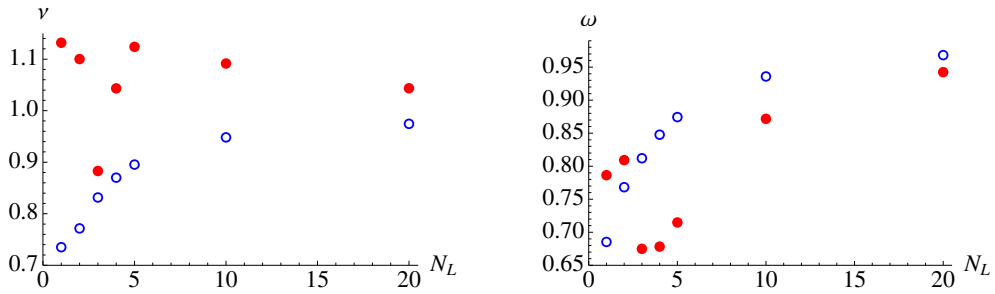

Figure 5.2: Critical exponents as a function of N_{L} in the chiral $\mathrm{U}(N_{\mathrm{L}})_{\mathrm{L}}\otimes\mathrm{U}(1)_{\mathrm{R}}$ model (red dots) in comparison with those of the analogous $\mathrm{O}(2N_{\mathrm{L}})$ model (blue circles).

in the right panel (purple diamonds and green triangles, respectively). For $N_{\mathrm{L}} = 1$, both anomalous dimensions agree as this corresponds to the left/right symmetric point. For larger N_{L}, η_{R}^* becomes significantly larger, as the massless fermionic and bosonic degrees of freedom contribute to the loop diagrams with a weight $\sim N_{\mathrm{L}}$.

The critical exponents ν and ω are shown in Fig. 5.2. Again, the red dots represent the values for our chiral $\mathrm{U}(N_{\mathrm{L}})_{\mathrm{L}}\otimes\mathrm{U}(1)_{\mathrm{R}}$ model which is compared with those of the analogous $\mathrm{O}(2N_{\mathrm{L}})$ model (blue circles). The results of both models approach each other for large N_{L} as expected but show sizable deviations at smaller N_{L}. We observe a rapid change of the critical exponents near $N_{\mathrm{L}} \simeq 3$, where the effective fixed point potential changes from the symmetric to the SSB regime.

We believe that especially the results for the universal fixed-point anomalous dimensions and critical exponents as summarized in Tab. 5.4 can provide for first benchmarks for these new universality classes. For any other nonperturbative approach to theories for chiral fermions near the symmetry-breaking phase transition, these universality classes can serve as a useful testing ground.

Discussion

A critical discussion of the accuracy of our NLO results can be based on the following indirect arguments: First, the large-N_{L} limit of our model corresponds to the purely scalar $\mathrm{O}(N)$ model with $N = 2N_{\mathrm{L}}$, which exhibits the well-known Wilson-Fisher fixed-point

N_{L}	h_*^2	κ_*	λ_2^*	η_ϕ^*	η_{L}^*	η_{R}^*	ν	ω
3	2.718	0.009	2.967	0.371	0.154	0.487	0.883	0.675
4	2.713	0.042	2.954	0.279	0.125	0.637	1.043	0.678
5	2.519	0.079	2.717	0.204	0.100	0.746	1.124	0.715
10	1.452	0.256	1.506	0.075	0.046	0.913	1.092	0.872
20	0.739	0.597	0.752	0.032	0.022	0.963	1.043	0.942
50	0.296	1.612	0.298	0.012	0.009	0.986	1.017	0.978
100	0.148	3.301	0.149	0.006	0.004	0.993	1.008	0.989

Table 5.4: Fixed point values and critical exponents in the SSB regime.

structure. In these models, the quantitative reliability of the derivative expansion has been verified to a high level of significance. We conjecture that this limit also provides a reasonable estimate for large finite values of N_{L}. Second, the derivative expansion is based on the implicit assumption that momentum dependencies of operators do not grow large. This includes the kinetic terms, such that self-consistency of the derivative expansion requires that the anomalous dimensions satisfy $\eta_{\phi,\mathrm{L,R}} \lesssim 1$, as is the case in our calculations. From the structure of the threshold functions, cf. App. B, we observe that even large anomalous dimensions of order $\eta_i \simeq 1$ do not change the LO flow qualitatively but contribute a correction on the 10-20% level to the potential flow. Third, the same NLO truncation has been used in the study of critical exponents in the 3d Gross-Neveu model [66]: the resulting critical exponents are in very good quantitative agreement with the available lattice data for $N_{\mathrm{f}} = 4, 12$ and other methods [122] even for large anomalous dimensions. Still, we emphasize that a direct quantitative estimate of the accuracy in our case requires a higher-order calculation. In particular, the anomalous dimensions and subleading exponents may be affected by larger corrections.

From our classification of all fermionic interaction terms compatible with the required symmetries, it is clear that the Higgs-like condensation channel is not the only possible channel. Aside from vector-like channels, there are two further pseudo-scalar channels, cf. Eq. (5.31), and further scalar and pseudo-scalar channels in the flavor-singlet Fierz transforms of Eqs. (5.30)-(5.33). In fact, the present analysis is a restricted study of a particular condensation process. We expect that the phase diagram of the general model is much more involved and might exhibit a variety of possible phases and corresponding transitions.

A special feature of our model arises in the symmetric regime: here, a fixed point within our truncation implies a sum rule for the anomalous dimensions, $\eta_\phi + \eta_{\mathrm{L}} + \eta_{\mathrm{R}} = 1 \equiv 4 - d$. This sum rule is relevant, since the underlying balancing between anomalous dimensions and dimensional power-counting scaling can be a decisive feature of many other models as well. Most prominently, the asymptotic-safety scenario in quantum gravity [20] as well as in extra-dimensional Yang-Mills theories [96] requires similar sum rules to be satisfied. In contrast to these latter models, the present models for $N_{\mathrm{L}} = 1, 2$ can serve as a much simpler example for a test of this sum rule at a fixed point. A verification of this sum rule also by other nonperturbative tools can shed light on this important mechanism for the generation of RG fixed points.

Chapter 6

Functional renormalization for the BCS-BEC crossover

Ultracold atomic Fermi gases with two accessible hyperfine spin states near a Feshbach resonance show a smooth crossover between Bardeen-Cooper-Schrieffer (BCS) superfluidity and Bose-Einstein condensation (BEC) of diatomic molecules [144, 145].

By means of an external magnetic field B the phenomenon of a Feshbach resonance allows to arbitrarily regulate the effective interaction strength of the atoms, parametrized by the s-wave scattering length a. We shortly discuss the example of ^{6}Li [146], which is besides ^{40}K realized in current experiments [147–152], see left panel of Fig. 6.1.

For magnetic fields larger than ~ 1200G the scattering length a is small and negative, giving rise to the many-body effect of Cooper-pairing and a BCS-type ground state below a critical temperature. The BCS ground state is superfluid described by a non-vanishing fermion bilinear order parameter $\phi_0 = \langle \psi_1 \psi_2 \rangle$. An increase of the temperature leads to a second order phase transition to a normal fluid, $\phi_0 = 0$. Magnetic fields below $B \sim 600$G induce a small and positive scattering length a and the formation of a diatomic bound state, a dimer. The ground state is a repulsive BEC of dimers and again a phase transition from a superfluid, $\phi_0 > 0$, to a normal fluid, $\phi_0 = 0$, can be observed at a critical temperature. For magnetic fields in the regime $700\text{G} \lesssim B \lesssim 1100\text{G}$ the modulus of the scattering length $|a|$ is large and diverges at the *unitarity point*, $B_0 = 834$G. At and near unitarity the fermions are in a strongly interacting regime. It connects the limits of BCS superfluidity and Bose-Einstein condensation by a continuous crossover and also shows a superfluid ground state, with $\phi_0 > 0$ [144, 145].

A convenient parametrization of the crossover is given by the inverse concentration $c^{-1} = (ak_F)^{-1}$. Here the density of atoms $n = k_F^3/(3\pi^2)$ defines the Fermi momentum k_F in natural units with $\hbar = k_B = 2M = 1$, and M the mass of the atoms. The dimensionless parameter c^{-1} varies from large negative values on the BCS side to large positive values on the BEC side. It crosses zero at the unitarity point, see right panel of Fig. 6.1.

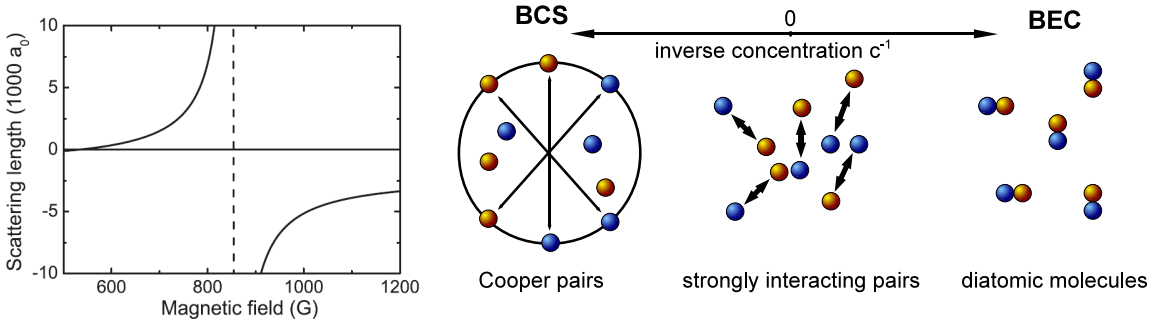

Figure 6.1: Left: Feshbach resonance, see [146]. Right: Sketch of the crossover physics.

A wide range of qualitative features of the BCS-BEC crossover is already well described by extended mean-field theories which account for the contribution of both fermionic and bosonic degrees of freedom [153, 154]. However, the quantitatively precise understanding of BCS-BEC crossover physics requires non-perturbative methods. The experimental realization of molecule condensates and the subsequent crossover to a BCS-like state of weakly attractively interacting fermions [147–152] pave the way to future experimental precision measurements and provide a testing ground for non-perturbative methods. Quantitative understanding of the crossover at and near the resonance has been developed through numerical Quantum Monte-Carlo (QMC) methods [155–159]. Computations of the complete phase diagram have been performed from functional field-theoretical techniques, as t-matrix approaches [160, 161], Dyson-Schwinger equations [162, 163], 2PI methods [164], and RG flow equations [68, 69, 165, 166]. These pictures of the whole phase diagram [68, 69, 160–167] do not yet reach a similar quantitative precision as the QMC calculations.

We intend to fill this gap and discuss the limit of broad Feshbach resonances for which all thermodynamic quantities can be expressed in terms of two dimensionless parameters,

$$\text{the concentration:} \qquad c = ak_F\,, \tag{6.1}$$

and the temperature in units of the Fermi temperature T/T_F where $T_F = k_F^2$. In the broad resonance regime, macroscopic observables are *universal* [68, 162, 167, 168], i.e. they are to a large extent independent of the concrete microscopic realization. This can be traced back to the existence of a NGFP in the RG flow, cf. Chaps. 3, 4 and 5, which is approached provided the Feshbach (Yukawa) coupling is large enough [69].

We shortly introduce the techniques and results from RG flow equations for cold atoms, see Secs. 6.1 - 6.4. Further, we include the quantitative effect of particle-hole fluctuations, Sec. 6.5, and systematically extend the truncation scheme, accounting for changes of the Fermi surface due to fluctuation effects, Sec. 6.6. Additionally, we also consider an atom-dimer interaction term.

6.1 Microscopic model

Microscopically the BCS-BEC crossover can be described by an action including a two-component Grassmann field $\psi = (\psi_1, \psi_2)$, describing non-relativistic fermions in two hyperfine states and a complex scalar field ϕ as the bosonic degrees of freedom. In different regimes of the crossover ϕ can be seen as a field describing molecules, Cooper pairs or simply an auxiliary field. Explicitly, the microscopic action at the ultraviolet scale Λ reads

$$S = \int_0^{1/T} d\tau \int d^3x \Big\{ \psi^\dagger(\partial_\tau - \Delta - \mu)\psi + \phi^*(\partial_\tau - \frac{\Delta}{2} - 2\mu + \nu_\Lambda)\phi - h_\Lambda(\phi^*\psi_1\psi_2 + h.c.) \Big\}. \quad (6.2)$$

In thermal equilibrium the system is described by the Matsubara formalism, see App. A. The variable μ is the chemical potential. The parameter $\nu_\Lambda = \nu(B) + \delta\nu(\Lambda)$ includes the detuning from the Feshbach resonance $\nu(B) = \mu_{\rm M}(B - B_0)$, with the magnetic moment of the boson field $\mu_{\rm M}$, and a renormalization counter term $\delta\nu(\Lambda)$ that has to be adjusted to match the conditions from the physical vacuum. The Yukawa coupling h_Λ is related to the width of the Feshbach resonance. Note that the bosonic field ϕ appears quadratically in Eq. (6.2) so the functional integral over ϕ can be carried out and our model is equivalent to a purely fermionic theory with an interaction term

$$S_{\rm int} = \int_{p_1,p_2,p_1',p_2'} \lambda_{\psi,\rm eff}(p_1 + p_2)\psi_1^*(p_1')\psi_1(p_1)\psi_2^*(p_2')\psi_2(p_2)\,\delta(p_1 + p_2 - p_1' - p_2'). \quad (6.3)$$

Here $p = (p_0, \vec{p})$ and the microscopic interaction between the fermions is described by the tree level expression with a classical inverse boson propagator in the denomiator

$$\lambda_{\psi,\rm eff}(q) = -\frac{h_\Lambda^2}{-\omega + \frac{\vec{q}^2}{2} + \nu_\Lambda - 2\mu}, \quad (6.4)$$

where ω is the real-time frequency of the exchanged boson ϕ. It is related to the Matsubara frequency q_0 via analytic continuation $\omega = -iq_0$. Further, $\vec{q} = \vec{p}_1 + \vec{p}_2$ is the center of mass momentum of the scattering fermions ψ_1 and ψ_2 with momenta $\vec{p}_1$ and $\vec{p}_2$, respectively. The limit of broad Feshbach resonances corresponds to $h_\Lambda \to \infty$, for which the microscopic interaction becomes pointlike, with strength $-h_\Lambda^2/\nu_\Lambda$.

6.2 Truncation and cutoff function

The functional renormalization group connects the microphysics to macrophysics and therefore to observable thermodynamics. which can be obtained from the grand canonical partition function Z or the corresponding grand canonical potential $\Omega_G = -T \ln Z$. It is related to the effective action via $\Gamma[\Phi_{eq}] = \Omega_G/T$, where Φ_{eq} is given by $\frac{\delta}{\delta\Phi}\Gamma[\Phi]|_{\Phi=\Phi_{eq}} = 0$.

Let s first present a basic version of a truncation which already captures all the qualitative features of the BCS-BEC crossover:

$$\Gamma_k[\Phi] = \int_{\tau,\vec{x}} \Big\{ \psi^\dagger(\partial_\tau - \Delta - \mu)\psi + \bar{\phi}^* \Big(\bar{Z}_\phi \partial_\tau - \frac{A_\phi \Delta}{2} \Big) \bar{\phi} + \bar{U}(\bar{\rho}, \mu) - \bar{h}(\bar{\phi}^* \psi_1 \psi_2 + \bar{\phi} \psi_2^* \psi_1^*) \Big\}. \quad (6.5)$$

The effective potential $\bar{U}(\bar{\rho}, \mu)$ is a function of $\bar{\rho} = \bar{\phi}^* \bar{\phi}$ and μ. This truncation can be motivated by a systematic derivative expansion and analysis of Ward identities, see [68, 169]. It does not yet incorporate the effects of particle-hole fluctuations and we will come back to this issue in Sect. 6.5.1. In terms of renormalized fields $\phi = A_\phi^{1/2} \bar{\phi}$, $\rho = A_\phi \bar{\rho}$ and renormalized couplings $Z_\phi = \bar{Z}_\phi / A_\phi$, $h = \bar{h} / \sqrt{A_\phi}$, Eq. (6.5) reads

$$\Gamma_k[\Phi] = \int_{\tau,\vec{x}} \Big\{ \psi^\dagger(\partial_\tau - \Delta - \mu)\psi + \phi^* (Z_\phi \partial_\tau - \frac{\Delta}{2})\phi + U(\rho, \mu) - h\,(\phi^* \psi_1 \psi_2 + \phi \psi_2^* \psi_1^*) \Big\}. \quad (6.6)$$

For the effective potential, we use an expansion around the k-dependent location of the minimum $\rho_0(k)$ and the k-independent value of the chemical potential μ_0 that corresponds to the physical particle number density n. We determine $\rho_0(k)$ and μ_0 by the requirements $(\partial_\rho U)(\rho_0(k), \mu_0) = 0$ for all k, and $-(\partial_\mu U)(\rho_0, \mu_0) = n$ at $k = 0$. More explicitly, we employ a truncation for $U(\rho, \mu)$ of the form

$$U(\rho, \mu) = U(\rho_0, \mu_0) - n_k(\mu - \mu_0) + (m^2 + \alpha(\mu - \mu_0))(\rho - \rho_0) + \frac{1}{2}\lambda(\rho - \rho_0)^2. \quad (6.7)$$

In the symmetric or normal gas phase, we have $\rho_0 = 0$, while in the phase with spontaneous breaking of $U(1)$-symmetry (superfluid phase), we have $\rho_0 > 0$ and $m^2 = 0$. The atom density $n = -\partial U / \partial \mu$ corresponds to n_k in the limit $k \to 0$.

In total, we have the running couplings $m^2(k)$, $\lambda(k)$, $\alpha(k)$, n_k, $Z_\phi(k)$ and $h(k)$. In the phase with spontaneous symmetry breaking m^2 is replaced by ρ_0. In addition, we need the anomalous dimension $\eta = -k\partial_k \ln A_\phi$. At the microscopic scale $k = \Lambda$ the initial values of our couplings are determined from Eq. (6.2). This gives $m^2(\Lambda) = \nu_\Lambda - 2\mu$, $\rho_0 = 0$, $\lambda(\Lambda) = 0$, $Z_\phi(\Lambda) = 1$, $h(\Lambda) = h_\Lambda$, $\alpha(\Lambda) = -2$ and $n_\Lambda = 3\pi^2 \mu \theta(\mu)$.

Finally, we have to employ a cutoff scheme. We use a purely space-like cutoff which in terms of the bare fields reads

$$\begin{aligned} \Delta S_k \;=\; & \int_p \Big\{ \psi^\dagger(p) \left(\mathrm{sign}(\vec{p}^2 - \mu) k^2 - (\vec{p}^2 - \mu) \right) \theta\left(k^2 - |\vec{p}^2 - \mu| \right) \psi(p) \\ & + \bar{\phi}^*(p) A_\phi \left(k^2 - \vec{p}^2/2 \right) \theta\left(k^2 - \vec{p}^2/2 \right) \bar{\phi}(p) \Big\}. \end{aligned} \quad (6.8)$$

For the fermions it regularizes fluctuations around the Fermi surface, while for the bosons fluctuations with small momenta are suppressed. The choice of ΔS_k is an optimized choice in the spirit of [16, 70].

6.3 Flow equations

For our choice of the regulator and with the basic approximation scheme Eq. (6.6) the flow equation for the effective potential can be computed:

$$k\partial_k U = \eta\rho\, U' + \frac{\sqrt{2}k^5}{3\pi^2 Z_\phi}\Big(1-\frac{2\eta}{5}\Big)s_{\mathrm{B}}^{(0)} - \frac{k^4}{3\pi^2}\big((\mu+k^2)^{\frac{3}{2}}\theta(\mu+k^2)-(\mu-k^2)^{\frac{3}{2}}\theta(\mu-k^2)\big)s_{\mathrm{F}}^{(0)}, \quad (6.9)$$

with the threshold functions

$$s_{\mathrm{B}}^{(0)} = \Big(\sqrt{\tfrac{k^2+U'}{k^2+U'+2\rho U''}}+\sqrt{\tfrac{k^2+U'+2\rho U''}{k^2+U'}}\Big)\Big(\tfrac{1}{2}+N_{\mathrm{B}}\Big[\tfrac{\sqrt{k^2+U'}\sqrt{k^2+U'+2\rho U''}}{Z_\phi}\Big]\Big), \quad (6.10)$$

$$s_{\mathrm{F}}^{(0)} = \tfrac{2}{\sqrt{k^4+h^2\rho}}\Big(\tfrac{1}{2}-N_{\mathrm{F}}\Big[\sqrt{k^4+h^2\rho}\Big]\Big). \quad (6.11)$$

The threshold functions include a temperature dependence via the Bose and Fermi functions $N_{\mathrm{B/F}}[\epsilon] = (e^{\epsilon/T}\mp 1)^{-1}$. From the effective potential flow we derive the flow equations for the running couplings m^2 or ρ_0 and λ. For details we refer to [169]. Further we need flow equations for A_ϕ and Z_ϕ that are obtained by the prescriptions

$$\partial_t \bar{Z}_\phi = -\partial_t \frac{\partial}{\partial q_0}(\bar{P}_\phi)_{12}(q_0,0)\Big|_{q_0=0}, \quad \text{and} \quad \partial_t A_\phi = 2\partial_t \frac{\partial}{\partial \vec{q}^2}(\bar{P}_\phi)_{22}(0,\vec{q})\Big|_{\vec{q}=0}, \quad (6.12)$$

with the momentum dependent part of the propagator

$$\frac{\delta^2\Gamma_k}{\delta\bar{\phi}_i(q)\delta\bar{\phi}_j(q')}\Big|_{\bar{\phi}_1=\sqrt{2\bar{\rho}_0},\bar{\phi}_2=0} = (\bar{P}_\phi)_{ij}(q)\delta(q+q'). \quad (6.13)$$

Here the boson field is expressed in a basis of real fields $\bar{\phi}(x) = \frac{1}{\sqrt{2}}(\bar{\phi}_1(x)+i\bar{\phi}_2(x))$. These flow equations are derived in [169] and have a rather involved structure. Finally, we need the flow of the Yukawa coupling. In the symmetric regime with $\rho_0 = 0$ there is no loop contribution and the flow is given by the anomalous dimension only,

$$\partial_t h = \frac{1}{2}\eta h, \quad \text{or in dimensionless units} \quad \partial_t \tilde{h}^2 = (-1+\eta)\tilde{h}^2, \quad (6.14)$$

where $\tilde{h}^2 = h^2/k$. For a nonvanishing order parameter ρ_0 there is a loop contribution $\sim h^3\lambda\rho_0$ from a diagram involving both fermions and bosons. This contribution is subleading and we verified numerically that this is indeed the case. For the basic approximation scheme, Eq. (6.6), we therefore omitted this contribution.

6.4 Vacuum limit

The vacuum limit establishes the contact to experiment. We find that for $n = T = 0$ the crossover at finite density turns into a second-order phase transition in vacuum [163, 167]

as a function of $m^2(\Lambda)$. In order to see this, we consider the momentum independent parts in both the fermion and the boson propagator, $-\mu$ (the "chemical potential" for the fermions in vacuum) and $m(k=0)^2$, which act as gaps for the propagation of fermions and bosons. We find the following constraints, separating two qualitatively different branches of the physical vacuum [163],

$$\begin{array}{llll} m^2(0) > 0, & \mu = 0 & \text{atom phase} & (a^{-1} < 0), \\ m^2(0) = 0, & \mu < 0 & \text{molecule phase} & (a^{-1} > 0), \\ m^2(0) = 0, & \mu = 0 & \text{resonance} & (a^{-1} = 0). \end{array} \tag{6.15}$$

Now, the initial values $m^2(\Lambda)$ and h_Λ can be connected to the two-particle scattering in vacuum close to a Feshbach resonance. For this purpose one follows the flow of $m^2(k)$ and $h(k)$ in vacuum, i.e. $\mu = T = n = 0$ and extracts the renormalized parameters $m^2 = m^2(k=0)$, $h = h(k=0)$. They have to match the physical conditions formulated in Eq. (6.15). We obtain the two relations

$$\bar{m}^2(\Lambda) = \mu_{\rm M}(B - B_0) - 2\mu + \frac{\bar{h}_\Lambda^2}{6\pi^2}\Lambda, \tag{6.16}$$

$$a = -\frac{h^2(k=0)}{8\pi\ m^2(k=0)} = -\frac{\bar{h}^2(\Lambda)}{8\pi\ \mu_{\rm M}(B - B_0)}. \tag{6.17}$$

For details we refer to [169]. These relations fix the initial conditions of our model completely and we can express the parameters $m^2(\Lambda)$ and $h^2(\Lambda)$ by the experimentally accessible quantities $B - B_0$ and a. They remain valid also for non-vanishing density and temperature. From the flow equations together with the inital conditions we can already recover all the qualitative features of the BCS-BEC crossover, e.g. compute the phase diagram for the phase transition to superfluidity. The result for this basic approximation is displayed in the right panel of Fig 6.7 by the dot-dashed line.

Fixed point and universality In the vacuum limit and in the regime where $k^2 \gg -\mu$ the flow of the anomalous dimension reads $\eta = h^2/(6\pi^2 k)$ [169]. Together with the dimensionless flow of the Yukawa coupling, Eq. (6.14), this reveals the existence of an IR attractive fixed point given by $\eta = 1$, $\tilde{h}^2 = 6\pi^2$. This fixed-point is approached rapidly if the initial value of $h^2(\Lambda)/\Lambda$ is large enough, i.e. the system is in the broad resonance limit. Then the memory of the microscopic value of $h^2(\Lambda)/\Lambda$ is lost. Also all of the other parameters, but the mass term m^2 are attracted to an IR fixed-point, giving rise to universality. The fixed-point structure remains similar for non-vanishing density and temperature and these findings also apply in this regime and determine the critical physics of these non-relativistic quantum fields. For a given temperature, this fixed point has only one relevant direction which related to the detuning of the resonance $B - B_0$.

6.5 Particle-hole fluctuations

For small and negative scattering length $c^{-1} < 0, |c| \ll 1$ (BCS side), the system can be treated the perturbative BCS theory of superfluidity [170, 171]. However, there is a significant decrease of the critical temperature as compared to the original BCS result due to a screening effect of particle-hole fluctuations in the medium [172, 173]. Here we will develop the technique to include the effect of particle-hole fluctuations in our functional RG treatment.

In an RG setting, the features of BCS theory can be described in a purely fermionic language with the fermion interaction vertex λ_ψ as the only scale dependent object. In general, the interaction vertex is momentum dependent, $\lambda_\psi(p_1', p_1, p_2', p_2)$, and its flow has two contributions which are depicted in Fig. 6.2, including the external momentum labels. For $k \to 0,\ \mu_0 \to 0,\ T \to 0$ and $n \to 0$ this coupling is related to the scattering length, $a = \frac{1}{8\pi}\lambda_\psi(p_i = 0)$.

In the BCS approximation only the first diagram in Fig. 6.2, the particle-particle (pp) loop, is kept and the momentum dependence of the fermion coupling is neglected, by replacing $\lambda_\psi(p_1', p_1, p_2', p_2)$ by the pointlike coupling evaluated at zero momentum. For $\mu > 0$ its effect increases as the temperature T is lowered. For small temperatures $T \leq T_{c,\mathrm{BCS}}$ the logarithmic divergence leads to the appearance of pairing, as $\lambda_\psi \to \infty$. In terms of the scattering length a, Fermi momentum k_F and Fermi temperature T_F, the critical temperature is found to be

$$T_{c,\mathrm{BCS}} \approx 0.61\ T_F\ e^{\pi/(2ak_F)}. \tag{6.18}$$

At zero temperature the expression for the second diagram in Fig. 6.2, the particle-hole (ph) loop, vanishes if it is evaluated for vanishing external momenta, as both poles of the frequency integration are always either in the upper or lower half of the complex plane. The dominant part of the scattering in a fermion gas occurs, however, for momenta on the Fermi surface rather than for zero momentum. For non-zero momenta of the external

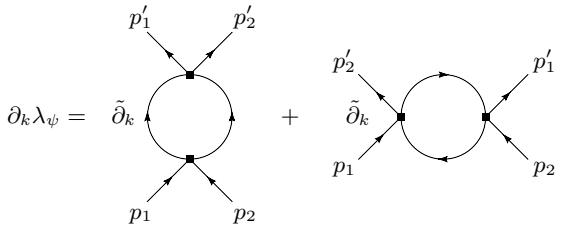

Figure 6.2: Running of the momentum dependent vertex λ_ψ. Here $\tilde{\partial}_k$ indicates derivatives with respect to the cutoff terms in the propagators and does not act on the vertices in the depicted diagrams.

particles the particle-hole loop makes an important contribution. Setting the external frequencies to zero, we find that the inverse propagators in the particle-hole loop are

$$P_\psi(q) = iq_0 + (\vec{q} - \vec{p}_1)^2 - \mu, \quad \text{and} \quad P_\psi(q) = iq_0 + (\vec{q} - \vec{p}_2')^2 - \mu. \tag{6.19}$$

Depending on the value of the momenta $\vec{p}_1$ and $\vec{p}_2'$, there are now values of the loop momentum $\vec{q}$ for which the poles of the frequency integration are in different halfplanes so that there is a nonzero contribution even for $T = 0$.

To include the effect of particle-hole fluctuations one could take the full momentum dependence of the vertex λ_ψ into account. However, this leads to complicated expressions which are hard to solve even numerically. One therefore often restricts the flow to the running of a single coupling λ_ψ by choosing an appropriate projection prescription to determine the flow equation. In the purely fermionic description this flow equation has a simple structure and the solution for λ_ψ^{-1} can be written as

$$\big(\lambda_\psi(k=0)\big)^{-1} = \big(\lambda_\psi(k=\Lambda)\big)^{-1} + \text{pp-loop} + \text{ph-loop}\,. \tag{6.20}$$

Since the ph-loop depends only weakly on the temperature, one can evaluate it at $T = 0$ and add it to the initial value $\lambda_\psi(k=\Lambda)^{-1}$. As T_c depends exponentially on the "effective microscopic coupling" $\big(\lambda_{\psi,\Lambda}^{\text{eff}}\big)^{-1} = (\lambda_\psi(k=\Lambda)^{-1} + \text{ph-loop})$, any shift in $\big(\lambda_{\psi,\Lambda}^{\text{eff}}\big)^{-1}$ results in a multiplicative factor for T_c. The numerical value of the ph-loop and therefore of the correction factor for T_c/T_F depends on the precise projection description.

Let us now choose the appropriate momentum configuration. For the formation of Cooper pairs, the relevant momenta lie on the Fermi surface and point in opposite directions

$$\vec{p}_1^{\,2} = \vec{p}_2^{\,2} = \vec{p}_1'^{\,2} = \vec{p}_2'^{\,2} = \mu, \quad \text{and} \quad \vec{p}_1 = -\vec{p}_2,\ \vec{p}_1' = -\vec{p}_2'\,. \tag{6.21}$$

This still leaves the angle between $\vec{p}_1$ and $\vec{p}_1'$ unspecified. Gorkov's approximation [173] uses Eqs. (6.21) and projects on the s-wave by averaging over the angle between $\vec{p}_1$ and $\vec{p}_1'$. One can shift the loop momentum such that the internal propagators depend on $\vec{q}^{\,2}$ and $(\vec{q} + \vec{p}_1 - \vec{p}_1')^2$. In terms of spherical coordinates the first propagator depends only on the magnitude of the loop momentum $q^2 = \vec{q}^{\,2}$, while the second depends additionally on the transfer momentum $\tilde{p}^2 = \frac{1}{4}(\vec{p}_1 - \vec{p}_1')^2$ and the angle α between $\vec{q}$ and $(\vec{p}_1 - \vec{p}_1')$,

$$(\vec{q} + \vec{p}_1 - \vec{p}_1')^2 = q^2 + 4\tilde{p}^2 + 4\,q\,\tilde{p}\cos(\alpha)\,. \tag{6.22}$$

Performing the loop integration involves the integration over q^2 and the angle α. The averaging over the angle between $\vec{p}_1$ and $\vec{p}_1'$ translates to an averaging over $\tilde{p}^2$. Both can be done analytically [172] for the particle-hole diagram and the result gives the well known Gorkov correction to BCS theory, resulting in $T_c = (4e)^{-1/3} T_{c,\text{BCS}}$. Here, we will use a

numerically simpler projection by choosing $\vec{p}_1' = \vec{p}_1$, $\vec{p}_2 = \vec{p}_2'$, without an averaging over the angle between $\vec{p}_1'$ and $\vec{p}_1$. The size of $\tilde{p}^2 = \vec{p}_1^2$ is chosen such that the one-loop result reproduces exactly the result of the Gorkov correction, namely $\tilde{p} = 0.7326\sqrt{\mu}$. Choosing different values of $\tilde{p}$ demonstrates the dependence of T_c on the projection procedure.

6.5.1 Scale-dependent bosonization

In Sect. 6.1 we describe an effective four-fermion interaction by the exchange of a boson. In this picture the phase transition to the superfluid phase is indicated by the vanishing of the bosonic "mass term" $m^2 = 0$. Negative m^2 leads to the spontaneous breaking of U(1)-symmetry, since the minimum of the effective potential occurs for a nonvanishing superfluid density $\rho_0 > 0$. For $m^2 \geq 0$ we can solve the field equation for the boson ϕ as a functional of ψ and insert the solution into the effective action. This leads to an effective four-fermion vertex describing the scattering $\psi_1(p_1)\psi_2(p_2) \to \psi_1(p_1')\psi_2(p_2')$

$$\lambda_{\psi,\text{eff}} = \frac{-h^2}{i(p_1+p_2)_0 + \frac{1}{2}(\vec{p}_1+\vec{p}_2)^2 + m^2}. \tag{6.23}$$

To investigate the breaking of U(1) symmetry and the onset of superfluidity, we first consider the flow of the bosonic propagator, which is mainly driven by the fermionic loop diagram. For the effective four-fermion interaction this accounts for the particle-particle loop (see left panel, r.h.s. of Fig. 6.3). In the BCS limit of a large microscopic m_Λ^2 the running of m^2 for $k \to 0$ reproduces the BCS result [170, 171].

The particle-hole fluctuations are not accounted for by the renormalization of the boson propagator. Indeed, we have neglected so far that a four-fermion interaction term λ_ψ in the effective action is generated by the flow. This holds even if the microscopic pointlike interaction is absorbed by a Hubbard-Stratonovich transformation into an effective boson exchange such that $\lambda_\psi(\Lambda) = 0$. The strength of the total interaction between fermions

$$\lambda_{\psi,\text{eff}} = \frac{-h^2}{i(p_1+p_2)_0 + \frac{1}{2}(\vec{p}_1+\vec{p}_2)^2 + m^2} + \lambda_\psi \tag{6.24}$$

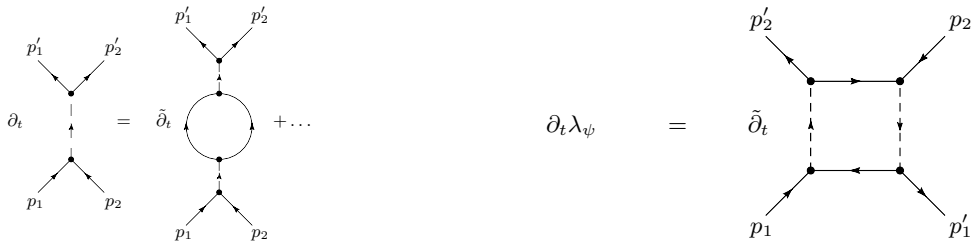

Figure 6.3: Left panel: Flow of the boson propagator. Right panel: Box diagram for the flow of the four-fermion interaction.

adds λ_ψ to the piece generated by boson exchange. In the partially bosonized formulation, the flow of λ_ψ is generated by the box diagrams depicted in the right panel of Fig. 6.3. We may interpret these diagrams and establish a direct connection to the particle-hole diagrams depicted in Fig. 6.2 on the BCS side of the crossover and in the microscopic regime. There the boson gap m^2 is large. In this case, the effective fermion interaction in Eq. (6.24) becomes momentum independent. Diagrammatically, this is represented by contracting the bosonic propagator. One can see, that the box-diagram in Fig. 6.3 is then equivalent to the particle-hole loop investigated in the last section with the pointlike approximation $\lambda_{\psi,\text{eff}} \to -\frac{h^2}{m^2}$ for the fermion interaction vertex. Therefore, we will evaluate $\partial_k \lambda_\psi$ for $\vec{p}_1 = \vec{p}_1' = -\vec{p}_2 = -\vec{p}_2'$, $|\vec{p}_1| = \tilde{p} = 0.7326\sqrt{\mu}$, as discussed in the preceding section to account for the particle-hole fluctuations.

In contrast to the particle-particle fluctuations (leading to SSB for decreasing T), the particle-hole fluctuations lead only to quantitative corrections and depend only weakly on temperature. This can be checked explicitly in the pointlike approximation, and holds not only in the BCS regime where $T/\mu \ll 1$, but also for moderate T/μ as realized at the critical temperature in the unitary regime. We therefore evaluate the box-diagrams in Fig. 6.2 for zero temperature. We note that an implicit temperature dependence, resulting from the couplings parameterizing the boson propagator, is taken into account.

After these preliminaries, we can now incorporate the effect of particle-hole fluctuations in the RG flow. An elegant way is provided by the method of bosonization [16, 174]. This method also preserves the picture that the divergence of $\lambda_{\psi,\text{eff}}$ is connected to the onset of a nonvanishing expectation value for the bosonic field ϕ_0. For this purpose, we use scale dependent fields in the average action. The scale dependence of $\Gamma_k[\chi_k]$ is modified by a term reflecting the k-dependence of the argument χ_k [174]

$$\partial_k \Gamma_k[\Phi_k] = \int \frac{\delta \Gamma_k}{\delta \Phi_k} \partial_k \Phi_k + \frac{1}{2} \text{STr} \left[\left(\Gamma_k^{(2)} + R_k \right)^{-1} \partial_k R_k \right] . \tag{6.25}$$

For our purpose it is sufficient to work with scale dependent bosonic fields $\bar{\phi}_k^*$, $\bar{\phi}_k$ and keep the fermionic field ψ scale independent. We employ

$$\partial_k \bar{\phi}_k(q) = (\psi_1 \psi_2)(q) \partial_k \upsilon, \quad \partial_k \bar{\phi}_k^*(q) = (\psi_2^\dagger \psi_1^\dagger)(q) \partial_k \upsilon. \tag{6.26}$$

In consequence, the flow equations in the symmetric regime get modified

$$\partial_k \bar{h} = \partial_k \bar{h}\big|_{\bar{\phi}_k} - \bar{P}_\phi(q) \partial_k \upsilon, \quad \partial_k \lambda_\psi = \partial_k \lambda_\psi\big|_{\bar{\phi}_k} - 2\bar{h} \partial_k \upsilon. \tag{6.27}$$

Here q is the center of mass momentum of the scattering fermions. In the notation of Eq. (6.23) we have $q = p_1 + p_2$ and we will take $\vec{q} = 0$, $q_0 = 0$. The first term on the right hand sides in Eqs. (6.27) gives the contribution of the flow equation which is valid for fixed

field $\bar{\phi}_k$. The second term comes from the explicit scale dependence of $\bar{\phi}_k$. The inverse propagator of the complex boson field $\bar{\phi}$ is denoted by $\bar{P}_\phi(q) = A_\phi(m^2 + iZ_\phi q_0 + \vec{q}^2/2)$.

We can choose $\partial_k \upsilon$ such that the flow of the coupling λ_ψ vanishes, i.e. that we have $\lambda_\psi = 0$ on all scales. This modifies the flow equation for the renormalized Yukawa coupling according to

$$\partial_k h = \partial_k h\big|_{\bar{\phi}_k} - \frac{m^2}{2h}\partial_k \lambda_\psi\big|_{\bar{\phi}_k}\,, \tag{6.28}$$

with $\partial_k h\big|_{\bar{\phi}_k}$ the contribution without bosonization and $\partial_k \lambda_\psi\big|_{\bar{\phi}_k}$ given by the box diagram in Fig. 6.3. Since λ_ψ remains zero during the flow, the effective four-fermion interaction $\lambda_{\psi,\text{eff}}$ is now purely given by the boson exchange. However, the contribution of the particle-hole exchange diagrams is incorporated via the second term in Eq. (6.28).

In the SSB regime we use a real basis for the bosonic field $\bar{\phi} = \bar{\phi}_0 + \frac{1}{\sqrt{2}}(\bar{\phi}_1 + i\bar{\phi}_2)$, where the expectation value $\bar{\phi}_0$ is chosen to be real without loss of generality. The real fields $\bar{\phi}_1$ and $\bar{\phi}_2$ then describe the radial and the Goldstone mode, respectively. To determine the flow equation of $\bar{h}$, we use the projection description

$$\partial_k h = i\sqrt{2}\Omega^{-1}\frac{\delta}{\delta\phi_2(0)}\frac{\delta}{\delta\psi_1(0)}\frac{\delta}{\delta\psi_2(0)}\partial_k\Gamma_k\,, \tag{6.29}$$

with the four volume $\Omega = \frac{1}{T}\int_{\vec{x}}$. Since the Goldstone mode has vanishing "mass", the flow of the Yukawa coupling is not modified by the box diagram (Fig. 6.3) in the SSB regime.

We emphasize that our non-perturbative flow equations go beyond the treatment by Gorkov and Melik-Barkhudarov [173] which includes the particle-hole diagrams only in a perturbative way. Furthermore, the inner bosonic lines $h^2/P_\phi(q)$ in the box diagrams represent the center of mass momentum dependence of the four-fermion vertex. This is neglected in Gorkov's pointlike treatment, and thus represents a further improvement of the classic calculation. Actually, this momentum dependence becomes substantial away from the BCS regime where the physics of the bosonic bound state sets in. We want to mention that there are also alternative approaches to the problem of scale dependent bosonization [61, 175].

Critical temperature including particle-hole fluctuations

To obtain the flow equations for the running couplings of our truncation Eq. (6.6) we use projection prescriptions similar to Eq. (6.29). The resulting system of ordinary coupled differential equations is then solved numerically for different chemical potentials μ and temperatures T. For temperatures sufficiently small compared to the Fermi temperature, $T/T_F \ll 1$, we find that the effective potential U at the macroscopic scale $k = 0$ develops a minimum at a nonzero field value $\rho_0 > 0$, $\partial_\rho U(\rho_0) = 0$. The system is then in the superfluid phase. For larger temperatures we find that the minimum is at $\rho_0 = 0$ and

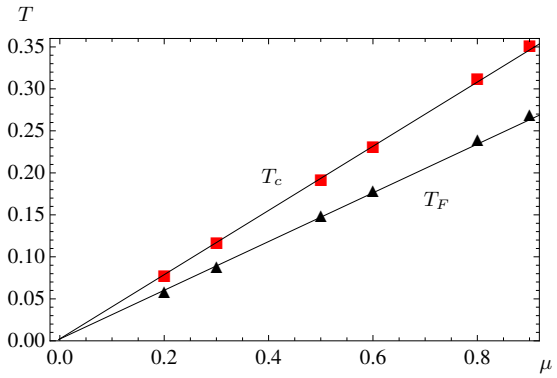

Figure 6.4: (Color online) Critical temperature T_c (boxes) and Fermi temperature $T_F = (3\pi^2 n)^{2/3}$ (triangles) as a function of the chemical potential μ. For convenience the Fermi temperature is scaled by a factor 1/5. We also plot the linear fits $T_c = 0.39\mu$ and $T_F = 1.48\mu$. The units are arbitrary and we use $\Lambda = e^7$.

that the "mass parameter" m^2 is positive, $m^2 = \partial_\rho U(0) > 0$. The critical temperature T_c of this phase transition between the superfluid and the normal phase is then defined as the temperature where one has

$$\rho_0 = 0, \quad \partial_\rho U(0) = 0 \quad \text{at} \quad k = 0. \tag{6.30}$$

Throughout the whole crossover the transition $\rho_0 \to 0$ is continuous as a function of T demonstrating that the phase transition is of second order.

In Fig. 6.4 we plot our result obtained for the critical temperature T_c and the Fermi temperature T_F as a function of the chemical potential μ at the unitarity point with $a^{-1} = 0$. From dimensional analysis it is clear that both dependencies are linear, $T_c, T_F \sim \mu$, provided that non-universal effects involving the ultraviolet cutoff scale Λ can be neglected. That this is indeed found numerically can be seen as a nontrivial test of our approximation scheme and the numerical procedures as well as the universality of the system. Dividing the slope of both lines gives $T_c/T_F = 0.264$, a result that will be discussed in more detail below. We emphasize that part of the potential error in this estimates is due to uncertainties in the precise quantitative determination of the density or T_F.

6.6 Running Fermion sector

In this section we aim at a systematic extension of the truncation scheme and consider a running fermion sector. Similar parametrizations of the fermionic self-energy have been studied in refs. [166, 176, 177]. Further, we include an atom-dimer interaction term.

Completion of the truncation

The extension of the truncation explicitely reads

$$\Gamma_k = \int_0^{1/T} d\tau \int d^3x \Big\{ \bar{\psi}^\dagger Z_\psi (\partial_\tau - \Delta)\bar{\psi} + \bar{m}_\psi^2 \bar{\psi}^\dagger \bar{\psi} + \bar{\phi}^* (\bar{Z}_\phi \partial_\tau - \frac{1}{2} A_\phi \Delta)\bar{\phi} + \bar{U}(\bar{\rho}, \mu) - \bar{h}(\bar{\phi}^* \bar{\psi}_1 \bar{\psi}_2 + \bar{\phi} \bar{\psi}_2^* \bar{\psi}_1^*) + \bar{\lambda}_{\phi\psi} \bar{\phi}^* \bar{\phi} \bar{\psi}^\dagger \bar{\psi} \Big\}. \tag{6.31}$$

In addition to the parameters used in our previous investigations, Secs. 6.2, our truncation includes now the k-dependent parameters $\bar{m}_\psi^2$ and Z_ψ by which we take into account fluctuation effects on the self-energy of the fermionic quasiparticles. The inclusion of the coupling constant $\bar{\lambda}_{\phi\psi}$ closes the truncation on the level of interaction terms quartic in the fields. The coupling $\bar{\lambda}_{\phi\psi}$ plays an important role for the three-body physics [178] and leads to quantitative modifications for the many-body problem. In contrast to [178] we do not resolve the momentum dependence of $\bar{\lambda}_{\phi\psi}$ in this work. In terms of renormalized fields $\phi = A_\phi^{1/2} \bar{\phi}$, $\rho = A_\phi \bar{\rho}$, $\psi = Z_\psi^{1/2} \bar{\psi}$ and couplings $Z_\phi = \bar{Z}_\phi / A_\phi$, $h = \bar{h}/(A_\phi^{1/2} Z_\psi)$, $\lambda_{\phi\psi} = \bar{\lambda}_{\phi\psi}/(A_\phi Z_\psi)$, $m_\psi^2 = \bar{m}_\psi^2 / Z_\psi$, Eq. (6.5) reads

$$\Gamma_k = \int_0^{1/T} d\tau \int d^3x \Big\{ \psi^\dagger (\partial_\tau - \Delta + m_\psi^2)\psi + \phi^* (Z_\phi \partial_\tau - \frac{1}{2}\Delta)\phi + U(\rho, \mu) - h(\phi^* \psi_1 \psi_2 + \phi \psi_2^* \psi_1^*) + \lambda_{\phi\psi} \phi^* \phi \psi^\dagger \psi \Big\}. \tag{6.32}$$

As before, we expand the effective potential in monomials of ρ, see Eq. (6.7). For $\rho_0 > 0$ the term $\sim \lambda_{\phi\psi}$ leads to a further modification of the Fermi surface, besides the gap $\sqrt{h^2 \rho_0}$. At the microscopic scale $k = \Lambda$ we have an additional initial value, $m_\psi^2(\Lambda) = -\mu$.

The infrared cutoff we use is again purely space-like and has to be completed as well, due to the running of the fermion mass. It reads in terms of the bare fields

$$\Delta S_k = \int_p \Big\{ \bar{\psi}^\dagger(p) Z_\psi \big[\mathrm{sign}(\vec{p}^2 - \tilde{\mu}_k) k^2 - (\vec{p}^2 - \tilde{\mu}_k) \big] \theta\left(k^2 - |\vec{p}^2 - \tilde{\mu}_k|\right) \bar{\psi}(p) + \bar{\phi}^*(p) A_\phi \left[k^2 - \vec{p}^2/2\right] \theta\left(k^2 - \vec{p}^2/2\right) \bar{\phi}(p) \Big\}, \tag{6.33}$$

where $\tilde{\mu}_k = -m_\psi^2 - \lambda_{\phi\psi}\rho_0$. For the fermions it regularizes fluctuations around the running Fermi surface, while for the bosons fluctuations with small momenta are suppressed.

The extension of the truncation by including the running couplings Z_ψ, m_ψ^2 and $\lambda_{\phi\psi}$ helps to improve the numerical precision of our results considerably all over the crossover, however especially in the limits of weak interactions. The effect of including the $\lambda_{\phi\psi}$-vertex can most prominently be observed in the result for the vacuum dimer-dimer scattering length a_M expressed in units of the atom-atom scattering length a. On the BEC side

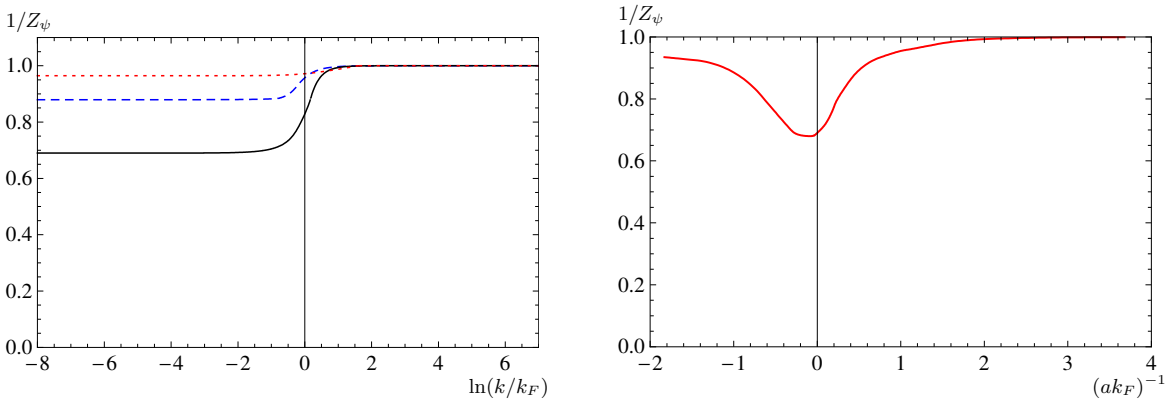

Figure 6.5: Left panel: Flow of the inverse fermionic wave function renormalization $1/Z_\psi$ at $T = 0$. The solid line is at the unitarity point ($c^{-1} = 0$). The dashed line corresponds to the BCS side at $c^{-1} = -1$ and the short dashed line to the BEC side at $c^{-1} = 1$. Right panel: Inverse fermionic wave function renormalization $1/Z_\psi$ at the macroscopic scale $k = 0$ as a function of the crossover parameter c^{-1}.

of the resonance we can derive this quantity from the corresponding couplings by the equation

$$\frac{a_M}{a} = 2\frac{\lambda}{\lambda_{\psi,\text{eff}}}, \quad \lambda_{\psi,\text{eff}} = 8\pi a = \frac{8\pi}{\sqrt{-\mu}}, \text{ for } \mu < 0 \text{ and } k = 0. \tag{6.34}$$

In this truncation we find $a_M/a = 0.59$, which is in very good agreement with the well-known result from a direct solution of the Schrödinger equation, $a_M/a = 0.60$ [179]. Our result is somewhat surprising since no momentum dependence of $\lambda_{\phi\psi}$ has been taken into account. As it has been found in [178], this turns out to be important for the atom-dimer scattering [178].

A study of the flow of the wave function renormalization Z_ψ shows, that its effect is strongest in the strongly interacting regime, when $|c^{-1}| < 1$, cf. Fig. 6.5.

Fermi sphere

The flowing coupling constants Z_ψ and m_ψ^2 as well as the coupling $\lambda_{\phi\psi}$ have an interesting effect on the dispersion relation of the fermions. In the regime with spontaneously broken $U(1)$ symmetry, the renormalized propagator of the fermionic field after analytic continuation to real frequencies ω reads

$$G_\psi^{-1} = \begin{pmatrix} -h\phi_0\epsilon & -\omega - (\vec{q}^2 + m_\psi^2 + \lambda_{\phi\psi}\rho_0) \\ -\omega + (\vec{q}^2 + m_\psi^2 + \lambda_{\phi\psi}\rho_0) & h\phi_0\epsilon \end{pmatrix}. \tag{6.35}$$

The dispersion relation follows from $\det G_\psi^{-1} = 0$ as $\omega = \pm\sqrt{\Delta^2 + (\vec{q}^2 - r_F^2)^2}$, where $\Delta = h\sqrt{\rho_0}$ is the gap and $r_F = \sqrt{-m_\psi^2 - \lambda_{\phi\psi}\rho_0}$ is the effective radius of the Fermi sphere. For small negative scattering lengths on the BCS side of the crossover the renormalization effects on r_F remain small. It takes the classical value $r_F = \sqrt{\mu} = k_F$ where $k_F =$

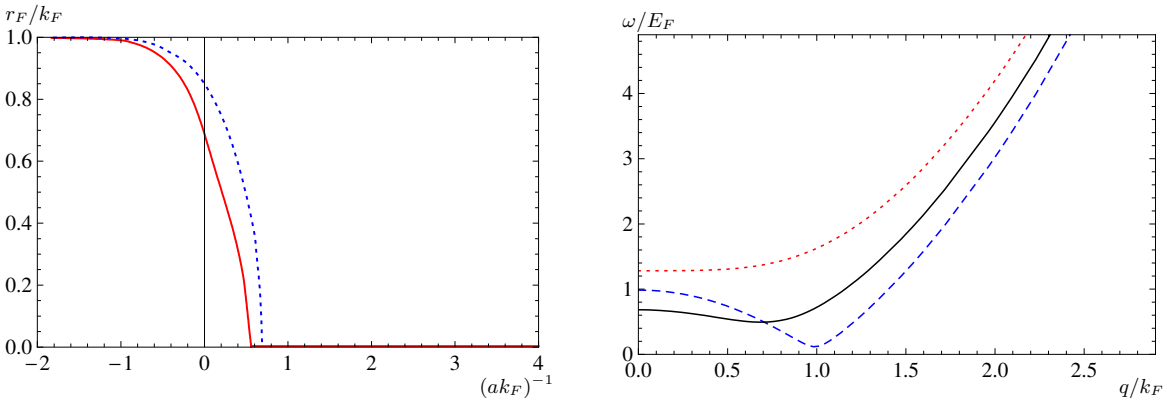

Figure 6.6: Left panel: Effective Fermi radius r_F/k_F as a function of the crossover parameter c^{-1} for vanishing temperature (solid line). We find that the Fermi sphere vanishes approximately $(ak_F)^{-1} \approx 0.6$. For comparison we also give the effective Fermi radius in an approximation, where we omitted the contribution of the atom-dimer vertex $\lambda_{\phi\psi}$ (dotted line). Right panel: Positive branch of the dispersion relation $\omega(q)$ in units of the Fermi energy for $c^{-1} = -1$ (dashed), $c^{-1} = 0$ (solid) and $c^{-1} = 1$ (short dashed). The gap and the Fermi radius are evaluated at the macroscopic scale $k = 0$.

$(3\pi^2 n)^{1/3}$. For large scattering length the Fermi sphere gets smaller and r_F finally vanishes at a point with $c^{-1} \approx 0.6$. For small and positive scattering length (BEC side), the Fermi surface has disappeared and the fermions are gapped even for $\Delta \to 0$ by a positive value of $m_\psi^2 + \lambda_{\phi\psi}\rho_0$. We plot our result for the Fermi radius and the dispersion relation in Fig. 6.6.

6.7 Results

For the studies in the previous section, we have omitted the effect of particle-hole fluctuations for simplicity. In the following, however, all the results are given for the correspondingly extended truncation inluding particle-hole fluctuations.

Single-particle gap at $T = 0$

On the BCS side for small negative values of c the single particle gap at zero temperature can be calculated from perturbation theory. The result first found by Gorkov and Melik-Bakhudarov is given by $\Delta/E_F = (2/e)^{7/3} e^{\pi/(2c)}$. In our approach we can extend this calculation to the strongly interacting regime and to the BEC side of the crossover. Our result for the gap in units of the Fermi energy, Δ/E_F, is shown in Fig. 6.7. We find perfect agreement with Gorkov and Melik-Bakhudarov on the BCS side. At the unitarity point, $(ak_F)^{-1} = 0$, we obtain $\Delta/E_F = 0.46$. Another benchmark for the comparison of different methods is the chemical potential in units of the Fermi energy at $(ak_F)^{-1} = 0$

	μ/E_F	Δ/E_F
Carlson *et al.* [155]	0.43	0.54
Perali *et al.* [161]	0.46	0.53
Haussmann *et al.* [164]	0.36	0.46
Bartosch *et al.* [177]	0.32	0.61
present work	0.51	0.46

Table 6.1: Results for the single-particle gap and the chemical potential at $T = 0$ and at the unitarity point by various authors.

and $T = 0$. We find $\mu/E_F = 0.51$. In Tab. 6.1 we compare the results from different (non-perturbative) approaches for this quantity as well as for Δ/E_F.

Phase diagram

With our approach we can compute the critical temperature for the phase transition to superfluidity throughout the crossover. The results are shown in Fig. 6.7. We plot the critical temperature in units of the Fermi temperature T_c/T_F as a function of the scattering length measured in units of the inverse Fermi momentum, i. e. the concentration $c = ak_F$.

Now, we discuss the three different regimes of the crossover. On the left side, where $c^{-1} < -1$, the BCS approximation and the effect of particle-hole fluctuations yield a critical temperature [173]

$$\frac{T_c}{T_F} = \frac{e^C}{\pi}\left(\frac{2}{e}\right)^{7/3} e^{\pi/(ak_F)} \approx 0.28 e^{\pi/(ak_F)}. \tag{6.36}$$

depicted by the short dashed line in the right panel of Fig. 6.7. Here, $C \approx 0.577$ is EulerÕs constant. On the BEC-side for very large and positive c^{-1} our result approaches the critical temperature of a free Bose gas where the bosons have twice the mass of the fermions $M_B = 2M$. In our units the critical temperature is then

$$\frac{T_{c,\mathrm{BEC}}}{T_F} = \frac{2\pi}{\left(6\pi^2\zeta(3/2)\right)^{2/3}} \approx 0.218. \tag{6.37}$$

In-between there is the unitarity regime, where the two-atom scattering length diverges ($c^{-1} \to 0$) and we deal with a system of strongly interacting fermions.

Our best result including also the particle-hole fluctuations is given by the solid line. This may be compared with a functional renormalization flow investigation leaving out particle-hole fluctuations (dot-dashed line) [68]. For $c \to 0_-$ the solid line of our result matches the BCS theory including the correction by Gorkov and Melik-Barkhudarov. Deviations from this pertubative regime appear only quite close to the regime of strong interactions $c^{-1} \to 0$.

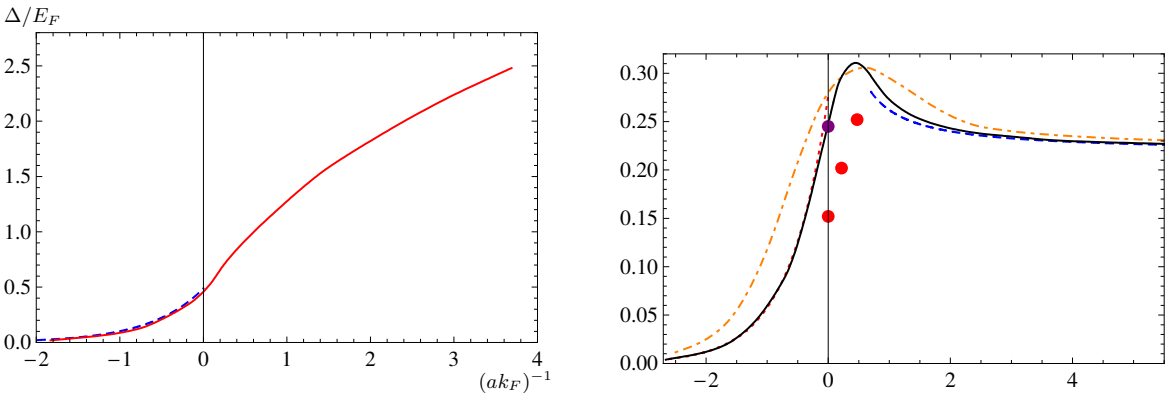

Figure 6.7: Left panel: Gap in units of the Fermi energy Δ/E_F as a function of $(ak_F)^{-1}$ (solid line). For comparison, we also plot the result found by Gorkov and Melik-Bakhudarov (left dahed) and extrapolate this to the unitarity point $(ak_F)^{-1} = 0$, where $\Delta_{\mathrm{GMB}}/E_F = 0.49$. Right panel: Critical temperature T_c/T_F in units of the Fermi temperature as a function of the crossover parameter $(ak_F)^{-1}$. The three red dots close to and at unitarity show the QMC results by Burovski *et al.* [158].

For $c \to 0_+$ this value is approached in the form [180]

$$\frac{T_c - T_{c,\mathrm{BEC}}}{T_{c,\mathrm{BEC}}} = \kappa a_M n_M^{1/3} = \kappa \frac{a_M}{a} \frac{c}{(6\pi^2)^{1/3}}. \tag{6.38}$$

Here, $n_M = n/2$ is the density of molecules and a_M is the scattering length between them. We use our result $a_M/a = 0.59$ obtained from solving the flow equations in vacuum, i. e. at $T = n = 0$, see also [68]. This has to be compared to the result obtained from solving the corresponding Schrödinger equation which gives $a_M/a = 0.6$ [179]. For the coefficients determining the shift in T_c compared to the free Bose gas we find $\kappa = 1.39$. In [181, 182] the result for an interacting BEC is given with $\kappa = 1.31$ (dashed curve on BEC side of 6.7), which is in reasonable agreement with our result . Other characteristic quantities are the maximum of the ratio $(T_c/T_F)_{\max} \approx 0.31$ and the location of the maximum $(ak_F)^{-1}_{\max} \approx 0.40$. For $c^{-1} > 0.5$ the effect of the particle-hole fluctuations vanishes. This is expected since the chemical potential is now negative $\mu < 0$ and there is no Fermi surface any more.

In the unitary regime ($c^{-1} \approx 0$) the particle-hole fluctuations still have a quantitative effect. We can give an improved estimate for the critical temperature at the resonance ($c^{-1} = 0$) where we find $T_c/T_F = 0.248$ and a chemical potential $\mu_c/T_F = 0.55$. A comparison to other methods and our previous work is given in Tab. 6.2. We observe reasonable agreement with QMC results for the chemical potential μ_c/T_F, however, our critical temperature T_c/T_F is larger.

	μ_c/E_F	T_c/T_F
Burovski *et al.* [158] (QMC)	0.49	0.15
Bulgac *et al.* [157] (QMC)	0.43	< 0.15
Akkineni *et al.* [159] (QMC)	-	0.245
Previous FRG estimate [60]	0.68	0.276
present work	0.55	0.248

Table 6.2: Results for T_c/T_F and μ_c/T_F at the unitarity point by various authors.

Discussion and Outlook

The inclusion of particle-hole fluctuations and further extensions of the truncation improve our numerical results in the perturbative domains of the crossover to match the results from well-known other field-theoretical methods. We obtain considerable quantitative precision on the BCS and BEC sides of the resonance.

Also our finding for the ratio a_M/a is in good agreement with the exact result [179]. This quantitative accuracy is remarkable in view of the fact that we have started with a purely fermionic microscopic theory, without propagating bosonic degrees of freedom or bosonic interactions.

In the strongly interacting regime where the scattering length diverges, no analytical treatments are available. Our results for the gap Δ/E_F and the chemical potential μ/E_F at zero temperature are in reasonable agreement with Monte-Carlo simulations. This holds also for the ratio μ_c/E_F at the critical temperature. The critical temperature T_c/T_F itself is found to be larger than the widely accepted Monte-Carlo result, however.

In future studies our approximations might be improved mainly at two points. One is the frequency- and momentum dependence of the boson propagator. In the strongly interacting regime this could be rather involved, developing structures beyond our current approximation. A more detailed resolution might lead to modifications in the contributions from bosonic fluctuations to various flow equations. Another point concerns structures in the fermion-fermion interaction that go beyond a diatom bound-state exchange process. Close to the unitarity point, other contributions might arise, for example in form of a ferromagnetic channel. While further quantitative modifications in the unitarity regime are conceivable, the present status of approximations already allows for a coherent description of the BCS-BEC crossover for all values of the scattering length, temperature and density by one simple method and microscopic model. This includes the critical behaviour of a second order phase transition as well as the temperature zero range.

However, also the QMC simulations have some weak points and as, e.g., finite size effects and the sign problem for fermions. In order to shed light on the relation between our method and QMC studies we started a study of finite size effects using the Wetterich RG [183].

Chapter 7

Curvature-ghost coupling in asymptotically safe gravity

The construction of an internally consistent and falsifiable theory of quantum gravity is one of the major challenges of modern theoretical physics. The perturbative quantization of the Einstein-Hilbert action yields a non-renormalizable theory [72–75]. Therefore several alternative approaches have been proposed: A change in the degrees of freedom and of the microscopic action, as well as a different approach to quantization, or assumptions about a discrete nature of spacetime offer possible routes to a predictive theory of quantum gravity. However, the possibility remains that the apparent non-renormalizability is not a failure of Einstein gravity but rather of the simple perturbative quantization scheme. It is Weinberg's asymptotic-safety scenario [19, 22, 85] that represents a possible non-perturbative way for a predictive theory of quantum gravity. A suitable tool to study this scenario is the functional RG formulated in terms of the Wetterich equation.

The functional RG for gravity has been pioneered by Reuter [20] and during the last years a substantial body of evidence for asymptotic safety of Quantum Einstein Gravity (QEG) has been accumulated [24–44, 46–49], for reviews see [21–23]. Therein not only the existence of a non-Gaußian fixed point has been confirmed in a variety of studies, but also the critical exponents classifying the relevant directions at the fixed point show a satisfactory convergence upon increasing the truncation. Moreover, implications of QEG for cosmology as well as black hole physics have been studied, see [50–52] for references.

In this chapter we contribute to this evidence by verifying the existence of a non-Gaußian fixed point by an alternative computation technique and including a running curvature-ghost coupling as a first step towards the flow of the ghost sector of the theory. Indeed, as is known from certain gauges in Yang-Mills theories ghosts can influence the strong-coupling regime of a gauge theory considerably [16, 184–188]. Thus it is important to check that the property of asymptotic saftey discovered so far within the Einstein-Hilbert truncation and beyond remains stable under the inclusion of the ghost flow.

7.1 Quantum Einstein Gravity

Early calculations [20, 24] have focussed on the Einstein-Hilbert truncation

$$\Gamma_{\rm EH} = 2\bar{\kappa}^2 Z_{\rm N}(k) \int d^d x \sqrt{\gamma}(-R(\gamma) + 2\bar{\lambda}(k)) + \text{classical gauge fixing}, \tag{7.1}$$

where $\bar{\kappa}^2 = \frac{1}{32\pi G_{\rm N}}$. The Einstein-Hilbert action $\Gamma_{\rm EH}$ contains the dimensionful Newton constant $G_{\rm N}$, the running graviton wave function renormalisation $Z_{\rm N}(k)$, and the running cosmological constant $\bar{\lambda}(k)$. The curvature scalar $R(\gamma)$ is constructed from the metric field $\gamma_{\mu\nu}$ and the gauge fixing terms will be discussed below. We introduce the dimensionless renormalized coupling G

$$G = \frac{G_{\rm N}}{Z_{\rm N} k^{2-d}} = \frac{1}{32\,\pi\,\bar{\kappa}^2\,Z_{\rm N}\,k^{2-d}}, \tag{7.2}$$

The flow equation for this coupling can be expressed by the dimensional rescaling terms and the graviton anomalous dimension $\eta = -\partial_t \ln Z_{\rm N}$, reading

$$\partial_t G = (d - 2 + \eta)G. \tag{7.3}$$

This already allows for a preliminary discussion of the fixed-point structure in the coupling G. The RG equation (7.3) shows a Gaußian fixed point (GFP), $G^* = 0 \to \eta = 0$, and further allows for a non-Gaußian fixed point (NGFP) if $\eta = \eta(G^*, \lambda^*, ...) = 2 - d$. In the vicinity of the GFP we observe scaling according to the canonical dimension of the gravitational coupling $[G_{\rm N}] = 2-d$, which is negative for $d = 4$ and so implies perturbative non-renormalizability.

For the NGFP, however, the anomalous dimension η counter-balances the canonical dimension of $G_{\rm N}$ facilitating non-perturbative renormalizability of Einstein gravity within the asymptotic safety scenario. The counter-balancing resembles closely to the sum rule found in the three dimensional Yukawa systems in Chap. 5, cf. Eq. (5.40). At the NGFP the gravitational coupling scales like

$$G_{\rm N,k} = G^* k^{2-d}. \tag{7.4}$$

If $G^* \neq 0$ the dimensionful Newton constant $G_{\rm N}$ becomes arbitrarily small for $d > 2$ indicating antiscreeing of gravity in the fixed-point regime.

This discussion has to be substantiated by the computation of explicit flow equations (e.g. in the Einstein-Hilbert truncation, Eq. (7.1)) for the anomalous dimension η and the dimensionless cosmological constant $\lambda = \bar{\lambda}(k)k^{-2}$. This has been done for the first time in [20] revealing the actual existence of a NGFP. In Sec. 7.4 we present the flow equations

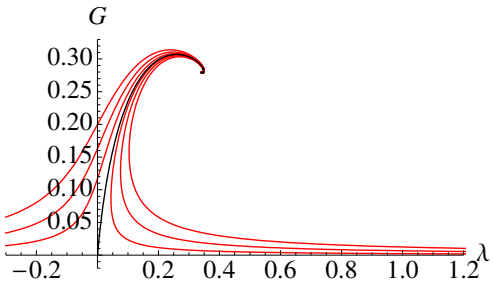

Figure 7.1: RG flow trajectories in the $G - \lambda$-plane.

for those couplings obtained with our truncation and cutoff scheme and applying the computational method that is introduced below.

The RG flow is found to be dominated by two fixed points, namely the Gaußian one, $(G^*, \lambda^*) = (0, 0)$, and a NGFP with $G^* > 0$ and $\lambda^* > 0$. The fact that the value of G^* is positive is important for stability reasons. We present the phase diagram of the RG trajectories in the (G, λ)-plane in Fig. 7.1, showing three classes of trajectories emanating from the NGFP: One trajectory is singled out by hitting the GFP for the limit $k \to 0$, the separatrix. The trajectories on the l.h.s. (r.h.s.) of the separatrix run towards negative (positive) cosmological constants in the infrared. This also stimulated studies of phenomenological implications of the existence of a fixed point, see e.g. [53, 54].

In the Einstein-Hilbert truncation we have two running couplings, G and λ, and the stability matrix at the NGFP yields a pair of complex conjugate RG eigenvalues with a positive real part. Thus, G and λ correspond to two RG relevant directions and the imaginary parts of the RG eigenvalues entail a spiralling of the trajectories running out of the NGFP, see Fig. 7.1.

The existence of the non-Gaußian fixed point has remains remarkably stable upon the inclusion of higher orders of the curvature [25–33, 36–38] and matter [43–46]. Recently, new techniques have allowed to go beyond the class of $f(R)$ truncations and include, e.g., the operator $C_{\mu\nu\kappa\lambda}C^{\mu\nu\kappa\lambda}$ involving the Weyl tensor among the gravitational interactions [41]. All these results do not only agree on the existence of a NGFP, but also on the classification of RG relevant and irrelevant directions. There are strong indications from high-order calculations that the number of relevant directions number is finite [36, 39–41].

Some features of QEG are also reminiscent to results obtained within other nonperturbative approaches to a quantum field theory of gravity [189–191].

7.2 Gauge fixing and ghost terms

The theory space of QEG consists, by definition, of functionals depending on the metric in a diffeomorphism invariant way and we have to specify a gauge fixing procedure for the functional integral as usual for gauge and gravity theories.

From certain gauges in Yang-Mills theories, e.g., the Landau gauge or the Coulomb gauge, it is known that ghosts can play an important if not dominant role in the strong-coupling regime of a gauge theory [16, 184–188]. This is due to the fact that the strong-coupling regime can be entropically dominated by field configurations near the Gribov horizon[1] which induce an enhancement of the ghost propagator. As the Gribov ambiguity is also present in standard gauges in general relativity [192], similar mechanisms may become relevant in QEG. However, investigations of the non-Gaußian fixed point in QEG have neglected running couplings in the ghost sector so far, mainly for technical reasons. Only a classical ghost term has been considered as the choice of truncations of the effective action in gravity has partly been guided by the available computational tools, most notably the heat-kernel expansion. We take a first step to go beyond the classical ghost term and examine the RG flow in the ghost sector. More specifically, we truncate the theory space of QEG down to the following action:

$$\Gamma_k \;=\; \Gamma_{\rm EH} + \Gamma_{\rm gf} + \Gamma_{\rm gh} + \Gamma_{\rm R\,gh}, \tag{7.5}$$

where we introduced the gauge-fixing action $\Gamma_{\rm gf}$, the Faddeev-Popov ghost term $\Gamma_{\rm gh}$ and a ghost-curvature term $\Gamma_{\rm R\,gh}$ explicitely reading

$$\Gamma_{\rm gf} \;=\; \frac{Z_{\rm N}(k)}{2\alpha}\int d^dx\sqrt{\bar g}\,\bar g^{\mu\nu}F_\mu[\bar g,h]F_\nu[\bar g,h], \tag{7.6}$$

$$\Gamma_{\rm gh} \;=\; -\sqrt{2}\,Z_{\rm c}(k)\int d^dx\,\sqrt{\bar g}\,\bar c_\mu\mathcal{M}^\mu{}_\nu c^\nu, \tag{7.7}$$

$$\Gamma_{\rm R\,gh} \;=\; \bar\zeta(k)\int d^dx\sqrt{\gamma}\,\bar c^\mu R c_\mu. \tag{7.8}$$

For the necessary gauge fixing of metric fluctuations, we apply the background-field method [20, 193–195], where the full metric $\gamma_{\mu\nu} = \bar g_{\mu\nu} + h_{\mu\nu}$ is decomposed into the background metric $\bar g_{\mu\nu}$ with its compatible covariant derivative $\bar D_\lambda$. $h_{\mu\nu}$ denotes the fluctuations around this background which do not have to obey any constraints concerning their amplitude. This is a crucial difference to a perturbative treatment on a fixed background. The curvature scalar constructed from the full metric is denoted by R, the one pertaining to the background metric by $\bar R$. The gauge-fixing action $\Gamma_{\rm gf}$ contains the gauge-fixing condition $F_\mu[\bar g,h]$, which for the background-covariant generalisation of the harmonic gauge reads

$$F_\mu[\bar g,h] = \sqrt{2}\bar\kappa\Big(\bar D^\nu h_{\mu\nu} - \frac{1+\rho}{d}\bar D_\mu h^\nu{}_\nu\Big). \tag{7.9}$$

[1]The gauge fixing condition ideally chooses one representative from each gauge orbit defining a submanifold in configuration space by the set of all representatives. However, in practice the gauge orbits may intersect this submanifold more than once which leads to the so-called the Gribov ambiguity. In order to resolve the problem of the Gribov ambiguity the functional integral is restricted to a single Gribov region whose boundary is called a Gribov horizon.

In Eq. (7.6), we ignore any independent running of $\alpha(k) \to \alpha$ =const and ρ. The appropriate ghost term $\Gamma_{\rm gh}$ contains the Faddeev-Popov operator

$$\mathcal{M}^{\mu}{}_{\nu} = \bar{g}^{\mu\rho}\bar{g}^{\sigma\lambda}\bar{D}_{\lambda}(\gamma_{\rho\nu}D_{\sigma} + \gamma_{\sigma\nu}D_{\rho}) - 2\frac{1+\rho}{d}\bar{g}^{\rho\sigma}\bar{g}^{\mu\lambda}\bar{D}_{\lambda}\gamma_{\sigma\nu}D_{\rho}, \tag{7.10}$$

and $Z_{\rm c}(k)$ denotes a wave function renormalisation for the ghosts, which we shall later set to $Z_{\rm c}(k) = 1$ in our calculations; this amounts to a classical treatment of the ghost "kinetic" term. Computations for this ghost kinetic term have been performed recently [48, 49]. The $\Gamma_{\rm R\,gh}$ term in Eq. (7.8) contains the running curvature-ghost coupling $\bar{\zeta}(k)$ which is of central interest here. In any dimension, it corresponds to a marginal coupling in a perturbative power-counting classification, as the ghosts carry canonical dimension $\frac{d-2}{2}$. Since such a classification does no longer hold at a non-Gaußian fixed point, it is a crucial question whether this curvature-ghost coupling becomes relevant or irrelevant because of the interactions.

In the remainder of this chapter, we drop the argument k of the couplings which are implicitly understood as running couplings.

7.3 Computational method

As before, our truncation (7.5) defines a hypersurface in theory space and the solution of the flow equation (2.20) provides us with an RG trajectory in this hypersurface, once an initial condition is specified. For unspecified initial conditions, the flow equation defines a vector field of β-functions on this hypersurface. In order to arrive at an explicit representation of this vector field in terms of the flow of the couplings, we need to project the right-hand side of the flow equation onto the operators of our truncation.

For this, we perform the computation on a maximally symmetric background metric of a d dimensional sphere of radius r in Euclidean space where

$$\bar{R} = \frac{d(d-1)}{r^2}, \quad \bar{R}_{\mu\nu} = \bar{g}_{\mu\nu}\frac{\bar{R}}{d}, \qquad \int d^dx\sqrt{\bar{g}} = \frac{\Gamma(d/2)}{\Gamma(d)}(4\pi r^2)^{\frac{d}{2}}. \tag{7.11}$$

Whereas this leads to an enormous simplification of the calculations, this background does not allow to disentangle the flow of $\Gamma_{\rm R\,gh}$ from that of, e.g., an operator of the form $\int d^dx\sqrt{\gamma}\,\bar{c}^{\mu}R_{\mu\nu}c^{\nu}$. Moreover, as we set $\gamma_{\mu\nu}$=$\bar{g}_{\mu\nu}$ in the flow equation, an operator of the form $\int d^dx\sqrt{\bar{g}}\bar{c}^{\mu}Rc_{\mu}$ can not be disentangled from $\Gamma_{\rm R\,gh}$. For a discussion of the relation between background-field couplings and couplings involving the full physical metric see [196]. Our calculation shares these ambiguities with most of the other works on the asymptotic-safety scenario for QEG, as the derivation of the flow equation with two distinct metrics and more complex backgrounds is highly non-trivial [196–198].

Past works in QEG evaluated the trace on the right-hand side of the flow equation (2.20) by invoking a proper-time representation and using heat-kernel techniques. For our purposes, we explicitly invert $\Gamma_k^{(2)}$ on a d sphere to get the graviton propagator in terms of a basis of hyperspherical harmonics. The trace operation over the eigenvalues can then be evaluated explicitly.

This technique has the advantage that it allows for a straightforward inclusion of external ghost fields, and hence the flow of the coupling parameter of the curvature-ghost term $\bar{\zeta}$ is accessible with our method. For the evaluation of ghost couplings using heat kernel techniques see [48]. Here, we use a decomposition of $\Gamma_k^{(2)} + R_k$ into an inverse propagator matrix contribution $\mathcal{P}_k = \Gamma_k^{(2)}[\bar{c} = 0 = c] + R_k$ containing the regulator but no external ghost fields and a fluctuation matrix $\mathcal{F}$ containing external ghost fields. The components of $\mathcal{F}$ are either linear or bilinear in the ghost fields. With this decomposition, the right-hand side of the flow equation can be expanded as follows:

$$\begin{aligned} \partial_t \Gamma_k &= \frac{1}{2}\mathrm{STr}\{[\Gamma_k^{(2)} + R_k]^{-1}(\partial_t R_k)\} = \frac{1}{2}\mathrm{STr}\tilde{\partial}_t \ln(\mathcal{P}_k + \mathcal{F}) \\ &= \frac{1}{2}\mathrm{STr}\tilde{\partial}_t \ln \mathcal{P}_k + \frac{1}{2}\sum_{n=1}^{\infty} \frac{(-1)^{n-1}}{n}\mathrm{STr}\tilde{\partial}_t (\mathcal{P}_k^{-1}\mathcal{F})^n, \end{aligned} \tag{7.12}$$

where the derivative $\tilde{\partial}_t$ in the second line acts by defintion only on the k dependence of the regulator, $\tilde{\partial}_t = \partial_t R_k \frac{d}{dR_k}$.

7.4 Evaluation of the Einstein-Hilbert sector

For the computation of the Einstein-Hilbert sector we have to evaluate the first term in the second line of Eq. (7.12). The second variation of the Einstein-Hilbert action including the gauge fixing with respect to the metric takes the form [26]

$$\begin{aligned} \delta^2\Gamma_{\mathrm{EH+gf}} &= 2\bar{\kappa}^2 Z_{\mathrm{N}} \int d^dx \sqrt{\bar{g}} h_{\mu\nu} \Big\{ -\Big(\frac{1}{2}\delta^\mu_\rho\delta^\nu_\sigma + \frac{1-2\alpha}{4\alpha}\bar{g}^{\mu\nu}\bar{g}_{\rho\sigma}\Big)\bar{D}^2 \\ &\quad + \frac{1}{4}(2\delta^\mu_\rho\delta^\nu_\sigma - \bar{g}^{\mu\nu}\bar{g}_{\rho\sigma})(\bar{R} - 2\bar{\lambda}) + \bar{g}^{\mu\nu}\bar{R}_{\rho\sigma} - \delta^\mu_\sigma \bar{R}^\nu{}_\rho - \bar{R}^\nu{}_\rho{}^\mu{}_\sigma \\ &\quad + \frac{1-\alpha}{\alpha}(\bar{g}^{\mu\nu}\bar{D}_\rho\bar{D}_\sigma - \delta^\mu_\sigma \bar{D}^\nu \bar{D}_\rho)\Big\} h^{\rho\sigma} \\ &= \int d^dx \sqrt{\bar{g}}\, h^{\mu\nu}\, (\Gamma_h^{(2)})_{\mu\nu\kappa\lambda}\, h^{\kappa\lambda}. \end{aligned} \tag{7.13}$$

We evaluate the fluctuation matrix entries in Landau-deWitt gauge $\alpha = 0$, as this is a fixed point of the RG flow [119, 120], and we set the second gauge parameter $\rho \to \alpha$ for our evaluation of the Einstein-Hilbert sector. For this choice the propagator matrix is diagonal in the gravitational sector and off-diagonal in the ghost sector.

We then apply the York decomposition [199] to the graviton $h_{\mu\nu}$ to identify its trace part $h = \bar{g}^{\mu\nu}h_{\mu\nu}$, its transverse traceless part $h^{\mathrm{T}}_{\mu\nu}$, and the transverse vector and scalar parts $\hat{\xi}_\mu$ and $\hat{\sigma}$:

$$h_{\mu\nu} = h^{\mathrm{T}}_{\mu\nu} + \bar{D}_\mu\hat{\xi}_\nu + \bar{D}_\nu\hat{\xi}_\mu + \bar{D}_\mu\bar{D}_\nu\hat{\sigma} - \frac{1}{d}\bar{g}_{\mu\nu}\bar{D}^2\hat{\sigma} + \frac{1}{d}\bar{g}_{\mu\nu}h. \tag{7.14}$$

Now, we introduce the notion of the "TT approximation" by the definition that only the transverse traceless mode in the gravitational sector is allowed to propagate and the vector and scalar modes are suppressed. The TT approximation only contains the information about the spin-2-mode, that is characteristic for gravity and it is able to capture the essential physics of the NGFP, allowing for its existence and conserving the number of relevant directions. For the Einstein-Hilbert truncation this is not an essential advantage, as we can straightforwardly compute the full set of modes along the lines we present here. However, we will employ the TT approximation here as it is technically much easier to compute the ghost-curvature term, assuming that it also captures the essential physics in the ghost sector. That this assumption is correct for the kinetic ghost operator has been checked in [49]. In the Landau-DeWitt gauge and TT approximation, we need only the inverse propagator for the transverse traceless tensor on the d sphere:

$$\left(\Gamma^{(2)}_{h^{\mathrm{T}}}\right)_{\mu\nu\kappa\lambda} = \bar{g}_{\mu\nu}\bar{g}_{\kappa\lambda}\,\bar{\kappa}^2 Z_{\mathrm{N}}\left(\frac{d(d-3)+4}{r^2} - 2\bar{\lambda} - \bar{D}^2\right). \tag{7.15}$$

Now we can invert the two-point function to arrive at the full regularized k-dependent propagator,

$$\left(\Gamma^{(2)}_{h^{\mathrm{T}}} + R_{k,h^{\mathrm{T}}}\right)_{\mu\nu\kappa\lambda} G^{\kappa\lambda}{}_{\rho\sigma} = \frac{1}{\sqrt{\bar{g}}}\delta^d(x-x')\bar{g}_{\mu\rho}\bar{g}_{\sigma\nu}, \tag{7.16}$$

where symmetrization of $\mu \leftrightarrow \nu$ and $\rho \leftrightarrow \sigma$ on the left-hand side is understood implicitly. At this stage, we take advantage of the existence of a basis for traceless tensor functions on the d sphere: the tensor hyperspherical harmonics $T^{lm}_{\mu\nu}(x)$. They fulfill a completeness and an orthogonality relation, and are eigenfunctions of the covariant Laplacean $\bar{D}^2$,

$$\frac{\delta^d(x-x')}{\sqrt{\bar{g}}}\bar{g}_{\mu\rho}\bar{g}_{\nu\sigma} = \sum_{l=2}^{\infty}\sum_{m=1}^{D_l} T^{lm}_{\mu\nu}(x)T^{lm}_{\rho\sigma}(x'), \tag{7.17}$$

$$\delta^{lk}\delta^{mn} = \int d^dx\,\sqrt{\bar{g}}\,\bar{g}^{\mu\rho}\bar{g}^{\nu\sigma}T^{lm}_{\mu\nu}(x)T^{kn}_{\rho\sigma}(x), \tag{7.18}$$

$$-\bar{D}^2T^{lm}_{\mu\nu}(x) = \Lambda_l T^{lm}_{\mu\nu}(x). \tag{7.19}$$

For the tensor mode the eigenvalues of the Laplacean are given by Λ_l and there is a D_l-fold degeneracy of the hyperspherical harmonics for fixed l but different m [200, 201] reading

$$\Lambda_l = \frac{l(l+d-1)-2}{r^2}\,,\; D_l = \frac{(d+1)(d-2)(l+d)(l-1)(2l+d-1)(l+d-3)!}{2(d-1)!(l+1)!}. \quad (7.20)$$

As the hyperspherical harmonics form a basis for functions on the d sphere, we can expand the Green's function as follows:

$$G(x-x')_{\mu\nu\rho\sigma} = \sum_{l=2}^{\infty}\sum_{m=1}^{D_l} a_{lm}\, T^{lm}_{\mu\nu}(x) T^{lm}_{\rho\sigma}(x'), \quad (7.21)$$

with expansion coefficients a_{lm}. We insert our expression Eq. (7.15) into Eq. (7.16), and use the eigenvalue equation Eq. (7.19). As the regulator is some function of $-\bar{D}^2$, it turns into the same function of Λ_l in the hyperspherical-harmonics basis.

Applying the completeness relation allows to rewrite the right-hand side of the definition of the Green's function Eq. (7.16). By a comparison of coefficients with respect to the hyperspherical-harmonics basis, we obtain

$$a_{lm} \;=\; \left(\bar{\kappa}^2 Z_{\rm N}\Big(\frac{d(d-3)+4}{r^2} - 2\bar{\lambda} + \Lambda_l\Big) + R_{k,l}\right)^{-1}, \quad (7.22)$$

for $l \geq 2$. Here, we have assumed that the argument of the regulator $R_k(x)$ is a function of the Laplacean, $x = x(\bar{D}^2)$, such that $R_{k,l} := R_k\Big(x\big(\Lambda_l\big)\Big)$. From the expression Eq. (7.22), it is obvious that the cosmological constant is similar to a wrong-sign mass term for the graviton modes. From this point on, we confine ourselves to $d = 4$, even though the calculations are straightforwardly generalizable to $d \neq 4$, see also [34, 35].

We parameterize the regulator function for the transverse traceless mode by

$$R_k(x) = x\,\mathfrak{r}\left(\frac{x}{Z_{\rm N}\bar{\kappa}^2 k^2}\right), \quad (7.23)$$

where the shape function $\mathfrak{r}(y)$ specifies the details of the Wilsonian momentum-shell integration. Different choices correspond to different RG schemes. As we need to expand in the curvature radius r in order to project the flow onto the truncation, an analytic shape function is required. Here, we work with an exponential shape function $\mathfrak{r}(y) = \frac{1}{e^y-1}$ as an example. Moreover, the regulator can be adjusted to the flow of the spectrum of the full propagator [202] by choosing $y = \frac{\Gamma^{(2)}_{h^{\rm T}}}{Z_{\rm N}\bar{\kappa}^2 k^2}$ evaluated on the background field. For the graviton, this yields

$$\partial_t R_k(y) = -(2-\eta) y\,\mathfrak{r}'\,\Gamma^{(2)}_{h^{\rm T}} + (\mathfrak{r} + y\,\mathfrak{r}')\partial_t \Gamma^{(2)}_{h^{\rm T}}, \quad (7.24)$$

where the prime denotes the derivative of $\mathfrak{r}(y)$ with respect to y. The resulting general structure of the flow with this type of regulator has first been discussed in [203]. Whereas a numerical integration of the resulting flow can become demanding due to the intricate structure of the resultig differential equation [204], this form of the flow can be advantageous for analytical studies, as will be the case in the following.

The spectrally adjusted flow equation for the flowing action has the following form in the Einstein-Hilbert sector

$$\partial_t \Gamma_k = \sum_{\{\mathfrak{m}\in\mathcal{M}\}} \left(\Gamma^{(2)}_{k\,\mathfrak{m}}\,(1+\mathfrak{r})\right)^{-1} \left[\partial_t \Gamma^{(2)}_{k\,\mathfrak{m}}\mathfrak{r} + \Gamma^{(2)}_{k\,\mathfrak{m}}\mathfrak{r}'\left(y(-2+\eta) + \frac{\partial_t \Gamma^{(2)}_{k\,\mathfrak{m}}}{Z_{\rm N} N_{\mathfrak{m}} \bar{\kappa}^2 k^2}\right)\right], \tag{7.25}$$

where $y = \Gamma^{(2)}_{k\,\mathfrak{m}}/(Z_{\rm N} N_{\mathfrak{m}} \bar{\kappa}^2 k^2)$ and $\mathcal{M}$ is the set of all modes of the York decomposition of the graviton as well as the ghost. We have also introduced a normalising factor $N_{\mathfrak{m}}$ which is chosen such that numerical factors in front of the eigenvalue of $-\bar{D}^2$ in the inverse propagator cancel in y. This guarantees that all Laplacean momentum modes are regularised by the same effective IR cutoff scale. In order to regularise the conformal instability, N_m may also acquire a negative sign. Here, we will only take the transvere traceless mode in the spirit of the TT approximation. This means that the sum $\sum_{\{\mathfrak{m}\in\mathcal{M}\}}$ which encodes the trace operation from the Wetterich equation explicitly reads

$$\sum_{\{\mathfrak{m}\in\mathcal{M}\}}\Big|_{\rm TT} = \int d^d x\sqrt{g}\int d^d y\sqrt{g}\frac{\delta^d(x-y)}{\sqrt{g}}\sum_{l=2}\sum_{m=1}^{D_l}. \tag{7.26}$$

The sum over m simply results in a multiplicative factor D_l, see Eq. (7.20), and the integrals can be carried out by use of the orthogonality relation Eq. (7.18). For the sum over l, we invoke the Euler-MacLaurin formula that transforms the sum over l into an integral. Inserting the transverse traceless propagator and using the Euler-MacLaurin formula, we project onto the two running couplings in the Einstein-Hilbert sector. For example, in four dimensions, $\partial_t Z_{\rm N}$ is accompanied by a factor of the curvature radius squared, whereas the combination $\partial_t(Z_{\rm N}\lambda)$ comes with a factor of r^4. Incidentally, all non-integral terms in the Euler-MacLaurin formula do not contribute to the scalar curvature-ghost coupling. This allows for a straightforward projection and yields the following β functions for the dimensionless couplings in TT approximation:

$$\partial_t G = (2+\eta)G, \tag{7.27}$$

$$\begin{aligned}\partial_t\lambda = {} & (-2+\eta)\lambda - \frac{5G}{4\pi}\Big\{e^{2\lambda}(4\lambda+\eta+2\partial_t\lambda) - 4\lambda(2\lambda+\partial_t\lambda)\big[\mathrm{Ei}(2\lambda) \\ & +\ln(1-e^{2\lambda}) - \ln(e^{2\lambda}-1) + i\pi\theta(-\lambda)\big] - 2\partial_t\lambda\mathrm{Li}_2(e^{2\lambda}) - 4\mathrm{Li}_3(e^{2\lambda})\Big\},\end{aligned} \tag{7.28}$$

and

$$\eta = \frac{25G}{12\pi}\Big\{e^{2\lambda}\eta - 2(2\lambda+\partial_t\lambda)\big[\mathrm{Ei}(2\lambda) - \ln(e^{2\lambda}-1) + i\pi\theta(-\lambda)\big] \\ -4\lambda\,\ln(1-e^{2\lambda}) - 2\mathrm{Li}_2(e^{2\lambda})\Big\}. \tag{7.29}$$

Note that branch cuts in the logarithm and the polylogarithm contribute imaginary parts which cancel for $\lambda > 0$. Thereby, the flow equations are completely real for all values of λ. At the fixed point, $\partial_t\lambda = 0$ and $\eta = -2$, implying (for $\lambda > 0$)

$$\begin{aligned} 0 &= 4\lambda + \frac{5G}{4\pi}\Big\{e^{2\lambda}(4\lambda-2) - 8\lambda^2\big[\mathrm{Ei}(2\lambda) + \ln(1-e^{2\lambda}) - \ln(e^{2\lambda}-1)\big] - 4\mathrm{Li}_3(e^{2\lambda})\Big\}, \\ -2 &= \frac{25G}{12\pi}\Big\{-2e^{2\lambda} - 4\lambda\big[\mathrm{Ei}(2\lambda) - \ln(e^{2\lambda}-1)\big] - 4\lambda\,\ln(1-e^{2\lambda}) - 2\mathrm{Li}_2(e^{2\lambda})\Big\}. \end{aligned}$$

A numerical solution yields the following fixed-point values

$$G_*^{\mathrm{TT}} = 0.2704, \quad \lambda_*^{\mathrm{TT}} = 0.3834. \tag{7.30}$$

The universal value $G_*^{\mathrm{TT}}\lambda_*^{\mathrm{TT}} = 0.1037$ is very close to the numerical values from other gauges and regulators [23]. The eigenvalues of the stability matrix appear as a complex conjugate pair,

$$\theta_{1,2}^{\mathrm{TT}} = 2.271 \pm i1.705, \tag{7.31}$$

inducing a spiral shape of the flow lines in the vicinity of the NGFP, see Fig. 7.1. It is straightforward to derive the full flow equations for the Einstein-Hilbert sector including all modes with our method. In the full treatment and Landau-deWitt gauge we find the slightly shifted fixed point values $G_* = 0.2701$ and $\lambda_* = 0.3785$ and the RG eigenvalues $\theta_{1,2} = 2.1015 \pm i1.685$. The full flow equations for the Einstein-Hilbert sector for arbitrary gauge parameters $\alpha = \rho$ can be found in [49].

As the combination of the Landau-DeWitt gauge $\alpha = 0$ together with the spectrally adjusted regulator has not been used before, our results represent an independent verification of the fixed-point scenario.

7.5 Ghost-Curvature Coupling in QEG

On the background of d spheres, the left-hand side of the flow equation for the scalar curvature-ghost coupling after setting $\gamma_{\mu\nu} = \bar{g}_{\mu\nu}$ takes the form

$$\partial_t\Gamma_{\mathrm{R\,gh}} = (\partial_t\bar{\zeta})\bar{c}^\mu c_\mu R\int d^dx\sqrt{\bar{g}} = (\partial_t\bar{\zeta})\bar{c}^\mu c_\mu\frac{\Gamma(d/2)}{\Gamma(d)}\,d(d-1)\,(4\pi)^{d/2}\,(r^2)^{\frac{d}{2}-1}. \tag{7.32}$$

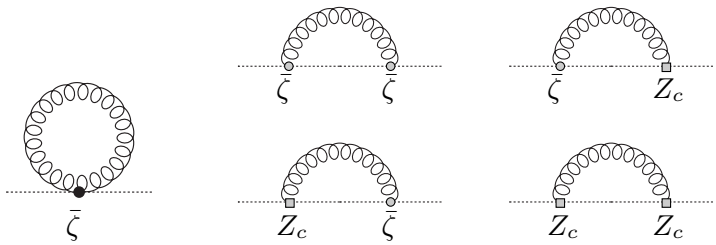

Figure 7.2: Single diagram on the left: tadpole contribution to the running of $\bar{\zeta}$. Four diagrams on the right: Two-vertex contribution to the wave function renormalisation of the ghost and the curvature-ghost coupling $\bar{\zeta}$. Spiral lines denote gravitons, dashed lines denote ghosts. The regulator insertion in the internal propagators is implicitly understood.

As $\mathcal{F}$ contains terms linear and bilinear in the ghosts, the flow of $\bar{\zeta}$ is fully determined by the $n = 1$ and $n = 2$ terms of the expansion of the flow equation Eq. (7.12).

Diagrammatically, we arrive at five contributions displayed in Fig. 7.2 in which only the transverse traceless graviton mode propagates as we employ the TT approximation: The two-vertex diagram appears in four different versions, as two different antighost-ghost-graviton vertices exist in our truncation, namely one $\propto \bar{\zeta}$ and one $\propto Z_c$. Accordingly, there is a diagram with two $\bar{\zeta}$ vertices, one with two Z_c vertices and two mixed ones. Now we can make use of the fact that the equation of motion for the transverse traceless part of $h^{\mu\nu}$ vanishes identically on d spheres for vanishing ghost fields,

$$(\delta(\sqrt{\gamma}R))\,|_{h^{\mathrm{T}}_{\mu\nu}} = \left(-h^{\mu\nu}R_{\mu\nu} + \bar{D}^{\mu}\bar{D}^{\nu}h_{\mu\nu} - \bar{D}^2 h + \frac{1}{2}hR\right)|_{h^{\mathrm{T}}_{\mu\nu}} \overset{d\ \text{sphere}}{=} 0. \tag{7.33}$$

Hence, the antighost-ghost-graviton vertex which is $\propto \bar{\zeta}$ does not receive a contribution from the transverse traceless mode, when evaluated on the Euclidean deSitter background. This fact is obvious for maximally symmetric spaces, where $R_{\mu\nu} \sim g_{\mu\nu}R$. Hence, a different choice of background would require the evaluation of some of the ghost self-energy diagrams. However, this does not imply that the final result for the β function is background dependent, as the fluctuation matrix entering the tadpole diagram would also change on a different background. A maximally symmetric background simply corresponds to a very efficient organisation of the flow equation also in terms of diagrams. As a result, three of the four selfenergy diagrams are zero.

Finally, we discuss the last diagram with two vertices $\propto Z_c$, which is obtained by the evaluation of the derivative operator of the ghost terms, cf. Eq. (7.10). Therefore, we introduce a simplifying choice for the background ghost fields: We choose them to be covariantly constant,

$$\bar{D}^{\mu}c^{\lambda} = 0, \tag{7.34}$$

which allows to disentangle the flow of $\bar{\zeta}$ from that of the ghost wave function renormalisation Z_c. This last diagram vanishes for covariantly constant ghost background fields,

as the ghost kinetic term can be brought into the following symbolic form by partial integration

$$\Gamma_{\rm gh} \sim \int d^dx\sqrt{\bar{g}}\left(\bar{D}\bar{c}\right)(Dc)\,. \tag{7.35}$$

Upon deriving the antighost-ghost-graviton vertex connected to the antighost from this equation, the result is always proportional to $\bar{D}\bar{c}$, and hence the diagram vanishes on the covariantly constant ghost background, cf. Eq. (7.34). This simply reflects the fact that this diagram contributes solely to the running of the ghost wave function renormalisation. Note that covariantly constant ghosts cannot be realized on d spheres with even d as a consequence of the hairy ball theorem, which is a shortcoming of our computation in $d = 4$. However, the background of d spheres has been chosen due to technical reasons only and we could have imposed covariantly constant ghosts in the first place to simplify the diagrammatic structure of the curvature-ghost-vertex. Therefore, we expect that this approach yields a qualitatively reliable result.

To summarize, only the tadpole diagram contributes to the running of $\bar{\zeta}$, corresponding to the $n = 1$ term in the expansion of the flow equation Eq. (7.12). To evaluate the tadpole diagram, the necessary fluctuation matrix entry projected onto a d sphere is

$$\delta^2\Gamma_{R\,\rm gh}|_{h^{\rm T}} = \bar{\zeta}\bar{c}^\alpha c_\alpha\, h^{{\rm T}\,\kappa\lambda}\delta^\mu_\kappa\delta^\nu_\lambda\left\{-\frac{d(d-3)+4}{2r^2}+\frac{\bar{D}^2}{2}\right\}h^{\rm T}_{\mu\nu}. \tag{7.36}$$

Together with the transverse traceless graviton propagator from the previous section the $n = 1$ term in the expansion of the flow Eq. (7.12) reads

$${\rm Tr}\left(\mathcal{P}^{-1}\mathcal{F}\right) = {\rm Tr}\left(\sum_{l=2}\sum_{m=1}^{D_l}\frac{\bar{\zeta}\,\bar{c}^\alpha c_\alpha\, T^{lm}_{\mu\nu}(x)T^{lm\,\kappa\lambda}(y)\delta^\mu_\kappa\delta^\nu_\lambda}{\bar{\kappa}^2 Z_{\rm N}\left(\frac{(d(d-3)+4)}{r^2}-2\bar{\lambda}+\Lambda_l\right)+R_{k,l}}\left\{-\frac{d(d-3)+4}{2r^2}-\frac{\Lambda_l}{2}\right\}\right),$$

where the trace implies an integration with measure $\int d^dx\sqrt{\bar{g}}\int d^dy\sqrt{\bar{g}}\frac{\delta^d(x-y)}{\sqrt{\bar{g}}}$. Invoking the orthogonality relation Eq. (7.18) and evaluating the $\tilde{\partial}_t$ derivative, we end up with the following expression:

$${\rm Tr}\tilde{\partial}_t\left(\mathcal{P}^{-1}\mathcal{F}\right) = \sum_{l=2}\frac{\bar{\zeta}\,\bar{c}^\alpha c_\alpha\, D_l\partial_t R_{k,l}}{\left(\bar{\kappa}^2 Z_{\rm N}\left(\frac{(d(d-3)+4)}{r^2}-2\bar{\lambda}+\Lambda_l\right)+R_{k,l}\right)^2}\left\{\frac{d(d-3)+4}{2r^2}+\frac{\Lambda_l}{2}\right\}. \tag{7.37}$$

We employ the regulator function for the transverse traceless mode, Eq. (7.23) and apply the Euler-MacLaurin formula to evaluate the trace. Then, we expand the result in powers of the d-sphere curvature and project the result onto the power of $(r^2)^{\frac{d}{2}-1}$ in order to perform a comparison of coefficients with respect to the scalar curvature-ghost term, cf. Eq. (7.32). Again, all non-integral terms in the Euler-MacLaurin formula do not contribute to the scalar curvature-ghost coupling.

7.6 Results

For the discussion of the fixed-point structure of QEG we introduce, additionally to the dimensionless renormalized coupling G (see Eq. (7.2)), the dimensionless renormalized version of ζ by $\zeta = \bar{\zeta}/Z_{\rm c}$. The running of the wave function renormalizations of graviton and ghost, $Z_{\rm N}$ and $Z_{\rm c}$, respectively, are governed by the corresponding anomalous dimensions, η, and $\eta_{\rm c} = -\partial_t \ln Z_{\rm c}$. With these prerequisites, we can now state our result for the graviton-tadpole induced flow of the coupling ζ in $d = 4$:

$$\begin{aligned}\partial_t\zeta &= \eta_c\zeta + \frac{25G\zeta}{6\pi}\Big\{(e^{4\lambda}-2e^{2\lambda})\left(2\lambda+\partial_t\lambda-\frac{\eta}{4}\right)-e^{2\lambda}\\ &\quad+\left((4\lambda-1)\left(\frac{\lambda}{2}+\partial_t\lambda\right)-\frac{\lambda\,\eta}{4}\right)\big(\mathrm{Ei}(2\lambda)-\mathrm{Ei}(4\lambda)\big)\Big\}. \qquad (7.38)\end{aligned}$$

This flow equation has a Gaußian fixed point $\zeta_* = 0$. This can already be concluded from the property that only the tadpole contributes in the TT approximation . Let us investigate the properties of this fixed point in the ghost sector for the case that the remaining system is at the non-Gaußian fixed-point of the Einstein-Hilbert sector, $G \to G_*$, $\lambda \to \lambda_*$. For this, we evaluate Eq. (7.38) at the NGFP and obtain

$$\partial_t\zeta = \eta_c\zeta + \frac{25G_*\zeta}{6\pi}f(\lambda_*), \qquad (7.39)$$

$$f(\lambda) = e^{4\lambda}\left(2\lambda+\frac{1}{2}\right)-e^{2\lambda}\left(\lambda+\frac{1}{2}\right)+8\lambda^2\big(\mathrm{Ei}(2\lambda)-\mathrm{Ei}(4\lambda)\big). \qquad (7.40)$$

In the present truncation involving a classical ghost kinetic term, we have $\eta_c = 0$. Together with the fact that $G > 0$ in the physical domain, this implies that the sign of $f(\lambda)$ decides about the sign of the linearised flow of ζ near its Gaußian fixed point. Indeed, this function is negative for all λ, see Fig. 7.3. The negative sign signals that ζ is asymptotically free. Inserting the fixed-point values from the Einstein-Hilbert sector in the Landau-DeWitt gauge $\alpha = 0$ with a spectrally adjusted cutoff, Eq. (7.30)), we get $\frac{25G_*}{6\pi}f(\lambda_*) = -1.528$. As long as the ghost anomalous dimension η_c remains sufficiently small, our conclusion

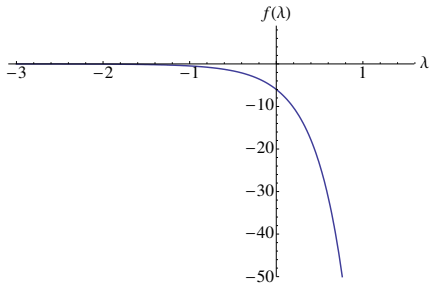

Figure 7.3: $f(\lambda)$ is negative for all values of λ and asymptotically tends to zero for $\lambda \to -\infty$, whereas it is unbounded for positive λ.

persists also for a larger truncation with a running ghost kinetic term. Our conclusions are supported by the results obtained in a recent computation where $\eta_c < 0$ [49].

Our result implies that (i) the non-Gaußian fixed point in the graviton sector is not influenced by the scalar curvature-ghost coupling, as the latter is zero at the fixed point, and (ii) this curvature-ghost coupling is RG relevant for the flow towards the IR. The latter property relates the initial value of this coupling to a physical parameter that has to be fixed by an RG condition (i.e., by an experiment). This does not necessarily imply that the scalar curvature-ghost coupling gives rise to an *independent* physical parameter. Since the background-field effective action has to satisfy (regulator-modified) Slavnov-Taylor and background-field identities [16, 17, 20, 193, 195, 205], this operator may be related to other purely gravitonic operators. An answer to this question requires to resolve the difference between background-metric and fluctuation-metric dependencies which is beyond the scope of this work.

Note that our arguments straightforwardly generalize to the coupling of any operator of the form $\int d^dx\sqrt{\gamma}R \cdot \mathcal{O}_{\rm s}$ in the TT approximation, where $\mathcal{O}_{\rm s}$ is a scalar operator of some fields, e.g., matter fields. The interaction part of the corresponding flow will always have a contribution $\sim Gf(\lambda)$ which supports an anti-screening flow. Of course, other contributions, such as other interaction terms, the anomalous dimensions of the matter fields, and dimensional rescaling terms, can eventually dominate the gravitational contributions.

Summary

To summarize we have provided further evidence for the asymptotic-safety scenario in Quantum Einstein Gravity by computing the RG flow of a scalar curvature-ghost coupling as another building block of the flowing action. In our present truncation involving an Einstein-Hilbert sector, a classical ghost kinetic term, and the curvature-ghost interaction, the coupling ζ is found to be asymptotically free and corresponds to a potentially relevant direction.

From a technical viewpoint, we have shown that a direct integration of gravity fluctuations in the functional RG equation is possible without relying on heat-kernel traces and propertime representations.

Ghost operators or a more general gauge-fixing sector may carry important pieces of information about the flow of a theory in certain gauges. We believe that a more detailed investigation of the ghost sector is important for a better understanding of the non-Gaußian fixed-point regime of Quantum Einstein Gravity. Next steps in this direction have recently been done by the evaluation of the ghost wave function renormalization [48, 49] and the inclusion of higher order curvature-ghost terms [206].

Chapter 8

Concluding remarks

In this thesis we have investigated various physical models with applications ranging from condensed matter physics via particle physics to quantum gravity. We have employed Wetterich's approach to functional renormalization which is a suitable method to investigate non-perturbative quantum field theoretical systems at and near criticality both qualitatively and quantitatively, especially for systems including fermionic as well as bosonic degrees of freedom.

Critical behavior of a quantum system is induced by a fixed point of the renormalization group flow implying an invariance of the system over a large range of scales. A fixed point that is approached in the infrared induces universal behaviour of an effective quantum field rendering it insensitive to its microscopic details. This results in universal scaling laws that are characterized by a set of pure numbers, the critical exponents. On the other hand, a fixed point, which is approached in the ultraviolet, provides a well-defined high-energy limit of a quantum system and as the number of relevant parameters is finite it constitutes a predictive and fundamental quantum field theory in the spirit of Weinberg's asymptotic safety scenario.

We have derived flow equations for left/right asymmetric chiral Yukawa models with and without gauge bosons and reveal fixed-point mechanisms in four and three spacetime dimensions. Furthermore, we computed the fixed point values and their renormalization group eigenvalues or critical exponents to characterize the universal behavior of our models.

The four-dimensional chiral Yukawa systems, see Chaps. 3 and 4, serve as toy models for the standard model Higgs sector and they show signatures of asymptotically safe fixed points by a balancing of contributions from the bosonic and fermionic degrees of freedom. The understanding of this mechanism by means of the very simple Z_2-symmetric Yukawa system in Chap. 3 allowed us to construct an asymptotically safe chiral Yukawa model as a toy model for an asymptotically safe standard model at a defined order in a derivative expansion. In the approximations investigated for the four-dimensional chiral Yukawa

system we solve the triviality problem and obtain predictions of the particle masses for the Higgs and the top quark by only fixing the vacuum expectation value of the Higgs field. Our scenario even provided a weakening of the hierarchy problem, which is a very appealing feature of the asymptotic safety scenario for the standard model.

Infrared fixed-points, as investigated in Chaps. 5 and 6 for effective quantum field theories, give rise to universal long-distance behavior. In the three-dimensional chiral Yukawa system, see Chap. 5, we give a classification of all four-fermion interaction terms. Fixed points in the three-dimensional chiral Yukawa system are induced by a balancing of dimensional rescaling terms and the anomalous dimensions of the quantum fields as well as by a balancing of bosonic and fermionic contributions. The critical exponents define new universality classes and provide benchmark values for systems of strongly correlated chiral fermions that could be tested using other approaches to non-perturbative quantum field theory, e.g. new lattice simulations that are suited to cope with chiral fermions.

In a system of non-relativistic two-component fermions a fixed-point dominates the renormalization group flow giving rise to universality in the BCS-BEC crossover, see Chap. 6. For BCS-BEC crossover physics, the experimental realization of molecule condensates and the subsequent crossover to a BCS-like state of weakly attractively interacting fermions pave the way to future precision measurements and provide an experimental testing ground for non-perturbative methods. To facilitate a sensible comparision we push the functional renormalization method on a quantitative level and include particle-hole fluctuations, fluctuations of the fermionic self energy and higher order interactions. With this ansatz we have computed universal properties as the critical temperature and the single particle gap with a considerable precision for the whole crossover.

Finally, in Chap. 7, we have provided further evidence for the asymptotic safety scenario in quantum gravity by confirming the existence of an ultraviolet fixed-point under inclusion of a curvature-ghost coupling. In our truncation this coupling is found to be asymptotically free and corresponds to a potentially relevant direction. Further steps completing our first approach have to be done in order to obtain an exhaustive picture of the role of the ghost sector. Work in this direction is on its way [48, 49, 206].

More generally, we have contributed to the understanding of fixed points and their properties by pointing out different mechanisms of how they can be generated as a result of a balancing of loop contributions. In conclusion we have shown that renormalization group flow equations are suitable to investigate effective and fundamental quantum fields at and near criticality. This applies to very different quantum field theories ranging from condensed matter systems to particle physics and gravity. We believe that our contributions may shed light on some basic underlying mechanism of quantum field theories and provide further insight into universal laws of nature.

Bibliography

[1] E. C. G. Stueckelberg and A. Petermann, Helv. Phys. Acta **26**, 499 (1953).

[2] M. Gell-Mann and F. E. Low, "Quantum Electrodynamics At Small Distances," Phys. Rev. **95**, 1300 (1954).

[3] L. P. Kadanoff, "Scaling laws for Ising models near T(c)," Physics **2** (1966) 263.

[4] K. G. Wilson, "Renormalization group and critical phenomena. 1. Renormalization group and the Kadanoff scaling picture," Phys. Rev. B **4**, 3174 (1971).

[5] F. J. Wegner and A. Houghton, "Renormalization group equation for critical phenomena," Phys. Rev. A **8** (1973) 401.

[6] F. J. Wegner, "The Critical State, General Aspects," *In *Phase Transitions and Critical Phenomena, Vol.6*, London 1976, 7-124*

[7] K. G. Wilson and J. B. Kogut, "The Renormalization group and the epsilon expansion," Phys. Rept. **12**, 75 (1974).

[8] C. Wetterich, "Average action and the renormalization group equations," Nucl. Phys. B **352**, 529 (1991).

[9] C. Wetterich, "The Average action for scalar fields near phase transitions," Z. Phys. C **57**, 451 (1993).

[10] C. Wetterich, "Improvement of the average action," Z. Phys. C **60**, 461 (1993).

[11] C. Wetterich, "Exact evolution equation for the effective potential," Phys. Lett. B **301**, 90 (1993).

[12] J. Berges, N. Tetradis and C. Wetterich, "Non-perturbative renormalization flow in quantum field theory and statistical physics," Phys. Rept. **363**, 223 (2002) [arXiv:hep-ph/0005122].

[13] C. Bagnuls and C. Bervillier, "Exact renormalization group equations: An introductory review," Phys. Rept. **348**, 91 (2001) [arXiv:hep-th/0002034].

[14] K. Aoki, "Introduction to the nonperturbative renormalization group and its recent applications," Int. J. Mod. Phys. B **14**, 1249 (2000).

[15] M. Salmhofer and C. Honerkamp, "Fermionic renormalization group flows: Technique and theory," Prog. Theor. Phys. **105**, 1 (2001).

[16] J. M. Pawlowski, "Aspects of the functional renormalisation group," Annals Phys. **322**, 2831 (2007) [arXiv:hep-th/0512261].

[17] H. Gies, "Introduction to the functional RG and applications to gauge theories," arXiv:hep-ph/0611146.

[18] S. Weinberg, "Critical Phenomena For Field Theorists," in *C76-07-23.1* HUTP-76/160, Erice Subnucl. Phys., 1, (1976).

[19] S. Weinberg, "Ultraviolet Divergences In Quantum Theories Of Gravitation," *In *Hawking, S.W., Israel, W.: General Relativity*, 790-831*

[20] M. Reuter, "Nonperturbative Evolution Equation for Quantum Gravity," Phys. Rev. D **57**, 971 (1998) [arXiv:hep-th/9605030].

[21] M. Niedermaier and M. Reuter, "The Asymptotic Safety Scenario in Quantum Gravity," Living Rev. Rel. **9**, 5 (2006).

[22] R. Percacci, "Asymptotic Safety," arXiv:0709.3851 [hep-th].

[23] D. F. Litim, "Fixed Points of Quantum Gravity and the Renormalisation Group," arXiv:0810.3675 [hep-th].

[24] W. Souma, "Non-trivial ultraviolet fixed point in quantum gravity," Prog. Theor. Phys. **102**, 181 (1999) [arXiv:hep-th/9907027].

[25] L. N. Granda and S. D. Odintsov, "Effective average action and nonperturbative renormalization group equation in higher derivative quantum gravity," Grav. Cosmol. **4**, 85 (1998) [arXiv:gr-qc/9801026].

[26] O. Lauscher and M. Reuter, "Ultraviolet fixed point and generalized flow equation of quantum gravity," Phys. Rev. D **65**, 025013 (2002) [arXiv:hep-th/0108040].

[27] M. Reuter and F. Saueressig, "Renormalization group flow of quantum gravity in the Einstein-Hilbert truncation," Phys. Rev. D **65**, 065016 (2002) [arXiv:hep-th/0110054].

[28] O. Lauscher and M. Reuter, "Is quantum Einstein gravity nonperturbatively renormalizable?," Class. Quant. Grav. **19**, 483 (2002) [arXiv:hep-th/0110021].

[29] O. Lauscher and M. Reuter, "Flow equation of quantum Einstein gravity in a higher-derivative truncation," Phys. Rev. D **66**, 025026 (2002) [arXiv:hep-th/0205062].

[30] P. Forgacs and M. Niedermaier, "A fixed point for truncated quantum Einstein gravity," arXiv:hep-th/0207028.

[31] M. Niedermaier, "On the renormalization of truncated quantum Einstein gravity," JHEP **0212**, 066 (2002) [arXiv:hep-th/0207143].

[32] D. F. Litim, "Fixed points of quantum gravity," Phys. Rev. Lett. **92**, 201301 (2004) [arXiv:hep-th/0312114].

[33] M. Niedermaier, "Dimensionally reduced gravity theories are asymptotically safe," Nucl. Phys. B **673**, 131 (2003) [arXiv:hep-th/0304117].

[34] P. Fischer and D. F. Litim, "Fixed points of quantum gravity in higher dimensions," AIP Conf. Proc. **861**, 336 (2006) [arXiv:hep-th/0606135].

[35] P. Fischer and D. F. Litim, "Fixed points of quantum gravity in extra dimensions," Phys. Lett. B **638**, 497 (2006) [arXiv:hep-th/0602203].

[36] A. Codello, R. Percacci and C. Rahmede, "Ultraviolet properties of f(R)-gravity," Int. J. Mod. Phys. A **23**, 143 (2008) [arXiv:0705.1769 [hep-th]].

[37] P. F. Machado and F. Saueressig, "On the renormalization group flow of f(R)-gravity," Phys. Rev. D **77**, 124045 (2008) [arXiv:0712.0445 [hep-th]].

[38] A. Codello, R. Percacci and C. Rahmede, "Investigating the Ultraviolet Properties of Gravity with a Wilsonian Renormalization Group Equation," Annals Phys. **324**, 414 (2009) [arXiv:0805.2909 [hep-th]].

[39] D. Benedetti, P. F. Machado and F. Saueressig, "Four-derivative interactions in asymptotically safe gravity," arXiv:0909.3265 [hep-th].

[40] D. Benedetti, P. F. Machado and F. Saueressig, "Taming perturbative divergences in asymptotically safe gravity," Nucl. Phys. B **824** (2010) 168 [arXiv:0902.4630 [hep-th]].

[41] D. Benedetti, P. F. Machado and F. Saueressig, "Asymptotic safety in higher-derivative gravity," Mod. Phys. Lett. A **24** (2009) 2233 [arXiv:0901.2984 [hep-th]].

[42] A. Eichhorn, H. Gies, M. M. Scherer "Asymptotically free scalar curvature-ghost coupling in Quantum Einstein Gravity" arXiv:0907.1828

[43] R. Percacci and D. Perini, "Constraints on matter from asymptotic safety," Phys. Rev. D **67**, 081503 (2003) [arXiv:hep-th/0207033];

[44] R. Percacci and D. Perini, "Asymptotic safety of gravity coupled to matter," Phys. Rev. D **68**, 044018 (2003) [arXiv:hep-th/0304222].

[45] G. Narain and R. Percacci, "Renormalization Group Flow in Scalar-Tensor Theories. I," Class. Quant. Grav. **27**, 075001 (2010) [arXiv:0911.0386 [hep-th]].

[46] G. Narain and C. Rahmede, "Renormalization Group Flow in Scalar-Tensor Theories. II," Class. Quant. Grav. **27**, 075002 (2010) [arXiv:0911.0394 [hep-th]].

[47] E. Manrique and M. Reuter, "Bare vs. Effective Fixed Point Action in Asymptotic Safety: The Reconstruction Problem," arXiv:0905.4220 [hep-th].

[48] K. Groh and F. Saueressig, "Ghost wave-function renormalization in Asymptotically Safe Quantum Gravity," arXiv:1001.5032 [hep-th].

[49] A. Eichhorn and H. Gies, "Ghost anomalous dimension in asymptotically safe quantum gravity," Phys. Rev. D **81** (2010) 104010 [arXiv:1001.5033 [hep-th]].

[50] A. Bonanno, "Astrophysical implications of the Asymptotic Safety Scenario in Quantum Gravity," arXiv:0911.2727 [hep-th].

[51] A. Bonanno, A. Contillo and R. Percacci, "Inflationary solutions in asymptotically safe f(R) gravity," arXiv:1006.0192 [gr-qc].

[52] K. Falls, D. F. Litim and A. Raghuraman, "Black holes and asymptotically safe gravity," arXiv:1002.0260 [hep-th].

[53] D. F. Litim and T. Plehn, "Virtual Gravitons at the LHC," arXiv:0710.3096 [hep-ph].

[54] D. F. Litim and T. Plehn, "Signatures of gravitational fixed points at the LHC," Phys. Rev. Lett. **100**, 131301 (2008) [arXiv:0707.3983 [hep-ph]].

[55] M. Shaposhnikov and C. Wetterich, Phys. Lett. B **683** (2010) 196 [arXiv:0912.0208 [hep-th]].

[56] H. Gies and M. M. Scherer, "Asymptotic safety of simple Yukawa systems," arXiv:0901.2459 [hep-th].

[57] H. Gies, S. Rechenberger and M. M. Scherer, "Towards an Asymptotic-Safety Scenario for Chiral Yukawa Systems," arXiv:0907.0327 [hep-th].

[58] M. M. Scherer, H. Gies and S. Rechenberger, "An asymptotic-safety mechanism for chiral Yukawa systems," arXiv:0910.0395 [hep-th].

[59] H. Gies, L. Janssen, S. Rechenberger and M. M. Scherer, "Phase transition and critical behavior of d=3 chiral fermion models with left/right asymmetry," arXiv:0910.0764 [hep-th].

[60] S. Floerchinger, M. Scherer, S. Diehl and C. Wetterich, "Particle-hole fluctuations in the BCS-BEC Crossover," Phys. Rev. B **78** (2008) 174528

[61] S. Floerchinger, M. M. Scherer and C. Wetterich, "Modified Fermi-sphere in the BCS-BEC crossover," arXiv:0912.4050 [cond-mat.quant-gas].

[62] D. U. Jungnickel and C. Wetterich, "Effective Action For The Chiral Quark-Meson Model," Phys. Rev. D **53**, 5142 (1996) [arXiv:hep-ph/9505267];

[63] B. J. Schaefer and H. J. Pirner, "The equation of state of quarks and mesons in a renormalization group flow picture," Nucl. Phys. A **660**, 439 (1999) [arXiv:nucl-th/9903003];

[64] H. Gies and C. Wetterich, "Universality of spontaneous chiral symmetry breaking in gauge theories," Phys. Rev. D **69**, 025001 (2004) [arXiv:hep-th/0209183];

[65] J. Braun, "The QCD Phase Boundary from Quark-Gluon Dynamics," arXiv:0810.1727 [hep-ph].

[66] L. Rosa, P. Vitale and C. Wetterich, "Critical exponents of the Gross-Neveu model from the effective average action," Phys. Rev. Lett. **86**, 958 (2001) [arXiv:hep-th/0007093];

[67] F. Hofling, C. Nowak and C. Wetterich, "Phase transition and critical behaviour of the d = 3 Gross-Neveu model," Phys. Rev. B **66**, 205111 (2002) [arXiv:cond-mat/0203588].

[68] S. Diehl, H. Gies, J. M. Pawlowski and C. Wetterich, "Flow Equations for the BCS-BEC Crossover," Phys. Rev. A **76**, 021602 (2007) [arXiv:cond-mat/0701198].

[69] S. Diehl, H. Gies, J. M. Pawlowski and C. Wetterich, "Renormalisation Flow and Universality for Ultracold Fermionic Atoms," Phys. Rev. A **76**, 053627 (2007) [arXiv:cond-mat/0703366].

[70] D. F. Litim, "Optimisation of the exact renormalisation group," Phys. Lett. B **486**, 92 (2000) [arXiv:hep-th/0005245].

[71] D. F. Litim, "Optimised renormalisation group flows," Phys. Rev. D **64**, 105007 (2001) [hep-th/0103195].

[72] G. 't Hooft and M. J. G. Veltman, "One loop divergencies in the theory of gravitation," Annales Poincare Phys. Theor. A **20**, 69 (1974).

[73] M. H. Goroff and A. Sagnotti, "Quantum Gravity At Two Loops," Phys. Lett. B **160**, 81 (1985).

[74] A. E. M. van de Ven, "Two loop quantum gravity," Nucl. Phys. B **378**, 309 (1992).

[75] S. M. Christensen and M. J. Duff, "Quantizing Gravity With A Cosmological Constant," Nucl. Phys. B **170**, 480 (1980).

[76] L.D. Landau, in *Niels Bohr and the Development of Physics*, ed. W. Pauli, Pergamon Press, London, (1955).

[77] M. Goeckeler, R. Horsley, V. Linke, P. Rakow, G. Schierholz and H. Stuben, "Is there a Landau pole problem in QED?," Phys. Rev. Lett. **80**, 4119 (1998); Nucl. Phys. Proc. Suppl. **63** (1998) 694.

[78] H. Gies and J. Jaeckel, "Renormalization flow of QED," Phys. Rev. Lett. **93**, 110405 (2004) [arXiv:hep-ph/0405183].

[79] M. Luscher and P. Weisz, "Scaling Laws and Triviality Bounds in the Lattice phi**4 Theory. 2. One Component Model in the Phase with Spontaneous Symmetry Breaking," Nucl. Phys. B **295**, 65 (1988);

[80] M. Luscher and P. Weisz, "Scaling Laws and Triviality Bounds in the Lattice phi**4 Theory. 3. N Component Model," Nucl. Phys. B **318**, 705 (1989).

[81] A. Hasenfratz, K. Jansen, C. B. Lang, T. Neuhaus and H. Yoneyama, "The Triviality Bound of the Four Component phi**4 Model," Phys. Lett. B **199**, 531 (1987).

[82] U. M. Heller, H. Neuberger and P. M. Vranas, "Large N Analysis Of The Higgs Mass Triviality Bound," Nucl. Phys. B **399**, 271 (1993) [arXiv:hep-lat/9207024].

[83] D. J. E. Callaway, "Triviality Pursuit: Can Elementary Scalar Particles Exist?," Phys. Rept. **167**, 241 (1988).

[84] O. J. Rosten, "Triviality from the Exact Renormalization Group," arXiv:0808.0082 [hep-th].

[85] S. Weinberg, "Living with Infinities" arXiv:0903.0568 [hep-th]

[86] B. Widom, "Equation of State in the Neighborhood of the Critical Point," J. Chem. Phys**43** (1965) 3898.

[87] Wolfram Research, Inc., Mathematica, Version 6.0, Champaign, IL (2007)

[88] R. Guida and J. Zinn-Justin, "Critical Exponents of the N-vector model," J. Phys. A **31**, 8103 (1998) [arXiv:cond-mat/9803240].

[89] D. F. Litim and L. Vergara, "Subleading critical exponents from the renormalisation group," Phys. Lett. B **581**, 263 (2004) [arXiv:hep-th/0310101].

[90] K. Gawedzki and A. Kupiainen, "Renormalizing The Nonrenormalizable," Phys. Rev. Lett. **55**, 363 (1985);

[91] B. Rosenstein, B. J. Warr and S. H. Park, "The Four Fermi Theory Is Renormalizable In (2+1)-Dimensions," Phys. Rev. Lett. **62**, 1433 (1989);

[92] C. de Calan, P. A. Faria da Veiga, J. Magnen and R. Seneor, "Constructing The Three-Dimensional Gross-Neveu Model With A Large Number Of Flavor Components," Phys. Rev. Lett. **66**, 3233 (1991).

[93] H. Gies, J. Jaeckel and C. Wetterich, "Towards a renormalizable standard model without fundamental Higgs scalar,"
Phys. Rev. D **69**, 105008 (2004) [arXiv:hep-ph/0312034].

[94] J. M. Schwindt and C. Wetterich, "Asymptotically free four-fermion interactions and electroweak symmetry breaking," arXiv:0812.4223 [hep-th].

[95] A. Codello and R. Percacci, "Fixed Points of Nonlinear Sigma Models in d¿2," arXiv:0810.0715 [hep-th].

[96] H. Gies, "Renormalizability of gauge theories in extra dimensions,"
Phys. Rev. D **68**, 085015 (2003) [arXiv:hep-th/0305208].

[97] N. Cabibbo, L. Maiani, G. Parisi and R. Petronzio, "Bounds On The Fermions And Higgs Boson Masses In Grand Unified Theories," Nucl. Phys. B **158**, 295 (1979);

[98] L. Maiani, G. Parisi and R. Petronzio, "Bounds On The Number And Masses Of Quarks And Leptons," Nucl. Phys. B **136**, 115 (1978).

[99] J. Kuti, L. Lin and Y. Shen, "Upper Bound On The Higgs Mass In The Standard Model," Phys. Rev. Lett. **61**, 678 (1988).

[100] T. Hambye and K. Riesselmann, "Matching conditions and Higgs mass upper bounds revisited," Phys. Rev. D **55**, 7255 (1997) [arXiv:hep-ph/9610272].

[101] Z. Fodor, K. Holland, J. Kuti, D. Nogradi and C. Schroeder, "New Higgs physics from the lattice," PoS **LAT2007**, 056 (2007) [arXiv:0710.3151 [hep-lat]].

[102] P. Gerhold, K. Jansen and J. Kallarackal, "Higgs mass bounds from a chirally invariant lattice Higgs-Yukawa model with overlap fermions," arXiv:0810.4447 [hep-lat].

[103] F. J. Yndurain, "Landau poles, violations of unitarity and a bound on the top quark mass," *In *Ann Arbor 1991, Proceedings, Gauge theories - past and future* 337-353.*

[104] H. Gies and C. Gneiting, in preparation; C. Gneiting, diploma thesis, Heidelberg (2005).

[105] V. A. Miransky, M. Tanabashi and K. Yamawaki, "Is the t Quark Responsible for the Mass of W and Z Bosons?," Mod. Phys. Lett. A **4**, 1043 (1989);

[106] V. A. Miransky, M. Tanabashi and K. Yamawaki, "Dynamical Electroweak Symmetry Breaking with Large Anomalous Dimension and t Quark Condensate," Phys. Lett. B **221**, 177 (1989);

[107] W. A. Bardeen, C. N. Leung and S. T. Love, "The Dilaton And Chiral Symmetry Breaking," Phys. Rev. Lett. **56**, 1230 (1986).

[108] J. Zinn-Justin, "Four fermion interaction near four-dimensions," Nucl. Phys. B **367**, 105 (1991).

[109] A. Hasenfratz, P. Hasenfratz, K. Jansen, J. Kuti and Y. Shen, "The Equivalence of the top quark condensate and the elementary Higgs field," Nucl. Phys. B **365**, 79 (1991).

[110] M. B. Halpern and W. Siegel, "The Particle Limit Of Field Theory: A New Strong Coupling Expansion," Phys. Rev. D **16**, 2486 (1977).

[111] H. Gies, J. Sanchez-Guillen and R. A. Vazquez, "Quantum effective actions from nonperturbative worldline dynamics," JHEP **0508**, 067 (2005) [arXiv:hep-th/0505275].

[112] J. Smit, "Standard model and chiral gauge theories on the lattice," Nucl. Phys. Proc. Suppl. **17**, 3 (1990);

[113] K. Jansen, "Domain Wall Fermions And Chiral Gauge Theories," Phys. Rept. **273**, 1 (1996) [arXiv:hep-lat/9410018],

[114] P. Gerhold and K. Jansen, "The phase structure of a chirally invariant lattice Higgs-Yukawa model - numerical simulations," JHEP **0710**, 001 (2007) [arXiv:0707.3849 [hep-lat]];

[115] P. Gerhold and K. Jansen, "The phase structure of a chirally invariant lattice Higgs-Yukawa model for small and for large values of the Yukawa coupling constant," JHEP **0709**, 041 (2007) [arXiv:0705.2539 [hep-lat]].

[116] O. Zanusso, L. Zambelli, G. P. Vacca and R. Percacci, "Gravitational corrections to Yukawa systems," Phys. Lett. B **689** (2010) 90 [arXiv:0904.0938 [hep-th]].

[117] A. H. Guth, "The Inflationary Universe: A Possible Solution To The Horizon And Flatness Problems," Phys. Rev. D **23** (1981) 347.

[118] J. M. Pawlowski and F. Lamprecht, in preparation; F. Lamprecht, diploma thesis, Heidelberg (2008)

[119] U. Ellwanger, M. Hirsch and A. Weber, "Flow equations for the relevant part of the pure Yang-Mills action," Z. Phys. C **69**, 687 (1996).

[120] D. F. Litim and J. M. Pawlowski, "Flow equations for Yang-Mills theories in general axial gauges," Phys. Lett. B **435**, 181 (1998).

[121] H. Gies, S. Rechenberger, and M. M. Scherer, *in preparation*

[122] S. Hands, A. Kocic and J. B. Kogut, "Four Fermi theories in fewer than four-dimensions," Annals Phys. **224**, 29 (1993) [arXiv:hep-lat/9208022];

[123] K. I. Aoki, K. i. Morikawa, J. I. Sumi, H. Terao and M. Tomoyose, "Non-perturbative renormalization group analysis of the chiral critical behaviors in QED," Prog. Theor. Phys. **97**, 479 (1997) [arXiv:hep-ph/9612459];

[124] J. A. Gracey, "Computation of Beta-prime (g(c)) at O(1/N**2) in the O(N) Gross-Neveu model in arbitrary dimensions," Int. J. Mod. Phys. A **9**, 567 (1994) [arXiv:hep-th/9306106];

[125] L. Karkkainen, R. Lacaze, P. Lacock and B. Petersson, "Critical behavior of the 3-d Gross-Neveu and Higgs-Yukawa models," Nucl. Phys. B **415**, 781 (1994) [Erratum-ibid. B **438**, 650 (1995)] [arXiv:hep-lat/9310020];

[126] A. N. Vasiliev, S. E. Derkachov, N. A. Kivel and A. S. Stepanenko, "The 1/n expansion in the Gross-Neveu model: Conformal bootstrap calculation of the index eta in order 1/n**3," Theor. Math. Phys. **94**, 127 (1993) [Teor. Mat. Fiz. **94**, 179 (1993)].

[127] R. D. Pisarski, "Chiral Symmetry Breaking In Three-Dimensional Electrodynamics," Phys. Rev. D **29**, 2423 (1984).

[128] T. Appelquist, M. J. Bowick, E. Cohler and L. C. R. Wijewardhana, "Chiral Symmetry Breaking In (2+1)-Dimensions," Phys. Rev. Lett. **55**, 1715 (1985);

[129] T. W. Appelquist, M. J. Bowick, D. Karabali and L. C. R. Wijewardhana, "Spontaneous Chiral Symmetry Breaking In Three-Dimensional QED," Phys. Rev. D **33**, 3704 (1986);

[130] T. Appelquist, M. J. Bowick, D. Karabali and L. C. R. Wijewardhana, "Spontaneous Breaking Of Parity In (2+1)-Dimensional QED," Phys. Rev. D **33**, 3774 (1986);

[131] T. Appelquist, D. Nash and L. C. R. Wijewardhana, "Critical Behavior In (2+1)-Dimensional QED," Phys. Rev. Lett. **60**, 2575 (1988);

[132] M. Gomes, R. S. Mendes, R. F. Ribeiro and A. J. da Silva, "Gauge structure, anomalies and mass generation in a three-dimensional Thirring model," Phys. Rev. D **43**, 3516 (1991);

[133] D. K. Hong and S. H. Park, "Large N analysis of (2+1)-dimensional Thirring model," Phys. Rev. D **49**, 5507 (1994) [arXiv:hep-th/9307186].

[134] S. J. Hands, J. B. Kogut and C. G. Strouthos, "Non-compact QED(3) with N(f) $\geq$ 2," Nucl. Phys. B **645**, 321 (2002) [arXiv:hep-lat/0208030];

[135] S. J. Hands, J. B. Kogut, L. Scorzato and C. G. Strouthos, "Non-compact QED(3) with N(f) = 1 and N(f) = 4," Phys. Rev. B **70**, 104501 (2004) [arXiv:hep-lat/0404013];

[136] S. Christofi, S. Hands and C. Strouthos, "Critical flavor number in the three dimensional Thirring model," Phys. Rev. D **75**, 101701 (2007) [arXiv:hep-lat/0701016].

[137] I. F. Herbut, "QED3 theory of underdoped high temperature superconductors," Phys. Rev. B **66**, 094504 (2002) [arXiv:cond-mat/0202491];

[138] K. Kaveh and I. F. Herbut, "Chiral symmetry breaking in QED(3) in presence of irrelevant interactions: A renormalization group study," Phys. Rev. B **71**, 184519 (2005) [arXiv:cond-mat/0411594].

[139] I. F. Herbut, V. Juricic and B. Roy, "Theory of interacting electrons on the honeycomb lattice," Phys. Rev. B **79**, 085116 (2009) [arXiv:0811.0610 [cond-mat.str-el]];

[140] V. P. Gusynin, S. G. Sharapov and J. P. Carbotte, "AC conductivity of graphene: from tight-binding model to 2+1-dimensional quantum electrodynamics," Int. J. Mod. Phys. B **21**, 4611 (2007) [arXiv:0706.3016 [cond-mat.mes-hall]].

[141] N. E. Mavromatos and J. Papavassiliou, arXiv:cond-mat/0311421.

[142] J. P. Blaizot, R. Mendez Galain and N. Wschebor, "A new method to solve the non perturbative renormalization group equations," Phys. Lett. B **632**, 571 (2006) [arXiv:hep-th/0503103].

[143] F. Benitez, J. P. Blaizot, H. Chate, B. Delamotte, R. Mendez-Galain and N. Wschebor, "Solutions of renormalization group flow equations with full momentum dependence," arXiv:0901.0128 [cond-mat.stat-mech].

[144] A. J. Leggett, in *Modern Trends in the Theory of Condensed Matter*, ed. A. Pekalski and R. Przystawa (Springer-Verlag, Berlin, 1980).

[145] D. M. Eagles, "Possible Pairing Without Superconductivity At Low Carrier Concentrations In Bulk And Thin-Film Superconducting Semiconductors," Phys. Rev. **186**, 456 (1969).

[146] K. M. O'Hara *et al.*, "Measurement Of The Zero Crossing In A Feshbach Resonance Of Fermionic Li-6," Phys. Rev. A **66**, 041401 (2002).

[147] C. A. Regal, M. Greiner and D. S. Jin, "Observation of Resonance Condensation of Fermionic Atom Pairs," Phys. Rev. Lett. **92** (2004) 040403.

[148] M. W. Zwierlein, C. A. Stan, C. H. Schunck, S. M. F. Raupach, A. J. Kerman and W. Ketterle, "Condensation of Pairs of Fermionic Atoms near a Feshbach Resonance," Phys. Rev. Lett. **92**, 120403 (2004).

[149] J. Kinast, S. L. Hemmer, M. E. Gehm, A. Turlapov and J. E. Thomas, "Evidence for Superfluidity in a Resonantly Interacting Fermi Gas," Phys. Rev. Lett. **92**, 150402 (2004).

[150] T. Bourdel *et al.*, "Experimental Study of the BEC-BCS Crossover Region in Lithium 6," Phys. Rev. Lett. **93**, 050401 (2004).

[151] M. Bartenstein, A. Altmeyer, S. Riedl, S. Jochim, C. Chin, J. H. Denschlag and R. Grimm, "Crossover from a Molecular Bose-Einstein Condensate to a Degenerate Fermi Gas," Phys. Rev. Lett. **92**, 120401 (2004).

[152] G. B. Partridge, K. E. Strecker, R. I. Kamar, M. W. Jack and R. G. Hulet, "Molecular Probe of Pairing in the BEC-BCS Crossover," Phys. Rev. Lett. **95**, 020404 (2005).

[153] P. Nozieres and S. Schmitt-Rink, "Bose condensation in an attractive fermion gas: From weak to strong coupling superconduct ivity," J. Low. Temp. Phys. **59** (1985) 195.

[154] C. A. R. Sa de Melo, M. Randeria, and J. R. Engelbrecht, Phys. Rev. Lett. **71**, 3202 (1993).

[155] J. Carlson, S. Y. Chang, V. R. Pandharipande and K. E. Schmidt, "Superfluid Fermi Gases with Large Scattering Length," Phys. Rev. Lett. **91**, 050401 (2003).

[156] G. E. Astrakharchik, J. Boronat, J. Casulleras and a. S. Giorgini, "Equation of State of a Fermi Gas in the BEC-BCS Crossover: A Quantum Monte Carlo Study," Phys. Rev. Lett. **93**, 200404 (2004).

[157] A. Bulgac, J. E. Drut and P. Magierski, "Spin 1/2 Fermions in the unitary regime: A Superfluid of a new type," Phys. Rev. Lett. **96**, 090404 (2006) [arXiv:cond-mat/0505374].

[158] E. Burovski, N. Prokof'ev, B. Svistunov and M. Troyer, "Critical Temperature And Thermodynamics Of Attractive Fermions At Unitarity," Phys. Rev. Lett. **96**, 160402 (2006).

[159] V. K. Akkineni, D. M. Ceperley, N. Trivedi, "Pairing and Superfluid Properties of Dilute Fermion Gases at Unitarity," Phys. Rev. B **76** 165116 (2007).

[160] P. Pieri and G. C. Strinati, "Strong-coupling limit in the evolution from BCS superconductivity to Bose-Einstein condensation," Phys. Rev. B **61**, 15370 (2000).

[161] A. Perali, P. Pieri, L. Pisani and G. C. Strinati, "BCS-BEC crossover at finite temperature for superfluid trapped Fermi atoms," Phys. Rev. Lett. **92**, 220404 (2004) [arXiv:cond-mat/0311309].

[162] S. Diehl and C. Wetterich, "Universality in Phase Transitions for Ultracold Fermionic Atoms," Phys. Rev. A **73**, 033615 (2006) [arXiv:cond-mat/0502534].

[163] S. Diehl and C. Wetterich, "Functional Integral for Ultracold Fermionic Atoms," Nucl. Phys. B **770**, 206 (2007) [arXiv:cond-mat/0510407].

[164] R. Haussmann, W. Rantner, S. Cerrito and W. Zwerger, "Thermodynamics of the BCS-BEC crossover," Phys. Rev. A **75**, 023610 (2007) [arXiv:cond-mat/0608282].

[165] M. C. Birse, B. Krippa, J. A. McGovern and N. R. Walet, "Pairing in many-fermion systems: An exact renormalisation group treatment," Phys. Lett. B **605**, 287 (2005) [arXiv:hep-ph/0406249].

[166] K. B. Gubbels and H. T. C. Stoof, "Renormalization Group Theory for the Imbalanced Fermi Gas," Phys. Rev. Lett. **100**, 140407 (2008).

[167] P. Nikolic and S. Sachdev, "Renormalization-group fixed points, universal phase diagram, and 1/N expansion for quantum liquids with interactions near the unitarity limit," Phys. Rev. A **75**, 033608 (2007) [arXiv:cond-mat/0609106].

[168] T. L. Ho, "Universal Thermodynamics of Degenerate Quantum Gases in the Unitarity Limit," Phys. Rev. Lett. **92**, 090402 (2004) [arXiv:cond-mat/0309109].

[169] S. Diehl, S. Floerchinger, H. Gies, J. M. Pawlowski and C. Wetterich, "Functional renormalization group approach to the BCS-BEC crossover," arXiv:0907.2193 [cond-mat.quant-gas].

[170] L. N. Cooper, "Bound electron pairs in a degenerate Fermi gas," Phys. Rev. **104**, 1189 (1956).

[171] J. Bardeen, L. N. Cooper and J. R. Schrieffer, "Theory Of Superconductivity," Phys. Rev. **108**, 1175 (1957).

[172] H. Heiselberg, C. J. Pethick, H. Smith and L. Viverit, "Influence of Induced Interactions on the Superfluid Transition in Dilute Fermi Gases," Phys. Rev. Lett. **85**, 2418 (2000) [arXiv:cond-mat/0004360].

[173] L. P. Gorkov and T. K. Melik-Barkhudarov, Sov. Phys.-JETP **13**, 1018 (1961).

[174] H. Gies and C. Wetterich, "Renormalization flow of bound states," Phys. Rev. D **65**, 065001 (2002) [arXiv:hep-th/0107221].

[175] S. Floerchinger and C. Wetterich, "Exact flow equation for composite operators," Phys. Lett. B **680**, 371 (2009) [arXiv:0905.0915 [hep-th]].

[176] P. Strack, R. Gersch and W. Metzner, "Renormalization group flow for fermionic superfluids at zero temperature," Phys. Rev. B **78**, 014522 (2008) [arXiv:0804.3994 [cond-mat.str-el]].

[177] L. Bartosch, P. Kopietz and A. Ferraz, "Renormalization of the BCS-BEC crossover by order parameter fluctuations," arXiv:0907.2687 [cond-mat.quant-gas].

[178] S. Diehl, H. C. Krahl and M. Scherer, "Three-Body Scattering from Nonperturbative Flow Equations," Phys. Rev. C **78** (2008) 034001

[179] D. S. Petrov, C. Salomon and G. V. Shlyapnikov, "Weakly Bound Dimers of Fermionic Atoms," Phys. Rev. Lett. **93**, 090404 (2004).

[180] G. Baym, J. P. Blaizot, M. Holzmann, F. Laloe and D. Vautherin, "The transition temperature of the dilute interacting Bose gas," Phys. Rev. Lett. **83**, 1703 (1999) [arXiv:cond-mat/9905430].

[181] P. Arnold and G. D. Moore, "Transition temperature of a dilute homogeneous imperfect Bose gas," Phys. Rev. Lett. **87**, 120401 (2001).

[182] V. A. Kashurnikov, N. V. Prokof'ev and B. V. Svistunov, "Critical Temperature Shift in Weakly Interacting Bose Gas," Phys. Rev. Lett. **87**, 120402 (2001).

[183] J. Braun, S. Diehl, and M. M. Scherer, *in preparation.*

[184] T. Kugo and I. Ojima, "Local covariant operator formalism of nonabelian gauge theories and quark confinement problem," Prog. Theor. Phys. Suppl. **66** (1979) 1.

[185] V. N. Gribov, "Quantization Of Non-Abelian Gauge Theories," Nucl. Phys. B **139**, 1 (1978).

[186] D. Zwanziger, "Non-perturbative Faddeev-Popov formula and infrared limit of QCD," Phys. Rev. D **69** (2004) 016002; [arXiv:hep-ph/0303028].

[187] R. Alkofer and L. von Smekal, "The infrared behavior of QCD Green's functions: Confinement, dynamical symmetry breaking, and hadrons as relativistic bound states," Phys. Rept. **353**, 281 (2001); [arXiv:hep-ph/0007355].

[188] C. S. Fischer, "Infrared properties of QCD from Dyson-Schwinger equations," J. Phys. G **32**, R253 (2006) [arXiv:hep-ph/0605173].

[189] J. Ambjorn, J. Jurkiewicz and R. Loll, "Spectral dimension of the universe," Phys. Rev. Lett. **95**, 171301 (2005) [arXiv:hep-th/0505113].

[190] J. Ambjorn, J. Jurkiewicz and R. Loll, "Semiclassical universe from first principles," Phys. Lett. B **607**, 205 (2005) [arXiv:hep-th/0411152].

[191] J. Ambjorn, J. Jurkiewicz and R. Loll, "Emergence of a 4D world from causal quantum gravity," Phys. Rev. Lett. **93**, 131301 (2004) [arXiv:hep-th/0404156].

[192] A. K. Das and M. Kaku, "The Gribov Ambiguity In General Relativity In The Coulomb Gauge," Nuovo Cim. **50B**, 303 (1979).

[193] M. Reuter and C. Wetterich, "Indications for gluon condensation for nonperturbative flow equations," arXiv:hep-th/9411227.

[194] L. F. Abbott, "The Background Field Method Beyond One Loop," Nucl. Phys. B **185**, 189 (1981).

[195] F. Freire, D. F. Litim and J. M. Pawlowski, "Gauge invariance and background field formalism in the exact renormalisation group," Phys. Lett. B **495**, 256 (2000) [arXiv:hep-th/0009110].

[196] E. Manrique, M. Reuter and F. Saueressig, "Bimetric Renormalization Group Flows in Quantum Einstein Gravity," arXiv:1006.0099 [hep-th].

[197] E. Manrique and M. Reuter, "Bimetric Truncations for Quantum Einstein Gravity and Asymptotic Safety," Annals Phys. **325**, 785 (2010) [arXiv:0907.2617 [gr-qc]].

[198] E. Manrique, M. Reuter and F. Saueressig, "Matter Induced Bimetric Actions for Gravity," arXiv:1003.5129 [hep-th].

[199] J. W. York, "Conformatlly Invariant Orthogonal Decomposition Of Symmetric Tensors On Riemannian Manifolds And The Initial Value Problem Of General Relativity," J. Math. Phys. **14**, 456 (1973).

[200] M. A. Rubin and C. R. Ordonez, "Symmetric Tensor Eigen Spectrum Of The Laplacian On N Spheres," J. Math. Phys. **26**, 65 (1985).

[201] M. A. Rubin and C. R. Ordonez, "Eigenvalues And Degeneracies For N-Dimensional Tensor Spherical Harmonics,"

[202] H. Gies, "Running coupling in Yang-Mills theory: A flow equation study," Phys. Rev. D **66**, 025006 (2002) [arXiv:hep-th/0202207].

[203] D. F. Litim and J. M. Pawlowski, "Completeness and consistency of renormalisation group flows," Phys. Rev. D **66**, 025030 (2002) [arXiv:hep-th/0202188].

[204] D. F. Litim and J. M. Pawlowski, "Wilsonian flows and background fields," Phys. Lett. B **546**, 279 (2002) [arXiv:hep-th/0208216].

[205] M. Reuter and C. Wetterich, "Gluon condensation in nonperturbative flow equations," Phys. Rev. D **56**, 7893 (1997) [arXiv:hep-th/9708051].

[206] A. Werner, diploma thesis, Jena (2010)

Appendix A

Technical supplements

Sketch for the derivation of the Wetterich equation

We modify the microscopic action by a scale k-dependent cutoff regulator term that will act as an infrared regulator,

$$S[\varphi] \to S_k[\varphi] = S[\varphi] + \Delta S_k[\varphi]\,, \quad \text{where} \quad \Delta S_k[\varphi] = \frac{1}{2}\int_q \varphi^T(-q)R_k(q)\varphi(q) \tag{A.1}$$

The implementation of the regulator term in Eq. (2.16) introduces a scale dependence of the generating functional, which now reads $W_k[J] = \ln Z_k[J]$, cf. Eq (2.15). Keeping the sources J scale independent, the derivative with respect to k reads

$$\begin{aligned} \partial_k W_k[J] &= -\frac{1}{2Z_k[J]}\int_q \int \mathcal{D}\varphi(\partial_k R_{k,ij}(q))\varphi_i(q)\varphi_j(q)\exp(-S_k[\varphi] + J\cdot\varphi) \\ &= -\frac{1}{2}\int_q (\partial_k R_{k,ij}(q))W^{(2)}_{k,ji}(q) - \partial_k \Delta S_k[\Phi]\,. \end{aligned} \tag{A.2}$$

From this equation we can deduce the scale-dependence of the effective average action $\Gamma_k[\Phi]$, Eq. (2.18). In Eq. (2.18) only the sup-part is convex and any non-convexity for finite k is introduced by the regulator term.

Eventually, we can derive the desired flow equation for Γ_k for fixed Φ at $J = J_{\text{sup}}$:

$$\begin{aligned} \partial_k \Gamma_k[\Phi] &= \partial_k J\cdot\Phi - \partial_k W[J]|_\Phi - \partial_k \Delta S_k[\Phi] = -\partial_k W[J]|_J - \partial_k \Delta S_k[\Phi] \\ &= \frac{1}{2}\int_Q (\partial_k R_{k,ij}(Q))W^{(2)}_{k,ji}(Q) = \frac{1}{2}\text{STr}\{(\partial_k R_k)[\Gamma^{(2)}_k[\Phi] + R_k]^{-1}\}\,. \end{aligned} \tag{A.3}$$

From the second to the third line, we have used equation (A.2) and in the following step equation (2.14) in momentum space. The "supertrace" STr introduced in the last line runs over field type, momentum and internal indices, and has an additional minus sign for fermionic entries.

Quantum field theory in thermal equilibrium

In the path integral formulation of thermodynamics, the Matsubara formalism, we find that quantum statistics is described by an euclidean functional integral where the imaginary time τ is compactified on a torus of circumference $L = 1/T = \beta$. Here T is the temperature in units with $k_{\mathrm{B}} = 1$ and the all possible field configurations are weighted with an exponential of the microscopic action S. We have

$$\langle A \rangle = Z^{-1} \int \mathcal{D}\varphi A e^{-S} \,. \tag{A.4}$$

$A = A(\varphi(x_1), \varphi(x_2), ...)$ is some operator function of the field $\varphi(x)$ and Z^{-1} is a normalization factor. This is found starting from the Hamiltonian operator formalism. Thermodynamics is described by the grand canonical partition function

$$Z(\beta) = \mathrm{Tr} e^{-\beta(H-\mu N)}, \tag{A.5}$$

where H is the Hamiltonian of the corresponding field theory, N is the particle number operator. For a bosonic field we require periodic boundary conditions,

$$\phi(\vec{x}, \tau) \;\; = \;\; \phi(\vec{x}, \tau + \beta), \quad \phi(\vec{x}, \tau) = \sum_n e^{i\omega_{\phi,n}} \phi_n(\vec{x}). \tag{A.6}$$

The compactified euclidean time τ leads to a discrete spectrum in Fourier space (Matsubara frequencies). We find for the *bosonic Matsubara frequencies*

$$\omega_{\phi,n} = 2\pi n T \tag{A.7}$$

For fermions we have antiperiodic boundary conditions and so we find the following relations and *fermionic Matsubara frequencies*

$$\psi(\vec{x}, \tau) = -\psi(\vec{x}, \tau + \beta), \quad \psi(\vec{x}, \tau) = \sum_n e^{-i\omega_{\psi,n}} \psi_n(\vec{x}), \quad \omega_{\psi,n} = 2\pi(n + \frac{1}{2})T \tag{A.8}$$

The lowest fermionic Matsubara frequency is found to be $\omega_0 = \pm\pi T$.

When we write the action in momentum space the integration over frequency is changed compared to the vacuum ($T = 0$) and now reads

$$\int \frac{dq_0}{2\pi} \longrightarrow T \sum_n \tag{A.9}$$

The Matsubara formalism recovers classical statistics in the limit $T \longrightarrow \infty$. For $T \longrightarrow 0$ one can recover scattering physics in the quantum vacuum.

Appendix B

Threshold Functions

For a compact notation we use threshold functions, see e.g. [12, 67]. We define $P_{\rm B}(p) = p^2(1 + r_{k\rm B}(p))$, $P_{\rm F}(p) = p^2(1 + r_{k\rm F}(p))^2$ and $v_d^{-1} = 2^{d+1}\pi^{d/2}\Gamma(d/2)$.

$$
\begin{aligned}
l_n^d(\omega) &= \frac{n+\delta_{n,0}}{4} v_d^{-1} k^{2n-d} \int \frac{d^dp}{(2\pi)^d} \left[\left(\frac{1}{Z_{\phi,k}} \partial_t R_k(p) \right) (P_{\rm B}(p) + \omega k^2)^{-(n+1)} \right], \\
l_{n,\rm L/R}^{({\rm F})d}(\omega) &= \frac{n+\delta_{n,0}}{2} v_d^{-1} k^{2n-d} \int \frac{d^dp}{(2\pi)^d} \times \\
&\quad \left[\frac{P_{\rm F}(p)}{1 + r_{k{\rm F}(p)}} \left(\frac{1}{Z_{{\rm L},k}} \partial_t (Z_{{\rm L},k} r_{k\rm F}) \right) (P_{\rm F}(p) + \omega k^2)^{-(n+1)} \right], \\
l_{n_1,n_2}^{({\rm FB})d}(\omega_1, \omega_2) &= -\frac{1}{4} v_d^{-1} k^{2(n_1+n_2)-d} \int \frac{d^dp}{(2\pi)^d} \tilde{\partial}_t \frac{1}{(P_{\rm F}(p) + \omega_1 k^2)^{n_1} (P_{\rm B}(p) + \omega_2 k^2)^{n_2}}, \\
l_{n_1,n_2,n_3}^{({\rm FB})d}(\omega_1, \omega_2, \omega_3) &= -\frac{k^{2(n_1+n_2+n_3)-d}}{4 v_d} \int \frac{d^dp}{(2\pi)^d} \times \\
&\quad \tilde{\partial}_t \frac{1}{(P_{\rm F}(p) + k^2\omega_1)^{n_1} (P_{\rm B}(p) + k^2\omega_2)^{n_2} (P_{\rm B}(p) + k^2\omega_3)^{n_3}}, \\
l_{n{\rm T}}^{({\rm GB})d}(\omega) &= \frac{n+\delta^{n0}}{4 v_d} k^{2n-d} \int \frac{d^dp}{(2\pi)^d} \frac{\frac{1}{Z_{\rm F}} \partial_t \left(Z_{\rm F} p^2 r_{k\rm GB} \right)}{(P_{\rm GB}(p) + \omega k^2)^{n+1}}, \\
l_{n{\rm L}}^{({\rm GB})d}(\omega) &= \frac{n+\delta^{n0}}{4 v_d} k^{2n-d} \int \frac{d^dp}{(2\pi)^d} \frac{\frac{1}{Z_\phi} \partial_t \left(Z_\phi p^2 r_{k\rm GB} \right)}{(P_{\rm GB}(p) + \omega k^2)^{n+1}}, \\
l_n^{({\rm G})d}(\omega) &= \frac{n+\delta^{n0}}{4 v_d} k^{2n-d} \int \frac{d^dp}{(2\pi)^d} \frac{\partial_t (p^2 r_{k\rm G}(p))}{(P_{\rm G}(p) + \omega k^2)^{n+1}}, \\
l_{n_1,n_2}^{({\rm BGB})d}(\omega_1, \omega_2) &= -\frac{k^{2(n_1+n_2)-d}}{8 v_d} \int \frac{d^dp}{(2\pi)^d} \tilde{\partial}_t \frac{1}{(P_{\rm B} + \omega_1 k^2)^{n_1} (P_{\rm GB} + \omega_2 k^2)^{n_2}}, \\
m_{n_1,n_2}^d(\omega_1, \omega_2) &= -\frac{1}{4} v_d^{-1} k^{2(n_1+n_2-1)-d} \int \frac{d^dp}{(2\pi)^d} p^2 \tilde{\partial}_t \times \\
&\quad \left[\frac{\frac{\partial}{\partial p^2} P_{\rm B}(p)}{(P_{\rm B}(p) + \omega_1 k^2)^{n_1}} \frac{\frac{\partial}{\partial p^2} P_{\rm B}(p)}{(P_{\rm B}(p) + \omega_2 k^2)^{n_2}} \right],
\end{aligned}
$$

$$
\begin{aligned}
m_2^{(\mathrm{F})d}(\omega) &= -\frac{1}{4}v_d^{-1}k^{6-d}\int\frac{d^dp}{(2\pi)^d}p^2\tilde{\partial}_t\left[\frac{\frac{\partial}{\partial p^2}P_{\mathrm{F}}(p)}{(P_{\mathrm{F}}(p)+\omega k^2)^2}\right]^2,\\
m_4^{(\mathrm{F})d}(\omega) &= -\frac{1}{4}v_d^{-1}k^{4-d}\int\frac{d^dp}{(2\pi)^d}p^4\tilde{\partial}_t\left[\frac{\partial}{\partial p^2}\frac{1+r_{k\mathrm{F}}(p)}{P_{\mathrm{F}}(p)+\omega k^2}\right]^2,\\
m_{n_1,n_2}^{(\mathrm{FB})d}(\omega_1,\omega_2) &= -\frac{1}{4}v_d^{-1}k^{2(n_1+n_2-1)-d}\int\frac{d^dp}{(2\pi)^d}p^2\times\\
&\quad\tilde{\partial}_t\left[\frac{1+r_{k\mathrm{F}}(p)}{(P_{\mathrm{F}}(p)+\omega_1k^2)^{n_1}}\frac{\frac{\partial}{\partial p^2}P_{\mathrm{B}}(p)}{(P_{\mathrm{B}}(p)+\omega_2k^2)^{n_2}}\right],\\
m^{(\mathrm{FBG})}(\omega_1,\omega_2,\omega_3) &= -\frac{k^{4-d}}{4v_d}\int\frac{d^dp}{(2\pi)^d}\tilde{\partial}_t\frac{p^2(1+r_{\mathrm{F}})}{(P_{\mathrm{B}}+\omega_1k^2)(P_{\mathrm{F}}+\omega_2k^2)(P_{\mathrm{GB}}+\omega_3k^2)},\\
m_{n_1,n_2}^{(\mathrm{BGB})d}(\omega_1,\omega_2) &= -\frac{k^{2(n_1+n_2-1)-d}}{4v_d}\int\frac{d^dp}{(2\pi)^d}\tilde{\partial}_t\frac{p^2\frac{\partial}{\partial p^2}P_{\mathrm{GB}}}{(P_{\mathrm{B}}+\omega_1k^2)^{n_1}(P_{\mathrm{GB}}+\omega_2k^2)^{n_2}},\\
m_4^{(\mathrm{BGB})d}(\omega_1,\omega_2) &= -\frac{k^{4-d}}{4v_d}\int\frac{d^dp}{(2\pi)^d}p^4\tilde{\partial}_t\frac{\left(\frac{\partial}{\partial p^2}P_{\mathrm{B}}\right)\left(\frac{\partial}{\partial p^2}P_{\mathrm{GB}}\right)}{(P_{\mathrm{B}}+\omega_1k^2)^2(P_{\mathrm{GB}}+\omega_2k^2)^2},\\
m_{n_1,n_2}^{(\mathrm{FGB})d}(\omega_1,\omega_2) &= -\frac{k^{2(n_1+n_2-1)-d}}{4v_d}\int\frac{d^dp}{(2\pi)^d}p^2\tilde{\partial}_t\left(\frac{1+r_{\mathrm{F}}}{(P_{\mathrm{F}}+\omega_1k^2)^{n_1}}\frac{\frac{\partial}{\partial p^2}P_{\mathrm{GB}}}{(P_{\mathrm{GB}}+\omega_2k^2)^{n_2}}\right).
\end{aligned}
$$

Here $\tilde{\partial}_t$ only acts on the regulator R_k (neither on $r_{k\mathrm{B}}$ nor $r_{k\mathrm{F}}$). For our purposes, we use a linear regulator function R_k which is optimized our truncations [71]. The boson cutoff is given by

$$
yr_{\mathrm{B}}(y) = (1-y)\theta(1-y), \tag{B.1}
$$

where $y = q^2/k^2$, and the fermion regulator $r_{\mathrm{F}}(y)$ is chosen such that $y(1+r_{\mathrm{B}}) = y(1+r_{\mathrm{F}})^2$. Using this regulator in the Wetterich equation, we can perform all momentum integrations analytically. For the ghost regulator and the gauge bosonic regulator we choose $r_{k\mathrm{GB}}(p) = r_{k\mathrm{G}}(p) = r_{k\mathrm{B}}(p)$.Further we define $\eta_\psi := \frac{1}{2}(\eta_{\mathrm{R}}+\eta_{\mathrm{L}})$. Performing the integrals with these definitions yields following threshold functions:

$$
\begin{aligned}
l_n^d(\omega) &= \frac{2(\delta_{n,0}+n)}{d}\Big(1-\frac{\eta_\phi}{d+2}\Big)\frac{1}{(1+\omega)^{n+1}},\\
l_{n,\mathrm{L/R}}^{(\mathrm{F})d}(\omega) &= \frac{2(\delta_{n,0}+n)}{d}\Big(1-\frac{\eta_{\mathrm{L/R}}}{d+1}\Big)\frac{1}{(1+\omega)^{n+1}},\\
l_{n_1,n_2}^{(\mathrm{FB})d}(\omega_1,\omega_2) &= \frac{2}{d}\frac{1}{(1+\omega_1)^{n_1}(1+\omega_2)^{n_2}}\times\\
&\quad\left[\frac{n_1}{1+\omega_1}\left(1-\frac{\frac{1}{2}(\eta_{\mathrm{R}}+\eta_{\mathrm{L}})}{d+1}\right)+\frac{n_2}{1+\omega_2}\left(1-\frac{\eta_\phi}{d+2}\right)\right],
\end{aligned}
$$

$$
\begin{aligned}
l^{(\mathrm{FB})d}_{n_1,n_2,n_3}(\omega_1,\omega_2,\omega_3) &= \frac{2}{d}\frac{1}{(1+\omega_1)^{n_1}(1+\omega_2)^{n_2}(1+\omega_3)^{n_3}} \times \\
&\quad \left[\frac{n_1}{1+\omega_1}\left(1-\frac{\frac{1}{2}(\eta_{\mathrm{L}}+\eta_{\mathrm{R}})}{d+1}\right)\right. \\
&\quad \left.+\frac{n_2}{1+\omega_2}\left(1-\frac{\eta_\phi}{d+2}\right)+\frac{n_3}{1+\omega_3}\left(1-\frac{\eta_\phi}{d+2}\right)\right], \\
l^{(\mathrm{GB})d}_{n\mathrm{T}}(\omega) &= \frac{2(\delta_{n,0}+n)}{d}\left(1-\frac{\eta_{\mathrm{F}}}{d+2}\right)\frac{1}{(1+\omega)^{n+1}}, \\
l^{(\mathrm{GB})d}_{n\mathrm{L}}(\omega) &= \frac{2(\delta_{n,0}+n)}{d}\left(1-\frac{\eta_\phi}{d+2}\right)\frac{1}{(1+\omega)^{n+1}}, \\
l^{(\mathrm{G})d}_{n}(\omega) &= \frac{2(\delta_{n,0}+n)}{d}\frac{1}{(1+\omega)^{n+1}}, \\
l^{(\mathrm{BGB})d}_{n_1,n_2}(\omega_1,\omega_2) &= \frac{1}{d(1+\omega_1)^{n_1}(1+\omega_2)^{n_2}} \times \\
&\quad \left[\frac{n_1}{1+\omega_1}\left(1-\frac{\eta_\phi}{d+2}\right)+\frac{n_2}{1+\omega_2}\left(1-\frac{\eta_{\mathrm{F}}}{d+2}\right)\right], \\
m^{d}_{n_1,n_2}(\omega_1,\omega_2) &= \frac{1}{(1+\omega_1)^{n_1}(1+\omega_2)^{n_2}}, \\
m^{(\mathrm{F})d}_{2}(\omega) &= \frac{1}{(1+\omega)^4}, \\
m^{(\mathrm{F})d}_{4}(\omega) &= \frac{1}{(1+\omega)^4}+\frac{1-\frac{1}{2}(\eta_{\mathrm{R}}+\eta_{\mathrm{L}})}{d-2}\frac{1}{(1+\omega)^3} \\
&\quad -\left(\frac{1-\frac{1}{2}(\eta_{\mathrm{R}}+\eta_{\mathrm{L}})}{2d-4}+\frac{1}{4}\right)\frac{1}{(1+\omega)^2}, \\
m^{(\mathrm{FB})d}_{n_1,n_2}(\omega_1,\omega_2) &= \left(1-\frac{\eta_\phi}{d+1}\right)\frac{1}{(1+\omega_1)^{n_1}(1+\omega_2)^{n_2}}, \\
m^{(\mathrm{FBG})}(\omega_1,\omega_2,\omega_3) &= \frac{1}{(1+\omega_1)(1+\omega_2)(1+\omega_3)} \times \\
&\quad \left[-\frac{1-\eta_\psi}{d+1}-\frac{\eta_\psi}{d+2}+\frac{\frac{\eta_\phi}{d+3}+\frac{2-\eta_\phi}{d+1}}{1+\omega_1}\right. \\
&\quad \left.+\frac{\frac{2(1-\eta_\psi)}{d+1}+\frac{2\eta_\psi}{d+2}}{1+\omega_2}+\frac{\frac{\eta_{\mathrm{F}}}{d+3}+\frac{2-\eta_{\mathrm{F}}}{d+1}}{1+\omega_3}\right], \\
m^{(\mathrm{BGB})d}_{n_1,n_2}(\omega_1,\omega_2) &= \frac{1}{(1+\omega_1)^{n_1}(1+\omega_2)^{n_2}}, \\
m^{(\mathrm{BGB})d}_{4}(\omega_1,\omega_2) &= \frac{1}{(1+\omega_1)^2(1+\omega_2)^2}, \\
m^{(FGB)d}_{n_1,n_2}(\omega_1,\omega_2) &= \frac{\left(1-\frac{\eta_{\mathrm{F}}}{d+2}\right)}{(1+\omega_1)^{n_1}(1+\omega_2)^{n_2}}.
\end{aligned}
$$

Appendix C

Flow equations for chiral Yukawa models

Flow of the effective potential

For the flow of the effective potential we project the Wetterich equation onto constant bosonic fields and vanishing fermionic fields,

$$\partial_t U_k = \frac{1}{2\Omega}\mathrm{STr}\{(\Gamma_k^{(2)} + R_k)^{-1}(\partial_t R_k)\}|_{\phi=\text{const.},\psi=0}. \tag{C.1}$$

Here Ω is the spacetime volume. For the evaluation of the r.h.s of Eq. (C.1) we need the $\Gamma_k^{(2)}$ matrix. We define $\Gamma_k^{(2)}$ explicitly by the prescription

$$\Gamma_k^{(2)} = \begin{pmatrix} \frac{\overrightarrow{\delta}}{\delta\phi_1(-p)} \\ \frac{\overrightarrow{\delta}}{\delta\phi_2(-p)} \\ \frac{\overrightarrow{\delta}}{\delta\psi_{\mathrm{L}}(-p)} \\ \frac{\overrightarrow{\delta}}{\delta\bar{\psi}_{\mathrm{L}}^{\mathrm{T}}(p)} \\ \frac{\overrightarrow{\delta}}{\delta\psi_{\mathrm{R}}(-p)} \\ \frac{\overrightarrow{\delta}}{\delta\bar{\psi}_{\mathrm{R}}^{\mathrm{T}}(p)} \end{pmatrix}^{\mathrm{T}} \Gamma_k \begin{pmatrix} \frac{\overleftarrow{\delta}}{\delta\phi_1(q)} \\ \frac{\overleftarrow{\delta}}{\delta\phi_2(q)} \\ \frac{\overleftarrow{\delta}}{\delta\psi_{\mathrm{L}}(q)} \\ \frac{\overleftarrow{\delta}}{\delta\bar{\psi}_{\mathrm{L}}^{\mathrm{T}}(-q)} \\ \frac{\overleftarrow{\delta}}{\delta\psi_{\mathrm{R}}(q)} \\ \frac{\overleftarrow{\delta}}{\delta\bar{\psi}_{\mathrm{R}}^{\mathrm{T}}(-q)} \end{pmatrix},$$

with $\phi_i^{\mathrm{T}} = (\phi_i^{1\mathrm{T}}, \ldots, \phi_i^{N_{\mathrm{L}}\mathrm{T}})$ and $\bar{\psi}_{\mathrm{L}} = (\bar{\psi}_{\mathrm{L}}^1, \ldots, \bar{\psi}_{\mathrm{L}}^{N_{\mathrm{L}}})$. The transposition refers to flavor as well as Dirac indices. For a proper IR regularization, a regulator which is diagonal in field space is sufficient and convenient,

$$R_k(q,p) = \delta(p-q)\begin{pmatrix} R_{k\mathrm{B}} & 0 \\ 0 & R_{k\mathrm{F}} \end{pmatrix},$$

with a $2N_{\mathrm{L}} \times 2N_{\mathrm{L}}$ matrix for the bosonic sector

$$R_{k\mathrm{B}} = \begin{pmatrix} Z_{\phi,k}\delta^{ab}p^2 r_{\mathrm{B}} & 0 \\ 0 & Z_{\phi,k}\delta^{ab}p^2 r_{\mathrm{B}} \end{pmatrix}, \tag{C.2}$$

cf. App. B and an $(2N_{\mathrm{L}}+2) \times (2N_{\mathrm{L}}+2)$ matrix for the fermionic sector

$$R_{k\mathrm{F}} = -\begin{pmatrix} 0 & Z_{\mathrm{L},k}\delta^{ab}\not{p}^{\mathrm{T}} & 0 & 0 \\ Z_{\mathrm{L},k}\delta^{ab}\not{p} & 0 & 0 & 0 \\ 0 & 0 & 0 & Z_{\mathrm{R},k}\not{p}^{\mathrm{T}} \\ 0 & 0 & Z_{\mathrm{R},k}\not{p} & 0 \end{pmatrix} r_{\mathrm{F}}. \tag{C.3}$$

The matrix $\Gamma_k^{(2)} + R_k$ has the same block form as the regulator. Therefore, we can evaluate the bosonic and fermionic parts separately. We start with the bosonic part. Inverting the matrix, multiplying with the derivative of the regulator, and taking the supertrace yields

$$\partial_t U_{k\mathrm{B}} = \frac{1}{2}\int \frac{d^dp}{(2\pi)^d}\partial_t R_k \Big[\frac{2N_{\mathrm{L}}-1}{Z_{\phi,k}P_{\mathrm{B}}(p)+U_k'} + \frac{1}{Z_{\phi,k}P_{\mathrm{B}}(p)+U_k'+2U_k''\rho}\Big],$$

where $P_{\mathrm{B}}(p) = p^2(1+r_{\mathrm{B}}(p))$. Introducing $P_{\mathrm{F}}(p) = p^2(1+r_{\mathrm{F}}(p))^2$ and d_γ as the dimension of the representation of the Dirac algebra, the fermionic contribution reads

$$\begin{aligned} \partial_t U_{k\mathrm{F}} \;=\; & -d_\gamma \int \frac{d^dp}{(2\pi)^d}\Big\{ \frac{\partial_t[Z_{\mathrm{L},k}r_{\mathrm{F}}(p)]}{Z_{\mathrm{L},k}(1+r_{\mathrm{F}}(p))}\Big[(N_{\mathrm{L}}-1) + \frac{Z_{\mathrm{L},k}Z_{\mathrm{R},k}P_{\mathrm{F}}(p)}{\bar{h}_k^2\rho + Z_{\mathrm{L},k}Z_{\mathrm{R},k}P_{\mathrm{F}}(p)}\Big] \\ & + \frac{\partial_t[Z_{\mathrm{R},k}r_{\mathrm{F}}(p)]}{Z_{\mathrm{R},k}(1+r_{\mathrm{F}}(p))}\frac{Z_{\mathrm{L},k}Z_{\mathrm{R},k}P_{\mathrm{F}}(p)}{\bar{h}_k^2\rho + Z_{\mathrm{L},k}Z_{\mathrm{R},k}P_{\mathrm{F}}(p)}\Big\}. \end{aligned}$$

Adding both parts and using the optimized regulator and the threshold functions introduced in App. B, we get

$$\begin{aligned} \partial_t U_k \;=\; & 2v_d k^d\Big[(2N_{\mathrm{L}}-1)l_0^d\Big(\frac{U_k'}{Z_{\phi,k}k^2}\Big) + l_0^d\Big(\frac{U_k'+2U_k''\rho}{Z_{\phi,k}k^2}\Big)\Big] \\ & -d_\gamma v_d k^d 2\Big[(N_{\mathrm{L}}-1)l_{0,\mathrm{L}}^{(\mathrm{F})d}(0) + l_{0,\mathrm{L}}^{(\mathrm{F})d}\Big(\frac{\bar{h}_k^2\rho}{k^2 Z_{\mathrm{L},k}Z_{\mathrm{R},k}}\Big) + l_{0,\mathrm{R}}^{(\mathrm{F})d}\Big(\frac{\bar{h}_k^2\rho}{k^2 Z_{\mathrm{L},k}Z_{\mathrm{R},k}}\Big)\Big]. \end{aligned}$$

In terms of dimensionless quantities defined in Eq. (4.1), the potential flow turns into Eq. (4.2) in the main text.

Derivation of the Yukawa coupling flow w.r.t. radial boson mode

For the derivation of the flow of the Yukawa coupling, we first separate the bosonic field into a vacuum expectation value (vev) v and a purely radial deviation from the vev.

$$\phi(p) = \frac{1}{\sqrt{2}}\begin{pmatrix}\phi_1^1(p)+i\phi_2^1(p)\\ \phi_1^2(p)+i\phi_2^2(p)\\ \vdots \\ \phi_1^{N_\mathrm{L}}(p)+i\phi_2^{N_\mathrm{L}}(p)\end{pmatrix} = \frac{1}{\sqrt{2}}\begin{pmatrix}v\\0\\\vdots\\0\end{pmatrix}\delta(p)+\frac{1}{\sqrt{2}}\begin{pmatrix}\Delta\phi_1^1(p)\\ \Delta\phi_1^2(p)\\ \vdots \\ \Delta\phi_1^{N_\mathrm{L}}(p)\end{pmatrix}, \tag{C.4}$$

setting all $\Delta\phi_2$ Goldstone components to zero. The projection of the Wetterich equation onto the flow of the Yukawa coupling reads

$$\partial_t \bar{h}_k = \frac{-1}{2}\frac{\overrightarrow{\delta}}{\delta\bar{\psi}_\mathrm{L}^1(p)}\frac{\sqrt{2}\overrightarrow{\delta}}{\delta\Delta\phi_1^1(p')}\partial_t\Gamma_k\frac{\overleftarrow{\delta}}{\delta\psi_\mathrm{R}(q)}\Bigg|. \tag{C.5}$$

The vertical line indicates that the equation is evaluated at $\psi_\mathrm{R}^a = \psi_\mathrm{L}^a = \Delta\phi = 0$, $p' = p = q = 0$. Next, we can decompose the matrix $(\Gamma_k^{(2)} + R_k)$ into two parts. One part, which we call $(\Gamma_{k,0}^{(2)} + R_k)$, contains only v and is independent of the fluctuations. The remaining part, $\Delta\Gamma_k^{(2)}$, contains all fluctuating fields. Inserting this into equation (C.5) and expanding the logarithm

$$\begin{aligned}\mathrm{STr}\left(\ln(\Gamma_k^{(2)}+R_k)\right) &= \mathrm{STr}\left(\ln\left[(\Gamma_{k,0}^{(2)}+R_k)\left(1+\frac{\Delta\Gamma_k^{(2)}}{\Gamma_{k,0}^{(2)}+R_k}\right)\right]\right) \\ &= \mathrm{STr}\left(\ln(\Gamma_{k,0}^{(2)}+R_k)\right)+\mathrm{STr}\frac{\Delta\Gamma_k^{(2)}}{\Gamma_{k,0}^{(2)}+R_k}-\frac{1}{2}\mathrm{STr}\left(\frac{\Delta\Gamma_k^{(2)}}{\Gamma_{k,0}^{(2)}+R_k}\right)^2+\ldots,\end{aligned} \tag{C.6}$$

only the term to third power in $\Delta\Gamma_k^{(2)}$ survives the projection onto $\Delta\phi_1^1\bar{\psi}_\mathrm{L}^1\psi_\mathrm{R}$. Performing the matrix calculations and taking the supertrace, we get

$$\begin{aligned}\partial_t\bar{h}_k = -\frac{\bar{h}_k^3}{2}\int\frac{d^dp}{(2\pi)^d}\tilde{\partial}_t\Bigg[&\frac{v}{Z_{\mathrm{L},k}Z_{\mathrm{R},k}P_\mathrm{F}(p)+\frac{\bar{h}_k^2}{2}v^2}\left(\frac{U_k''v}{(Z_{\phi,k}P_\mathrm{B}(p)+U_k')^2}-\frac{3U_k''v+U_k'''v^3}{(Z_{\phi,k}P_\mathrm{B}(p)+U_k'+U_k''v^2)^2}\right)\\ &+\frac{\bar{h}_k^2v^2}{(Z_{\mathrm{L},k}Z_{\mathrm{R},k}P_\mathrm{F}(p)+\frac{\bar{h}_k^2}{2}v^2)^2}\left(\frac{1}{Z_{\phi,k}P_\mathrm{B}(p)+U_k'}-\frac{1}{Z_{\phi,k}P_\mathrm{B}(p)+U_k'+U_k''v^2}\right)\\ &-\frac{1}{Z_{\mathrm{L},k}Z_{\mathrm{R},k}P_\mathrm{F}(p)+\frac{\bar{h}_k^2}{2}v^2}\left(\frac{1}{Z_{\phi,k}P_\mathrm{B}(p)+U_k'}-\frac{1}{Z_{\phi,k}P_\mathrm{B}(p)+U_k'+U_k''v^2}\right)\Bigg],\end{aligned}$$

where the potential on the right hand side is evaluated at the minimum $\frac{1}{2}v^2$. Using the optimized regulator and the threshold functions as defined in App. B and switching over to dimensionless quantities, we end up with the representation (4.3) given in the main text.

Derivation of the anomalous dimensions w.r.t. the radial boson mode

For the derivation of the flow of $Z_{\phi,k}$, we decompose the bosonic field as in Eq. (C.4). The projection of the Wetterich equation onto the boson kinetic term leads us to

$$\partial_t Z_{\phi,k} = -\frac{\partial}{\partial(p'^2)}\frac{\delta}{\delta\Delta\phi_1^1(p')}\frac{\delta}{\delta\Delta\phi_1^1(q')}\frac{1}{4}\mathrm{STr}\left[\tilde{\partial}_t\left(\frac{\Delta\Gamma_k^{(2)}}{\Gamma_k^{(2)}+R_k}\right)^2\right]\Bigg|_{\Delta\phi=\psi_{\mathrm{L}}^a=\psi_{\mathrm{R}}=0,p'=q'=0}. \quad \text{(C.7)}$$

Again, we have decomposed the matrix into two parts, one part containing the vev and the other part containing all fluctuating fields. We have expanded the logarithm as in Eq. (C.6), but this time only the second order contributes. Calculating the r.h.s of Eq. (C.7), results in

$$\begin{aligned}
\partial_t Z_{\phi,k} &= \frac{1}{d}\int\frac{d^dp}{(2\pi)^d}\tilde{\partial}_t\Bigg[(3U_k''v+U_k'''v^3)^2p^2Z_{\phi,k}^2\left(\frac{\frac{\partial}{\partial p^2}P_{\mathrm{B}}(p)}{(Z_{\phi,k}P_{\mathrm{B}}(p)+U_k'+U_k''v^2)^2}\right)^2 \\
&\quad +(2N_{\mathrm{L}}-1)(U_k''v)^2p^2Z_{\phi,k}^2\left(\frac{\frac{\partial}{\partial p^2}P_{\mathrm{B}}(p)}{(Z_{\phi,k}P_{\mathrm{B}}(p)+U_k')^2}\right)^2 \\
&\quad +2h_k^2d_\gamma p^4Z_{\mathrm{L},k}Z_{\mathrm{R},k}\left(\frac{\partial}{\partial p^2}\frac{(1+r_{\mathrm{F}}(p))}{Z_{\mathrm{L},k}Z_{\mathrm{R},k}P_{\mathrm{F}}(p)+\frac{h_k^2}{2}v^2}\right)^2 \\
&\quad -h_k^4d_\gamma v^2p^2\left(\frac{\partial}{\partial p^2}\frac{1}{Z_{\mathrm{L},k}Z_{\mathrm{R},k}P_{\mathrm{F}}(p)+\frac{h_k^2}{2}v^2}\right)^2\Bigg],
\end{aligned}$$

where the potential is evaluated at the minimum. Using the optimized regulator together with the threshold functions as defined in App. B and again introducing dimensionless quantities, we end up with

$$\begin{aligned}
\eta_\phi &= \frac{8v_d}{d}\tilde{\rho}(3u_k''+2\tilde{\rho}u_k''')^2m_{22}^d(u_k'+2\tilde{\rho}u_k'')+\frac{(2N_{\mathrm{L}}-1)8v_d}{d}\tilde{\rho}u_k''^2m_{22}^d(u_k') \qquad \text{(C.8)} \\
&\quad +\frac{8v_dd_\gamma}{d}h_k^2m_4^{(\mathrm{F})4}(\tilde{\rho}h_k^2)-\frac{8v_dd_\gamma}{d}\tilde{\rho}h_k^4m_2^{(\mathrm{F})4}(\tilde{\rho}h_k^2),
\end{aligned}$$

where we have used $\eta_\phi=-\frac{\partial_t Z_{\phi,k}}{Z_{\phi,k}}$, and the right hand side has to be evaluated on the vev.

For the fermionic anomalous dimensions, the procedure is the same. We start with

$$\partial_t Z_{\mathrm{L/R},k} = \frac{1}{4v_dd_\gamma}\mathrm{tr}\gamma^\mu\frac{\partial}{\partial p'^\mu}\frac{\overrightarrow{\delta}}{\delta\bar{\psi}_{\mathrm{L/R}}^1(p')}\mathrm{STr}\left[\left(\frac{\Delta\Gamma_k^{(2)}}{\Gamma_{k,0}^{(2)}+R_k}\right)^2\right]\frac{\overleftarrow{\delta}}{\delta\psi_{\mathrm{L/R}}^1(q')}\Bigg|_{\Delta\phi=\psi_{\mathrm{L}}=\psi_{\mathrm{R}}=0,p'=q'=0},$$

and get

$$\partial_t Z_{\mathrm{L},k} = \frac{2\bar{h}_k^2}{d}\int\frac{d^dp}{(2\pi)^d}p^2\tilde{\partial}_t\Big[\frac{Z_{\mathrm{L},k}(1+r_\mathrm{F}(p))}{Z_{\mathrm{L},k}Z_{\mathrm{R},k}P_\mathrm{F}(p)+\frac{\bar{h}_k^2}{2}v^2}Z_{\phi,k}\frac{\partial}{\partial p^2}\times P_\mathrm{B}(p)\Big(\frac{1}{(Z_{\phi,k}P_\mathrm{B}(p)+U_k'+U_k''v^2)^2}+\frac{1}{(Z_{\phi,k}P_\mathrm{B}(p)+U_k')^2}\Big)\Big]$$

and

$$\begin{aligned}\partial_t Z_{\mathrm{R},k} = {}& \frac{2\bar{h}_k^2}{d}\int\frac{d^dp}{(2\pi)^d}p^2\tilde{\partial}_t\Big[\frac{Z_{\mathrm{R},k}(1+r_\mathrm{F}(p))}{Z_{\mathrm{L},k}Z_{\mathrm{R},k}P_\mathrm{F}(p)+\frac{\bar{h}_k^2}{2}v^2}Z_{\phi,k}\frac{\partial}{\partial p^2}\times\\ & P_\mathrm{B}(p)\left(\frac{1}{(Z_{\phi,k}P_\mathrm{B}(p)+U_k'+U_k''v^2)^2}\right)+\frac{1}{(Z_{\phi,k}P_\mathrm{B}(p)+U_k')^2}\\ & +\frac{2(N_\mathrm{L}-1)Z_{\mathrm{R},k}(1+r_\mathrm{F}(p))}{Z_{\mathrm{L},k}Z_{\mathrm{R},k}P_\mathrm{F}(p)}Z_{\phi,k}\frac{\partial}{\partial p^2}P_\mathrm{B}(p)\frac{1}{(Z_{\phi,k}P_\mathrm{B}(p)+U_k')^2}\Big],\end{aligned}$$

respectively. Using the optimized regulator the result reads in terms of dimensionless quantities

$$\eta_\mathrm{L}=\frac{8v_d}{d}h_k^2[m_{12}^{(\mathrm{FB})d}(\tilde{\rho}h_k^2,u_k'+2\tilde{\rho}u_k'')+m_{12}^{(\mathrm{FB})d}(\tilde{\rho}h_k^2,u_k')] \tag{C.9}$$

$$\eta_\mathrm{R}=\frac{8v_d}{d}h_k^2[m_{12}^{(\mathrm{FB})d}(\tilde{\rho}h_k^2,u_k'+2\tilde{\rho}u_k'')+m_{12}^{(\mathrm{FB})d}(\tilde{\rho}h_k^2,u_k')+2(N_\mathrm{L}-1)m_{12}^{(\mathrm{FB})d}(0,u_k')] \tag{C.10}$$

Yukawa flow and anomalous dimensions w.r.t. the Goldstone mode

The flow equations for the dimensionless effective potential $\partial_t u_k$ and the anomalous dimensions η_L and η_R remain the same.

For deriving the flow of the squared Yukawa coupling constant h^2 we again split the bosonic field into its vev v and the deviation from the vev (the relation between the dimensionful vev v and the dimensionless squared vev κ is $\kappa=\frac{1}{2}Z_\phi k^{2-d}v^2$),

$$\phi(p)=\frac{1}{\sqrt{2}}\begin{pmatrix}\phi_1^1(p)+\mathrm{i}\phi_2^1(p)\\ \phi_1^2(p)+\mathrm{i}\phi_2^2(p)\\ \vdots\\ \phi_1^{N_\mathrm{L}}(p)+\mathrm{i}\phi_2^{N_\mathrm{L}}(p)\end{pmatrix}=\frac{1}{\sqrt{2}}\begin{pmatrix}v\\0\\\vdots\\0\end{pmatrix}\delta(p)+\frac{1}{\sqrt{2}}\begin{pmatrix}\Delta\phi_1^1(p)+\mathrm{i}\Delta\phi_2^1(p)\\ \Delta\phi_1^2(p)+\mathrm{i}\Delta\phi_2^2(p)\\ \vdots\\ \Delta\phi_1^{N_\mathrm{L}}(p)+\mathrm{i}\Delta\phi_2^{N_\mathrm{L}}(p)\end{pmatrix}. \tag{C.11}$$

Here, we are interested in the Yukawa coupling between the fermions and the Goldstone boson. Thus we use the $\Delta\phi_2^1$ part for the projection. This yields

$$\partial_t\bar{h}_k=-\frac{\mathrm{i}}{2}\frac{\overrightarrow{\delta}}{\delta\bar{\psi}_\mathrm{L}^1(p)}\frac{\sqrt{2}\overrightarrow{\delta}}{\delta\Delta\phi_2^1(p')}\mathrm{STr}\left[\tilde{\partial}_t\ln(\Gamma_k^{(2)}+R_k)\right]\frac{\overleftarrow{\delta}}{\delta\psi_\mathrm{R}(q)}\bigg|_{\substack{\psi_\mathrm{R}^a=\psi_\mathrm{L}^a=\Delta\phi=0\\ p'=p=q=0}}. \tag{C.12}$$

Next, we split $(\Gamma_k^{(2)} + R_k)$ into a propagator part $\mathcal{P}$, which contains only the vev, and a fluctuation part $\mathcal{F}$, which contains the fluctuating fields. Inserting this into Eq. (C.12) the expansion of the logarithm reads

$$\ln\left(\Gamma_k^{(2)} + R_k\right) = \ln\left[\mathcal{P}\left(1 + \frac{\mathcal{F}}{\mathcal{P}}\right)\right] = \ln(\mathcal{P}) + \frac{\mathcal{F}}{\mathcal{P}} - \frac{1}{2}\left(\frac{\mathcal{F}}{\mathcal{P}}\right)^2 + \frac{1}{3}\left(\frac{\mathcal{F}}{\mathcal{P}}\right)^3 - \dots \quad \text{(C.13)}$$

Only the term to third power survives the projection. Performing the matrix calculations and taking the supertrace, we get

$$\partial_t \bar{h}_k^2 = \int \frac{d^d p}{(2\pi)^d} \tilde{\partial}_t \frac{h_k^4 U_k'' v^2}{\left(Z_\phi P_{\mathrm{B}}(p) + U_k' + U_k'' v^2\right)\left(Z_\phi P_{\mathrm{B}}(p) + U_k'\right)\left(Z_{\mathrm{L}} Z_{\mathrm{R}} P_{\mathrm{F}}(p) + \frac{\bar{h}_k^2}{2} v^2\right)}.$$

The potential on the right-hand side is evaluated at the minimum $\frac{1}{2}v^2$. Using the threshold function and switching over to dimensionless quantities, we end up with Eq. (5.37).

For the derivation of the flow of η_ϕ, we use the decomposition of (C.11). Again we use $\Delta\phi_2^1$ for the projection and expand the logarithm as in (C.13). This time only the quadratic term survives the projection,

$$\partial_t Z_\phi = -\frac{1}{4}\frac{\partial}{\partial p^2}\frac{\delta}{\delta\Delta\phi_2^1(p)}\frac{\delta}{\delta\Delta\phi_2^1(q)}\mathrm{STr}\left[\tilde{\partial}_t\left(\frac{\mathcal{F}}{\mathcal{P}}\right)^2\right]\Bigg|_{\psi=\Delta\phi=0=p=q}.$$

After performing the matrix calculations and taking the supertrace, we use $\eta_\phi = -\frac{\partial_t Z_\phi}{Z_\phi}$ and switch over to dimensionless quantities. By use of the threshold functions, we obtain Eq. (5.38) in the main text.

Appendix D

Flow Equations for the gauged chiral Yukawa model

Here, we calculate the flow equations for the effective potential, the Yukawa coupling and the anomalous dimensions including gauge fields as defined in Sec. 4.5. We shall see that there are new contributions due to the gauge fields and the ghost fields. The flow equation of the gauge coupling will not be considered. First we write down the truncation in momentum space:

$$
\begin{aligned}
\Gamma_k = &\int d^dx U_k(\rho) + \int \frac{d^dp}{(2\pi)^d} \left\{ \frac{Z_\phi p^2}{2} (\phi_1^a(p)\phi_1^a(-p) + \phi_2^a(p)\phi_2^a(-p)) - Z_{\mathrm{L}} \bar{\psi}_L^a \not{p} \psi_L^a \right. \\
&- Z_{\mathrm{R}} \bar{\psi}_{\mathrm{R}} \not{p} \psi_{\mathrm{R}} + \frac{Z_{\mathrm{F}}}{2} W_\mu^i(p) \left(p^2 \delta^{\mu\nu} - p_\mu p_\nu \left(a - \frac{Z_\phi}{\alpha Z_{\mathrm{F}}} \right) \right) - \bar{c}^i(p) p^2 c^i(p) \\
&+ \int \frac{d^dq}{(2\pi)^d} [ig \bar{c}^i(p) q_\mu W_\mu^k(q) f^{ikj} c^j(p-q) - 2\alpha v g^2 \bar{c}^i(p) T_{Na}^i T_{ab}^i \phi^b(q) c^j(p-q)] \\
&+ \int \frac{d^dq}{(2\pi)^d} \bar{h}_k [\bar{\psi}_{\mathrm{R}}(p) \phi^{a\dagger}(p-q) \psi_{\mathrm{L}}^a(q) - \bar{\psi}_{\mathrm{L}}^a(p) \phi^a(p-q) \psi_{\mathrm{R}}(q)] \\
&+ \int \frac{d^dq}{(2\pi)^d} Z_{\mathrm{L}} g \bar{\psi}_{\mathrm{L}}^a(p) \not{W}^i(q) T_{ab}^i \psi_{\mathrm{L}}(p-q) \\
&+ \int \frac{d^dq}{(2\pi)^d} i Z_{\mathrm{F}} g f^{jki} p_\mu W_\nu^i(p) W_\mu^j(q) W_\nu^k(-p-q) \\
&+ \int \frac{d^dq}{(2\pi)^d} \int \frac{d^dr}{(2\pi)^d} \frac{Z_{\mathrm{F}}}{4} g^2 f^{jki} f^{lmi} W_\mu^j(p) W_\nu^k(q) W_\mu^l(r) W_\nu^m(-p-q-r) \\
&+ \int \frac{d^dq}{(2\pi)^d} \int \frac{d^dr}{(2\pi)^d} Z_\phi g^2 W_\mu^i(p) W_\mu^j(q) \phi^{a\dagger}(r) T_{ab}^i T_{bc}^j \phi^c(-p-q-r) \\
&+ Z_\phi v g W_\mu^i(p) \left(p_\mu \phi^{a\dagger}(-p) T_{aN}^i - p_\mu T_{Na}^i \phi^a(-p) \right) \\
&+ \left. \int \frac{d^dq}{(2\pi)^d} Z_\phi g W_\mu^i(p) \left(q_\mu \phi^{a\dagger}(q) T_{ab}^i \phi^b(-p-q) - q_\mu \phi^{a\dagger}(-p-q) T_{ab}^i \phi^b(q) \right) \right\}.
\end{aligned}
$$

Here we neglected terms proportional to α. The first two lines contain the kinetic terms of all fields, the third line contains interactions which include ghost fields, the fourth line includes all Yukawa interactions and the rest represents higher order interaction terms.

Fluctuation Matrix and Regulator

The fluctuation matrix is a $(3N_{\mathrm{L}}^2 + 4N_{\mathrm{L}} - 1) \times (3N_{\mathrm{L}}^2 + 4N_{\mathrm{L}} - 1)$ matrix:

$$\begin{pmatrix}
\Gamma_{\phi_1\phi_1} & \Gamma_{\phi_1\phi_2} & \Gamma_{\phi_1\psi_{\mathrm{L}}} & \Gamma_{\phi_1\bar{\psi}_{\mathrm{L}}} & \Gamma_{\phi_1\psi_{\mathrm{R}}} & \Gamma_{\phi_1\bar{\psi}_{\mathrm{R}}} & \Gamma_{\phi_1 W} & \Gamma_{\phi_1 c} & \Gamma_{\phi_1\bar{c}} \\
\Gamma_{\phi_2\phi_1} & \Gamma_{\phi_2\phi_2} & \Gamma_{\phi_2\psi_{\mathrm{L}}} & \Gamma_{\phi_2\bar{\psi}_{\mathrm{L}}} & \Gamma_{\phi_2\psi_{\mathrm{R}}} & \Gamma_{\phi_2\bar{\psi}_{\mathrm{R}}} & \Gamma_{\phi_2 W} & \Gamma_{\phi_2 c} & \Gamma_{\phi_2\bar{c}} \\
\Gamma_{\psi_{\mathrm{L}}\phi_1} & \Gamma_{\psi_{\mathrm{L}}\phi_2} & \Gamma_{\psi_{\mathrm{L}}\psi_{\mathrm{L}}} & \Gamma_{\psi_{\mathrm{L}}\bar{\psi}_{\mathrm{L}}} & \Gamma_{\psi_{\mathrm{L}}\psi_{\mathrm{R}}} & \Gamma_{\psi_{\mathrm{L}}\bar{\psi}_{\mathrm{R}}} & \Gamma_{\psi_{\mathrm{L}} W} & \Gamma_{\psi_{\mathrm{L}} c} & \Gamma_{\psi_{\mathrm{L}}\bar{c}} \\
\Gamma_{\bar{\psi}_{\mathrm{L}}\phi_1} & \Gamma_{\bar{\psi}_{\mathrm{L}}\phi_2} & \Gamma_{\bar{\psi}_{\mathrm{L}}\psi_{\mathrm{L}}} & \Gamma_{\bar{\psi}_{\mathrm{L}}\bar{\psi}_{\mathrm{L}}} & \Gamma_{\bar{\psi}_{\mathrm{L}}\psi_{\mathrm{R}}} & \Gamma_{\bar{\psi}_{\mathrm{L}}\bar{\psi}_{\mathrm{R}}} & \Gamma_{\bar{\psi}_{\mathrm{L}} W} & \Gamma_{\bar{\psi}_{\mathrm{L}} c} & \Gamma_{\bar{\psi}_{\mathrm{L}}\bar{c}} \\
\Gamma_{\psi_{\mathrm{R}}\phi_1} & \Gamma_{\psi_{\mathrm{R}}\phi_2} & \Gamma_{\psi_{\mathrm{R}}\psi_{\mathrm{L}}} & \Gamma_{\psi_{\mathrm{R}}\bar{\psi}_{\mathrm{L}}} & \Gamma_{\psi_{\mathrm{R}}\psi_{\mathrm{R}}} & \Gamma_{\psi_{\mathrm{R}}\bar{\psi}_{\mathrm{R}}} & \Gamma_{\psi_{\mathrm{R}} W} & \Gamma_{\psi_{\mathrm{R}} c} & \Gamma_{\psi_{\mathrm{R}}\bar{c}} \\
\Gamma_{\bar{\psi}_{\mathrm{R}}\phi_1} & \Gamma_{\bar{\psi}_{\mathrm{R}}\phi_2} & \Gamma_{\bar{\psi}_{\mathrm{R}}\psi_{\mathrm{L}}} & \Gamma_{\bar{\psi}_{\mathrm{R}}\bar{\psi}_{\mathrm{L}}} & \Gamma_{\bar{\psi}_{\mathrm{R}}\psi_{\mathrm{R}}} & \Gamma_{\bar{\psi}_{\mathrm{R}}\bar{\psi}_{\mathrm{R}}} & \Gamma_{\bar{\psi}_{\mathrm{R}} W} & \Gamma_{\bar{\psi}_{\mathrm{R}} c} & \Gamma_{\bar{\psi}_{\mathrm{R}}\bar{c}} \\
\Gamma_{W\phi_1} & \Gamma_{W\phi_2} & \Gamma_{W\psi_{\mathrm{L}}} & \Gamma_{W\bar{\psi}_{\mathrm{L}}} & \Gamma_{W\psi_{\mathrm{R}}} & \Gamma_{W\bar{\psi}_{\mathrm{R}}} & \Gamma_{WW} & \Gamma_{Wc} & \Gamma_{W\bar{c}} \\
\Gamma_{c\phi_1} & \Gamma_{c\phi_2} & \Gamma_{c\psi_{\mathrm{L}}} & \Gamma_{c\bar{\psi}_{\mathrm{L}}} & \Gamma_{c\psi_{\mathrm{R}}} & \Gamma_{c\bar{\psi}_{\mathrm{R}}} & \Gamma_{cW} & \Gamma_{cc} & \Gamma_{c\bar{c}} \\
\Gamma_{\bar{c}\phi_1} & \Gamma_{\bar{c}\phi_2} & \Gamma_{\bar{c}\psi_{\mathrm{L}}} & \Gamma_{\bar{c}\bar{\psi}_{\mathrm{L}}} & \Gamma_{\bar{c}\psi_{\mathrm{R}}} & \Gamma_{\bar{c}\bar{\psi}_{\mathrm{R}}} & \Gamma_{\bar{c}W} & \Gamma_{\bar{c}c} & \Gamma_{\bar{c}\bar{c}}
\end{pmatrix},$$

and the regulator matrix contains parts for gauge bosons ($R_{k\mathrm{GB}}$) and ghost fields ($R_{k\mathrm{G}}$)

$$R_k(q,p) = \delta(p-q) \begin{pmatrix}
R_{k\mathrm{B}} & 0 & 0 & 0 \\
0 & -R_{k\mathrm{F}} & 0 & 0 \\
0 & 0 & R_{k\mathrm{GB}} & 0 \\
0 & 0 & 0 & R_{k\mathrm{G}}
\end{pmatrix}.$$

The regulators for the bosons and the fermions are given as in App. C by Eq. (C.2) and Eq. (C.3). Further, we define

$$R_{k\mathrm{G}} = \begin{pmatrix}
0 & p^2\delta^{ij} r_{k\mathrm{G}}(p) \\
-p^2\delta^{ij} r_{k\mathrm{G}}(p) & 0
\end{pmatrix}$$

and

$$R_{k\mathrm{GB}} = Z_{\mathrm{F}}(p^2 P_{\mathrm{T}} + \frac{p^2 Z_\phi}{\alpha Z_{\mathrm{F}}} P_{\mathrm{L}})\delta^{ij} r_{k\mathrm{GB}}(p),$$

with the longitudinal and transversal projectors

$$P_{\mathrm{T}} = \delta^{\mu\nu} - \frac{p^\mu p^\nu}{p^2} \quad \text{and} \quad P_{\mathrm{L}} = \frac{p^\mu p^\nu}{p^2}.$$

Flow Equation of the Effective Potential

In this subsection we discuss how the flow equation of the effective potential changes by introducing the gauge field and the ghosts as compared to App. C. First we project our truncation onto the effective potential by:

$$\delta(0)\partial_t U_k = \partial_t \Gamma_k|_{\substack{\psi,W,c=0\\ \phi=const}} = \frac{1}{2}\mathrm{STr}\left(\frac{\partial_t R_k}{\Gamma_k^{(2)}+R_k}\right)\Bigg|_{\substack{\psi,W,c=0\\ \phi=const}}.$$

Using this projection the fluctuation matrix is block diagonal. Thus the bosonic, fermionic, gauge bosonic and the ghost block can be calculated separately. We employ Landau gauge ($\alpha = 0$) so the bosonic block and the fermionic block do not change. Using $P_{\mathrm{G}}(p) = p^2(1+r_{\mathrm{G}})$, the ghost block can be computed very easily and reads

$$(\partial_t U_k)_{\mathrm{G}} = -(N_{\mathrm{L}}^2-1)\int \frac{d^dp}{(2\pi)^d}\frac{\partial_t(p^2 r_{\mathrm{G}})}{P_{\mathrm{G}}(p)}.$$

The gauge-boson block is more involved: $\Gamma_k^{(2)}+R_k$ is now given by

$$\begin{aligned}(\Gamma_k^{(2)}+R_k)_{ij}^{\rho\gamma} &= \delta^{ij}\left[\left(Z_{\mathrm{F}}p^2P_{\mathrm{T}}+\frac{Z_\phi}{\alpha}p^2P_{\mathrm{L}}\right)(1+r_{\mathrm{GB}})+Z_\phi g^2\delta^{\rho\gamma}\phi^{a\dagger}\{T^i,T^j\}_{ab}\phi^b\right]\delta(p-q)\\ &= \left[\delta^{ij}\left(Z_{\mathrm{F}}p^2P_{\mathrm{T}}+\frac{Z_\phi}{\alpha}p^2P_{\mathrm{L}}\right)(1+r_{\mathrm{GB}})+\delta^{\rho\gamma}\sum_{A=1}^{N_{\mathrm{L}}^2-1}m_A^2P_A^{ij}\right]\delta(p-q).\end{aligned}$$

Here we diagonalised the matrix $Z_\phi g^2\phi^{a\dagger}\{T^i,T^j\}_{ab}\phi^b$. Since P_A, P_{T} and P_{L} are projectors we can write down the inverse as

$$\left((\Gamma_k^{(2)}+R_k)_{ij}^{\rho\gamma}\right)^{-1} = \delta_{p,q}\sum_A P_A^{ij}\left[P_{\mathrm{T}}^{\rho\gamma}\frac{1}{Z_{\mathrm{F}}p^2(1+r_{\mathrm{GB}})+m_A^2}+P_{\mathrm{L}}^{\rho\gamma}\frac{1}{\frac{Z_\phi}{\alpha}p^2(1+r_{\mathrm{GB}})+m_A^2}\right].$$

Using $\mathrm{Tr}_{\rho\gamma}P_{\mathrm{T}} = d-1, \mathrm{Tr}_{\rho\gamma}P_{\mathrm{L}} = 1$ and $\mathrm{Tr}_{ij}P_A^{ij} = 1$ we get the gauge boson part of the flow equation of the effective potential as

$$(\partial_t U_k)_{\mathrm{GB}} = \frac{1}{2}\int\frac{d^dp}{(2\pi)^d}\sum_A\left[\frac{(d-1)\partial_t(Z_{\mathrm{F}}p^2r_{\mathrm{GB}})}{Z_{\mathrm{F}}p^2(1+r_{\mathrm{GB}})+m_A^2}+\frac{\partial_t\left(\frac{Z_\phi}{\alpha}p^2r_{\mathrm{GB}}\right)}{\frac{Z_\phi}{\alpha}p^2(1+r_{\mathrm{GB}})+m_A^2}\right].$$

Altogether we have the following flow equation for the effective potential:

$$\begin{aligned}\partial_t U_k =& v_d k^d 2\left[(2N_\mathrm{L}-1) l_0^d\left(\frac{U_k'}{Z_\phi k^2}\right)+l_0^d\left(\frac{U_k'+2\rho U_k''}{Z_\phi k^2}\right)\right]\\ &- d_\gamma v_d k^d 2\left[(N_\mathrm{L}-1) l_{0\mathrm{L}}^{(\mathrm{F})d}(0)+l_{0\mathrm{L}}^{(\mathrm{F})d}\left(\frac{\rho\bar{h}_k^2}{k^2 Z_\mathrm{L} Z_\mathrm{R}}\right)+l_{0\mathrm{R}}^{(\mathrm{F})d}\left(\frac{\rho\bar{h}_k^2}{k^2 Z_\mathrm{L} Z_\mathrm{R}}\right)\right]\\ &+\frac{1}{2}\sum_A\int\frac{d^dp}{(2\pi)^d}\left[(d-1)\frac{\partial_t(Z_\mathrm{F}p^2 r_\mathrm{GB}(p))}{Z_\mathrm{F}P_\mathrm{GB}(p)+m_A^2}+\frac{\partial_t(Z_\phi p^2 r_\mathrm{GB}(p))}{Z_\phi P_\mathrm{GB}(p)+\alpha m_A^2}\right]\\ &-(N_\mathrm{L}^2-1)\int\frac{d^dp}{(2\pi)^d}\frac{p^2\partial_t r_\mathrm{G}(p)}{P_\mathrm{G}(p)},\end{aligned}$$

where we introduced $P_\mathrm{G}=p^2(1+r_\mathrm{G})$ and $P_\mathrm{GB}=p^2(1+r_\mathrm{GB})$. Rewriting this equation by using the threshold functions defined in App. B yields

$$\begin{aligned}\partial_t U_k =& v_d k^d 2\left[(2N_\mathrm{L}-1) l_0^d\left(\frac{U_k'}{Z_\phi k^2}\right)+l_0^d\left(\frac{U_k'+2\rho U_k''}{Z_\phi k^2}\right)\right]\\ &- d_\gamma v_d k^d 2\left[(N_\mathrm{L}-1) l_{0\mathrm{L}}^{(\mathrm{F})d}(0)+l_{0\mathrm{L}}^{(\mathrm{F})d}\left(\frac{\rho\bar{h}_k^2}{k^2 Z_\mathrm{L} Z_\mathrm{R}}\right)+l_{0\mathrm{R}}^{(\mathrm{F})d}\left(\frac{\rho\bar{h}_k^2}{k^2 Z_\mathrm{L} Z_\mathrm{R}}\right)\right]\\ &+2v_d k^d\sum_A\left[(d-1) l_{0\mathrm{T}}^{(\mathrm{GB})d}\left(\frac{m_A^2}{Z_\mathrm{F}k^2}\right)+l_{0\mathrm{L}}^{(\mathrm{GB})d}\left(\frac{\alpha m_A^2}{Z_\phi k^2}\right)\right]\\ &-4v_d k^d\left(N_\mathrm{L}^2-1\right) l_0^{(\mathrm{G})d}(0).\end{aligned}$$

The last step is to introduce dimensionless quantities and use the specific regulators as discussed in App. B. Using the dimensionless quantities

$$\tilde{\rho}=Z_\phi k^{2-d}\rho,\quad \tilde{h}_k^2=\frac{k^{d-4}h_k^2}{Z_\phi Z_\mathrm{L} Z_\mathrm{R}},\quad \tilde{u}_k=U_k k^{-d},\quad \tilde{m}_A^2=\frac{m_A^2}{Z_\mathrm{F}k^2},\quad \tilde{g}^2=\frac{g^2}{Z_\mathrm{F}k^{4-d}},\tag{D.1}$$

the flow equation for the effective potential is given by Eq. (4.17).

Flow Equation of the Yukawa Coupling

In order to derive the flow equation for the Yukawa coupling we divide our bosonic field into vacuum expectation value and fluctuations. This time we choose the vacuum expectation value v to be in the N_L direction:

$$\phi(p)=\frac{1}{\sqrt{2}}\begin{pmatrix}\phi_1^1(p)+i\phi_2^1(p)\\ \phi_1^2(p)+i\phi_2^2(p)\\ \vdots\\ \phi_1^{N_\mathrm{L}}(p)+i\phi_2^{N_\mathrm{L}}(p)\end{pmatrix}=\begin{pmatrix}0\\ \vdots\\ 0\\ v\end{pmatrix}\delta(p)+\frac{1}{\sqrt{2}}\begin{pmatrix}\Delta\phi_1^1(p)+i\Delta\phi_2^1(p)\\ \Delta\phi_1^2(p)+i\Delta\phi_2^2(p)\\ \vdots\\ \Delta\phi_1^{N_\mathrm{L}}(p)+i\Delta\phi_2^{N_\mathrm{L}}(p)\end{pmatrix}.\tag{D.2}$$

We are interested in the Yukawa coupling between the radial mode $\Delta\phi_1^{N_\mathrm{L}}$ and the fermions. Thus the projection onto the coupling constant $\bar{h}_k$ is given by

$$\frac{\overrightarrow{\delta}}{\delta\bar{\psi}_\mathrm{L}^{N_\mathrm{L}}(p)}\frac{\sqrt{2}\overrightarrow{\delta}}{\delta\Delta\phi_1^{N_\mathrm{L}}(p')}\Gamma_k\frac{\overleftarrow{\delta}}{\delta\psi_\mathrm{R}(q)}\bigg|_{\substack{\psi=\Delta\phi=W=c=0\\p'=p=q=0}} = -\bar{h}_k\delta(0).$$

Again, we divide $\Gamma_k^{(2)}+R_k$ into the propagator part and the fluctuation part. Expanding the logarithm as in Eq. (C.6) only the third power survives and we obtain

$$\delta(0)\partial_t\bar{h}_k = -\frac{\sqrt{2}}{6}\frac{\overrightarrow{\delta}}{\delta\bar{\psi}_\mathrm{L}^{N_\mathrm{L}}(p)}\frac{\overrightarrow{\delta}}{\delta\Delta\phi(p')}\mathrm{STr}\left[\tilde{\partial}_t\left(\frac{\Delta\Gamma_k^{(2)}}{(\Gamma_{k0}^{(2)}+R_k)}\right)^3\right]\frac{\overleftarrow{\delta}}{\delta\psi_\mathrm{R}(q)}\bigg|_{\substack{\psi=\Delta\phi=W=c=0\\p'=p=q=0}}.$$

The matrix calculations are tedious but straightforward and the flow equation reads

$$\begin{aligned}\partial_t\bar{h}_k = &-\int\frac{d^dp}{(2\pi)^d}\tilde{\partial}_t\left[\frac{v\bar{h}^3}{Z_\mathrm{L}Z_\mathrm{R}P_\mathrm{F}(p)+v^2\bar{h}^2}\left(\frac{vU''}{(Z_\phi P(p)+U')^2}-\frac{3vU''+2v^3U'''}{(Z_\phi P(p)+U'+2v^2U'')^2}\right)\right.\\
&+\frac{v^2\bar{h}^5}{(Z_\mathrm{L}Z_\mathrm{R}P_\mathrm{F}(p)+v^2\bar{h}^2)^2}\left(\frac{1}{Z_\phi P(p)+U'}-\frac{1}{Z_\phi P(p)+U'+2v^2U''}\right)\\
&-\frac{\frac{1}{2}\bar{h}^3}{Z_\mathrm{L}Z_\mathrm{R}P_\mathrm{F}(p)+v^2\bar{h}^2}\left(\frac{1}{Z_\phi P(p)+U'}-\frac{1}{Z_\phi P(p)+U'+2v^2U''}\right)\\
&\left.-\bar{h}\sum_{a=1}^{N}\sum_{i=1}^{N^2-1}\frac{Z_\phi Z_\mathrm{L}Z_\mathrm{R}g^2p^2d_\gamma(1+r_{k\mathrm{F}})T_{Na}^iT_{aN}^i}{(Z_\phi P+U')(Z_\mathrm{L}Z_\mathrm{R}P_\mathrm{F}+v^2\bar{h}^2\delta^{aN})}\frac{(d-1)}{Z_\mathrm{F}P_\mathrm{GB}+m_i^2}\right].\end{aligned}$$

Using the threshold functions defined in App. B and the dimensionless quantities, Eq. (D.1), we obtain Eq. (4.18) as given in the main text.

Anomalous Dimensions

Finally we derive the equations for the anomalous dimensions, starting with the bosonic anomalous dimension. The projection onto the wave-function renormalisation is given by

$$\delta(0)\partial_tZ_\phi = \frac{\partial}{\partial(p'^2)}\frac{\delta}{\delta\Delta\phi(p')}\frac{\delta}{\delta\Delta\phi(q')}\frac{-1}{4}\mathrm{STr}\left[\tilde{\partial}_t\left(\frac{\Delta\Gamma_k^{(2)}}{\Gamma_{k,0}^{(2)}+R_k}\right)^2\right]\bigg|_{\substack{\Delta\phi=\psi=W=c=0\\p'=q'=0}},$$

where we divided the bosonic field as in Eq. (D.2) into its vacuum expectation value and the fluctuation contributions.

We also expanded the logarithm and this time the second power is the only one which survives the projection:

$$(\partial_t Z_{\phi,k})_{\mathrm{GB}} = -\frac{1}{d}\int \frac{d^dp}{(2\pi)^d}\tilde{\partial}_t \left\{ \frac{Z_\phi^2 g^2}{2}\sum_{a=1}^{N}\sum_{i=1}^{N^2-1} T^i_{Na}T^i_{aN}\left[\frac{2d}{(Z_\phi P_{\mathrm{B}}+U')(Z_{\mathrm{F}}P_{\mathrm{GB}}+m_i^2)}\right.\right.$$
$$\left.\left. +\frac{12p^2 Z_{\mathrm{F}}\frac{\partial}{\partial p^2}P_{\mathrm{GB}}}{(Z_\phi P_{\mathrm{B}}+U')(Z_{\mathrm{F}}P_{\mathrm{GB}}+m_i^2)^2} - \frac{4p^4 Z_\phi Z_{\mathrm{F}}\left(\frac{\partial}{\partial p^2}P_{\mathrm{B}}\right)\left(\frac{\partial}{\partial p^2}P_{\mathrm{GB}}\right)}{(Z_\phi P_{\mathrm{B}}+U')^2(Z_{\mathrm{F}}P_{\mathrm{GB}}+m_i^2)^2}\right]\right\}.$$

Introducing the threshold functions defined in App. B and switching to dimensionless quantities leads to Eq. (4.19).

For the calculation for the anomalous dimension of the left-handed fermion the projection reads

$$\delta(0)\partial_t Z_{\mathrm{L}} = \frac{1}{4dd_\gamma}\mathrm{tr}\gamma_\mu \frac{\partial}{\partial p'_\mu}\frac{\overrightarrow{\delta}}{\delta\bar{\psi}^N_{\mathrm{L}}(p')}\mathrm{STr}\left[\tilde{\partial}_t\left(\frac{\Delta\Gamma^{(2)}_k}{\Gamma^{(2)}_{k0}+R_k}\right)^2\right]\frac{\overleftarrow{\delta}}{\delta\psi^N_{\mathrm{L}}(q')}\Bigg|_{\substack{\Delta\phi=\psi=W=c=0\\ p'=q'=0}},$$

where we expanded the logarithm and only keep the second order since all other orders do not survive the projection. We find the same terms as in the chiral Yukawa model without gauge bosons, cf. Eq. (C.9), and one additional loop term for the gauge bosons. This new contribution reads

$$(\partial_t Z_{\mathrm{L},k})_{\mathrm{GB}} = \int \frac{d^dp}{(2\pi)^d}p^2\tilde{\partial}_t$$
$$\left[-2d_\gamma Z_{\mathrm{L}}^2 g^2\sum_{a=1}^{N}\sum_{i=1}^{N^2-1} T^i_{aN}T^i_{Na}\frac{Z_{\mathrm{R}}(1+r_{\mathrm{F}})}{Z_{\mathrm{L}}Z_{\mathrm{R}}P_{\mathrm{F}}+\delta^{aN}v^2h_k^2}\frac{Z_{\mathrm{F}}\frac{\partial}{\partial p^2}P_{\mathrm{GB}}}{(Z_{\mathrm{F}}P_{\mathrm{GB}}+m_i^2)^2}\right].$$

The threshold functions and the dimensionless quantities enable us to write the complete equation in a compact notation, see Eq. (4.20) in the main text.

Since the right-handed fermions do not couple to the gauge bosons the equation for the right-handed anomalous dimension does not change, cf. Eq. (4.20).

Fixed-points for the gauged chiral Yukawa model

We identified a number of interesting fixed-points in this system for various values of N_{L} ranging from 3 to 5 as a function of the gauge coupling g. This is summarized in the figures below. Investigations about the underlying fixed-point mechanisms still go on and we therefore refer to our work in preparation [121]. Corresponding to the discussion in Sec. 4.5.3 we show the plots for $N_{\mathrm{L}} \in \{4, 5\}$.

We start with $N_{\mathrm{L}} = 4$:

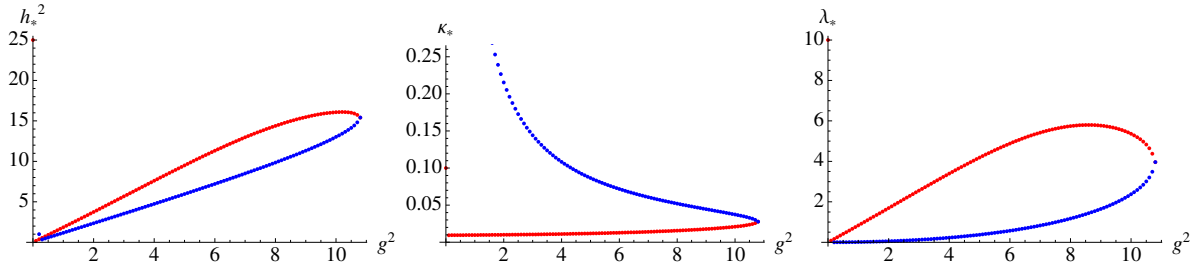

Figure D.1: Fixed points for $N_{\mathrm{L}} = 4$ at NLO with u up to 6th order in ρ.

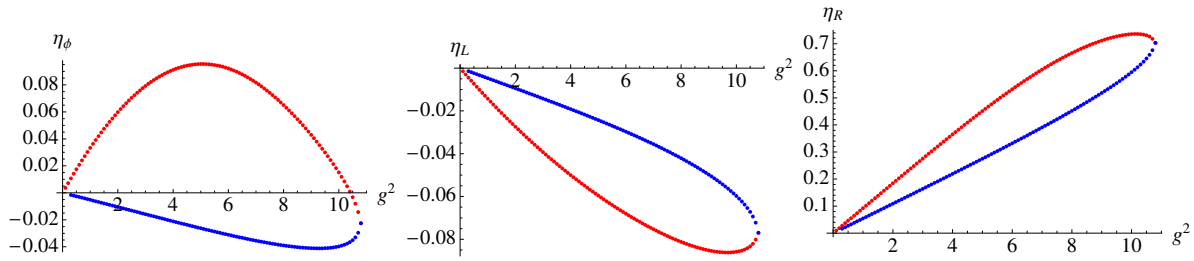

Figure D.2: FP anomalous dimensions for $N_{\mathrm{L}} = 4$ at NLO with u up to 6th order in ρ.

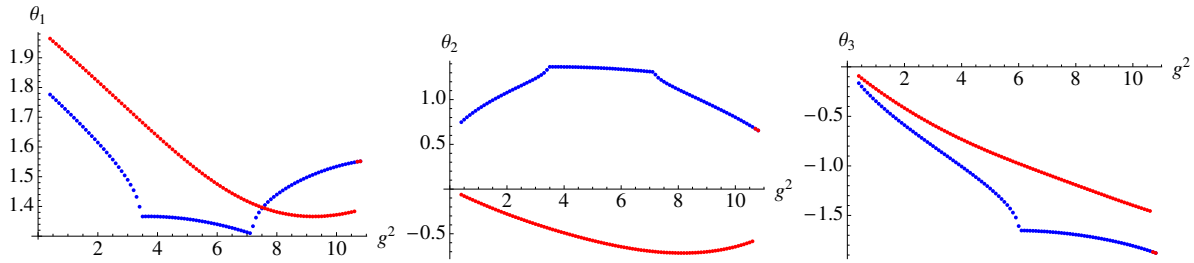

Figure D.3: RG eigenvalues for $N_{\mathrm{L}} = 4$ at NLO with u up to 6th order in ρ.

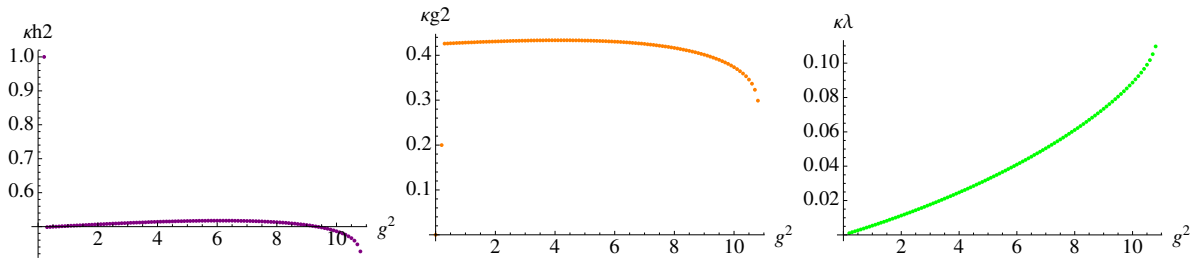

Figure D.4: Mass terms for $N_{\mathrm{L}} = 4$ at NLO with u up to 6th order in ρ.

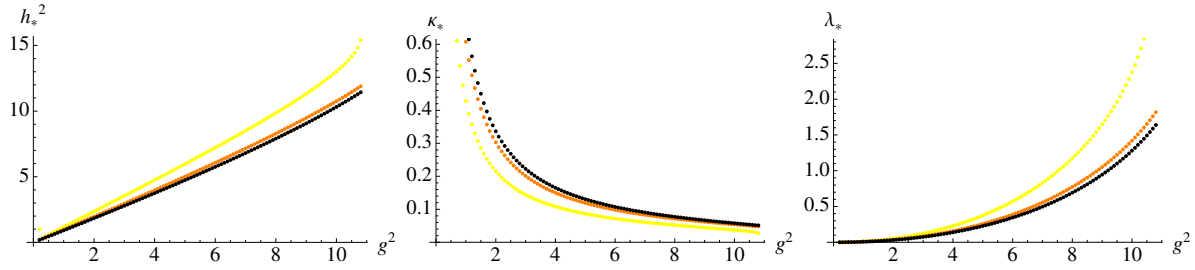

Figure D.5: Convergence for $N_\mathrm{L} = 4$ at NLO with u up to 2nd, 4th and 6th order in ρ.

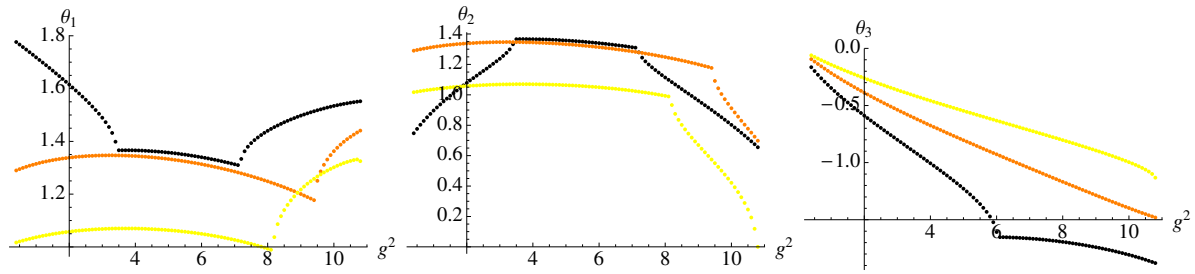

Figure D.6: Convergence of RG eigenvalues for $N_\mathrm{L} = 4$ at NLO.

The results for $N_\mathrm{L} = 5$ are:

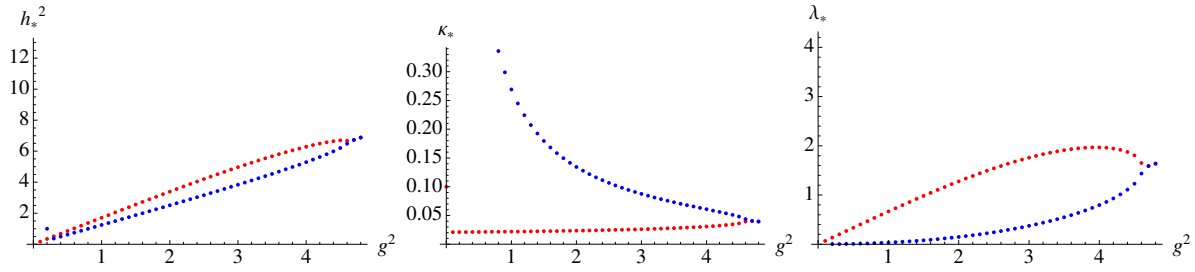

Figure D.7: Fixed points for $N_\mathrm{L} = 5$ at NLO with u up to 6th order in ρ.

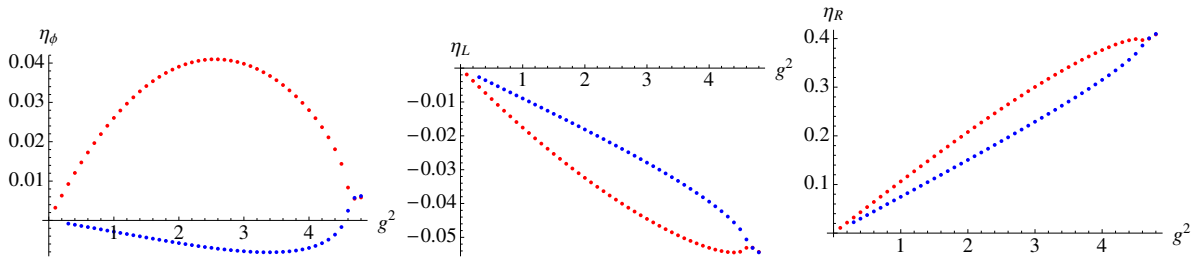

Figure D.8: Anomalous dimensions for $N_\mathrm{L} = 5$ at NLO with u up to 6th order in ρ.

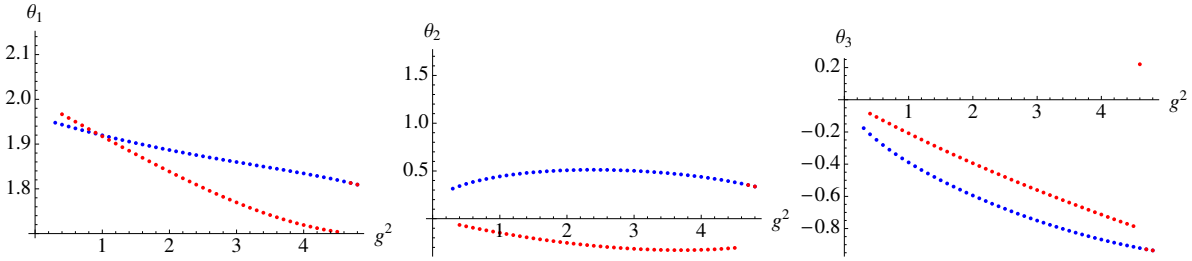

Figure D.9: RG eigenvalues for $N_{\mathrm{L}} = 5$ at NLO with u up to 6th order in ρ.

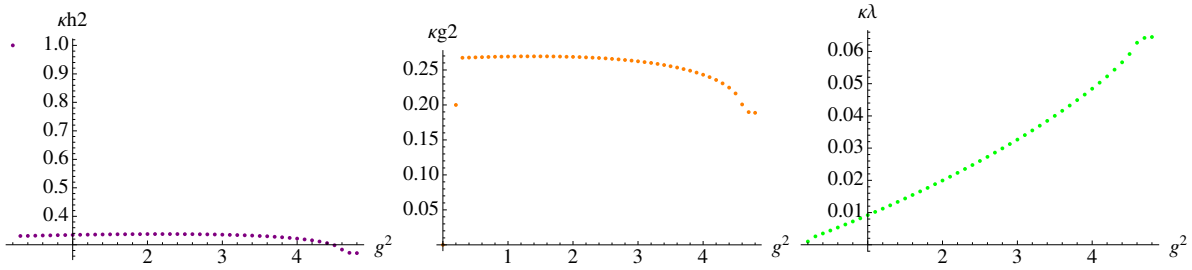

Figure D.10: Mass terms for $N_{\mathrm{L}} = 5$ at NLO with u up to 6th order in ρ.

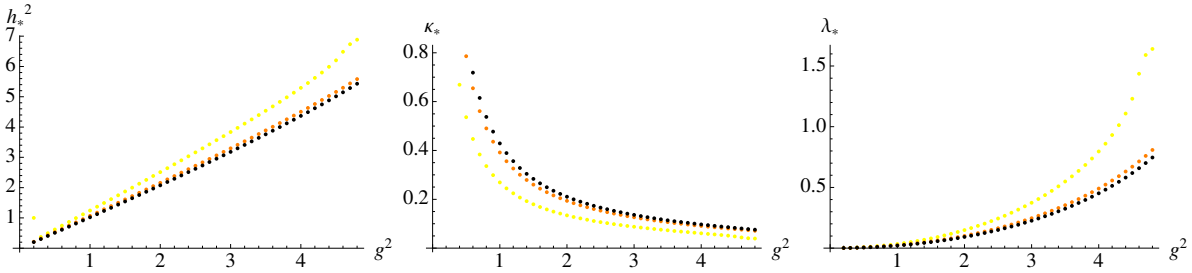

Figure D.11: Convergence for $N_{\mathrm{L}} = 5$ at NLO with u up to 2nd, 4th and 6th order in ρ.

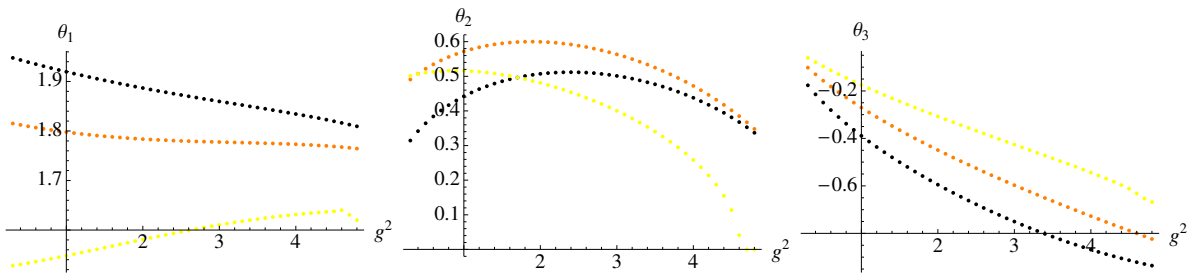

Figure D.12: Convergence of RG eigenvalues for $N_{\mathrm{L}} = 5$ at NLO.

Acknowledgments,...

Danksagung, Remerciements, Ringraziamento

Für die kompetente und freundliche Betreuung dieser Doktorarbeit und für die ausgezeichnete Zusammenarbeit möchte ich mich bei Prof. Dr. Holger Gies bedanken. Aus unseren Gesprächen und Diskussionen habe ich sehr viel gelernt. Im Besonderen danke ich auch für die zahlreichen Möglichkeiten an Konferenzen und Workshops in aller Welt teilzunehmen, Gäste einzuladen und einen Forschungsaufenthalt in Triest zu machen.

Mein Forschungsaufenthalt in Triest wurde durch die Gastfreundschaft von Prof. Dr. Roberto Percacci ermöglicht, dem ich für diese lehrreiche Zeit sehr dankbar bin.

Großer Dank gebührt Dr. Jens Braun für erhellende Diskussionen und das mühevolle Korrekturlesen des Manuskriptes zu dieser Arbeit.

Für die gute Zusammenarbeit und zahlreiche inspirierende Diskussionen mit Dr. Stefan Flörchinger, Stefan Rechenberger, Astrid Eichhorn, Lukas Janssen, Dr. Sebastian Diehl und Prof. Dr. Christof Wetterich bedanke ich mich ganz herzlich.

Besonders bedanken möchte ich mich für zahlreiche motivierende und klärende Gespräche mit Prof. Dr. Jan Martin Pawlowski, Dr. Hans Christian Krahl, Dr. Philipp Strack und Omar Zanusso.

Der Deutschen Forschungsgemeinschaft und im Besonderen der DFG Forschergruppe 723 bin ich für die finanzielle Unterstützung meiner Doktorarbeit zu großem Dank verpflichtet.

Ich möchte mich herzlich bei meinen Eltern bedanken, die mich stets unterstützt haben. Dank gebührt auch meiner Schwester und meinen Freunden für sehr Vieles.

Ehrenwörtliche Erklärung

Ich erkläre hiermit ehrenwörtlich, daß ich die vorliegende Arbeit selbständig, ohne unzulässige Hilfe Dritter und ohne Benutzung anderer als der angegebenen Hilfsmittel und Literatur angefertigt habe. Die aus anderern Quellen direkt oder indirekt übernommenen Daten und Konzepte sind unter Angabe der Quelle gekennzeichnet. Auch die Ergebnisse, die in Zusammenarbeit mit den Mitgliedern des Lehrstuhles für Quantenfeldtheorie in Jena und anderen Kooperationen entstanden sind, sind in der Arbeit entsprechend benannt.

Weitere Personen waren an der inhaltlich-materiellen Erstellung der vorliegenden Arbeit nicht beteiligt. Insbesondere habe ich hierfür nicht die entgeltliche Hilfe von Vermittlungsbzw. Beratungsdiensten (Promotionsberater oder andere Personen) in Anspruch genommen. Niemand hat von mir unmittelbar oder mittelbar geldwerte Leistungen für Arbeiten erhalten, die im Zusammenhang mit dem Inhalt der vorgelegten Dissertation stehen. Die Arbeit wurde bisher weder im In- noch im Ausland in gleicher oder ähnlicher Form einer anderen Prüfungsbehörde vorgelegt.

Die geltende Promotionsordnung der Physikalisch-Astronomischen Fakultät ist mir bekannt.

Ich versichere ehrenwörtlich, dass ich nach bestem Wissen die reine Wahrheit gesagt und nichts verschwiegen habe.

Jena, 27.6.2010

Michael Scherer

Curriculum Vitae

Personal Information

Name	Michael Scherer
Born	November 2, 1981, Furtwangen, Germany

Education and University Studies

11/2008	Continuation of Ph.D. at the University of Jena
11/2007	Start of Ph.D. at the Institute for Theoretical Physics, University of Heidelberg supervisor: Prof. H. Gies
2006–2007	Diploma at the Institute for Theoretical Physics, University of Heidelberg supervisor: Prof. C. Wetterich
09/2004 – 06/2005	Physics at the Joseph Fourier University Grenoble (Erasmus-Fellowship)
10/2002 – 11/2007	Physics at the Universitiy of Heidelberg
09/2001 – 06/2002	Civil service with the German Red Cross, Education as an Emergency Medical Technician
2001	High school graduation at the Friedrich-Hecker-Gymnasium Radolfzell, Abitur

Teaching and Seminar organization

10/2009–03/2010	Organization of an undergraduate seminar on quantum effects on curved spacetimes, Jena University
03/2009–	Organization of a graduate seminar at the Theoretisch-Physikalisches Institut, Jena University
2006–2008	Organization of a seminar for graduate students at the Institute for Theoretical Physics, University of Heidelberg (the Cold Quantum Coffee)
2006–2008	Tutorials for lectures in theoretical physics and mathematics at the Institute for Theoretical Physics, University of Heidelberg

Talks (to be found on `http://www.tpi.uni-jena.de/qfphysics/homepage/scherer/`)

1. "FRG approach for the BCS-BEC crossover: Many-body effects and scattering physics", RWTH Aachen, 2010/03/17

2. "Interacting fixed-points in chiral Yukawa systems – critical behaviour and asymptotic safety", Sussex University, Brighton, 2010/03/08

3. "Towards a quantitative FRG approach for the BCS-BEC crossover", INT-10-45, Seattle, 2010/02/26

4. "Chiral Yukawa systems in 3 and 4 dimensions - critical behaviour and asymptotic safety", Workshop Graduiertenkolleg 1523, Oppurg, 2009/11/21

5. "A mechanism for Asymptotic Safety of chiral Yukawa systems", Perimeter Institute, Waterloo, 2009/11/07

6. "Asymptotic Safety in chiral Yukawa Systems", SISSA, Trieste, 2009/07/17

7. "Towards asymptotic safety in chiral Yukawa Systems", Cracow School of Theoretical Physics, Zakopane, 2009/06/07

8. "Asymptotic Safety in simple Yukawa Systems", ITP Heidelberg, 2009/04/28

9. "Asymptotic Safety in simple Yukawa Systems", Theoretisch Physikalisches Institut at the University of Jena, 2009/02/26

10. "Ultracold Gases and Functional Renormalization II", Ladenburg, 2008/11/20, FOR 723 Retreat

11. "Particle-hole fluctuations in the BCS-BEC crossover", Theoretisch Physikalisches Institut at the University of Jena, 2008/09/24

November 25, 2010

List of publications

Refereed publications

1. S. Floerchinger, M. M. Scherer, and C. Wetterich (2009): Modified Fermi-sphere in the BCS-BEC crossover, Phys. Rev. A **81**, 063619, 063619-1 – 063619-7

2. H. Gies, L. Janssen, S. Rechenberger and M. M. Scherer (2010): Phase transition and critical behavior of d=3 chiral fermion models with left/right asymmetry, Phys. Rev. D **81** 025009, 025009-1 – 025009-14.

3. H. Gies, S. Rechenberger and M. M. Scherer (2010): Towards an Asymptotic-Safety Scenario for Chiral Yukawa Systems, The European Physical Journal C - Particles and Fields, DOI - 10.1140/epjc/s10052-010-1257-y, 16 pages (online first).

4. H. Gies and M. M. Scherer (2010): Asymptotic safety of simple Yukawa systems, The European Physical Journal C - Particles and Fields, DOI - 10.1140/epjc/s10052-010-1256-z, 16 pages (online first).

5. A. Eichhorn, H. Gies and M. M. Scherer (2009): Asymptotically free scalar curvature-ghost coupling in Quantum Einstein Gravity, Phys. Rev. D **80** 104003, 104003-1 – 104003-8.

6. S. Flörchinger, M. M. Scherer, S. Diehl and C. Wetterich (2008): Particle-hole fluctuations in the BCS-BEC Crossover, Phys. Rev. B **78** (2008) 174528, 174528-1 – 174528-10.

7. S. Diehl, H. C. Krahl, and M. M. Scherer (2008): Three-Body Scattering from Non-perturbative Flow Equations, Phys. Rev. C **78** (2008) 034001, 034001-1 – 034001-10.

Published conference proceedings

1. M. M. Scherer, H. Gies and S. Rechenberger (2009): Proceedings Supplement of Acta Physica Polonica B, Vol. 2, No. 3, December 2009, 541 – 554.